Identification of target proteins of furan reactive metabolites in rat liver

Dissertation

Zur Erlangung des naturwissenschaftlichen Doktorgrades

der Bayerischen Julius-Maximilians-Universität Würzburg

vorgelegt von

Sabrina Moro

aus Elsenfeld

Würzburg 2011

Eingereicht am …….

bei der Fakultät für Chemie und Pharmazie

1. Gutachter …….

2. Gutachter …….

der Dissertation

1. Prüfer …….

2. Prüfer …….

3. Prüfer …….

des öffentlichen Promotionskolloquiums

Datum des öffentlichen Promotionskolloquiums

……

Doktorurkunde ausgehändigt am

……

Für Mama, Papa und Marco

"Wir glauben, Erfahrungen zu machen,

aber die Erfahrungen machen uns."

(Eugène Ionesco)

TABLE OF CONTENTS

ABBREVIATIONS

2D-GE	two-dimensional gel electrophoresis
3α-HSD	3α-hydroxysteroid dehydrogenase
4-HNE	4-hydroxy-2-nonenal
4-ONE	4-oxo-2-nonenal
8-oxo-dG	8-oxo-7,8-dihydro-2´-deoxyguanosine
AAT	α1-antiproteinase
ALAD	δ-aminolevulinic acid dehydratase
ALDH-2	mitochondrial aldehyde dehydrogenase
ATF-6	activating transcription factor-6
ATP	adenosine triphosphate
BDA	*cis*-2-butene-1,4-dial
BHMT1	betaine-homocysteine S-methyltransferase 1
bp	base pairs
BSA	bovine serum albumin
bw	body weight
cDNA	complementary deoxyribonucleic acid
CEB	cytosol extraction buffer
CHAPS	3-[(3-cholamidopropyl)dimethylammonio]-1-propanesulfonate
CHO cells	chinese hamster ovary cells
CID	collision-induced dissociation
Ck	cytoskeleton
CK-8	cytokeratin 8
CM	cell membrane
CoA	coenzyme A
COPII	coat protein complex II
Cp	cytoplasm
Cs	cytosol
C_t	threshold cycle
CYP	cytochrome P450
cys	cysteine
d	days
dAdo	2'-deoxyadenosine
DAVID	Database for Annotation, Visualization and Integrated Discovery
DBP	vitamin D binding protein
dCyd	2'-deoxycytidine
DEPC	diethylpyrocarbonate (diethyldicarbonate)
dGuo	2'-deoxyguanosine
DNA	deoxyribonucleic acid
dNTP	deoxyribonucleoside triphosphate
dpm	disintegrations per minute
dRib	2-deoxyribose
DTT	1,4-dithiothreitol
EBP50	ezrin-radixin-moesin-binding phosphoprotein 50
EDTA	ethylenediaminetetraacetic acid
EFSA	European Food Safety Authority

ER	endoplasmic reticulum
ERAD	endoplasmic reticulum-associated degradation
ES	extracellular space
ESI	electrospray ionization
ESI-MS	electrospray ionization-mass spectrometry
EtBr	ethidium bromide
EU	European Union
FAD	flavin adenine dinucleotide
FAM	6-carboxyfluorescein
FDA	U.S. Food and Drug Administration
FGG	fibrinogen γ chain
FTCD	formimidoyltransferase-cyclodeaminase
FT-ICR	fourier transform ion cyclotron resonance
fw	forward
GAPDH	glyceraldehyde-3-phosphate dehydrogenase
GGT	γ-glutamyltransferase
GO	Gene Ontology
GPDH-C	cytosolic glycerol-3-phosphate dehydrogenase
GRP78	78 kDa glucose-regulated protein
GSH	glutathione
GST	glutathione S-transferase
h	hours
H&E	hematoxylin and eosin
HDL	high density lipoprotein
Herpud1 = HERP	homocysteine-inducible, endoplasmic reticulum stress-inducible, ubiquitin-like domain member 1
his	histidine
hnrnp H1	heterogeneous nuclear ribonucleoprotein H1
HPLC	high performance liquid chromatography
IAA	iodoacetamide
IARC	International Agency for Research on Cancer
IEF	isoelectric focusing
IPG	immobiline pH gradient
IRE1	inositol-requiring protein-1
KEGG	Kyoto Encyclopedia of Genes and Genomes
LC	liquid chromatography
LCFA	long chain fatty acid
LD_{50}	median lethal dose
L-FABP	liver fatty acid binding protein
LOD	limit of detection
LOQ	limit of quantification
LSC	liquid scintillation counting
lys	lysine
MALDI-TOF	matrix-assisted laser desorption/ionization time of flight
MAP kinase	mitogen-activated protein kinase
MAT1	S-adenosylmethionine synthetase isoform type-1
MDH1	cytosolic malate dehydrogenase
MEB	membrane extraction buffer

MGB	dihydrocyclopyrroloindole tripeptide minor groove binder
min	minutes
Mito	mitochondrion
M_r	molecular mass
mRNA	messenger ribonucleic acid
Ms	microsome
MS	mass spectrometry
MS/MS	tandem mass spectrometry
MST	3-mercaptopyruvate sulfurtransferase
N-AcCys	N-acetylcysteine
N-AcLys	N-acetyllysine
NAD^+	nicotinamide adenine dinucleotide
NDRG2	N-myc downstream-regulated gene 2
NEB	nuclear extraction buffer
NFQ	nonfluorescent quencher
NHERF3	Na^+/H^+ exchanger regulatory factor 3
NL	non-linear
NPC	nuclear pore complex
NRK cells	normal rat kidney cells
NTP	National Toxicology Program
Nu	nucleus
oatp	organic anion transporting polypeptide
PBS	phosphate buffered saline
PCR	polymerase chain reaction
PDI	protein disulfide isomerase
PERK	protein kinase RNA-like ER kinase
pI	isoelectric point
PIC	protease inhibitor cocktail
p.o.	per os
ppa1 protein	inorganic pyrophosphatase 1
PUFA	polyunsaturated fatty acid
Px	peroxisome
QTOF	quadrupole time of flight
rAFAR2-2	aflatoxin B1 aldehyde reductase member 2
RNA	ribonucleic acid
rpm	rounds per minute
RT	reverse transcriptase
RT-PCR	real-time polymerase chain reaction
rv	reverse
SAM	S-adenosylmethionine
SCE	sister chromatid exchange
SD	standard deviation
SDS	sodium dodecyl sulfate
SDS-PAGE	sodium dodecyl sulfate- polyacrylamide gel electrophoresis
sec	secreted
SEC13l	protein SEC13 homolog
serpin	serine protease inhibitor
SILAC	stable isotope labeling by amino acids in cell culture

SO	sulfite oxidase
TAE	tris-acetate-EDTA
TCA	trichloroacetic acid
TOF	time of flight
Tris	tris(hydroxymethyl)aminomethane
Trx	thioredoxin
Txl-1	thioredoxin-like protein 1
ufd1	ubiquitin fusion degradation protein 1
UDS	unscheduled DNA synthesis
UPR	unfolded protein response
VDAC1	voltage-dependent anion-selective channel protein 1
XBP1	X-box binding protein 1

1 INTRODUCTION

In 2004, the U.S. Food and Drug Administration (FDA) published results from studies identifying the chemical furan in a variety of food items that undergo heat treatment. Furan, originally known as an industrial chemical, is known to be a potent hepatotoxin and liver carcinogen in rodents. In a 2-year bioassay, chronic furan administration to rats caused hepatocellular adenomas and carcinomas (NTP, 1993). In addition, high incidences of cholangiocarcinomas were observed even at the lowest furan dose tested (2.0 mg/kg bw) (NTP, 1993). Although data on human intake of furan are limited, it appears that there is a relatively narrow margin between human exposure and doses which cause liver tumors in rodents, suggesting that the presence of furan in food may present a potential risk to human health. However, the currently available data on furan toxicity is insufficient to perform a risk assessment and more research regarding the mechanism of furan carcinogenicity is needed (EFSA, 2004).

Hepatotoxic effects of furan are thought to be mediated by bioactivation. Furan is oxidized by cytochrome P450 to yield a chemically reactive α,β-unsaturated dialdehyde, cis-2-butene-1,4-dial, which has been identified as the key cytotoxic metabolite of furan (Chen et al., 1995; Peterson et al., 2000). In vitro studies demonstrate that cis-2-butene-1,4-dial covalently modifies nucleosides (Byrns et al., 2002; Byrns et al., 2004) and amino acid residues (Chen et al., 1997) (Fig. 1), suggesting that both genotoxicity (via formation of DNA adducts) and chronic cytotoxicity mediated through binding of cis-2-butene-1,4-dial to critical target proteins may contribute to the mechanism of tumor formation by furan. While the important question as to whether or not furan forms DNA adducts in vivo has not been fully resolved, support for a role of cytotoxic/non-genotoxic mechanism(s) in furan toxicity/carcinogenicity has come from in vivo studies demonstrating that i) 80 % of the radioactivity present in livers of rats administered ^{14}C-labeled furan is associated with proteins (Burka et al., 1991), ii) degraded protein adducts are major urinary metabolites of furan (Lu et al., 2009), and iii) increased cell proliferation secondary to furan induced hepatocyte necrosis is a critical event in furan carcinogenicity (Wilson et al., 1992).

Based on these studies, it appears that inactivation of protein function through covalent binding may present a key event in the toxicity of furan. However, it has long been recognized that the formation of adducts at some proteins may be critical to injury, whereas covalent binding to others is not (Zhou et al., 2005). For a comprehensive understanding of the molecular events involved in furan toxicity, identification of target proteins of reactive furan intermediates, which may play a causal role in the pathogenesis of furan-associated liver toxicity, and characterization of the cellular and functional consequences of protein adduct formation are needed.

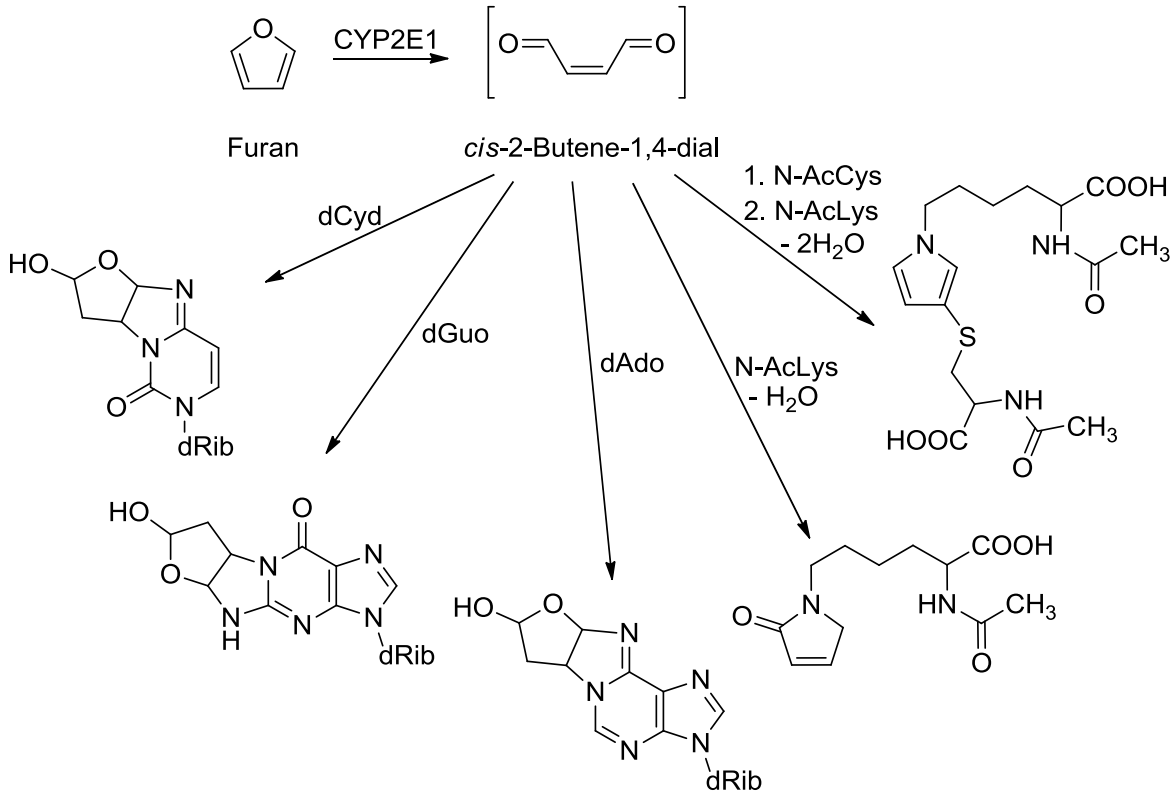

Figure 1 *Reaction products of nucleophilic additions to the furan metabolite cis-2-butene-1,4-dial exemplified for 2'-deoxycytidine (dCyd), 2'-deoxyguanosine (dGuo), 2'-deoxyadenosine (dAdo), N-acetyllysine (N-AcLys), and N-acetylcysteine (N-AcCys) (modified from Chen et al. 1997 and Byrns et al. 2002). CYP2E1 = cytochrome P 450 2E1, dRib = 2-deoxyribose*

2 STATE OF KNOWLEDGE ON FURAN

2.1 Structure and occurrence of furan

2.1.1 Properties of furan

Furan is a heterocyclic and aromatic organic compound. It is a colorless, inflammable, and volatile liquid with a boiling point of 31.4 °C. It is insoluble in water, but soluble in alcohol, acetone, benzene, and ether (IARC, 1995). It is used in various industrial processes, e.g. the manufacturing of lacquers and resins and the production of pharmaceuticals and agricultural chemicals (insecticides) (IARC, 1995). Furan also occurs in the environment as a constituent of cigarette smoke, wood smoke and exhaust gas from diesel and gasoline engines (IARC, 1995). Furthermore, furan was shown to occur in a variety of food items that undergo heating processes (see 2.1.3) (EFSA, 2004).

2.1.2 Formation of furan in food

Furan in food can be formed through a variety of pathways. The most important precursors appear to be ascorbic acid, sugars, amino acids, and unsaturated fatty acids (Fig. 2) (Crews and Castle, 2007). Experiments with single compounds or mixtures of different substances at high temperatures showed that the most efficient precursor for the formation of furan was ascorbic acid, followed by dehydroascorbic acid, glycolaldehyde/alanine, and erythrose (Perez Locas and Yaylayan, 2004). It was also observed that furan formation is strongly influenced by the reaction conditions (temperature, time, pH) (EFSA, 2009a; Fan et al., 2008).

In contrast to model reactions using only one or two educts, food items usually consist of more complex mixtures, in which several competing reactions may influence each other. Therefore, it is hypothesized that furan formation in foods is much lower than observed in reaction models (Limacher et al., 2007). Nevertheless, labeling experiments using reaction models have provided important insight as to how furan may be formed during heating processes (Fig. 2).

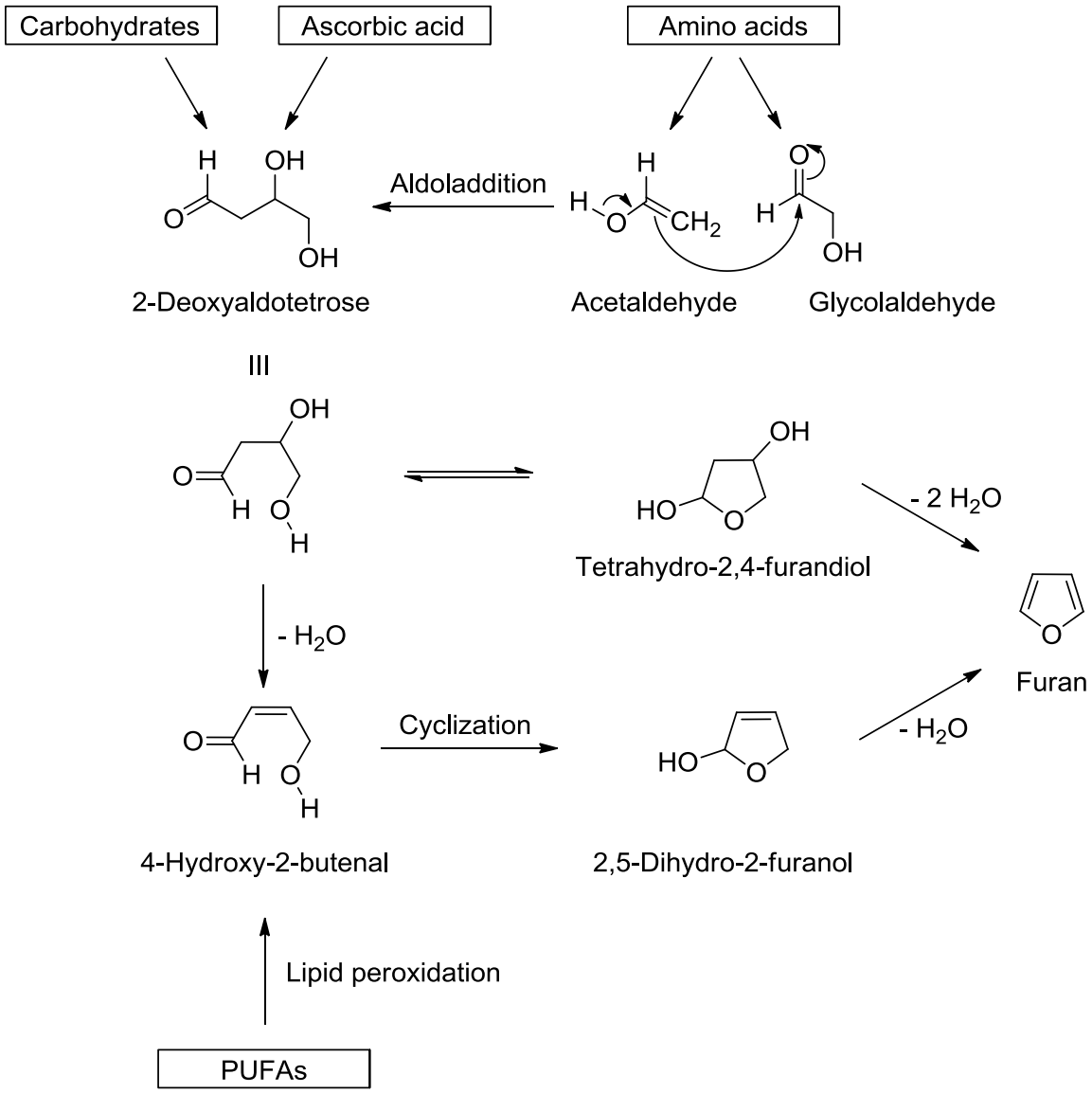

Figure 2 *Summary of potential routes of furan formation from different components present in food (modified from Perez Locas and Yaylayan 2004); PUFAs = polyunsaturated fatty acids*

Mechanisms of furan formation from polyunsaturated fatty acids

The formation of furan from polyunsaturated fatty acids (PUFAs) was suggested to start with the oxidative degradation of PUFAs to form lipid peroxides and hydroperoxides either by lipoxygenases or by reactive oxygen species. In further steps, the lipid hydroperoxides are transformed into 2-alkenals, 4-oxo-alkenals, and 4-hydroxy-2-alkenals, e.g. 4-hydroxy-2-butenal which can form furan through cyclization and dehydration (Fig. 2) (Perez Locas and Yaylayan, 2004).

Mechanism of furan formation through degradation of amino acids

The mechanism of furan formation from amino acids involves the two key molecules acetaldehyde and glycolaldehyde (Perez Locas and Yaylayan, 2004). Both aldehydes occur as important intermediates in the degradation of amino acids and are able to undergo aldol addition, thereby forming aldotetrose, which can then further react to yield furan (Fig. 2) (Perez Locas and Yaylayan, 2004).

The degradation of the amino acids serine and cysteine can generate both acetaldehyde and glycolaldehyde, whereas aspartic acid, alanine, and threonine can only yield acetaldehyde and thus need reducing sugars for the production of glycolaldehyde (Perez Locas and Yaylayan, 2004). This is consistent with findings that heating of serine or cysteine leads to small amounts of furan, whereas heating of aspartic acid, alanine, and threonine alone did not result in detectable furan formation (Perez Locas and Yaylayan, 2004). However, when glucose (a source of glycolaldehyde) was added to the single amino acids and the mixtures were heated, furan formation occurred and heating of glycolaldehyde and alanine resulted in high amounts of furan (Perez Locas and Yaylayan, 2004).

Mechanism of furan formation through degradation of carbohydrates and ascorbic acid

The formation of furan through degradation of sugars mostly involves formation of the reactive intermediates 1-deoxyosone and 3-deoxyosone, which further react to an aldotetrose derivative, such as aldotetrose itself, 2-deoxyaldotetrose, and 2-deoxy-3-ketoaldotetrose (Fig. 2). These molecules occur during degradation of hexoses, pentoses, and tetroses. Aldotetrose derivatives as intermediates are also involved in the formation of furan from the degradation of ascorbic acid and dehydroascorbic acid.

2.1.3 Furan content in food and human exposure

Furan occurs in a variety of food items (Tab. 1). By far the highest furan contents are found in ground roasted coffee and instant coffee. Moreover, maximal furan contents of more than 100 µg furan/kg food were found in baby food, soups, meat products, cereal products, sauces and fruit juices. For most food groups, the measured levels of furan vary over a wide range.

Table 1 *Furan content in food per category as reported by the EFSA (EFSA, 2009b). LOQ = limit of quantification, LOD = limit of detection*

Food group	Total number of samples	Number of samples > LOQ	Number of samples ≤ LOD	Number of samples ≤ LOQ	Range of furan content [µg furan/kg food]	Mean furan content [µg furan/kg food]
Roasted coffee (ground)	66	50	0	16	5 - 5749	1114
Instant coffee	48	41	0	7	8 - 2200	589
Baby food	985	778	59	148	0.03 - 215	25
Soups	198	158	15	25	0.7 - 225	24
Meat products	65	36	15	14	2 - 115	22
Infant formulas	35	27	3	5	2 - 56	19
Milk products	20	14	0	6	1 - 80	15
Cereal products	99	37	44	18	0.2 - 168	14
Sauces	207	10	19	88	0.1 - 120	12
Vegetables	95	28	7	60	1 - 74	12
Fruits	84	22	7	55	0.6 - 27	7
Vegetable juices	45	7	10	28	1 - 20	7
Beer	86	36	17	33	1 - 28	6
Fruit juices	203	69	32	102	0.5 - 420	6

The exposure of humans against furan was assessed using data on food consumption in Europe in connection with the furan contents determined in various food items. The estimated mean exposure of adults to furan in food ranges from 0.34 µg/kg bw/d to 1.23 µg/kg bw/d in the different states of the EU, with a median of 0.78 µg/kg bw/d (EFSA, 2009b). For infants at 3-12 months age, an estimated mean exposure between 0.27 µg/kg bw/d and 1.01 µg/kg bw/d was calculated (EFSA, 2009b). In the case of adults, coffee was identified as the main source of furan from food, while in infants exposure to furan is predominantly caused through intake of infant formulas and jarred baby food (EFSA, 2009b). Considering these estimated daily intakes, the difference between human exposure to furan and furan doses which cause carcinogenic effects in rodents after chronic administration (2 mg/kg bw) appears to be rather small (NTP, 1993). Thus, the presence of furan in food may present a potential risk to human health.

2.2 Toxicology of furan

2.2.1 Toxicokinetics of furan

Furan toxicokinetics have been studied extensively. After a single oral administration of [2,5-^{14}C]-furan to rats, more than 80 % of the radioactivity were eliminated during the first 24 hours, with 14 % exhaled as unchanged furan, 26 % exhaled as CO_2, 20 % excreted via urine and 22 % via feces (Burka et al., 1991). The formation of CO_2 presumably occurs through opening of the furan ring followed by complete oxidation of at least one of the labeled carbons (Burka et al., 1991). Measurement of the radioactivity still present in rats after 24 hours revealed that by far the highest amount was present in the liver, where it was reported to be mainly covalently bound to proteins (Burka et al., 1991). Repeated administration of [2,5-^{14}C]-furan (daily dose of 8 mg/kg bw) to rats resulted in accumulation of radioactivity in the liver, levelling off after the 4th dose (Burka et al., 1991).

Furan was found to be metabolized by cytochrome P450 (CYP) enzymes, predominantly CYP2E1, to its major metabolite *cis*-2-butene-1,4-dial (BDA, maleic dialdehyde) (Chen et al., 1995; Kedderis et al., 1993). BDA is a highly reactive electrophilic compound that can easily react with cellular nucleophiles in nucleophilic addition reactions (Michael additions and/or 1,2-additions) and is thus assumed to be the key mediator of furan toxicity and carcinogenicity (Fig. 3). This is supported by a study on furan toxicity in freshly isolated rat hepatocytes in vitro, which demonstrated that furan-mediated glutathione depletion and reduction of cell viability could be suppressed by the CYP inhibitor 1-phenylimidazole and increased by acetone pretreatment (a CYP2E1 inductor), indicating that furan cytotoxicity depends on its metabolic activation (Carfagna et al., 1993). In line with these findings, furan-induced hepatotoxic effects in vivo could be prevented by cotreatment with the irreversible CYP450 inhibitor aminobenzotriazole (Fransson-Steen et al., 1997).

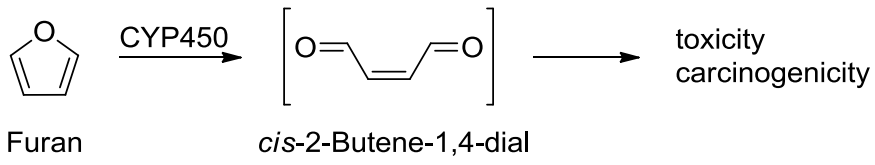

Figure 3 *Initial step in the metabolism of furan. Furan is metabolized by cytochrome P450 2E1 (CYP2E1) to its key metabolite cis-2-butene-1,4-dial (BDA). By nucleophilic addition reactions (Michael addition and/or 1,2-addition), BDA can react with cellular nucleophiles. Thus, BDA is assumed to be the key mediator of furan toxicity and carcinogenicity.*

To address the reactivity of the furan metabolite *cis*-2-butene-1,4-dial (BDA) against cellular nucleophiles and further elucidate furan metabolism, several in vitro and in vivo studies were conducted.

In vitro, BDA was shown to react with both thiol and amino groups and to cause cross-link formation between compounds containing these residues (Chen et al., 1997). Model reactions of BDA with N-acetyllysine, N-acetylcysteine, and glutathione (GSH) yielded molecules containing lactam or pyrrole structures (Fig. 4 and 5). According to the hard and soft acids and bases concept, the compounds formed after reaction of BDA with thiol groups were still reactive towards nucleophiles, such as amino groups, whereas molecules formed after reaction of BDA with amino groups did not show further reactivity towards thiol groups (Fig. 4). Consistently, *cis*-2-butene-1,4-dial was reported to react in vitro with glutathione, which contains a thiol group and a free amino group to form inter- and intramolecular cross-links, i.e. mono- and bis-glutathione conjugates (Peterson et al., 2005) (Fig. 5).

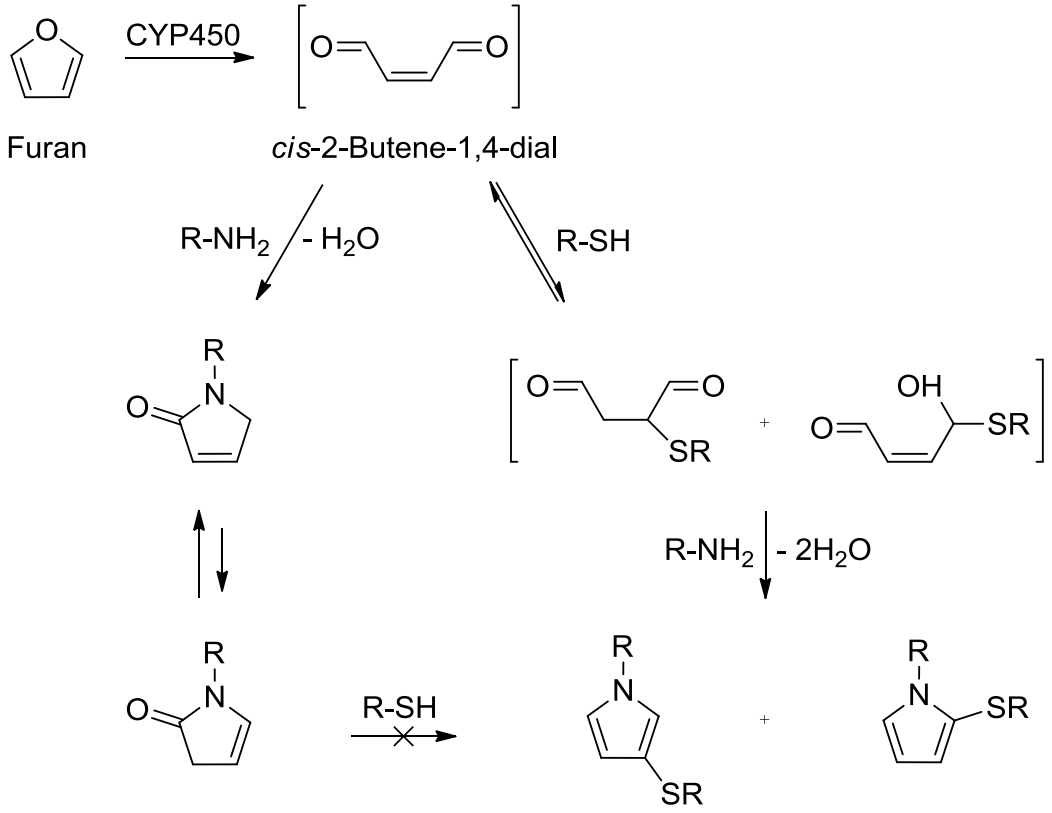

Figure 4 *Reactivity of the furan metabolite cis-2-butene-1,4-dial towards amines (R-NH_2) and/or thiols (R-SH) (modified from Chen et al. 1997). CYP2E1 = cytochrome P 450 2E1*

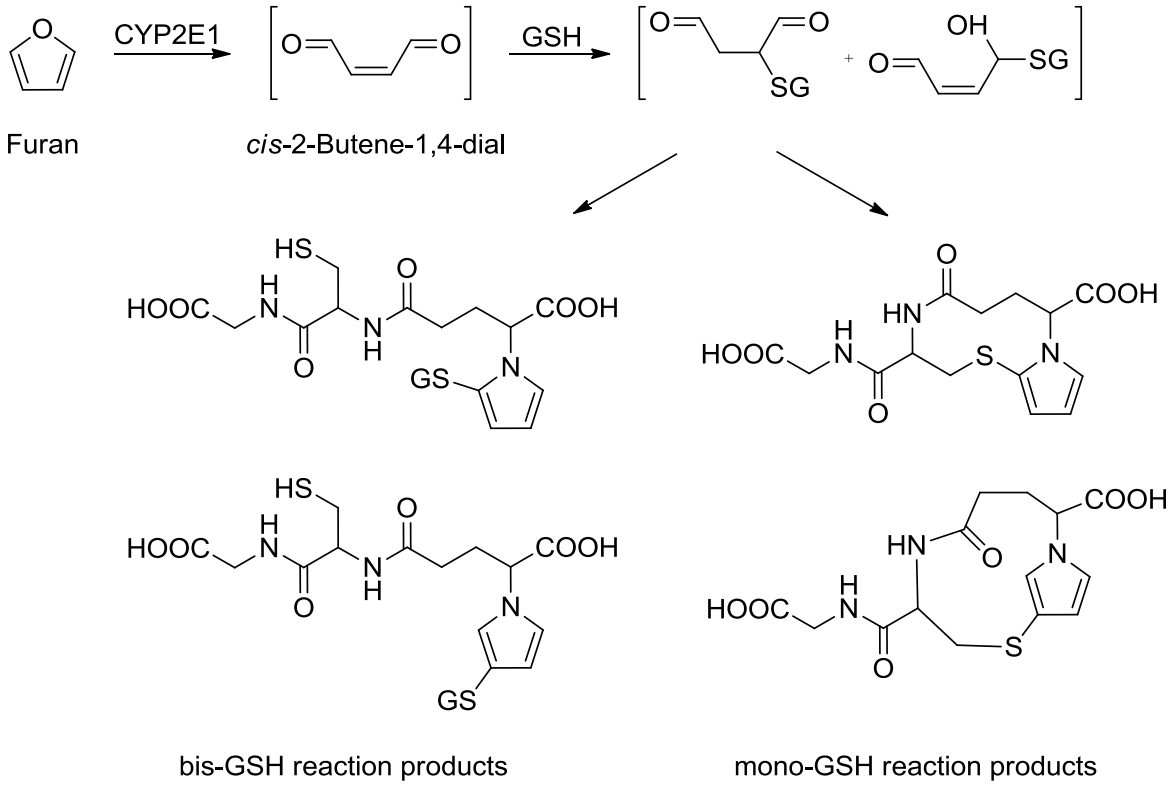

Figure 5 *Formation of mono- and bis-glutathione conjugates from cis-2-butene-1,4-dial (modified from Peterson et al. 2005). CYP2E1 = cytochrome P 450 2E1, GSH = glutathione*

In in vivo studies, the cyclic mono-glutathione conjugates but not the bis-glutathione conjugates were observed in urine of furan-treated rats (Peterson et al., 2006). This may be due to the fact that the bis-glutathione conjugates show a high molecular weight and thus are more likely to be excreted via bile than via urine. Similarly, a recent study aimed at identifying furan metabolites in bile of furan-treated rats did not show the presence of the bis-glutathione conjugates per se. However, degradation products resulting from enzymatic processing by γ-glutamyltransferase and dipeptidase (cysteinylglycine-GSH-conjugate and cysteine-GSH-conjugate) were found in bile, suggesting that the bis-glutathione conjugates are formed, but are rapidly cleaved by GSH-processing enzymes (Hamberger et al., 2010a).

Besides the mono-glutathione conjugate, further metabolites have recently been identified in urine and bile of rats treated with furan (Hamberger et al., 2010a; Kellert et al., 2008b; Lu et al., 2009). Based on these studies, it was suggested that the observed furan metabolites not only represent products derived from the reaction of BDA with glutathione and free amino acids, but also degradation products of protein adducts formed through the reaction of BDA with cysteine and/or lysine residues of proteins (Fig. 6).

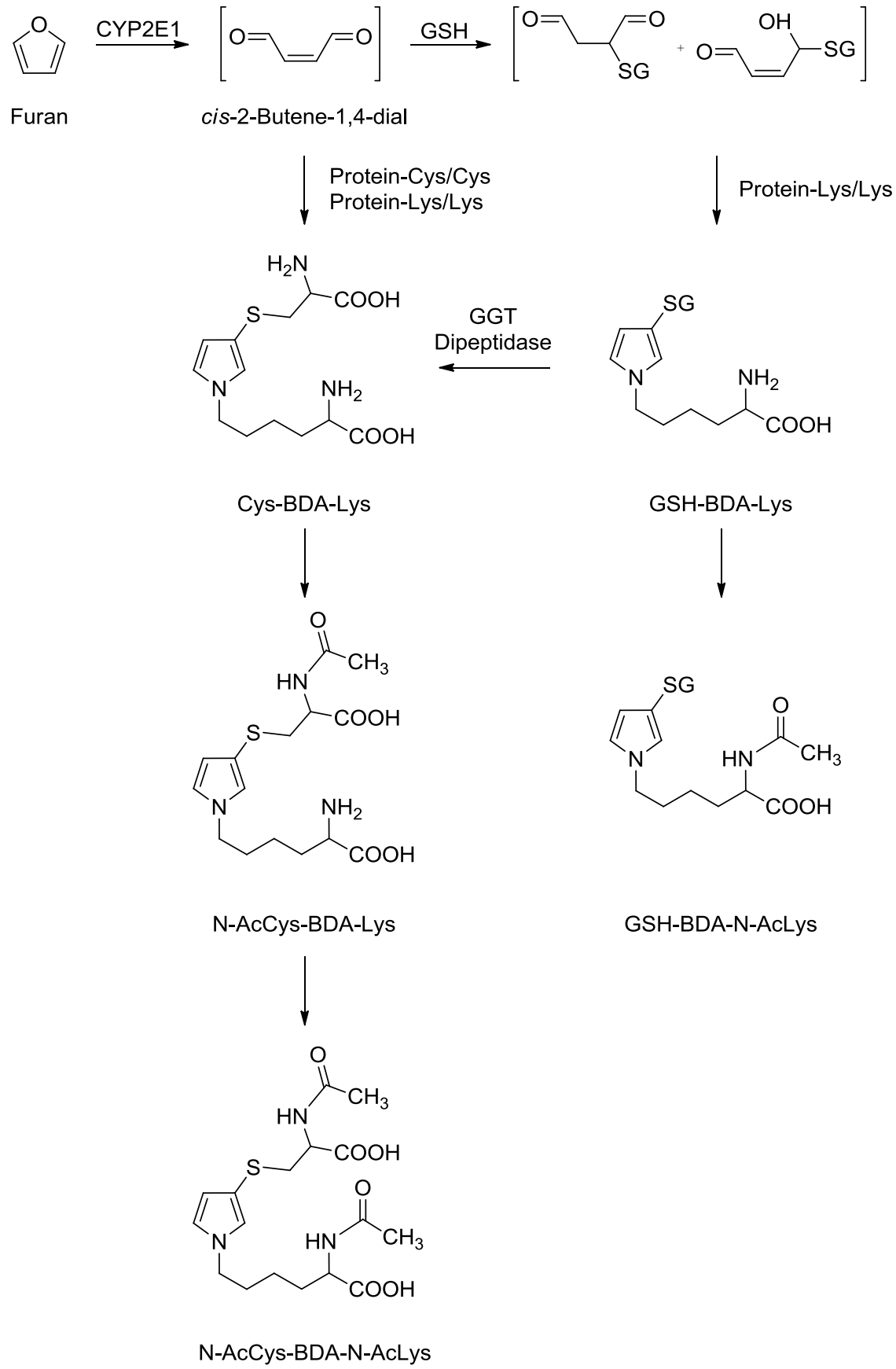

Figure 6 *Proposed metabolic pathways of furan by conjugation with cysteine (cys) and lysine (lys) either as free amino acids or protein residues (modified from Hamberger et al. 2010). CYP2E1 = cytochrome P 450 2E1, GGT = γ-glutamyltransferase, N-AcCys = N-acetylcysteine, N-AcLys = N-acetyllysine, BDA = cis-2-butene-1,4-dial, GSH = glutathione*

Besides its ability to form adducts with amino acid residues, BDA has also been demonstrated to form adducts with nucleosides in vitro (Byrns et al., 2002). Moreover, recent results from our group indicate the potential to form DNA adducts in vivo (Hamberger et al., 2010b).

Taken together, some of the metabolites identified in bile and urine of rats treated with furan appear to represent degradation products of protein adducts formed through the reactions of BDA with cysteine and lysine residues in proteins (Hamberger et al., 2010a; Kellert et al., 2008b; Lu et al., 2009), providing additional support that significant protein binding of furan reactive metabolites occurs in vivo and is likely to contribute to furan toxicity and carcinogenicity.

2.2.2 Acute and subchronic toxicity of furan

Furan was reported to cause toxic effects in several organs, but the main target organ of furan toxicity and carcinogenicity is the liver (NTP, 1993). LD_{50} values determined after intraperitoneal administration of furan were 5.2 mg/kg bw (rats) and 7.0 mg/kg bw (mice) (Egle and Gochberg, 1979). In a study conducted by Wilson et al., rats received a single furan dose (30 mg/kg bw) by gavage and were sacrificed 12 h, 24 h, 48 h, 4 days or 8 days after administration (Wilson et al., 1992). Histopathological examination of liver sections revealed that furan induced hepatocellular necrosis already at 12 h after administration, showing maximal necrotic lesions at 24 h. Moreover, inflammation and elevated liver enzyme activities in plasma were observed at the 24 h timepoint. At 48 h post-dosing, an increase in regenerative cell proliferation was found, indicative of the liver trying to replace the loss of cells. After 8 days, livers showed scarring and some residual inflammation. In another study also using doses of 30 mg/kg bw, furan administration for up to 3 months resulted in extensive hepatocellular necrosis and inflammation, followed by proliferation of hepatocytes and biliary cells and fibrosis (Hickling et al., 2010a). Furthermore, an oral 13-week study with higher furan doses (0, 4, 8, 15, 30, or 60 mg/kg bw) showed increased liver weights and hepatotoxic effects such as bile duct hyperplasia and cholangiofibrosis in rats of all dose groups (NTP, 1993). In this study, 9/10 male and 4/10 female rats treated with 60 mg/kg bw died before the end of the study.

In a further study, furan administration by gavage (4 and 40 mg/kg bw, 1-14 d) was found to induce hepatocellular degeneration, hepatic inflammation and compensatory cell

proliferation (Hamadeh et al., 2004). Moreover, furan treatment resulted in elevated plasma levels of endogenous metabolites normally excreted in bile such as cholesterol and bilirubin, suggesting that furan may interfere with hepatobiliary transport mechanisms (Hamadeh et al., 2004).

In a recent study conducted with furan doses of 0.0, 0.03, 0.12, 0.5, 2.0, and 8.0 mg/kg bw, macroscopic and histological changes were also observed after 90 days of treatment (Gill et al., 2010). In the high dose group, nodular structures were reported to be present within the caudate and left liver lobes of all animals (Gill et al., 2010). Apoptosis of hepatocytes, alterations in Kupffer cells, and inflammation occurred in the caudate lobes at doses ≥ 0.12 mg/kg bw and were also detected in the left lobe at doses of ≥ 0.5 mg/kg bw (Gill et al., 2010). At the lower doses, the subcapsular toxic effects were mild and were only observed at the visceral surface of the left lateral and caudate lobes. However, with increasing doses the lesions became more pronounced and extended deeper into the liver lobe. At the highest dose of 8 mg/kg bw, subcapsular inflammation, hyperplasia of biliary epithelial cells and cholangiofibrosis with fibrotic tissue replacing the liver parenchyma were reported (Gill et al., 2010). Supporting the abovementioned hypothesis that furan may affect hepatobiliary transport mechanisms, Gill et al. also found elevated serum levels of bilirubin and cholesterol (Gill et al., 2010).

2.2.3 Chronic toxicity and carcinogenicity of furan

Chronic toxicity and carcinogenicity of furan were investigated in a 2-year bioassay conducted by the National Toxicology Program (NTP) with furan doses of 0, 2, 4, 8 mg/kg bw (NTP, 1993). In this study, various nonneoplastic hepatic lesions were reported in F344/N rats of both sexes, including bile duct hyperplasia, cholangiofibrosis, necrosis, chronic inflammation, biliary cell proliferation, hepatocellular cytomegaly and degeneration, and nodular hyperplasia of hepatocytes (NTP, 1993).

Additionally, in animals dosed with 2 and 4 mg/kg bw furan for 9 months, toxic furan effects, i.e. nodular changes and scarring of the liver, were observed to be most pronounced at the visceral surfaces of the left lateral and caudate liver lobes facing the forestomach (Maronpot et al., 1991). In line with these findings, furan administration (8 mg/kg bw) was reported to result in hepatic lesions including necrosis, inflammation, cholangiofibrosis and slight bile duct proliferation extending from the subcapsular visceral

surface of the left and caudate liver lobes (Wilson et al., 1992). Although the reasons for these regionally specific effects remain to be established, it was suggested that furan may directly diffuse through the stomach into the subcapsular area of the liver where it can cause toxic effects (Wilson et al., 1992). Another possible explanation for the selective toxic effects may be intra- and interlobular differences in blood flow (Hamadeh et al., 2004; Metzger and Schywalsky, 1992). Furthermore, vascular lesions or formation of thrombi may constrict the blood flow in the specific areas and thus induce hypoxia and subsequent necrosis (Mally et al., 2010).

Furan administration for 2 years significantly increased the combined incidence of hepatocellular adenomas and carcinomas in male and female B6C3F1 mice and in male F344/N rats (Tab. 2). Furthermore, furan was found to cause high incidences of cholangiocarcinomas in male and female F344/N rats after 2 years of furan administration (Tab. 2). High incidences of cholangiocarcinomas were also observed in F344/N rats at the 9- or 15- months interim evaluations (NTP, 1993). Interestingly, no cholangiocarcinomas were found in mice after 2 years of furan administration.

Table 2 *Tumor incidences in F344/N rats and B6C3F1 mice in the rodent bioassay on furan conducted by the National Toxicology Program (NTP, 1993). m = male, f = female*

Rats	**Sex**	**0 mg/kg bw**	**2 mg/kg bw**	**4 mg/kg bw**	**8 mg/kg bw**
Cholangiocarcinoma	m	0/50	43/50	48/50	49/50
	f	0/50	49/50	50/50	48/50
Hepatocellular adenoma or carcinoma	m	1/50	5/50	22/50	35/50
	f	0/50	2/50	4/50	8/50

Mice	**Sex**	**0 mg/kg bw**	**8 mg/kg bw**	**15 mg/kg bw**
Hepatocellular adenoma or carcinoma	m	26/50	44/50	50/50
	f	7/50	34/50	50/50

2.2.4 Mechanisms contributing to furan carcinogenicity

Depending on their mode of action, carcinogenic compounds can be separated into two groups. Genotoxic carcinogens directly react with DNA to form covalent DNA adducts. The formation of these adducts can then lead to mutations. Multiple mutations can induce loss of function of tumor suppressors (e.g. p53) or transformation of proto-oncogenes (e.g. ras) into oncogenes, thus resulting in loss of cell growth regulation and subsequent tumor formation.

The second group of carcinogens consists of substances that act in a non-genotoxic manner, i.e. they do not show direct reactivity against DNA. Instead, non-genotoxic carcinogens can exert carcinogenic effects through disruption of tissue homeostasis leading to increased cell proliferation (Klaunig et al., 2000). Increased mitosis may result from either mitogenic mechanisms (interaction with cellular receptors, modulation of growth factors, disruption of cell growth regulation) or regenerative cell proliferation secondary to cytotoxicity. Furthermore, escape from apoptosis as a protective process to eliminate altered and potentially mutagenic cells may contribute to disruption of tissue homeostasis. An additional factor involved in non-genotoxic carcinogenesis may be the decrease of intercellular communication via gap junctions, presumably leading to inhibited growth control through neighboring cells (Klaunig et al., 2000). Moreover, increased oxidative stress in cells exposed to non-genotoxic carcinogens may participate in cancer development through oxidative damage to DNA, proteins, and lipids, leading to mutations and/or disrupted cellular functions. Oxidative stress may also result in altered gene expression through directly activating transcriptional pathways or indirectly causing hypomethylation (Klaunig et al., 2000). In addition, non-genotoxic carcinogens may elicit effects on intracellular signaling pathways, transcription factors, and DNA methylation status. Hyper- and hypomethylation of genes is associated with decreased and increased gene expression, respectively. Thus, non-genotoxic carcinogens may influence gene expression of oncogenes and tumor suppressor genes.

In the case of furan-induced carcinogenicity, it is still unclear to what extent genotoxic or non-genotoxic mechanisms contribute to tumor formation. Findings of studies addressing both genotoxic and non-genotoxic effects are briefly summarized below.

2.2.4.1 Genotoxicity of furan

Data on furan genotoxicity in vitro and in vivo are inconsistent. Furan was reported not to be mutagenic in the Ames test conducted with 4 different Salmonella typhimurium strains (NTP, 1993), but to induce chromosomal aberrations and sister chromatid exchanges (SCEs) in chinese hamster ovary (CHO) cells (NTP, 1993) and double-strand breaks in isolated rat hepatocytes (Mugford et al., 1997). No genotoxic effects were observed after treatment of L5178Y tk(+/-) mouse lymphoma cells with furan (Kellert et al., 2008a). Furthermore, chromosomal aberrations, but no SCEs were found in mouse bone marrow cells after intraperitoneal administration of furan (NTP, 1993). Unscheduled DNA synthesis (UDS) was not detected in mouse or rat hepatocytes in vivo and in vitro (Wilson et al., 1992). Furan was also negative in the micronucleus-test in mice (Durling et al., 2007). Importantly, no radioactivity was found to be associated with liver DNA after administration of [2,5-^{14}C]-furan to rats (Burka et al., 1991). However, detection of furan-derived DNA adducts in this study may have been compromised by the low specific activity (90 µCi/mmol), which may have been too low to detect DNA adducts, and the positions of the radiolabel (2 and 5) at the labile carbons, which may give rise to CO_2 (EFSA, 2004). Moreover, it is possible that DNA adducts are unstable and are cleaved by the isolation method used (EFSA, 2004). Thus, results from this study were considered inconclusive and recent data from our group suggest that furan covalently binds to DNA in vivo (Hamberger et al., 2010b).

In contrast to furan, *cis*-2-butene-1,4-dial, the reactive metabolite of furan, was shown to increase mutant frequency in L5178Y tk+/− mouse lymphoma cells and tail length in the comet assay (Kellert et al., 2008a). In these studies, however, a strong cytotoxic effect of BDA on the cells was apparent. BDA was also found to be mutagenic in the Ames test in a strain sensitive to aldehydes (TA 104) (Peterson et al., 2000) and to cause DNA single-strand breaks and cross-links in CHO cells (Marinari et al., 1984). Furthermore, BDA was found to form adducts with 2'-deoxyribonucleosides in vitro (Byrns et al., 2002). However, under BDA treatment no cross-link formation in mouse lymphoma cells was observed and BDA was not positive in the micronucleus test (Kellert et al., 2008a).

The inconsistency of the in vitro data may in part be due to the fact that furan is highly volatile and may evaporate easily from the reaction mixture, resulting in a need to

monitor the actual furan concentration in the cell medium (Wilson et al., 1992), which may not have been conducted in all studies.

Taken together, the available information on furan and BDA genotoxicity is insufficient to establish whether the mechanism of furan-induced toxicity and carcinogenicity involves direct genotoxic effects. Furthermore, it seems likely that toxic furan effects are mediated by BDA rather than by furan itself. This is in line with findings that furan toxicity requires metabolic activation to BDA (Fransson-Steen et al., 1997; Mugford et al., 1997).

2.2.4.2 Non-genotoxic mechanisms of furan toxicity and carcinogenicity

Besides studies addressing genotoxic effects of furan, results from a range of studies suggest that furan carcinogenicity may in part be mediated through non-genotoxic mechanisms. This includes protein binding followed by cytotoxicity and secondary cell proliferation, leading to tumor formation.

It is well established that protein binding of reactive intermediates may lead to cell death (Evans et al., 2004). In the case of furan, covalent binding of BDA to amino acids and glutathione was observed in vitro (Chen et al., 1997). Furthermore, Burka et al. reported that 24 hours after administration of ^{14}C-labeled furan most of the radioactivity still present in the rat was detected in the liver and that it was associated with proteins (Burka et al., 1991). This finding shows that BDA covalently binds to proteins in vivo.

Consistent with a non-genotoxic mechanism of furan-induced carcinogenicity, sustained cell proliferation without induction of DNA repair was detected in mice and rats after furan treatment, leading to the suggestion that enhanced cell proliferation may play a key role in tumor development in rodents exposed to furan (Wilson et al., 1992). In these and other experiments, subcapsular necrosis and inflammation were observed and it was concluded that cell proliferation occurred as a regenerative mechanism secondary to cell death (Wilson et al., 1992). In line with these data, a study in female mice showed that furan induced a substantial increase in the rate of apoptosis and slightly enhanced cell proliferation (Fransson-Steen et al., 1997). Thus, both forms of cell death, necrosis and apoptosis, may play a role in furan-induced toxicity and carcinogenesis. It was suggested that dose and duration of furan treatment determine which form of cell death occurs depending on factors such as cellular ATP level (Fransson-Steen et al., 1997; Richter et al., 1996). Indeed, furan was found to uncouple oxidative phosphorylation, leading to the

hypothesis that furan-induced ATP depletion and mitochondrial injury represent early events in cell death (Mugford et al., 1997).

In a rat study to elucidate the sequential events during the process of furan-induced carcinogenicity (daily furan dose of 30 mg/kg bw; several timepoints for sacrifice from 8 hours to 3 months), furan administration was shown to cause subcapsular and centrilobular necrosis and inflammation already at 24 hours after the first dose (Hickling et al., 2010a). By day 3 of the study, the centrilobular necrosis was mostly repaired through proliferation of hepatocytes and inflammation was absent in these areas. Conversely, in focal regions with more severe injury (subcapsular and portal) the damage could not be repaired by hepatocyte proliferation only and the response to injury consisted of bile duct proliferation and sustained inflammation. The biliary cells derived from the expanding bile ducts later transformed into hepatocytes to replace the necrotic tissue. Altogether, this is assumed to represent a normal response to liver injury. However, in some regions where the initial injury had been severe, biliary cells did not differentiate into hepatocytes and the biliary ducts kept extending into the parenchyma, finally leading to cholangiofibrosis. It was suggested that lack of signals supposed to terminate the repair response caused by chronic furan administration may be involved in the development of cholangiofibrosis, which may represent a precursor of cholangiocarcinomas (Hickling et al., 2010a).

Although the genotoxic potential of furan has not been conclusively elucidated yet, the findings described here indicate that non-genotoxic effects may play a significant role in the mechanisms of furan-induced toxicity and carcinogenicity.

3 ROLE OF PROTEIN BINDING AND METHODS FOR THE IDENTIFICATION OF TARGET PROTEINS

3.1 Covalent protein binding and cytotoxicity

First insights into a role of covalent protein adduct formation in toxicity and carcinogenicity were provided in the late 1940s (Miller and Miller, 1948). Based on results from their studies, Miller and Miller suggested that the carcinogenic effect of the azo dye 4-dimethylaminoazobenzene was associated with binding of its metabolite, 4-monomethylaminoazobenzene to liver proteins.

In the following decades, further research concerning the link between protein modification and toxicity has been conducted. It was observed that both acetaminophen and its regioisomer 3'-hydroxyacetanilide form similar levels of covalent protein adducts in the liver (Tirmenstein and Nelson, 1989). However, acetaminophen administration resulted in hepatotoxicity, whereas 3'-hydroxyacetanilide was not toxic. Thus, it was suggested that there may be proteins whose adduction may result in toxicity, while modification of other proteins does not lead to toxic effects (Evans et al., 2004). However, there is still little information as to which proteins might be critical for the development of cytotoxicity.

3.2 Methods for the identification of target proteins

From the beginning of the 1980s until 1998, methods used for the identification of target proteins of various chemical compounds had been very labor- and time-consuming. Thus, in this time span only 28 target proteins of chemicals were identified (Hanzlik et al., 2009).

In 1998, Qiu et al. published a newly developed method, which combined separation of proteins by two-dimensional gel electrophoresis (2D-GE) with peptide mass mapping and tandem mass spectrometry (MS/MS) sequencing to identify target proteins of reactive metabolites (Qiu et al., 1998). This method represented a milestone in the field of target protein identification. Using the new approach, Qiu et al. were able to identify more than 20 target proteins of reactive acetaminophen metabolites in a single workflow, which is about as many as had been found in total in the previous two decades. Using methods similar to the workflow developed by Qui et al., more than 320 target proteins of reactive

metabolites are known today, which can be found in the target protein database (TPDB; http://tpdb.medchem.ku.edu:8080/protein_database/).

Today, most methodological approaches are similar to the one used by Qiu et al., i.e. they apply 2D-GE (or two-dimensional liquid chromatography) to separate modified and unmodified proteins and subsequent mass spectrometry to identify the detected target proteins. Detection of the adducted proteins is usually conducted using either radiolabeling or specific antibodies.

The power of the approach using radiolabeled compounds was demonstrated by Koen et al. (2007). In their studies, rats received ^{14}C-labeled bromobenzene (specific activity 5.17 Ci/mol, 2 mmol/kg bw, intraperitoneal) and proteins were isolated from liver. After subcellular fractionation, liquid scintillation counting revealed the amount of radioactivity covalently bound to liver cytosolic proteins (3900 pmol equiv ^{14}C-bromobenzene/mg protein). Following separation by 2D-GE, proteins were transferred to a membrane by electroblotting and radioactive spots were detected by phosphorimaging. Protein identification was conducted using matrix-assisted laser desorption/ionization time-of-flight (MALDI-TOF) mass spectrometry and MS/MS and database search, resulting in the identification of 33 target proteins of bromobenzene. Methods using radiolabeled compounds have been widely applied for the detection of adducted proteins due to their high sensitivity and simplicity. However, disadvantages of this approach are special safety issues, which have to be regarded when using radioactive material. Moreover, it may be difficult and expensive to obtain the radiolabeled material needed for the study since many radiolabeled compounds show a limited availability and have to be specifically synthesized.

In contrast to the use of radiolabeled compounds, Druckova et al. (2007) detected adducted proteins on a Western blot using a specific antibody against teucrin A, a hepatotoxic furan-containing compound found in the herb germander. Teucrin A is bioactivated to an 1,4-enedial derivative structurally similar to *cis*-2-butene-1,4-dial and was found to react with both lysine and cysteine residues of proteins (Druckova and Marnett, 2006). Moreover, the teucrin-A specific antibody was also used for immunoprecipitation to enrich modified proteins from rat liver homogenates. After enrichment, the proteins were digested and analyzed by liquid chromatography-MS/MS (LC-MS/MS). In this study, 46 target proteins of the furan derivative teucrin A were

identified. Antibody-based methods are easier to handle compared to radioactive material. However, problems may occur if no specific antibody against the metabolite-protein adduct is commercially available. In this case, a specific antiserum has to be manufactured, which needs the use of laboratory animals and may be very expensive.

4 AIMS OF THIS WORK

Furan, a potent hepatotoxin and liver carcinogen in rodents, was reported to be present in a variety of food items that undergo heat treatment (Crews and Castle, 2007; NTP, 1993). The toxic and carcinogenic effects of furan were found to depend on the formation of its reactive metabolite *cis*-2-butene-1,4-dial (BDA) (Fransson-Steen et al., 1997). However, the mechanisms of furan-induced tumor formation are still poorly understood and both genotoxic and non-genotoxic mechanisms have been proposed.

Despite possible genotoxic effects of furan (Byrns et al., 2002; Hamberger et al., 2010b), results from several studies indicate that furan covalently binds to proteins in vitro and in vivo (Burka et al., 1991; Chen et al., 1997; Hamberger et al., 2010a; Lu et al., 2009). Since it is well established that protein binding of reactive intermediates may lead to cell death (Evans et al., 2004), it has been suggested that inactivation of protein function through covalent binding of reactive furan metabolites and subsequent cell death leading to regenerative cell proliferation may present key events in furan-induced carcinogenicity. However, it has long been recognized that adduction of some proteins may be critical to injury, whereas covalent binding to others is not (Zhou et al., 2005). For a comprehensive understanding of the molecular events involved in furan toxicity, identification of target proteins of reactive furan intermediates, which may play a causal role in the pathogenesis of furan-associated liver toxicity, and characterization of the cellular and functional consequences of protein adduct formation are needed.

Therefore, the major aims of this work were to identify target proteins of furan reactive intermediates in rat liver by employing state-of-the-art proteomics methods involving administration of ^{14}C-labeled furan to rats, separation of unmodified and furan-adducted proteins present in liver by two-dimensional gel electrophoresis, detection of protein spots containing radiolabel by fluorography, and identification of proteins by modern mass spectrometry techniques (Chapter 6) and to discuss the potential relationship between loss of target protein function and furan toxicity (Chapter 8).

To determine the cellular and functional consequences associated with protein damage, a further aim of this work was to characterize the effects of subacute furan administration to rats at a known carcinogenic dose and at doses closer to estimated human exposure (Chapter 7). In this regard, we also want to establish if the administration of furan at either a known carcinogenic dose or at a clearly hepatotoxic dose results in activation of

the unfolded protein response (UPR). The UPR is a cellular pathway, which is activated upon stress in the endoplasmic reticulum (ER) caused by accumulation of unfolded or misfolded proteins and which serves to increase the cells capacity to recognize misfolded proteins and target them for degradation by the proteasome.

5 MATERIALS

5.1 Equipment

A list containing information on the equipment used for this work is provided in Tab. 3.

Table 3 *Equipment used for this work*

Equipment	Provider
Autoradiography cassette	Hartenstein, Würzburg, Germany
DC Power Supply PS 3000	Hoefer, Holliston, MA, USA
Electrode strips	GE Healthcare, München, Germany
Electrophoresis Power Supply EPS 3500	GE Healthcare, München, Germany
E-Pure Water Purification Systems, Barnstead	Thermo Fisher Scientific, Dreieich, Germany
Eppendorf Centrifuge 5403	Eppendorf, Hamburg, Germany
Eppendorf Concentrator	Eppendorf, Histon, UK
ExcelGel 2-D Homogeneous 12.5	GE Healthcare, München, Germany
ExcelGel SDS Buffer Strips	GE Healthcare, München, Germany
FluorChemQ imaging system	Cell Biosciences, Santa Clara, CA, USA
Rotanta/RP	Hettich, Tuttingen, Germany
Glass capillary (100 x 1.5 mm)	Hartenstein, Würzburg, Germany
Glassware	Schott, Mainz, Germany
Capillary liquid chromatography system CapLC including autosampler	Waters, Elstree, UK
HP ScanJet 5550C Flatbed Scanner	Hewlett-Packard, Germany
Hyperfilm MP	GE Healthcare, München, Germany
Immobiline DryStrip Kit	GE Healthcare, München, Germany
Immobiline DryStrip pH 3-11 NL (non-linear), 18 cm	GE Healthcare, München, Germany
Immobiline DryStrip pH 4-7, 18 cm	GE Healthcare, München, Germany
Immobiline DryStrip pH 6-9, 18 cm	GE Healthcare, München, Germany
Immobiline DryStrip Reswelling Tray	GE Healthcare, München, Germany
Integrafrit column (10 cm/ 75 µm C8)	New Objective, Woburn, MA, USA
Kodak X-OMAT 1000 Processor	Kodak, Stuttgart, Germany
LTQ FT Ultra mass spectrometer	Thermo Fisher Scientific, Dreieich, Germany
Makrolon® type-4 cages	Bayer Makrolon, Leverkusen, Germany
Megafuge 1.0R	Heraeus, Hanau, Germany
Mettler Toledo AG 245	Mettler-Toledo, Giessen, Germany
Micro AS autosampler	Thermo Fisher Scientific, Dreieich, Germany
Microspin FV-2400 mini-centrifuge	Biosan, Riga, Latvia
Multiphor II Electrophoresis System	GE Healthcare, München, Germany
MultiTemp cooling unit	GE Healthcare, München, Germany
Nanodrop 2000C	Thermo Fisher Scientific, Dreieich, Germany
Owl Separation Systems Model B1	Thermo Fisher Scientific, Dreieich, Germany
Pelleted standard rat maintenance diet	SSNIFF Spezialdiäten GmbH, Soest, Germany

Polypropylene reaction tubes (0.5 ml, 1.5 ml, 2.0 ml)	Sarstedt, Nümbrecht, Germany
Polystyrene cuvettes (10 x 4 x 45 mm)	Sarstedt, Nümbrecht, Germany
PTC-200™ Programmable Thermal Controller	MJ Research, Waltham, USA
Qiagen BioRobot 3000	Qiagen, Hilden, Germany
Q-TOF Ultima Global mass spectrometer	Waters, Elstree, UK
LC Packings column (15 cm/75 µm C18, 3 µm, 100 Å)	Dionex-LC Packings, Amsterdam, The Netherlands
LightCycler 480	Roche, Mannheim, Germany
Rotho Clear Box	Rotho, Görwihl, Germany
Sample application pieces, large (0.5 x 2.5 cm)	GE Healthcare, München, Germany
Sample application pieces, small (0.5 x 1 cm)	GE Healthcare, München, Germany
Sample cups	GE Healthcare, München, Germany
Sample cup bar	GE Healthcare, München, Germany
Saran foil	Dow, Schwalbach/Ts, Germany
Sero-Wel 96 Well Plates, V-well, I/W sterile, Sterilin	Appleton Woods, Birmingham, UK
Shaker L-40	Hartenstein, Würzburg, Germany
Sigma 4-15C	Qiagen, Hilden, Germany
Surveyor MS pump	Thermo Fisher Scientific, Dreieich, Germany
Tri-Carb 2900 TR Liquid Scintillation Analyzer	PerkinElmer, Rodgau, Germany
TriVersa NanoMate (ESI) source	Advion BioSciences, Ithaca, NY, USA
Polypropylene tubes (15 ml, 50 ml)	Sarstedt, Nümbrecht, Germany
Ultrospec 2000	Pharmacia Biotech, Cambridge, UK
Vortex Duo Press_To_Mix 525	Labinco, Giessen, Germany

5.2 Chemicals and reagents

Tab. 4 shows the chemicals and reagents used for this work.

Table 4 *Chemicals and reagents used for this work*

Chemical/Reagent	Provider
Acetone	AppliChem, Darmstadt, Germany
Acetonitrile	Sigma-Aldrich, Taufkirchen, Germany
Agarose (Biozym LE Agarose)	Biozym, Hessisch Oldendorf, Germany
Amersham Amplify™ Fluorographic Reagent	GE Healthcare, München, Germany
Ammonium bicarbonate (NH_4HCO_3)	Thermo Fisher Scientific, Dreieich, Germany
Bromophenol blue	Carl Roth, Karlsruhe, Germany
3-[(3-Cholamidopropyl)dimethylammonio]-1-propanesulfonate (CHAPS)	AppliChem, Darmstadt, Germany
Corn oil	Sigma-Aldrich, Taufkirchen, Germany
Deionized water	see E-Pure Water Purification Systems
DEPC-H_2O (DNase free, RNase free, sterile)	Carl Roth, Karlsruhe, Germany
1,4-Dithiothreitol (DTT)	Carl Roth, Karlsruhe, Germany

Dry Strip Cover Fluid	GE Healthcare, München, Germany
Ethylenediaminetetraacetic acid (EDTA)	Sigma-Aldrich, Taufkirchen, Germany
Ethanol	Carl Roth, Karlsruhe, Germany
Ethidium bromide solution for fluorescence	Sigma-Aldrich, Taufkirchen, Germany
Formic acid	Sigma-Aldrich, Gillingham, UK
[3,4-^{14}C]-Furan	Tjaden Biosciences, Burlington IA,USA
Furan (Cat. 18,592-2)	Sigma-Aldrich, Taufkirchen, Germany
Gel loading dye	New England Biolabs, Frankfurt, Germany
Glacial acetic acid	Carl Roth, Karlsruhe, Germany
[Glu^{1}]-Fibrinopeptide B, human	Sigma-Aldrich, Taufkirchen, Germany
Glycerol 86 %	Carl Roth, Karlsruhe, Germany
Hydrochloric acid (HCl) 25 %	Carl Roth, Karlsruhe, Germany
Water, HPLC Grade	J.T. Baker, Philipsburg, NJ, USA
Iodoacetamide (IAA)	GE Healthcare, München, Germany
IPG Buffer pH 3-11 non-linear (NL)	GE Healthcare, München, Germany
IPG Buffer pH 4-7	GE Healthcare, München, Germany
IPG Buffer pH 6-11	GE Healthcare, München, Germany
Isopropanol	Sigma-Aldrich, Taufkirchen, Germany
MassPREP™ Digestion Standard Enolase	Waters, Elstree, UK
Methanol	Carl Roth, Karlsruhe, Germany
Potassium chloride (KCl)	Merck, Darmstadt, Germany
Potassium dihydrogen phosphate (KH_2PO_4)	Ferak, Berlin, Germany
Primers for XBP1 and GAPDH, reverse and forward	Biomers, Ulm, Germany
Protease Inhibitor Cocktail	Carl Roth, Karlsruhe, Germany
peqGOLD Orange 50 bp ladder	PEQLAB, Erlangen, Germany
peqGOLD Prestained Protein-Marker IV	PEQLAB, Erlangen, Germany
RotiBlue	Carl Roth, Karlsruhe, Germany
Rotiszint 22	Carl Roth, Karlsruhe, Germany
Sodium dodecyl sulfate (SDS) Pellets	Carl Roth, Karlsruhe, Germany
Sodium chloride (NaCl)	Carl Roth, Karlsruhe, Germany
Sodium hydrogen phosphate dihydrate ($Na_2HPO4 * 2H_2O$)	Merck, Darmstadt, Germany
TaqMan® Gene Expression Master Mix	Applied Biosystems, Darmstadt, Germany
Tissue-Tek® O.C.T™ Compound	Sakura Finetek, Staufen, Germany
Thermo-Start PCR Master Mix (2x)	Thermo Fisher Scientific, Dreieich, Germany
Thiourea	AppliChem, Darmstadt, Germany
Trichloroacetic acid (TCA)	Sigma-Aldrich, Taufkirchen, Germany
Tris(hydroxymethyl)aminomethane (Tris) base	Carl Roth, Karlsruhe, Germany
Tris(hydroxymethyl)aminomethane (Tris) HCl	AppliChem, Darmstadt, Germany
Trypsin Gold, Mass Spectrometry Grade	Promega, Southampton, UK
Urea	Carl Roth, Karlsruhe, Germany

5.3 Kits

Names and providers of the kits used for this work are listed in Tab. 5.

Table 5 *Kits used for this work*

Product	Provider
2-D Quant Kit	GE Healthcare, München, Germany
FractionPREP™ Cell Fractionation Kit	Biocat, Heidelberg, Germany
RNase-Free DNase Set	Qiagen, Hilden, Germany
RNeasy® Mini Kit	Qiagen, Hilden, Germany
Silver staining Kit	GE Healthcare, München, Germany
TaqMan® Gene Expression Assays	Applied Biosystems, Darmstadt, Germany
Verso™ cDNA Kit	Thermo Fisher Scientific, Dreieich, Germany

5.4 Software

Names and providers of the software tools used for this work are listed in Tab. 6.

Table 6 *Software used for this work*

Product	Provider
DAVID 6.7	National Institute of Allergy and Infectious Diseases, Bethesda, Maryland, USA
LightCycler®480 SW 1.5	Roche, Mannheim, Germany
Mascot	Matrix Science, London, UK
Masslynx 4.0	Waters, Elstree, UK
Qiasoft4	Qiagen, Crawley, UK
REDFIN 3, 2D gel image analysis software	Ludesi, Malmö, Sweden
Xcalibur 2.0.7	Thermo Fisher Scientific, Dreieich, Germany

6 IDENTIFICATION OF FURAN TARGET PROTEINS BY PROTEIN MASS SPECTROMETRY

6.1 Introduction

Furan is known to be a potent hepatotoxin and liver carcinogen in rodents. In a 2-year bioassay, chronic furan administration to rats caused hepatocellular adenomas and carcinomas as well as cholangiocarcinomas (NTP, 1993). To date, the mechanisms of furan-induced toxicity and carcinogenicity are still unknown. However, there are findings indicative of involvement of a non-genotoxic mechanism including protein adduct formation, cell death and regenerative cell proliferation (Burka et al., 1991; Lu et al., 2009; Wilson et al., 1992). Covalent binding of furan reactive metabolites to cellular proteins may result in loss of their functions and subsequent cell death. Thus, it is important to identify the target proteins of furan reactive metabolites in order to better understand a possible role in the cellular events leading to cell death.

A common approach addressing this issue includes the administration of a radiolabeled compound to animals and subsequent protein extraction from target and non-target tissues. The obtained protein extracts are then measured by liquid scintillation counting to determine the extent of protein adduct formation, i.e. the amount of compound covalently bound to proteins. Moreover, for identification of target proteins, adducted and unmodified proteins are separated by two-dimensional gel electrophoresis (2D-GE), radiolabeled protein spots in the gel are detected by fluorography, and proteins contained in selected spots were cleaved into peptides by in-gel digestion (Fig. 7). The resulting peptides are then used for identification of modified proteins by mass spectrometry and protein sequence database search.

In our study, male rats received [3,4-^{14}C]-furan at a single dose of 2 mg/kg bw (known carcinogenic dose) or 0.1 mg/kg bw (dose closer to estimated human exposure) and were sacrificed 2h after administration. Protein extracts were used to determine the extent of protein adducts formation in liver (target) and kidney (non-target) tissue and to identify furan target proteins in rat liver.

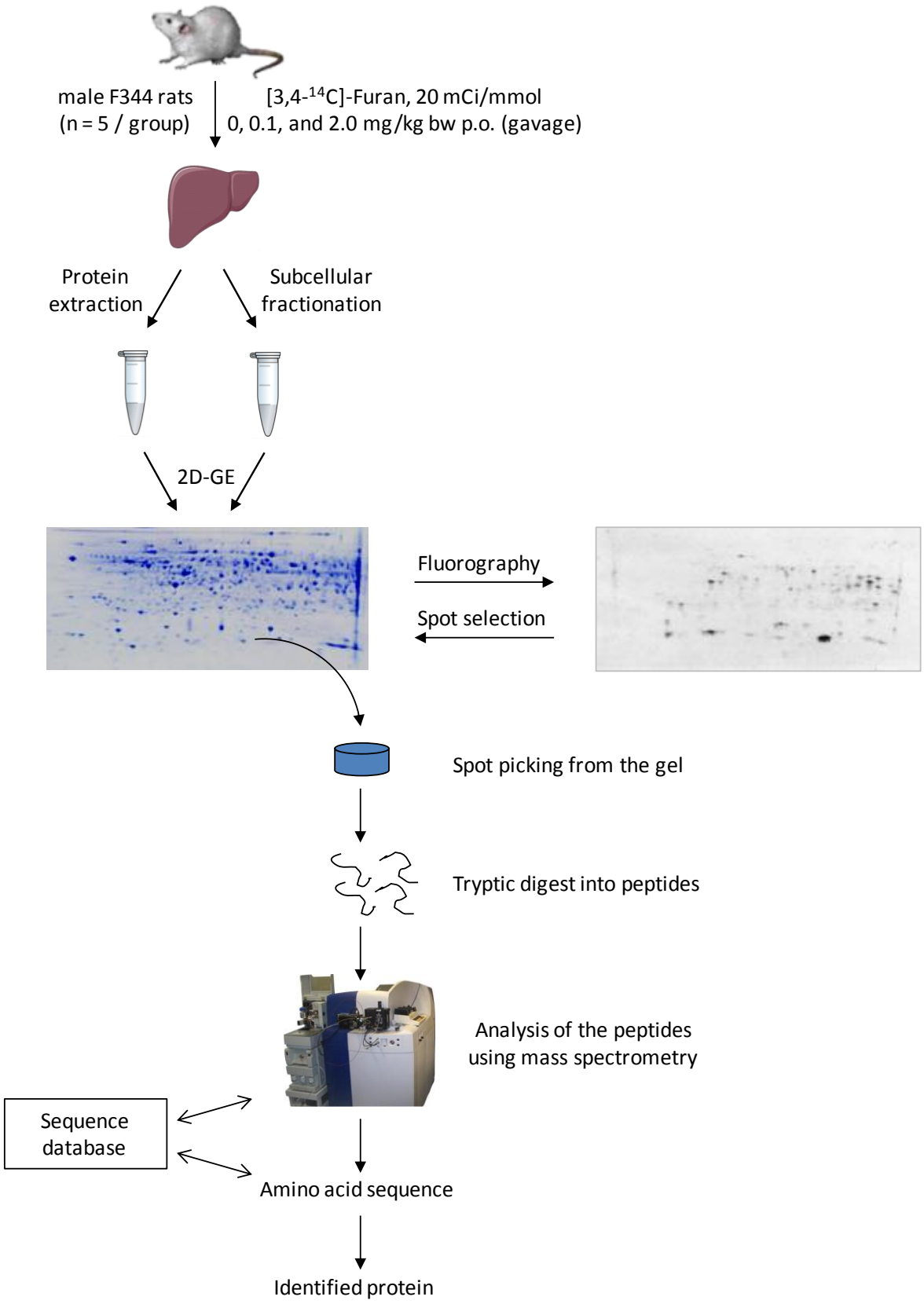

Figure 7 *Study design and methodological approach to identify furan target proteins in liver of rats treated with [3,4-^{14}C]-furan. 2D-GE = two-dimensional gel electrophoresis*

In addition to the quantification of covalent binding to proteins and the identification of the target proteins, the use of radiolabeled compounds also enables to visualize the distribution of a compound in a tissue. Thus, it is possible to establish whether there are locally different concentrations of furan in the different liver lobes and in various areas of the single lobes. This is of interest, because the left and the caudate lobes represent the main target lobes of furan toxicity and the subcapsular region is most susceptible to toxic effects (Gill et al., 2010; Maronpot et al., 1991; Wilson et al., 1992). Since the liver lobe areas most affected by furan toxicity are located close to the stomach, it has been suggested that diffusion of furan from the stomach, resulting in higher exposure against furan, might be involved in the different responses of liver lobes after furan administration (Hamadeh et al., 2004; Wilson et al., 1992). Moreover, it has been suggested that blood flow was limited in the more susceptible areas and that resulting hypoxia may lead to necrosis (Mally et al., 2010).

To investigate if furan is evenly distributed or if there are areas of higher furan concentrations in the liver after oral administration, rats received a single dose of [3,4-^{14}C]-furan and liver slices were examined using autoradiography.

6.2 Methods

6.2.1 Housing and treatment of animals

15 Male Fischer F344/N rats (200-250g on arrival, Harlan-Winkelmann GmbH, Borchen, Germany) were housed under standard laboratory conditions (climate cabinets, temperature 22 ± 2 °C, relative humidity 30-70 %, 12-15 air changes per hour, 12 hour light/dark cycle) in groups of 5 in Makrolon® type-4 cages with wire meshtops and standard softwood bedding. Rats received pelleted standard rat maintenance diet and tap-water ad libitum. After acclimatization, animals received [3,4-^{14}C]-furan (specific activity 20 mCi/mmol) in corn oil (4 ml/kg bw) by gavage at single doses of 0.0 mg/kg bw, 0.1 mg/kg bw and 2.0 mg/kg bw. The doses were chosen, because 2.0 mg/kg bw was the lowest dose tested in a 2-year bioassay known to cause carcinogenic effects (NTP, 1993) and 0.1 mg/kg bw represents a dose closer to the estimated human exposure (EFSA, 2004). Rats were sacrificed 2 h after administration by cardiac puncture under CO_2 anesthesia and livers were removed, separated into their lobes, flash frozen in liquid nitrogen, and stored at - 80 °C for further analyses. The time point of 2 h after

administration was chosen to allow distribution and bioactivation of furan based on the rapid excretion of furan metabolites with bile (Hamberger et al., 2010a), whilst avoiding metabolic incorporation of ^{14}C.

6.2.2 Extraction of proteins from liver and kidney tissue for determination of covalent protein binding and identification of furan target proteins

- **Extraction solution:** 7M urea, 2M thiourea, 4 % CHAPS, 2 % IPG Buffer pH 3-11 non-linear (NL), 65mM DTT, 1 tablet protease inhibitor cocktail
- **TCA (Trichloroacetic acid) solution**: 10 % TCA in acetone containing 20 mM DTT
- **Washing solution**: acetone containing 20 mM DTT
- **Sample solution:** 7M urea, 2M thiourea, 4 % CHAPS, 2 % IPG Buffer pH 3-11 NL, and 40 mM DTT

The extraction solution contained urea and thiourea to denature and thus solubilize and unfold the proteins in the solution, thereby exposing the amino acid residues for ionization. This results in better resolution in the first dimension where proteins are separated according to their isoelectric point. 3-[(3-Cholamidopropyl)dimethylammonio]-1-propanesulfonate (CHAPS), a zwitterionic detergent, was included to enhance solubilization and to avoid aggregation of the proteins. An immobiline pH gradient (IPG) buffer containing a mixture of carrier ampholytes (not specified by the manufacturer GE Healthcare) was added to the solution to improve protein solubility by decreasing protein aggregation through charge-charge interactions and to produce a more homogeneous conductivity across the pH gradient during the first dimension. Dithiothreitol (DTT) acts as a reducing agent in the extraction solution, breaking disulfide bonds and keeping the proteins in their completely unfolded and reduced form. DTT was added to the solution shortly before use. The protease inhibitor cocktail was added to the solution to prevent protease-mediated protein degradation during the homogenizing process.

All centrifugation steps for the protein extraction were conducted at 4 °C using the Megafuge 1.0R and the samples were kept on ice during the process. Frozen tissue (200 mg) from the left liver lobe or right kidney were homogenized in 2.5 ml extraction solution and the homogenate was centrifuged for 30 min at 1000 x g. The supernatant was transferred to a fresh tube and the proteins were precipitated with 2.5 ml TCA solution over night at -20 °C. The next day, the samples were centrifuged for 30 min at

4000 x g and the supernatant was discarded. The obtained pellet was washed 9 times with 2.5 ml acetone containing 20 mM DTT (15 min, 4000 x g) to remove non-covalently bound radioactivity. Subsequent liquid scintillation counting (Tri-Carb 2900 TR Liquid Scintillation Analyzer) of the homogenate and the supernatants obtained during the washing procedure showed a decreasing content of radioactivity until background levels were achieved after the final washing step (Fig. 8). The washed protein pellet was dissolved in 2 ml sample solution. However, if the pellet did not dissolve completely, the solution was centrifuged again, the supernatant was transferred to a fresh tube, and the pellet was discarded. The protein extract was aliquoted and stored at -80 °C.

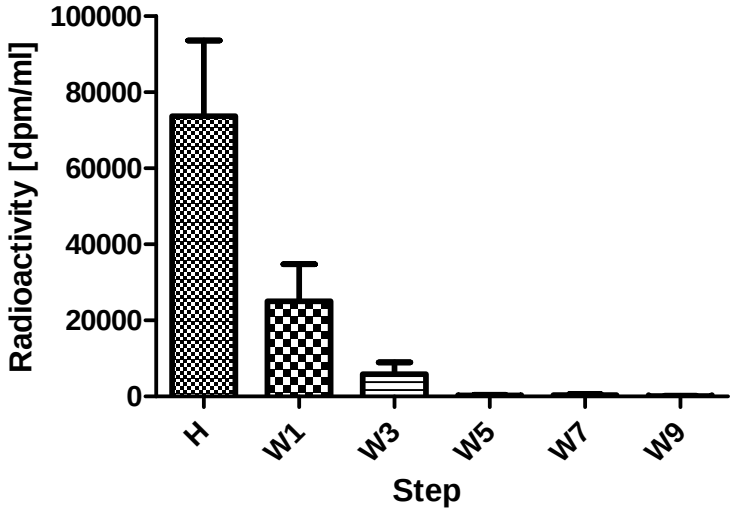

Figure 8 *Radioactivity [dpm/ml] present in the homogenate (H) and after the washing steps (W1-9). Radioactivity was determined by liquid scintillation counting of proteins extracted from livers of high dose animals (n=5). Values are expressed as mean +SD. Radioactivity decreased during the washing procedure until background levels were achieved. dpm = disintegrations per minute*

6.2.3 Protein quantification

Since high concentrations of denaturating agents, detergents and reductants in the sample solution are known to interfere with standard protein quantification methods such as the Bradford assay, protein solutions were quantified using the 2D Quant Kit (GE Healthcare). In brief, this protein quantification is conducted by quantitatively precipitating the proteins, while the interfering substances stay in the supernatant. After centrifugation, the supernatant is removed and the pellet is resolved in an alkaline solution containing cupric ions, which bind to the protein backbone. The unbound rest of the cupric ions reacts with a colorimetric agent (not further specified by the manufacturer) that is added to the solution. Thus, the color density inversely correlates

with the amount of protein in the sample. The protein concentration in the sample can be calculated using a BSA (bovine serum albumin) standard curve (Fig. 9).

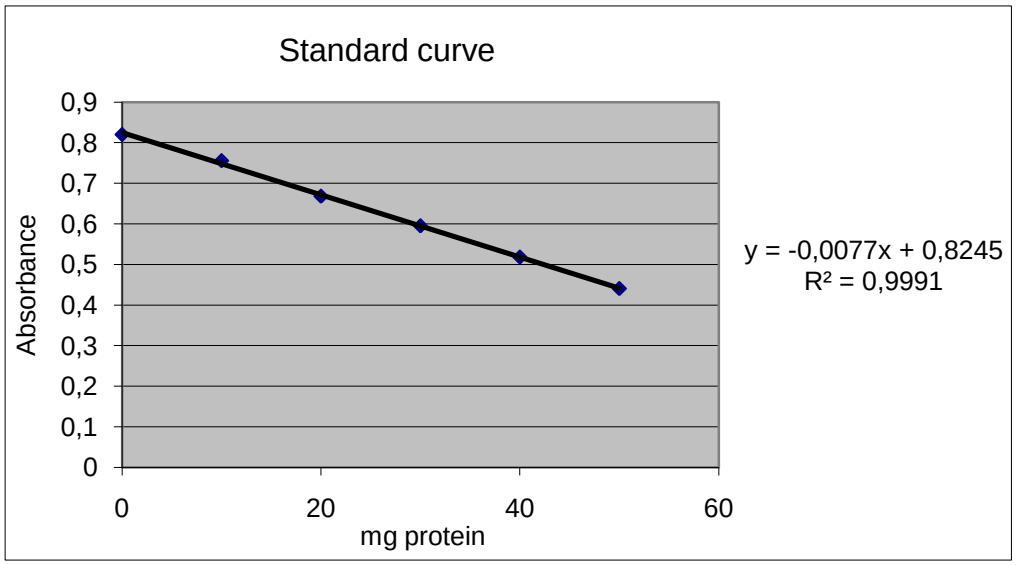

Figure 9 *Representative standard curve for protein quantification using the 2D Quant Kit. The higher the amount of protein present in the sample, the lower is the absorbance.*

- **2D Quant Kit** containing the following solutions:
  - Bovine serum albumin (BSA) standard solution (2 µg/µl)
  - Precipitant
  - Co-Precipitant
  - Copper solution
  - Working color reagent A
  - Working color reagent B

The composition of the solutions contained in the 2D Quant Kit is not further specified by the manufacturer (GE Healthcare). All steps of the protein quantification were carried out at room temperature. In the first step, the working color reagent was prepared (100 parts of reagent A + 1 part color reagent B), from which 1 ml per sample was needed. Then, the standard curve (0, 10, 20, 30, 40, 50 µg BSA) and the protein extracts (5 µl) were pipetted into tubes. 500 µl precipitant were added to each tube, the samples were shortly vortexed, incubated for 2 min at room temperature, and 500 µl co-precipitant was added. After shortly vortexing, the samples were centrifuged at 15.000 rpm for 10 min (Eppendorf Centrifuge 5403) and the supernatants were removed and discarded. The samples were briefly centrifuged again with a mini-centrifuge (Microspin FV-2400) and the remaining liquid was removed and discarded. 100 µl copper solution and 400 µl

deionized water were added to the pellet and the sample was vortexed until the pellet dissolved completely. 1 ml working color reagent was added and the samples were mixed immediately by inverting them several times. The samples were incubated for 20 min at room temperature and the absorbance at 480 nm was measured using the UV/Vis spectrophotometer Ultrospec 2000 and deionized water as blank reference. The protein concentrations were calculated using a standard curve.

6.2.4 Liquid scintillation counting of protein extracts

In our study, furan labeled with ^{14}C was used. ^{14}C is a radioactive isotope of carbon whose nucleus contains 6 protons and 8 neutrons. Through transformation of a neutron to a proton and an electron in the nucleus, ^{14}C decays to ^{14}N with a radioactive half life of 5730 years, thereby emitting β^- radiation.

To conduct liquid scintillation counting (LSC), a scintillation fluid was added to the sample. In our studies, we used Rotiszint 22, a liquid scintillator based on toluene and Triton X-100. In general, the essential components of a scintillation fluid are a solvent such as toluene and a scintillator, e.g. 2,5-diphenyloxazole. The solvent collects the energy emitted by ^{14}C and transfers it to the scintillator molecules, which convert the absorbed energy into light, thereby emitting photons with a characteristic wavelength. The resulting signal is detected by a photomultiplier and displayed as disintegrations per minute (dpm).

150 µl of the obtained protein extract were used for liquid scintillation counting. Rotiszint 22 (10 ml) was added to the sample and the sample was vortexed. LSC was conducted in a Tri-Carb 2900 TR Liquid Scintillation Analyzer with a counting time of 10 min per sample. Using the data obtained by protein quantification, the dpm values were then converted into pmol furan equivalent/mg protein (furan equiv/mg protein).

Example:

Samples measured using LSC (mean): 15903 dpm = 265 Bq = 7164 pCi

Protein content in the samples (mean): 1254 µg protein

→ 5.7 pCi/µg protein

Specific activity of furan (20 pCi/pmol) → 5.7 pCi ≡ 0.286 pmol → 286 pmol/mg protein

6.2.5 Subcellular fractionation of the liver proteome

Since furan treatment was shown to result in elevated plasma levels of endogenous metabolites normally excreted in bile such as cholesterol and bilirubin (Hamadeh et al., 2004), it has been suggested that furan may interfere with hepatobiliary transport mechanisms (2.2.2). Furthermore, it has been hypothesized that the underlying mechanism of this interference may include covalent binding of furan reactive metabolites to transport proteins located in the cell membranes of hepatocytes, which may then result in impaired transport function of these proteins. To obtain a fraction enriched with membrane proteins for improved detection of adducted membrane proteins, subcellular fractionation of the liver proteome was conducted.

The FractionPREP^{TM} Cell Fractionation Kit (Biocat) was used to obtain four subcellular protein fractions (cytosolic, nuclear, membrane/particulate, and cytoskeletal fraction) from each sample. This fractionation kit works on a principle similar to the differential detergent fractionation (Ramsby et al., 1994). In the method described by Ramsby et al. (Ramsby et al., 1994), the buffer for the first step contains the nonionic detergent digitonin. Low digitonin concentrations (0.01-0.05 %) cause cell permeabilization and release of cytosolic proteins, thereby not disrupting membranes of organelles such as endoplasmic reticulum (ER) or mitochondrion. In the second step, a buffer including the nonionic detergent Triton X-100 is used. When using isomolar and isotonic buffer conditions and low concentrations of Triton (0.5 %), membrane and organellar proteins are efficiently extracted, while nuclear integrity remains unaffected. The last extraction step is conducted using a buffer which contains the non-ionic detergent tween-40 and the anionic deoxycholate. An hypoosmotic and hypotonic buffer including tween-40 (1 %) and deoxycholate (0.5 %) disrupts nuclear integrity and extracts nuclear proteins. The remaining pellet contains the cytoskeletal proteins.

A workflow overview for subcellular fractionation using the FractionPREP™ Cell Fractionation Kit is provided in Fig. 10.

- **10x PBS:** 1g KCl, 41g NaCl, 2.86g Na_2HPO_4 x 2 H_2O, 1g KH_2PO_4, deionized water was added up to 500 ml, the pH was adjusted to 7.2
- **1x PBS:** 10x PBS was diluted 1:10 with deionized water
- **FractionPREP™ Cell Fractionation Kit** containing the following solutions:
  - Cytosol Extraction Buffer (CEB)
  - Membrane Extraction Buffer-A (MEB-A)
  - Membrane Extraction Buffer-B (MEB-B)
  - Nuclear Extraction Buffer (NEB)
  - DTT (1 M)
  - Protease Inhibitor Cocktail (PIC) dissolved in DMSO
- **TCA solution**: 10 % TCA in acetone containing 20 mM DTT
- **Sample solution:** 7M urea, 2M thiourea, 4 % CHAPS, 2 % IPG Buffer pH 3-11 NL, and 40 mM DTT

Before starting, working solutions CEB-Mix (2.5 ml CEB + 5 µl PIC + 5 µl DTT), MEB-A-Mix (2.5 ml MEB-A + 5 µl PIC + 5 µl DTT), and NEB-Mix (1.5 ml NEB + 3 µl PIC + 3 µl DTT) were prepared.

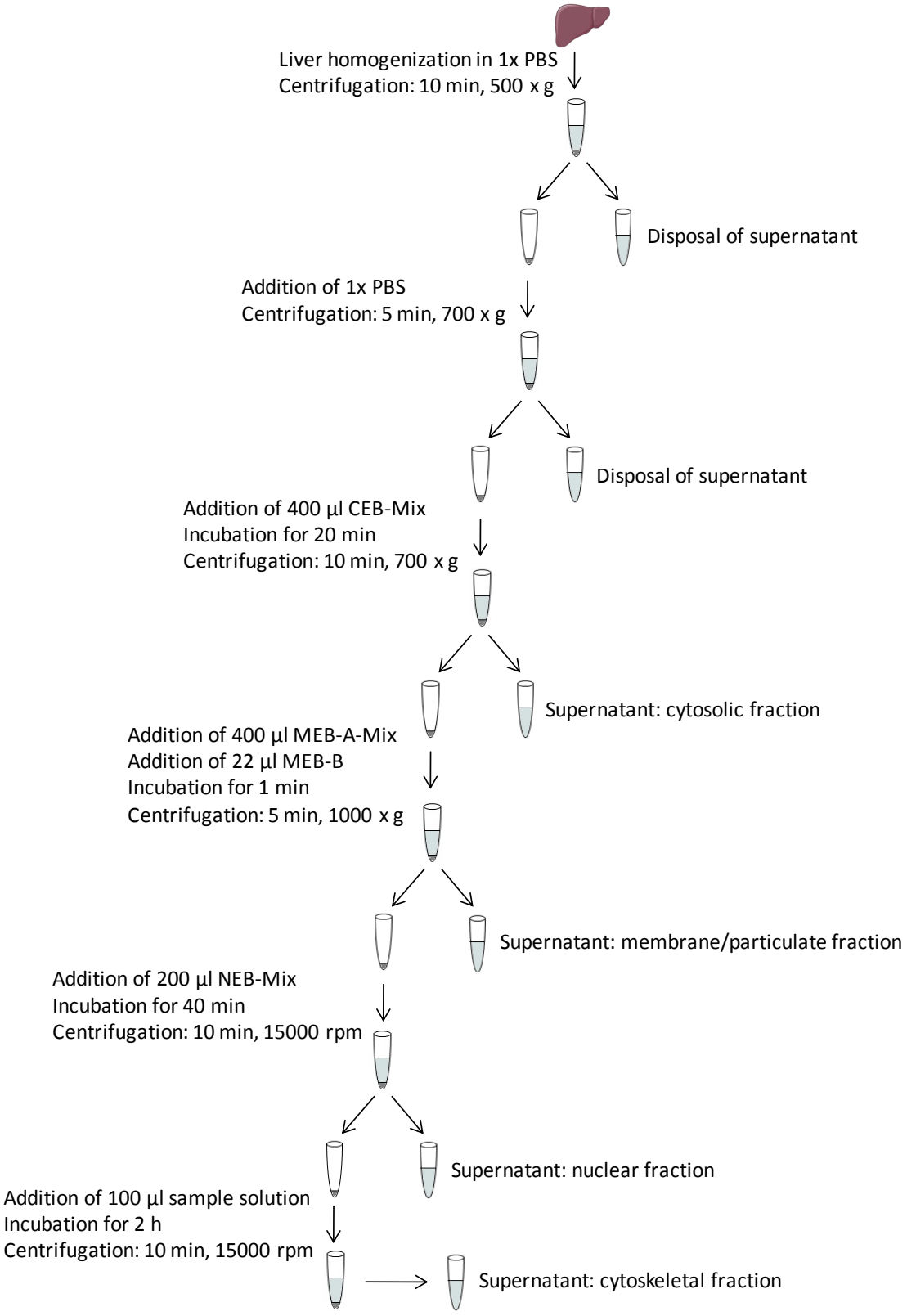

Figure 10 *Workflow for subcellular fractionation of proteins using FractionPREP™ Cell Fractionation Kit. PBS = Phosphate Buffered Saline, CEB = Cytosol Extraction Buffer, MEB-A = Membrane Extraction Buffer-A, MEB-B = Membrane Extraction Buffer-B, NEB = Nuclear Extraction Buffer*

During the procedure, buffers and samples were kept on ice. Unless stated otherwise, all centrifugation steps were performed using an Eppendorf Centrifuge 5403 at 4 °C.

Frozen liver tissue (400 mg) was cut into small pieces, 1 ml ice cold 1x PBS was added, and the tissue was homogenized in a manual tissue homogenizer. The homogenate was transferred to a 15 ml tube and 1.5 ml ice cold 1x PBS was added to the sample. The sample was centrifuged for 10 min at 500 x g (Megafuge 1.0R) and the supernatant was discarded. The pellet was resuspended in 1 ml ice cold 1x PBS, transferred to an Eppendorf tube, centrifuged for 5 min at 700 x g, and the supernatant was discarded. CEB-Mix (400 µl) containing DTT and protease inhibitor cocktail was added to the pellet and mixed well by pipetting up and down several times. The sample was incubated on ice for 20 min with gentle tapping 3-4 times every 5 min and centrifuged for 10 min at 700 x g. The supernatant representing the cytosolic fraction was collected in a clean and prechilled tube and kept on ice. The pellet was resuspended in 400 µl of MEB-A-Mix containing DTT and protease inhibitor cocktail by pipetting up and down several times and vortexed for 15 seconds. Membrane Extraction Buffer-B (22 µl) was added. The sample was vortexed for 5 seconds, incubated on ice for 1 minute, vortexed again for 5 seconds, and centrifuged for 5 min at 1000 x g. The supernatant representing the membrane/particulate fraction was immediately transferred to a clean prechilled tube and kept on ice. The pellet was resuspended in 200 µl of ice-cold NEB-Mix containing DTT and protease inhibitor cocktail, vortexed for 15 seconds, and kept on ice for 40 min with vortexing for 15 seconds every 10 min. The sample was centrifuged for 10 min at 15000 rpm. The supernatant representing the nuclear fraction was transferred to a clean prechilled tube. The pellet representing the cytoskeletal fraction was dissolved in 100 µl sample solution by pipetting up and down and vortexing several times. After incubation for 2 hours on ice, the cytoskeletal fraction was again centrifuged for 10 min at 15000 rpm, the supernatant was transferred to a clean prechilled tube.

The proteins contained in the fractions were precipitated with TCA solution (volume 1+1) overnight at -20 °C. The next day, the samples were centrifuged for 30 min at 4000 x g, the supernatant was discarded, and the resulting pellet was dissolved in 450 µl sample solution. The protein concentrations of all fractions were determined using the 2D Quant Kit as described in 6.2.3. The fractions were stored at –80 °C until further use.

6.2.6 Two-dimensional gel electrophoresis (2D-GE)

6.2.6.1 Principle of two-dimensional electrophoresis

Proteins are amphoteric molecules and as such can be either positively or negatively charged or carry no net charge, depending on the pH of the surrounding medium. Each protein has a specific isoelectric point representing the pH value at which the net charge of the protein is zero. If the protein is kept in a medium with a pH lower than its isoelectric point, the side chains, the carboxylic terminus, and the amino terminus are protonated and the protein carries a positive net charge. If the medium in which the protein is dissolved has a pH higher than its isoelectric point, the proteins will be negatively charged. During the first dimension of the two-dimensional gel electrophoresis, proteins are separated according to their isoelectric points along a pH gradient which is fixed in a gel strip, the Immobiline pH gradient (IPG) strip. This process is called isoelectric focusing (IEF). After IEF, the IPG strips are equilibrated to the conditions of the second dimension, which consists of a SDS-PAGE (sodium dodecyl sulfate-polyacrylamide gel electrophoresis). SDS, an anionic detergent, denatures the proteins and coats them with many negative charges, thus leading to unfolded and negatively charged amino acid chains. During the second dimension of the two-dimensional gel electrophoresis, the proteins are separated according to their molecular mass. Small proteins move faster through the gel than big ones. At the beginning of the second dimension, the proteins move out of the IPG strip into the SDS gel where the separation process takes place. Fig. 11 depicts the different steps of the two-dimensional gel electrophoresis.

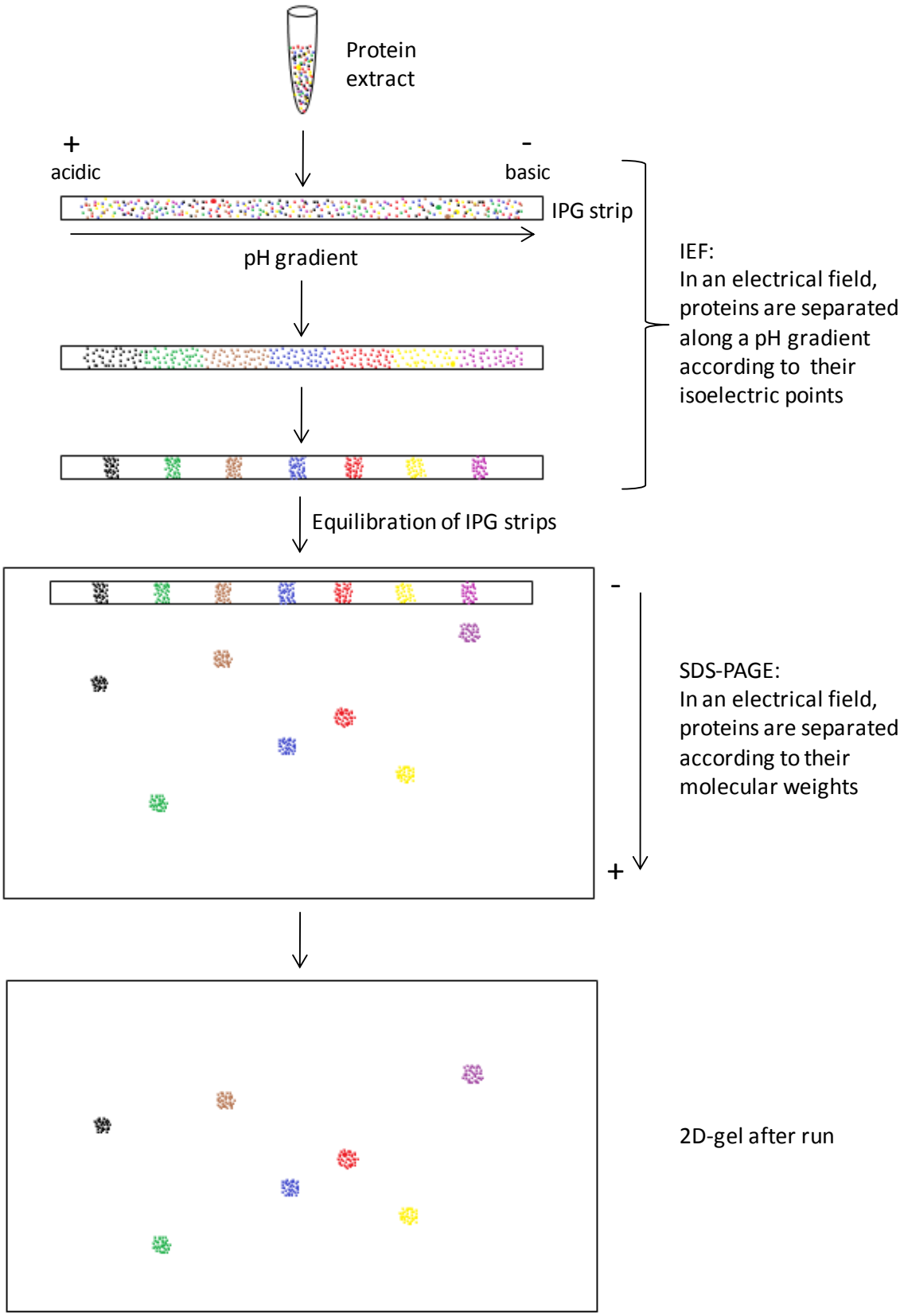

Figure 11 *Workflow for two-dimensional (2D) gel electrophoresis, modified from http://www.ucl.ac.uk/ich/services/lab-services/mass_spectrometry/proteomics/technologies/2d_page. During the isoelectric focusing (IEF), proteins are separated according to their isoelectric points using an immobiline pH gradient (IPG) strip. After equilibration, proteins are separated according to their molecular mass using SDS-PAGE (sodium dodecyl sulfate- polyacrylamide gel electrophoresis).*

6.2.6.2 The first dimension of 2D-GE

In this work, isoelectric focusing was conducted using a Multiphor II electrophoresis unit equipped with an additional frame (Immobiline Dry Strip Tray), a cooling unit (MultiTemp) and a power supply (Electrophoresis Power Supply EPS 3500).

At first, IPG strips with a pH range of 3-11 NL (non-linear) were used in the first dimension to obtain a broad range overview. In further experiments, IPG strips with narrow pH ranges were used (pH 4-7 and pH 6-9) to improve resolution and to decrease the streaking typically observed in the basic parts of the gel. Moreover, samples consisting of either whole tissue extracts or membrane fractions were analyzed. Since the running conditions depend on several factors, such as strip length and protein load, the processes were optimized for each type of IPG strip (Tab. 7).

Table 7 *Running conditions used for protein separation during the first dimension (isoelectric focusing). IPG = immobiline pH gradient*

Samples	IPG strip	Amount of protein loaded [µg]	Length of strip [cm]	Settings for the first dimension
Whole tissue protein extract	Immobiline DryStrip pH 3-11 non-linear	500	18	2 mA, 5 W, 20 °C Step 1: 500 V, 1700 Vh Step 2: 500-3500 V, 1300 Vh Step 3: 3500 V, 22 kVh
Whole tissue protein extract Membrane fraction	Immobiline DryStrip pH 4-7	900	18	2 mA, 5 W, 20 °C Step 1: 500 V, 3 kVh Step 2: 3500 V, 33 kVh
Whole tissue protein extract Membrane fraction	Immobiline DryStrip pH 6-9	500	18	2 mA, 5 W, 20 °C Step1: 150 V, 150 Vh Step 2: 300 V, 600 Vh Step 3: 600 V, 600 Vh Step 4: 3500 V, 50 kVh

First dimension of pH 3-11 NL (non-linear)

- **Rehydration solution:** 7M urea, 2M thiourea, 2 % CHAPS, 0.5 % IPG Buffer pH 3-11 NL, 20 mM DTT, 0.002 % bromophenol blue
- **DTT solution:** 3 % (m/v) DTT in deionized water

Liver protein extracts containing the required amount of protein (Tab. 7) were diluted with rehydration solution to a final volume of 360 µl and pipetted into the Immobiline DryStrip Reswelling Tray. The dehydrated IPG gel strips (Immobiline DryStrip pH 3-11 NL) were placed onto the protein solutions in the tray and, after adding a layer of Dry Strip Cover Fluid to prevent drying of the strips, were left to rehydrate over night. The next

day, the strips were washed and blotted dry before they were placed on the cooling plate of a Multiphor II system equipped with an Immobiline Dry Strip Tray, a temperature control unit (MultiTemp) and a power supply (Electrophoresis Power Supply EPS 3500). The strips were held in the right position by a strip aligner. To ensure an even flow of current through all IPG strips and to improve the electrical conductivity between electrodes and IPG strips, electrode strips were placed orthogonally on top of both sides of the IPG strips. The electrode strip at the anodic side was soaked with deionized water. For the cathodic electrode strip a 3 % DTT solution was used since DTT migrates to the anode during the run of the first dimension, the IPG strip loses DTT, and the proteins are at risk to oxidize and form disulfide bridges, which would alter their position in the IPG strip. After setup of the system, the chamber with the IPG strips was filled up with Dry Strip Cover Fluid to prevent drying of IPG strips. The running conditions applied for the pH range 3-11 NL are shown in Tab. 7. After the run, the IPG strips were wrapped in Saran foil and stored at -80 °C until further use.

First dimension of pH 4-7

- **Rehydration solution:** 7M urea, 2M thiourea, 2 % CHAPS, 0.5 % IPG Buffer pH 4-7, 20 mM DTT, 0.002 % bromophenol blue

The first dimension of the pH 4-7 was conducted as described for pH 3-11 NL, the only difference representing the pH range of the IPG Buffer used for preparation of the rehydration solutions.

First dimension of pH 6-9

- **Rehydration solution:** 7M urea, 2M thiourea, 4 % CHAPS, 0.5 % IPG Buffer pH 6-11, 10 % isopropanol, 65 mM DTT, 0.002 % bromophenol blue
- **Sample buffer:** 7M urea, 2M thiourea, 4 % CHAPS, 0.5 % IPG Buffer pH 6-11, 10 % isopropanol, 85 mM DTT, 0.002 % bromophenol blue

IPG strips (Immobiline DryStrip pH 6-9) were rehydrated over night in 360 µl rehydration solution using the Immobiline DryStrip Reswelling Tray. The next day, the amount of sample containing 500 µg protein was diluted with sample buffer to a volume of 200 µl and each sample was pipetted onto a large sample application piece (0.5 x 2.5 cm). The rehydrated strips were placed on the cooling plate of a Multiphor II system equipped with

an Immobiline Dry Strip Tray, a temperature control unit (MultiTemp) and a power supply (Electrophoresis Power Supply EPS 3500). The large sample application pieces containing the samples were positioned on top of the anodic end of the rehydrated strips and fixed with sample cups on a sample cup bar so that close contact between sample application piece and IPG strip was assured. To ensure an even flow of current through all IPG strips and to improve the electrical conductivity between electrodes and IPG strips, electrode strips were placed orthogonally on top of the IPG strips. The electrode strip at the anodic side was soaked with deionized water while for the cathodic electrode strip rehydration solution was used. For isoelectric focusing of IPG strips with a pH range of 6-9, a specific program was applied (Tab. 7).

6.2.6.3 Equilibration of IPG strips

- **Equilibration solution A:** 6M urea, 75 mM Tris-HCl pH 8.8, 30 % glycerol, 2 % SDS, 0.002 % bromophenol blue, 65 mM DTT
- **Equilibration solution B:** 6M urea, 75 mM Tris-HCl pH 8.8, 30 % glycerol, 2 % SDS, 0.002 % bromophenol blue, 135 mM IAA

IPG strips were left in equilibration solution A for 20 min followed by incubation in equilibration solution B for 20 min. The strips were then air-dried for 6 min.

6.2.6.4 The second dimension of 2D-GE

After cooling the ceramic plate of the Multiphor II to 15 °C, 5 ml Dry Strip Cover Fluid was poured onto the plate and the precast gel (ExcelGel SDS 2-D Homogeneous 12.5) and buffer strips (ExcelGel SDS Buffer Strips) were positioned on top of it. The gel was left to dry slightly for 30 min. The equilibrated IPG strip was laid face down onto the gel, trapped air bubbles were removed, and small sample application pieces were placed underneath each side of the strip in order to absorb water leaking from the IPG strip during the process. A small sample application piece, which was cut to 1/4 of its original size, was placed beside the IPG strip and was soaked with 5 µl of protein marker solution (peqGOLD Prestained Protein-Marker IV, diluted 1:5). The Multiphor II was connected to the power supply and in the first step 600 V, 20 mA, and 30 W were applied for 40 min. After this step, the IPG strip and the sample application pieces were removed from the gel and 600 V, 50 mA, and 30 W were applied for 60 to 75 min. The current was switched

off when the dye front had reached the anodic buffer strip, then the buffer strips were removed and the gel was placed in a Rotho Clear Box for further treatment.

6.2.6.5 Coomassie Blue staining of 2D-gels

- **Fixing solution:** 125 ml deionized water, 100 ml ethanol, 25 ml glacial acetic acid
- **Coomassie Blue solution:** 120 ml deionized water, 40 ml methanol, 40 ml RotiBlue (Carl Roth)

The gel was left in the fixing solution for 2 hours to prevent the proteins from further migrating in the gel, washed for 10 min in deionized water and stained in the Coomassie Blue solution over night. During the staining procedure, the dye associates with the basic amino acid side chains of the proteins and thus stains the proteins unspecifically. The next day, the gel was washed in deionized water for 10 min to remove the precipitated dye and, after drying for some minutes, the gel was scanned on a HP ScanJet 5550C flatbed scanner to obtain digital images.

6.2.7 Fluorography for the detection of radiolabeled protein spots

In the case of ^{14}C, which emits low energy β-particles with a short path length, the detection of signals from a polyacrylamide gel can be dramatically impaired by internal absorption of the radiation by the gel matrix. Thus, signals are likely to be only inefficiently detected by autoradiography. To overcome this problem, fluorography instead of direct autoradiography was conducted in this study. Impregnation of the polyacrylamide gel with the fluorographic reagent Amplify™ (GE Healthcare) can improve the sensitivity by more than 10-fold and can thus significantly reduce exposure times required for the detection of ^{14}C. Through impregnation of the polyacrylamide gel with Amplify™, the scintillator contained in the fluorographic reagent comes in close contact with the isotope, which can then transfer its energy to the scintillator molecules. After absorption of the β-radiation, the scintillator converts the energy into light, which can penetrate the polyacrylamide gel much further than the original β-particle and can efficiently be detected by the radiographic film, forming an image on the adjacent region of the film.

After impregnation, the gels need to be dried since the formation of ice crystals during the exposure at -70 °C can distort the gel and decrease the resolution.

However, a disadvantage of fluorography is that photographic emulsions are disproportionately insensitive to very low intensities of light, resulting in non-linear signal generation on the film. The reason lies in the reversibility of the initial stage of latent image formation in the film at room temperature. In order to yield a blackening signal during development of the film, a silver halide crystal (grain) in the film emulsion must accumulate several atoms of metallic silver, which then catalyze the reduction of the entire silver halide grain (or large parts of it) to metallic silver during developing. A single silver atom in a silver halide crystal is unstable and reverts to a silver ion with a half-life of about one second, whereas two or more silver atoms in a grain are stable. While a single hit by a β-particle has the ability to produce hundreds of silver atoms, a hit by a photon of light can only yield one silver atom. Thus, each photon produces only one silver atom, which means that the latent image can only accumulate when two photons are captured by a grain within one second to produce a stable pair of silver atoms, which is quite unlikely in the case of low intensities of light. If the temperature is lowered, the half-life of the single silver atoms is increased, thus enhancing the probability for a second photon to arrive in time to prevent the first silver atom from reverting to a silver ion and stabilizing the grain. Therefore, the exposure of the film was conducted at -80 °C, which was reported to greatly increase sensitivity of the film to very low intensities of light.

For impregnation, the gel was soaked for 30 min in 150 ml Amplify™ to which 20 ml of glycerol was added to prevent the gel from cracking during the following drying process. The gel was dried at 70 °C for 2.5 hours under vacuum. After drying, the supporting foil was peeled off and the gel was positioned in an autoradiography cassette (Hartenstein) using adhesive strips. A Hyperfilm MP (GE Healthcare) was placed on the gel and the cassette was stored at -80 °C for up to 28 weeks. After this time, the films were allowed to warm to room temperature in order to avoid the formation of artifacts and were then developed using Kodak X-OMAT 1000 Processor. Developed films were scanned on a HP ScanJet 5550C flatbed scanner to obtain digital images.

6.2.8 Spot selection and spot picking for protein identification

For spot selection, the developed films were matched with the Coomassie Blue-stained gel images (Fig. 12). Spots that occurred consistently on the fluorographic images of high dose animals and corresponded to protein spots on the gel were determined and chosen for protein identification. Protein spots corresponding to the spots on the film were cut from the gels using a glass capillary (100 x 1.5 mm), and placed into 96-well plates.

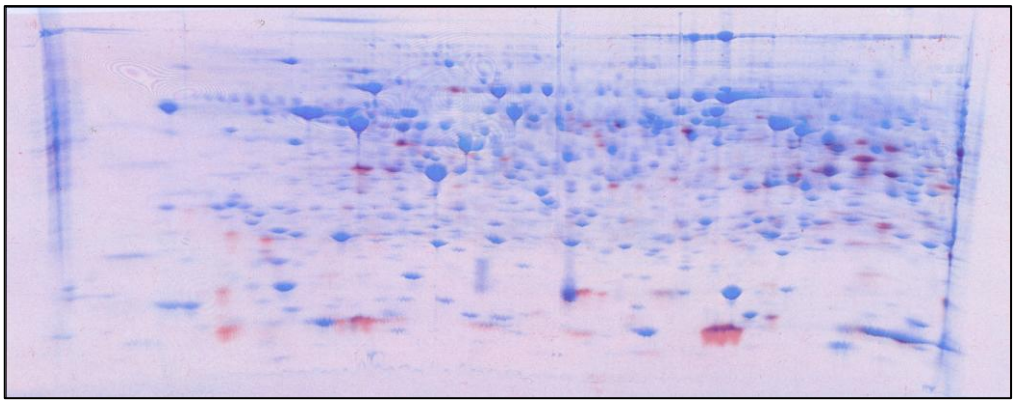

Figure 12 *Matched Coomassie Blue-stained gel (blue) and fluorographic image (colored in red for better visibility of the spots) obtained after separation of proteins over the pH range 4-7 (high dose). Several spots detected by fluorography correspond to Coomassie-Blue stained spots, indicating that these spots contain radiolabeled proteins.*

6.2.9 In-gel tryptic digest of proteins

The tryptic digests and the following mass spectrometry analyses were conducted at the laboratories of the Functional Genomics and Proteomics Unit (Q-TOF Ultima Global mass spectrometer) and the Advanced Mass Spectrometry Facility (LTQ FT Ultra mass spectrometer) at the School of Biosciences, University of Birmingham, United Kingdom, in cooperation with the external collaborator J.K. Chipman.

Before analysis by mass spectrometry, the proteins present in the gel plugs were digested into peptides. This step is required, because tryptic peptides can efficiently be extracted from the gel and show a suitable length for electrospray ionization-mass spectrometry (ESI-MS) analysis. Furthermore, tryptic peptides contain arginine or lysine, which are both basic amino acids, at the C-terminus, thus enhancing ionization of the peptide for mass spectrometry.

- **NH_4HCO_3 solution:** 100 mM in HPLC grade water
- **1,4-Dithiothreitol (DTT) solution:** 10 mM DTT in NH_4HCO_3 solution
- **Iodoacetamide (IAA) solution:** 50 mM IAA in NH_4HCO_3 solution
- **Trypsin stock solution:** 100 µg lyophilized trypsin (Trypsin Gold, Promega) is dissolved in 925 µl acetic acid (50mM)
- **Trypsin solution:** 46 µl trypsin stock solution, 360 µl NH_4HCO_3 solution, 400 µl HPLC grade water
- **Extraction solution A:** 53 µl formic acid, 100 µl acetonitrile, filled up to 5 ml with HPLC grade water
- **Extraction solution B:** 53 µl formic acid, 2 ml acetonitrile, filled up to 5 ml with HPLC grade water
- **Resuspension solution:** 53 µl formic acid, 250 µl acetonitrile, filled up to 5 ml with HPLC grade water

Tryptic digest was conducted at room temperature using a Qiagen BioRobot 3000. The values given in the protocol are the amounts of liquid used per well, i.e. per gel plug. The 96-well plate containing the picked gel plugs was centrifuged for 3 min at 1000 x g (Sigma 4-15C) to bring the plugs to the bottoms of the wells. The cover foil was removed and the plate was positioned on the right plate shaker in the robot. The robot was controlled by the software Qiasoft4. The program was started and the robot conducted the pipetting steps as follows: The gel plugs were destained by first adding 60 µl acetonitrile and incubating for 5 min. After the liquid was removed, 50 µl acetonitrile and 50 µl NH_4HCO_3 solution were added and the plate was incubated for 10 min. The liquid was discarded and the gel plugs were washed twice with 50 µl NH_4HCO_3 solution. To dehydrate the gel plugs, 10 µl acetonitrile was added and the plate was incubated for 15 min. After removal of the liquid and addition of 50 µl NH_4HCO_3 solution to rehydrate the gel plugs, the plate was incubated for 10 min. Then again, dehydration was achieved by adding 10 µl acetonitrile and incubating for 15 min. The liquid was discarded and the gel plugs were dried in the Eppendorf concentrator 5301 for 45 min at 45 °C. After drying, the plate was again placed in the robot, 25 µl DTT solution was added to reduce protein disulfide bonds, and the plate was left on a heating block for 15 min at 60 °C. The plate was placed in the robot and left to cool for 5 min. The DTT solution was removed and 25 µl IAA solution was added to alkylate the thiol groups of the proteins, thus preventing the formation of

disulfide bonds. The plate was kept in the dark for 45 min and the IAA solution was discarded. The gel plugs were washed with 25 µl NH_4HCO_3 solution and dehydrated, rehydrated, and again dehydrated as described above. The plate was removed from the robot, dried in the Eppendorf concentrator 5301 at 45 °C, and placed back in the robot. Trypsin solution (20 µl) was added and the plate was incubated for 20 min so that the gel plugs could soak up the trypsin solution. NH_4HCO_3 solution (20 µl) was added and the plate was incubated over night at 37° C. After placing the plate back in the robot the next day, 30 µl extraction solution A was added and the plate was incubated for 30 min. The solution was transferred into the corresponding wells of a fresh plate, 12 µl extraction solution B and 12 µl acetonitrile were added to the original plate and the plate was incubated for 30 min. The solution was then added to the wells of the fresh plate and the fresh plate was dried in the Eppendorf concentrator 5301 at 45 °C, while the original plate was discarded. 10 µl resuspension solution was added and the samples were stored at -80 °C for further analyses.

6.2.10 Mass spectrometry

The first set of samples from the pH range 4-7 (whole tissue extract) was measured on a Q-TOF Ultima Global mass spectrometer. The second set of samples, i.e. the samples from the pH range 6-9 (whole tissue extract) and from the pH range 4-7 (membrane fraction), was analyzed using a LTQ FT Ultra mass spectrometer, because the Q-TOF Ultima Global mass spectrometer was out of service. To confirm the results obtained by the Q-TOF Ultima Global mass spectrometer, selected samples from the pH range 4-7 (whole tissue extract) were reanalyzed using the LTQ FT Ultra mass spectrometer.

Before the peptides extracted from the gel plugs were subjected to mass spectrometry, they were separated by liquid chromatography to make the mixture less complex.

6.2.10.1 Electrospray ionization (ESI)

In both cases, an electrospray ionization (ESI) source was used to produce positively charged peptide ions, which were online transferred into the mass analyzer. Predominantly, ESI leads to the formation of doubly charged peptide ions, but if the peptide consists of more than 15 amino acids or includes several amino acids with basic residues, such as lysine, arginine, and histidine, it can also carry three or more charges.

ESI is a gentle ionization method and causes only slight fragmentation of the ionized peptides. Weak acids support the formation of positively charged molecules and organic solvents support the spray formation. Thus, the mobile phase used for separation of the peptides by liquid chromatography before mass spectrometry analysis (6.2.10.3 and 6.2.10.5) consisted of a mixture of 0.1 % formic acid in HPLC grade water and 0.1 % formic acid in acetonitrile.

During introduction of the sample into the mass spectrometer via a capillary, a very high voltage is applied and the peptides in the mobile phase become charged. Since all the peptides carry one or more positive charges, they strongly repel each other. Thus, the solvent containing the peptides forms a cone shape (Taylor cone), before it is dispersed into a fine spray. After entering the evaporation chamber, the solvent in these small droplets gradually evaporates with the help of the nebulizer gas nitrogen and the positive charges in the droplet are forced closer to each other. When the repelling Coulomb force exceeds the surface tension of the solvent, the formation of even smaller droplets occurs repeatedly until the solvent is completely evaporated and the charged peptide molecules are introduced into the mass analyzer.

6.2.10.2 QTOF mass spectrometry

QTOF mass spectrometers are very suitable for the determination of peptide masses, because they show high resolution over a wide m/z range.

The acronym QTOF stands for quadrupole time-of-flight and describes the kind of mass analyzer that is used for the determination of peptide masses (Fig. 13). Before entering the QTOF analyzer, the ions from the source pass two cones and are accelerated using an electrical field, thereby gaining a specific speed, which depends on their m/z ratio, for every type of ion. In the next step, the accelerated ions pass a quadrupole and a hexapole and then enter a field-free vacuum tube (= time-of-flight analyzer), which is arranged orthogonally to the trajectory of the ions. In MS mode, the first quadrupole can be used as an ion guide, while in MS/MS mode it can act as a precursor mass selector, filtering out the peptide ions that are further fragmented in the collision cell (hexapole). The charged ions from either MS or MS/MS mode are directed orthogonally into the tube while neutral and solvent molecules are lost. The ions in the tube are redirected by a special reflector plate, which doubles the path length in the tube and improves resolution. The

time, which the ions need to fly through the tube until they reach the detector (photomultiplier), is measured and with this information, the masses of the ions can be calculated.

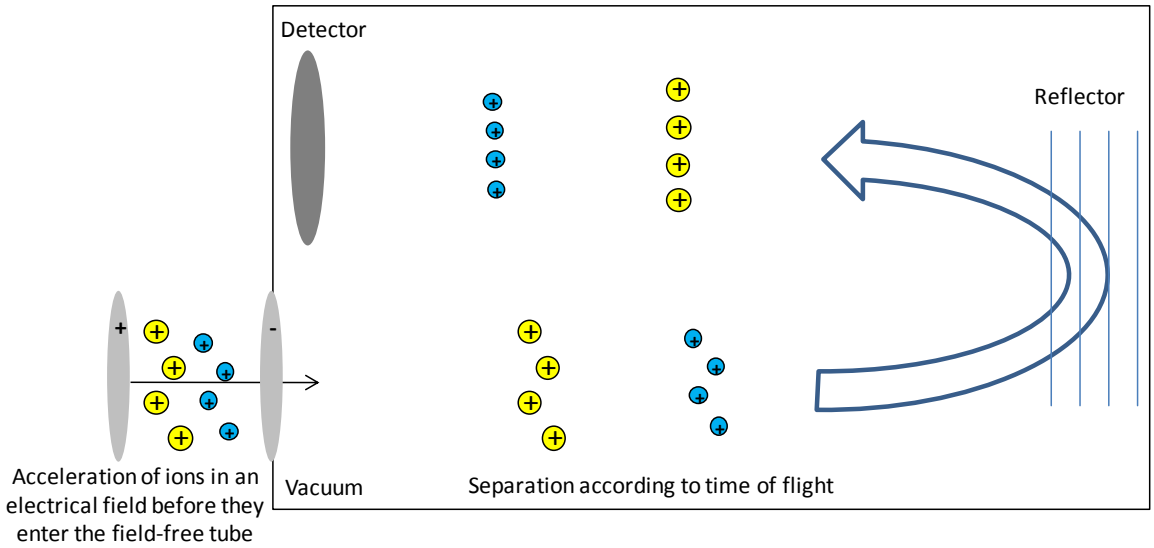

Figure 13 *Time-of-flight tube showing separation of ions according to their time of flight and signal focusing through a reflector, modified from (Rehm, 2006).*

6.2.10.3 Peptide analysis using the Q-TOF Ultima Global mass spectrometer

- **Solvent A:** 0.1 % formic acid in HPLC grade water
- **Solvent B:** 0.1 % formic acid in acetonitrile

After the tryptic digest, peptide extracts were analyzed on a Q-TOF Ultima Global mass spectrometer connected with a Waters capillary HPLC system (CapLC pump). 5 µl of sample was injected by a Waters autosampler and run on a LC Packings column (15 cm/75 µm C18, 3 µm, 100 Å) with a 45 min gradient, consisting of 7 % to 90 % solvent B in 38 min followed by 6 min 7 % solvent B, and a flow rate of 4 µl/min to separate the peptides. The sample was inserted into the mass spectrometer via a Waters ESI source with capillary voltage 3.0-3.5 kV, cone voltage 80-100 kV, source temperature 80 °C and the nebulizer gas nitrogen. The mass spectrometer was controlled by the software Masslynx 4.0 and altered between a full scan (m/z 400-1800, positive ion mode) and subsequent Collision-Induced Dissociation (CID) MS/MS scans of the three most abundant ions with charges of 2+ or 3+ (resolution 10,000 over 50-2000 m/z). The collision gas argon had a collision energy of 10 eV for MS and 32 eV for MS/MS mode. Weekly calibrations with the

standard peptide [Glu^1]-Fibrinopeptide and daily control samples of MassPREP^{TM} Digestion Standard Enolase assured the proper function of the mass spectrometer.

After the analyses were completed, the software Masslynx 4.0 converted the information obtained through the MS and MS/MS spectra into monoisotopic peak lists and produced data files containing this information in a compressed form. These data files were then directly uploaded into the Mascot search engine to determine the amino acid sequences of the peptides and to identify proteins from which the peptides may be derived. For the Mascot search (MS/MS Ions Score) the following settings were used: database: MSDB, enzyme: trypsin, up to 2 missed cleavages allowed, taxonomy: rattus, fixed modifications: Carbamidomethyl (C), variable modifications: Oxidation (M), peptide tolerance ± 2 Da, MS/MS tolerance ± 0.8 Da, peptide charge 2+ and 3+, monoisotopic peak list, data format: micromass (.pkl), instrument: ESI-QUAD-TOF.

6.2.10.4 FT-ICR mass spectrometry

For parts of this study, the LTQ FT Ultra mass spectrometer was used for peptide analyses. The LTQ FT Ultra represents a hybrid mass spectrometer, which combines Ion Trap and Fourier Transform Ion Cyclotron Resonance (FT-ICR) technologies into a single instrument and is able to analyze masses with very high accuracy, ultra high resolution (> 750,000), and attomole sensitivity.

The ionized molecules from the ESI source are funneled into the analyzer cell (Fig. 14) with the use of an ion guide. The cell is located in the center of a superconducting magnet. Ions entering the cell begin to circle the magnetic field, thereby describing tiny orbits. While the radius of the orbit is the same for all ions, the speed of the flying ions depends on their mass and thus all ions with the same mass travel at the same speed around the orbits, which is called their cyclotron frequency. The lighter ions are faster than the heavier ones and therefore have higher cyclotron frequencies. This is the criterion how the machine will eventually differentiate between the various ions. With increasing power of the magnet and thus enhanced strength of the magnetic field, not only the cyclotron frequencies themselves increase, but also the differences between the ICR frequencies, thus making it easier to differentiate between various types of ions with different masses, i.e. the stronger the magnetic field is, the better a resolution can be obtained.

Ions of the same mass travelling at the same speed have to be focused in order to measure them. When the ions inside the cell pass the detector plates close enough to the electrodes on each plate, a flow of negatively-charged electrons (equal in charge to the packet) is induced and can be measured in the connected electric circuit outside the cell. However, without excitation the ions travel on orbits too small (0.1 millimeter) for them to reach the detection plates. Using an external circuit connected to the excitation plates, a series of oscillating radio frequency pulses (chirp) is transferred to the excitation plates. Each chirp excites only the one mass-type of ions whose particular cyclotron frequency corresponds to the chirp. The chirps start at a low frequency, which is increased with time, and thus the heavier ions will respond first. The ions absorb the additional energy from the radiofrequency pulse and use it to increase the size of their orbits. Travelling on the new and bigger orbits, the ions are focused into a "packet" and come close enough to the electrodes on the detector plates to induce a signal without crashing into the walls of the cell.

Once the ions have induced a signal at an electrode, they continue on their orbit and circle back toward the electrode at the opposite side, where they also induce a flow of electrons. These currents in the external circuit are measured by a resistor. When the ion packets have reached their biggest orbits and the radio frequency chirp is removed, the packets lose their energy and spiral back down to the original orbit, thereby inducing gradually less current. The machine detects the decay of the orbits over time while it simultaneously measures the packets corresponding to all the masses in the sample, a process which takes about one second.

After amplification and digitalization of the voltages measured in the external circuit, a signal composed of all of the cyclotron frequencies of all of the ions present is obtained. In order to acquire readable signals from raw data, a mathematical algorithm called Fourier transform is applied, which shows the amplitude of each of the different frequencies detected. This amplitude corresponds to the number of ions associated with that frequency. Finally, the results of the Fourier transform are translated to produce a mass spectrum.

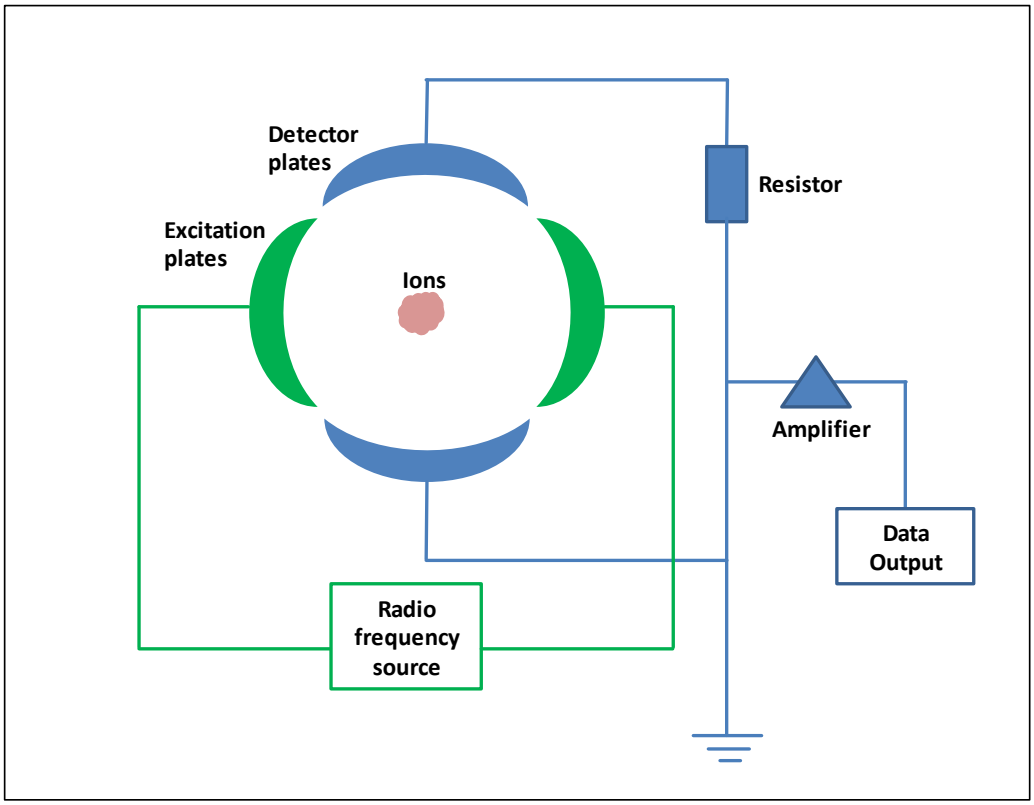

Figure 14 *Schematic setup of an analyzer cell as used for Fourier Transform-Ion Cyclotron Resonance (FT-ICR) mass spectrometry.*
Figure modified from http://www.magnet.fsu.edu/education/tutorials/magnetacademy/fticr/.

6.2.10.5 Peptide analysis using the LTQ FT Ultra mass spectrometer

- **Solvent A:** 0.1 % formic acid in HPLC grade water
- **Solvent B:** 0.1 % formic acid in acetonitrile

The digested samples (5 µl) were injected into a system consisting of a Micro AS autosampler, a Surveyor MS pump, an Integrafrit column (10 cm/ 75 µm, C8), a TriVersa NanoMate (ESI) source and a LTQ FT Ultra mass spectrometer. For the separation of the peptides, a linear gradient with a flow rate of 300 nl per minute was used during which the fraction of solvent B was increased from 5 % to 40 % in 40 min. The nanospray source sprayed the eluted peptides into the mass spectrometer using a voltage of +1.7 kV. Data acquisition by data-dependent scanning in the mass spectrometer was performed under control of the Xcalibur 2.0.7 software. The mass spectrometer conducted a full FT-MS scan (m/z 380-2000) followed by Collision-Induced Dissociation (CID) MS/MS scans of the three most frequent ions.

The CID MS/MS data were uploaded into the in-house Mascot search engine to determine the amino acid sequences of the peptides and to identify proteins from which the peptides may be derived. For the Mascot search (MS/MS Ions Search), the following

search parameters were used: database: NCBInr, enzyme: trypsin, up to 3 missed cleavages allowed, taxonomy: rattus, fixed modifications: Carbamidomethyl (C), variable modifications: Acetyl (K), Deamidated (NQ), Oxidation (M), Phospho (ST), Phospho (Y), peptide tolerance ± 20 ppm, MS/MS tolerance ± 0.5 Da, and the error tolerant search was not used.

6.2.10.6 Protein identification with the Mascot search engine

During CID, the peptides break at various sites and thus disintegrate into smaller fragments. Although breaking of the amino acid side chains can also be observed, cleavage mainly occurs at the peptide backbone. Depending on whether the charge remains at the N-terminus or at the C-terminus, the ions are called a, b, c fragment ions or x, y, z fragment ions (Fig. 15), respectively. When the peptide bond is cleaved, b and y fragment ions occur and these ion pairs are the most important ones for the identification of a peptide's amino acid sequence. The number in the index of the fragment ion corresponds to the number of amino acids contained in the fragment ion. The localization of the charge and the preferred position of the cleavage depend on the amino acid sequence of the peptide.

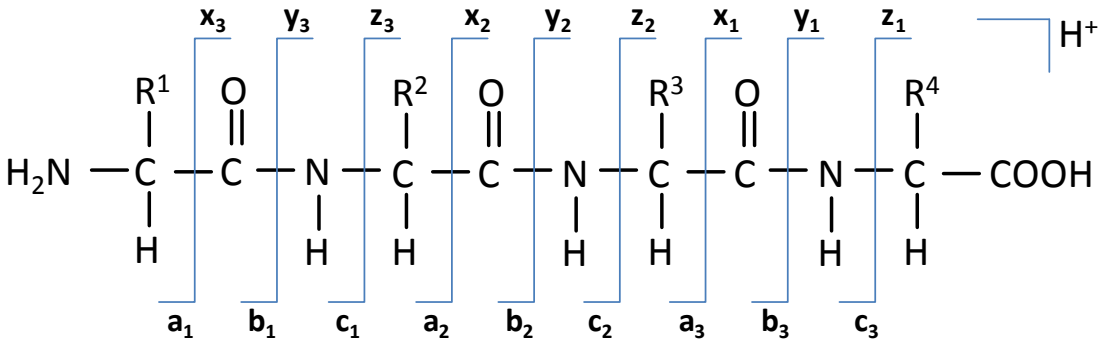

Figure 15 *Possible cleavage sites of a peptide during MS/MS fragmentation. Despite possible breaking of amino acid side chains, cleavage mainly occurs at the protein backbone. Depending on whether the charge remains at the N-terminus or at the C-terminus, the ions are called a, b, c fragment ions or x, y, z fragment ions, respectively. For subsequent database search, b- and y-ions are the most important ones. Figure modified from http://www.matrixscience.com/help/fragmentation_help.html.*

For MS/MS Ions Search using Mascot search engine (www.matrixscience.com), the monoisotopic peak lists and spectra contained in the data files or in the raw data were directly uploaded into the online search engine or into the in-house search engine at the University of Birmingham, respectively. By comparison of theoretical mass values present

in the database with experimentally determined masses, the Mascot search engine assigns the peaks to the various fragments, thus revealing the amino acid sequence of the peptide.

The Mascot search engine applies a scoring system based on the Mowse score, which can be calculated for each entry by giving a certain statistical weight to each match according to an empirically determined frequency factor matrix. Mascot combines the Mowse score with a probability based scoring system and reports a "probability based Mowse score" for each peptide (= ions score) on the results page shown after the search. This probability based Mowse score represents the absolute probability that the obtained match occurred at random. The probability is transformed into the score using the equation $-10*LOG_{10}(P)$ (with P being the probability) and thus a high score stands for a high probability that the hit is not a random event. Using the probability and the known size of the searched database, Mascot calculates the minimum score that is needed for a hit to be a significant match ($p < 0.05$) and shows this confidence threshold on the results page for every peptide. If the peptide has an ions score higher than the confidence threshold, this indicates that the experimentally determined peptide is identical or extensively homologous to the peptide in the database.

However, the protein scores which are reported for every protein match, as opposed to the ions scores reported for every peptide match, represent the combined ions scores of all peptides that are assigned to a single protein. The more peptides are assigned to a protein hit, the higher the protein score is. The protein score functions as a non-probabilistic basis for ranking protein hits. Also for the protein scores, a threshold is given on the results page, which gives a clue as to which proteins are the most probable hits. If a hit has a protein score higher than this threshold, this also indicates that the protein is a significant hit ($p<0.05$).

In our study, the protein score thresholds were in the range of 35-36 or 29-43 for samples measured with Q-TOF Ultima Global mass spectrometer or LTQ FT Ultra mass spectrometer, respectively.

Besides the scores, further important information needed to determine whether a match is accepted as an identified protein, can also be obtained by Mascot. This information includes the number of peptides assigned to a protein and the sequence coverage.

It often happens that a peptide occurs several times on the results list. This can be due to different charge states or various modifications. To obtain the number of peptides assigned to one protein, only unique peptide sequences were counted. This means that if a peptide sequence occurs three times in the peptide list with different modifications or charges, it was only counted as one peptide. The minimal number of peptides assigned to one protein should be at least 2 since finding only a single peptide matched to a protein strongly increases the risk of a false-positive protein assignment (Nesvizhskii and Aebersold, 2004).

The sequence coverage is the percentage of the protein sequence for which matching peptides were detected. The higher the sequence coverage is, the more of the amino acid sequence was confirmed by the analyses. The ideal case of 100 % protein coverage has already been obtained (Meyer et al., 2010), but only after special sample preparation, which included digests with different enzymes to obtain many peptides with various cleavage sites. In standard high-throughput screening workflows, only cleavage with the enzyme trypsin is conducted. Thus, only reduced sequence coverages are obtained. A further factor contributing to limited sequence coverage may be the amino acid composition and thus the hydrophobicity of peptides in connection to the ionization technique applied. It was observed that for small and hydrophobic peptides ESI is the preferred ionization method, whereas basic and polar peptides are better detectable using MALDI (Meyer et al., 2010). Moreover, the amount of sample available for analysis can influence the sequence coverage. It is possible that proteins in the gel plugs excised from the gels are not properly digested or extracted from the gel plugs and hence the amount of peptides available for analysis is reduced.

However, reduced sequence coverage does not prevent the reliable identification of a protein. In studies using similar high-throughput screening approaches to identify target proteins of reactive metabolites, sequence coverages of 5-57 % (Dooley et al., 2008), 11-83 % (Koen et al., 2007), and 4-39 % (Druckova et al., 2007) were obtained. There are no fixed rules as to how the sequence coverage should be to get definitive protein identification. In our study, we used a cut-off of 10 % sequence coverage in an attempt to exclude proteins identified with a low level of confidence.

To obtain the target protein list for our study, in the first step all proteins with protein scores higher than their protein score thresholds were listed. Then, all protein hits

consisting of only one peptide hit and/or showing less than 10 % sequence coverage were excluded. Since only highly consistent proteins should be subjected to the subsequent functional analysis, only proteins found in all three high dose animals were picked for the target protein list. In summary, in our study a protein was regarded as identified if detected in all high dose animals (n=3), each with a protein score above the confidence threshold, a sequence coverage of at least 10 % based on at least 2 identified peptides. The online database Protein Knowledgebase (UniProtKB; http://www.uniprot.org/) was used to gain further information on the proteins, such as protein family, function and subcellular localization.

As an example to illustrate how data obtained by mass spectrometry were processed, the peptide CLLFVDIPSK, which was assigned to the protein regucalcin, is used. Fig. 16 depicts the MS/MS spectrum of the peptide. Tab. 8 shows the fragment masses that may theoretically be found after CID fragmentation, while the ions that were actually observed are marked in red. The more complete the fragment series are, predominantly the b and y series, the more information on the peptide sequence is present and the better the ions score is. In our example, it is clearly visible that a, b, and y fragment ions were detected and that the b-y series is nearly complete. Thus, the amino acid sequence of the peptide can be determined. In this example, a peptide from the protein regucalcin, the results page showed that an ions score > 33 indicates identity or extensive homology ($p < 0.05$). Considering this confidence threshold, the peptide with an ions score of 75 represents a significant hit.

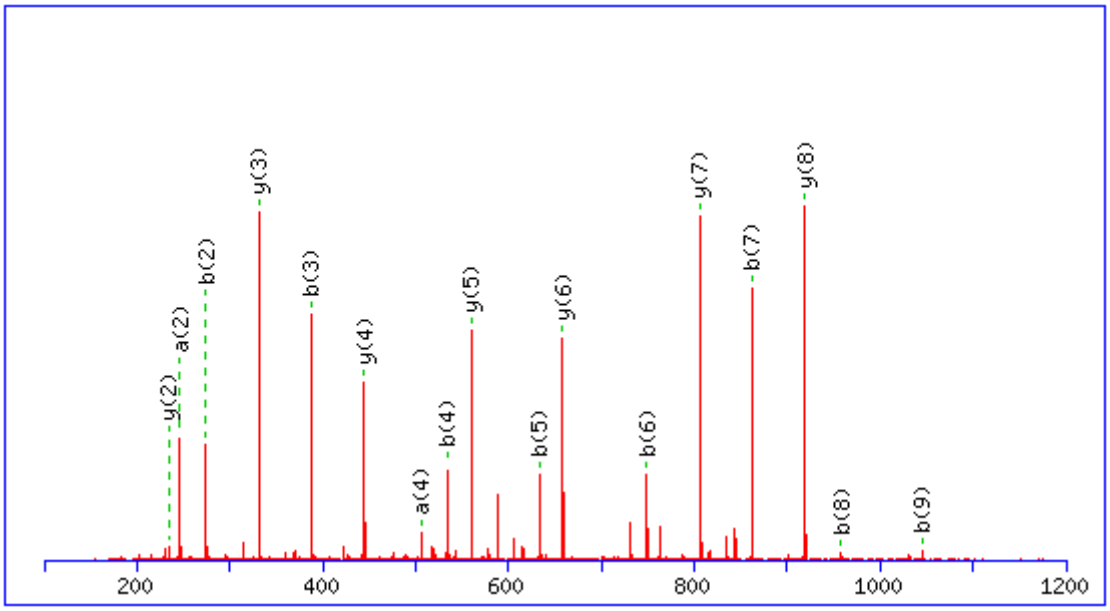

Figure 16 *MS/MS spectra of the peptide CLLFVDIPSK belonging to the protein regucalcin. The detected peaks are assigned to a-, b-, and y-ions. The number in brackets correspond to the number of amino acids contained in the fragment ion.*

Table 8 *All a-, b-, and y-fragment ions of the peptide CLLFVDIPSK that can theoretically be obtained by MS/MS are listed in the table. Fragments that were actually found in the analysis are marked in red.*

#	a	a^{++}	b	b^{++}	Sequence	y	y^{++}	y*	y^{*++}	#
1	133.0430	67.0251	161.0379	81.0226	C					10
2	246.1271	123.5672	274.1220	137.5646	L	1031.6136	516.3104	1014.5870	507.7971	9
3	359.2111	180.1092	387.2061	194.1067	L	918.5295	459.7684	901.5029	451.2551	8
4	506.2796	253.6434	534.2745	267.6409	F	805.4454	403.2264	788.4189	394.7131	7
5	605.3480	303.1776	633.3429	317.1751	V	658.3770	329.6921	641.3505	321.1789	6
6	720.3749	360.6911	748.3698	374.6886	D	559.3086	280.1579	542.2821	271.6447	5
7	833.4590	417.2331	861.4539	431.2306	I	444.2817	222.6445	427.2551	214.1312	4
8	930.5117	465.7595	958.5067	479.7570	P	331.1976	166.1024	314.1710	157.5892	3
9	1017.5438	509.2755	1045.5387	523.2730	S	234.1448	117.5761	217.1183	109.0628	2
10					K	147.1128	74.0600	130.0863	65.5468	1

In the case of our example, 30 peptides were assigned to regucalcin, 19 of which represented significant hits, i.e. had ions scores higher than their respective confidence thresholds. This led to a very high protein score of 1263, which is by far higher than the range of protein score threshold of 29-43 for samples measured with the LTQ FT Ultra

mass spectrometer, and a very high sequence coverage of 86 %. Thus, regucalcin is identified with very high confidence.

6.2.11 Autoradiographic analysis of furan distribution in rat liver after oral administration

3 Male Fischer F344/N rats (140-170 g on arrival, Harlan-Winkelmann GmbH, Borchen, Germany) were housed at standard laboratory conditions (climate cabinets, temperature 22 ± 2 °C, relative humidity 30-70 %, 12-15 air changes per hour, 12 hour light/dark cycle) in Makrolon® type-4 cages with wire meshtops and standard softwood bedding. Rats received pelleted standard rat maintenance diet and tap-water ad libitum. After acclimatization, animals received a single oral dose of [3,4-^{14}C]-furan (0.8 mg/kg bw; specific activity 20 mCi/mmol) in corn oil (4 ml/kg bw) by gavage. Rats were sacrificed 2 hours after administration by cardiac puncture under CO_2 anesthesia and livers were removed and mounted without disrupting the anatomical order on a precast base of frozen Tissue-Tek® O.C.T^{TM} Compound, which was placed in a cube formed of aluminum foil. After documentation of the liver position on the base, the cube was filled up with Tissue-Tek® O.C.T^{TM} Compound and frozen at -20 °C to yield a solid block in which the liver was embedded. The tissue block including the liver was cut into slices, which were mounted on plastic foil. The liver slices were dried under vacuum at -70 °C and were placed into an autoradiography cassette. A Hyperfilm MP was placed onto the dried slices and the cassette was kept at -80 °C for two weeks. After the exposure time, the film was developed and scanned on a HP ScanJet 5550C flatbed scanner to obtain digital images.

6.3 Results and discussion

6.3.1 Determination of covalent binding of furan to proteins

To determine covalent binding of furan to proteins, the radioactivity contained in the protein extracts isolated from liver and kidney tissue was determined by liquid scintillation counting. Following treatment with [3,4-^{14}C]-furan, a dose-dependent increase in the amount of radiolabeled furan covalently bound to proteins was observed in both target (liver) and non-target (kidney) tissue of furan carcinogenicity (Tab. 9). In the high dose group (2 mg/kg bw), protein binding in the liver was 286 ± 25 pmol furan equiv/mg protein, a level of protein adduction roughly three times higher than measured in kidney (88 ± 49 pmol furan equiv/mg protein). The difference between target and non-

target organ was even more pronounced in the low dose group (0.1 mg/kg bw) in which 29 ± 7 pmol furan equiv/mg protein (liver) and 3 ± 1 pmol furan equiv/mg protein (kidney) were measured.

Thus, the level of covalent adducts in livers of rats given a single dose of [3,4-^{14}C]-furan, which is not expected to cause significant hepatotoxicity (Mally et al., 2010), was about 1/3 of what is typically observed following treatment with a dose of a prototypical drug inducing hepatocellular necrosis (1 nmol drug equiv/mg protein) (Evans et al., 2004) and indicates for a 25 kDa protein an average labeling density of approximately 0.01 adducts per molecule of protein (Ikehata et al., 2008).

Table 9 *Amount of furan equivalents covalently bound to proteins in target and non-target tissue of furan carcinogenicity following treatment of rats with [3,4-^{14}C]-furan. Data are expressed as mean ± SD (n=5). The amount of furan bound to proteins increased with increasing dose in both organs, but was higher in liver than in kidney tissue.*

Dose group (mg/kg bw)	**^{14}C-furan bound to proteins in rat liver** (pmol furan equiv/mg protein)	**^{14}C-furan bound to proteins in rat kidney** (pmol furan equiv/mg protein)
0	0 ± 0	0 ± 0
0.1	29 ± 7	3 ± 1
2.0	286 ± 25	88 ± 49

6.3.2 Identification of target proteins of reactive furan metabolites

Two-dimensional gel electrophoresis and fluorography

Using wide range IPG strips (pH 3-11), separation of unmodified and furan-adducted proteins from whole liver extracts by two-dimensional gel electrophoresis and subsequent detection by fluorography (exposure ≥ 10 weeks) revealed highly consistent spot patterns of adducted proteins in all high dose animals (Fig. 17). However, the resolution of the protein spots was not satisfying and streaking occurred to a great extent in the basic part of the gel. Thus, to improve spot resolution and facilitate spot picking for subsequent analysis by mass spectrometry, narrow range IPG strips (pH 4-7 and pH 6-9) were used and optimized independently. This procedure led to gel images with better resolution and less streaking in both narrow pH ranges (Fig. 18).

Furthermore, subcellular fractionation was conducted and membrane fractions were analyzed in addition to total liver extracts. This was done since it had been hypothesized

that furan reactive metabolites may bind to transport proteins located in the canalicular membrane of hepatocytes, resulting in disruption of membrane integrity and/or interference with hepatobiliary transport (6.2.5).

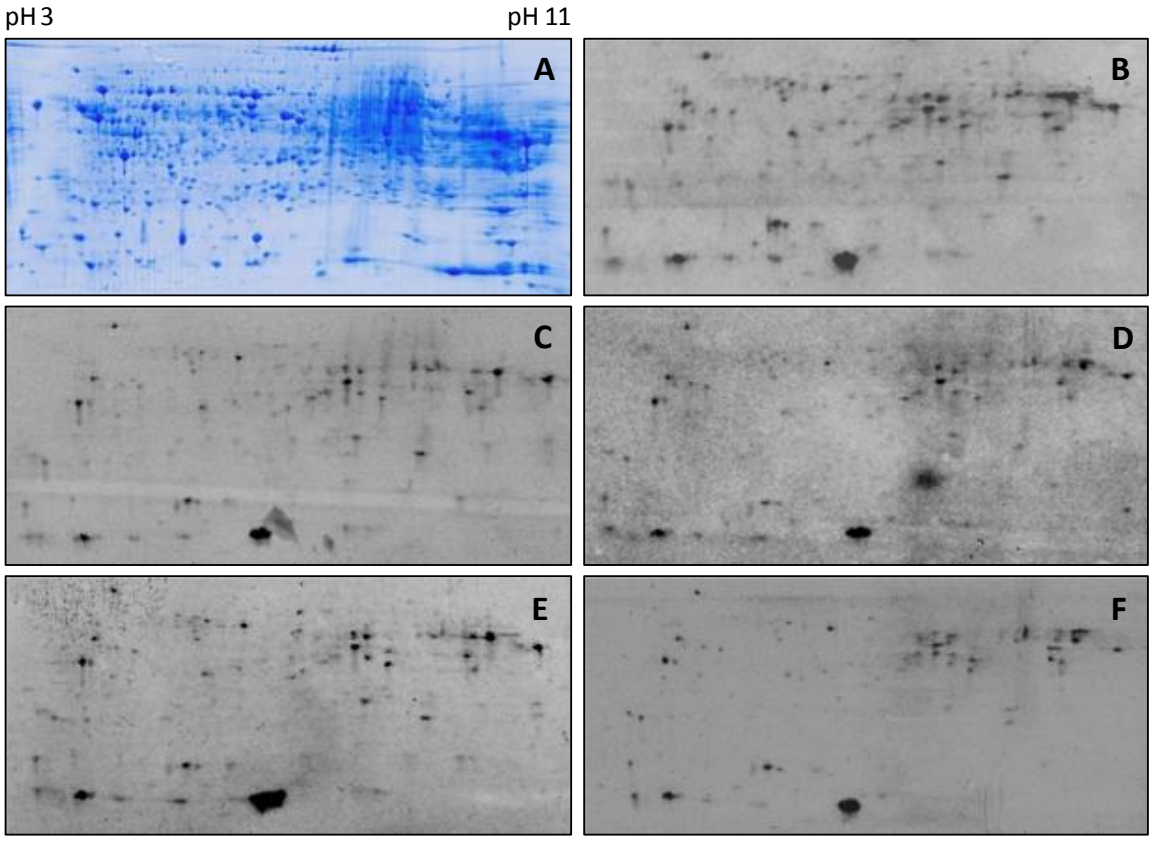

Figure 17 *Images of a representative Coomassie Blue-stained gel (A) and fluorographic film images (B-F) obtained from 5 different rats treated with 2 mg/kg bw furan. Modified and unmodified proteins were separated by two-dimensional gel electrophoresis (pH range 3-11, whole liver extract) and adducted proteins were detected by fluorography. Spot patterns appeared to be consistent in all animals, but strong streaking in the basic part (right side) of the gels made spot selection difficult.*

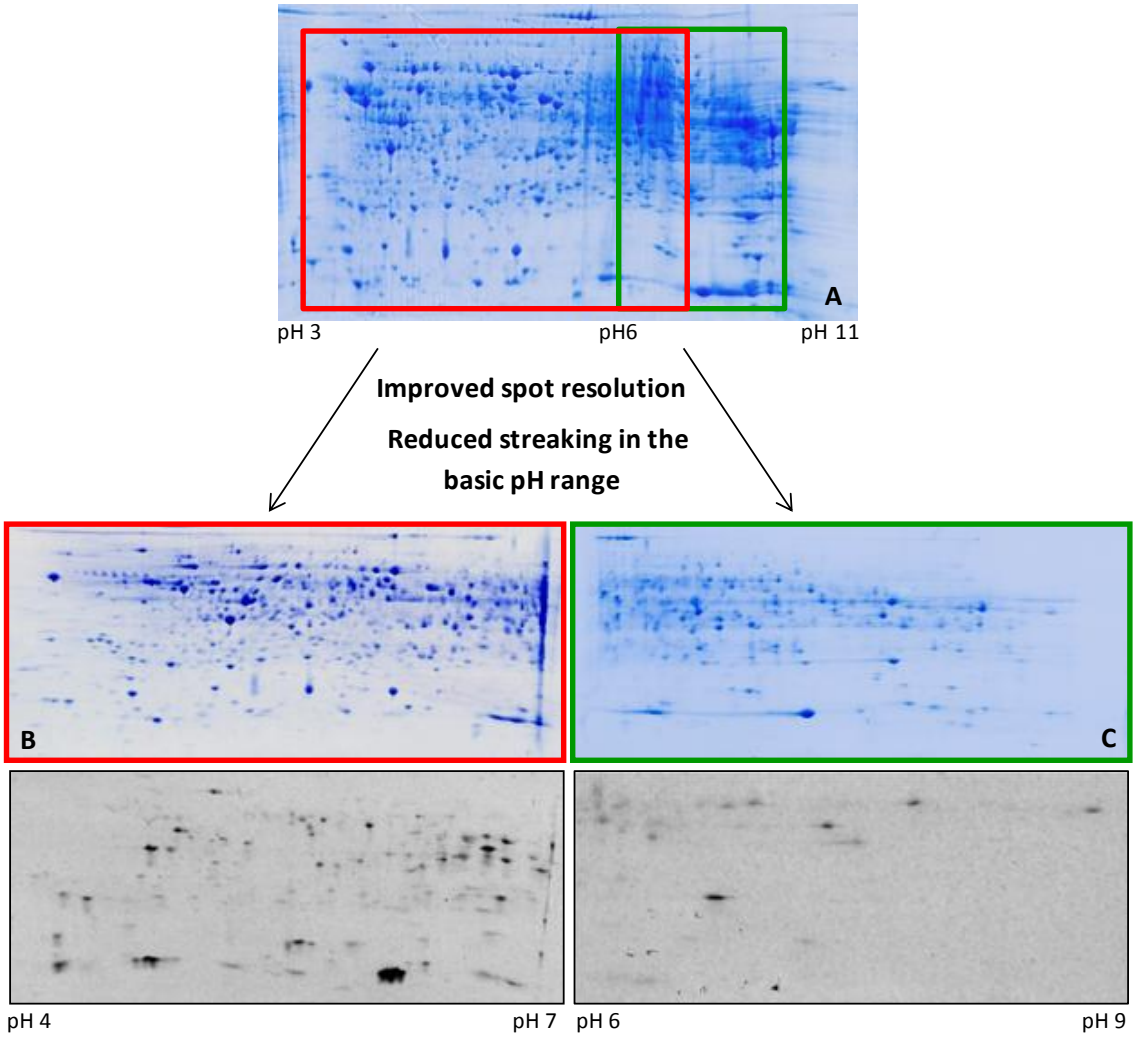

Figure 18 *Using narrow range pH ranges, improved spot resolution and reduced streaking in the basic pH range was obtained. Representative images shown are Coomassie Blue-stained gel images obtained after separation of proteins over a broad (A: pH 3-11) and two different narrow pH ranges (B: pH 4-7, C: pH 6-9) with their corresponding fluorographic film images (D, E).*

As expected, no spots were observed on fluorographic films prepared from control animals (Fig. 19). In contrast, a total of 83 radioactive spots were consistently detected in high dose animals (Fig. 20) and were selected for identification by mass spectrometry. 37, 15, and 31 of the 83 spots were detected after separation of modified and unmodified proteins by two-dimensional gel electrophoresis using pH ranges 4-7 (whole tissue homogenate,), 6-9 (whole tissue homogenate), and 4-7 (membrane fraction), respectively. On the fluorographic films obtained from the pH range 6-9 (membrane fraction) only very few spots were detected in proteins isolated from a single animal. Thus, these few spots were excluded from further identification.

Figure 19 *Representative fluorographic film image obtained from a control animal (pH range 4-7, whole tissue extract, 26 weeks exposure time). As expected, no spots derived from radioactively labeled proteins were observed.*

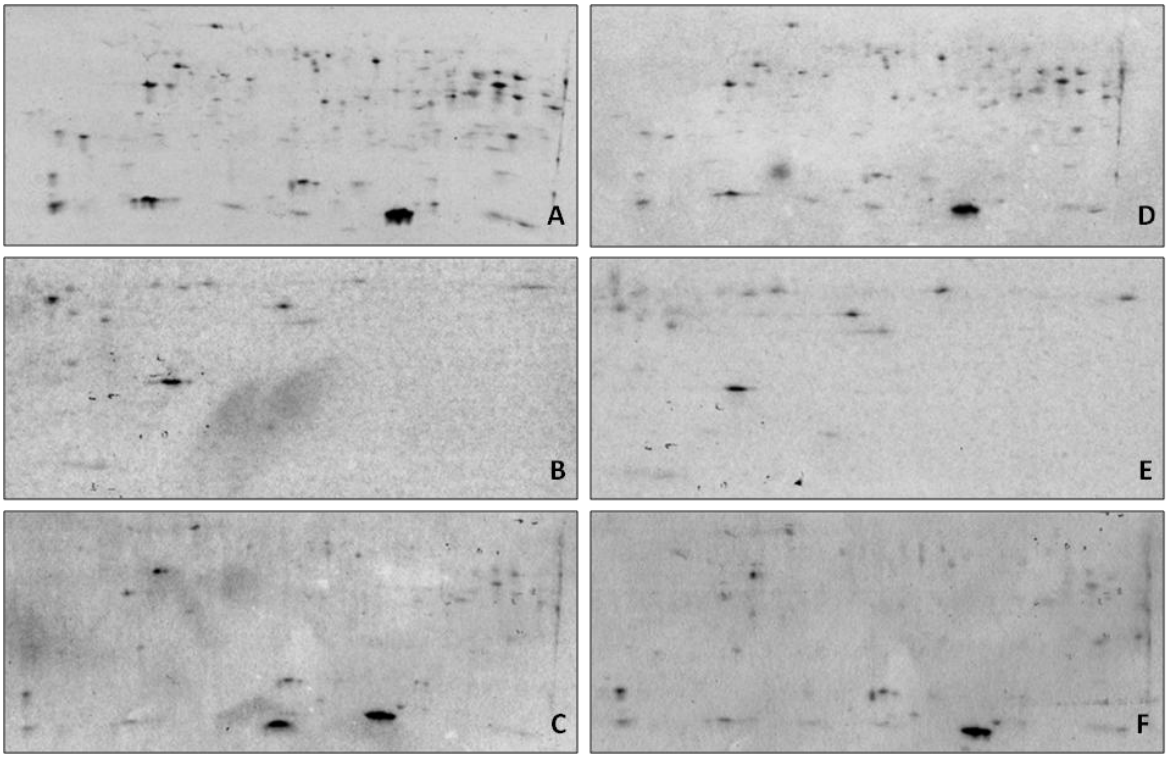

Figure 20 *Representative film images obtained from high dose animals. The top (A, D), middle (B, E), and bottom (C,F) row each show two representative film images of whole tissue extract (pH range 4-7), whole tissue extract (pH range 6-9), and membrane fraction (pH range 4-7), respectively. The spot patterns of A and D, B and E, and C and F show high consistency.*

Protein identification by mass spectrometry

Analysis of the selected spots using Q-TOF Ultima Global mass spectrometer (QTOF) and LTQ FT Ultra mass spectrometer (FT-ICR) followed by a Mascot database search identified 61 proteins as putative targets of furan reactive metabolites (Tab. 10 and Fig. 21). A protein was regarded as identified if it was detected in all high dose animals (n=3), in each case showing a sequence coverage of at least 10 % and the identification of at least 2 peptides. Since the spots were analyzed using two different mass spectrometers with the FT-ICR being far more sensitive and accurate than the QTOF, the overall protein scores, sequence coverages, and peptide numbers obtained by the FT-ICR were higher than the

ones observed during analysis with the QTOF. For this reason, some spots for which insufficient sequence coverage was obtained with QTOF were confirmed by repeating mass spectrometry analysis using the FT-ICR. For instance, in the case of thioredoxin-1, analyses using the QTOF yielded a maximum of only two peptides (21 % sequence coverage) assigned to the protein whereas using the FT-ICR 8 peptides (65 % sequence coverage) of the protein could be detected.

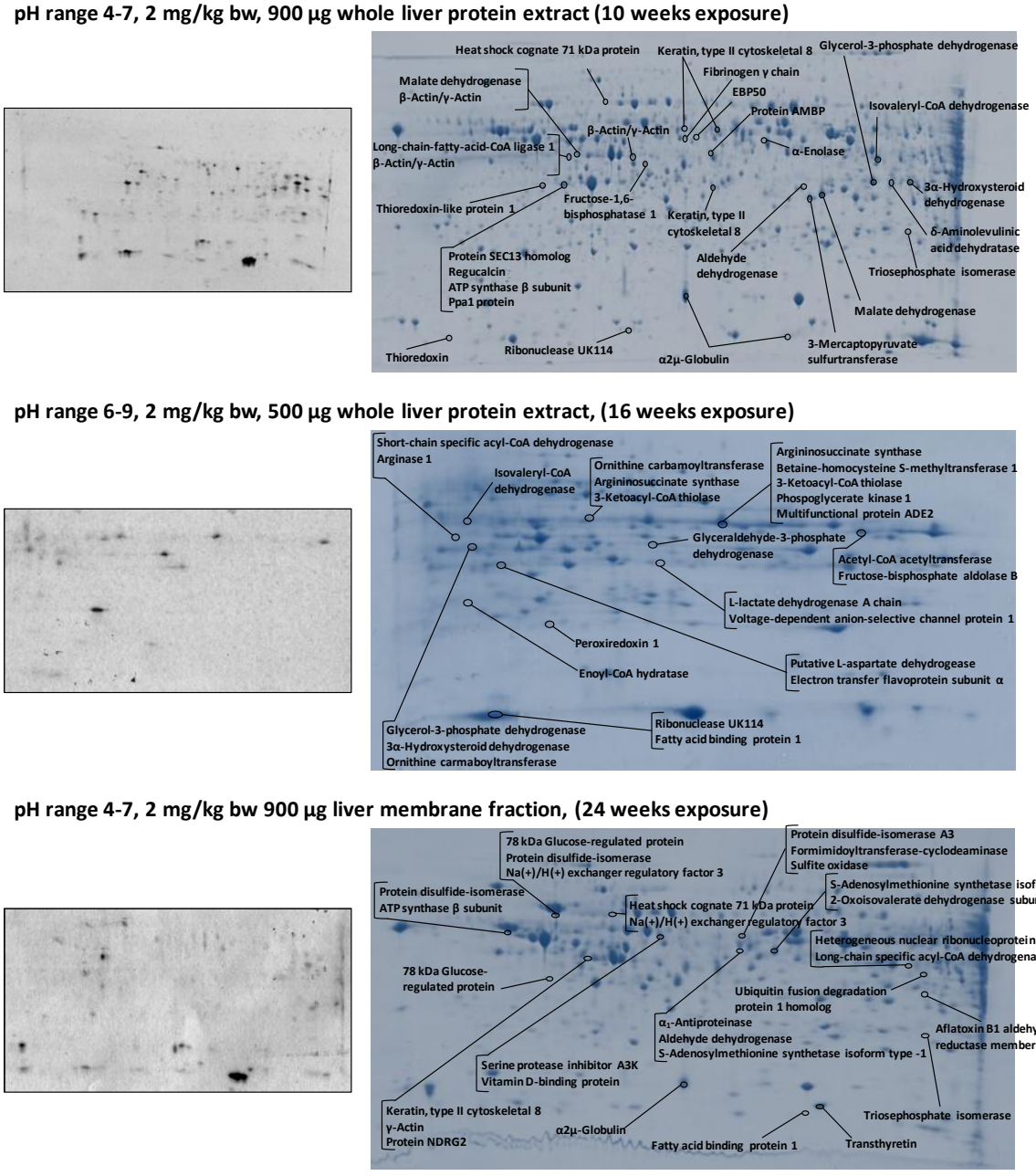

Figure 21 *Putative furan target proteins identified by mass spectrometry following separation by two-dimensional gel electrophoresis and detection by fluorography. EBP50 = ezrin-radixin-moesin-binding phosphoprotein 50*

Table 10 Target proteins of reactive furan metabolites *(continued on next pages)*

*Protein data obtained from Mascot search engine and UniProtKB database following peptide analysis by *FT-ICR (LTQ FT Ultra™, Thermo Fisher Scientific) or +ESI-QTOF-MS/MS (Q-TOF Ultima Global, Waters). Proteins were regarded as identified if present in three different animals, each with a peptide score above the confidence threshold (> 36 or > 43 for samples measured with +ESI-QTOF-MS/MS or *FT-ICR, respectively), a sequence coverage of at least 10 % and at least 2 identified peptides. For proteins identified in more than one spot, data shown represent the maximum scores, sequence coverages, and peptide numbers (derived from the bold and underlined spot). Protein molecular mass (M_r) and isoelectric point (pI) represent the theoretical values. Cs = cytosol, CM = cell membrane, Cp = cytoplasm, Mito = mitochondrion, ER = endoplasmic reticulum, Ck = cytoskeleton, ES = extracellular space, sec = secreted, Nu = nucleus, Ms = microsome, Px = peroxisome. Several proteins are also reported to present targets of [1]mycophenolic acid (Asif et al., 2007), [2]diaminochlorotriazine (Dooley et al., 2008), [3]teucrin A (Druckova et al., 2007), [4]thiobenzamide (Ikehata et al., 2008), [5]bromobenzene (Koen et al., 2007; Koen and Hanzlik, 2002), [6]acetaminophen (Qiu et al., 1998).*

Protein Name	Spot	UniProt ID	M_r [Da]	pI	Protein scores	Sequence coverage [%]	Peptides assigned to protein	Location
Carbohydrate metabolism								
+α-Enolase[1,2,4,5]	27	P04764	47128	6.2	70, 80, 57	17, 13, 12	9,6,7	Cs, CM
*Fructose-bisphosphate aldolase B[1,3,4]	50	P00884	39618	8.7	232, 291, 277	26, 31, 26	8, 9, 10	Cs
+Fructose-1,6-bisphosphatase 1	6	P19112	39609	5.5	88, 115, 38	19, 20, 12	7, 11, 4	Cs
*Glyceraldehyde-3-phosphate dehydrogenase[1,3,4]	52	P04797	35828	8.4	258, 145, 195	28, 20, 19	8, 8, 8	Cs
*L-Lactate dehydrogenase A chain	53	P04642	36451	8.5	90, 101, 80	12, 15, 12	4, 5, 4	Cs
+Malate dehydrogenase[4]	2b, **31**	O88989	36483	6.2	103, 251, 155	22, 31, 24	9, 9, 9	Cs
*Phosphoglycerate kinase 1[2,4,5]	51	P16617	44538	8.0	104, 239, 113	14, 36, 17	4, 11, 5	Cs
*Triosephosphate isomerase[1,2,5]	47, **97**	P48500	26849	6.5	157, 264, 706	15, 41, 81	3, 9, 19	Cs
Lipid metabolism								
*Enoyl-CoA hydratase	64	P14604	31516	6.4	110, 67, 121	13, 13, 19	3, 3, 5	Mito
*3-Ketoacyl-CoA thiolase[3]	**51**, 55	P13437	41871	8.1	159, 223, 160	17, 20, 17	5, 6, 5	Mito
+Long-chain fatty acid CoA ligase 1[3]	2a	P18163	78179	6.6	46, 221, 59	10, 18, 10	7, 12, 7	ER, Mito, Ms, Px
*Long-chain specific acyl-CoA dehydrogenase[1,3]	93	P15650	47873	7.6	71, 291, 731	10, 26, 43	5, 10, 21	Mito
*Short-chain specific acyl-CoA dehydrogenase	59	P15651	44765	8.5	179, 237, 225	20, 31, 23	8, 12, 9	Mito
Amino acid metabolism, urea cycle								
*Arginase 1[4,5]	59	P07824	34973	6.8	145, 157, 108	20, 16, 12	6, 5, 4	Cp
*Argininosuccinate synthase[3]	**51**, 55	P09034	46496	7.6	257, 239, 321	29, 31, 34	19, 18, 21	Mito, ER
*Betaine-homocysteine S-methyltransferase 1[3]	51	O09171	44976	8.0	215, 124, 103	51, 31, 33	14, 10, 10	Cs, CM
*Formimidoyltransferase-cyclodeaminase	83	O88618	58914	5.8	189, 311, 487	14, 23, 39	8, 13, 22	Ck, Golgi
*Isovaleryl-CoA dehydrogenase	33c, **58**	P12007	46435	8.0	201, 141, 97	22, 16, 14	9, 8, 7	Mito
*Ornithine carbamoyltransferase	**55**, 60	P00481	39886	9.1	197, 87, 133	31, 14, 28	10, 5, 9	Mito
*2-Oxoisovalerate dehydrogenase subunit α	85	P11960	50164	7.7	275, 198, 521	29, 18, 45	11, 8, 19	Mito
*S-Adenosylmethionine synthetase isoform type-1	**85**, 86	P13444	43698	5.6	309, 251, 547	31, 34, 50	13, 14, 20	Cs
Redox regulation								
*Electron transfer flavoprotein subunit α[2,3]	61	P13803	34951	8.6	233, 183, 203	31, 36, 31	8, 11, 9	Mito
*Peroxiredoxin-1[4,6]	62	Q63716	22109	8.3	104, 274, 160	41, 57, 47	10, 14, 11	Cs
+*Thioredoxin-1[4,5]	12	P11232	11673	4.8	155, 41, 67	65, 21, 21	8, 2, 2	Cp
+*Thioredoxin-like protein 1	3	Q920J4	32249	4.8	61, 43, 1271	20, 19, 76	5, 6, 27	Cp

Table 10 *(continued)*

Protein Name	Spot	UniProt ID	M_r [Da]	pI	Protein scores	Sequence coverage [%]	Peptides assigned to protein	Location
Protein folding								
*78 kDa Glucose-regulated protein[3,4,5]	**75**, 76	P06761	72347	5.1	2066, 2250, 7714	58, 53, 60	48, 45, 49	ER lumen
*Heat shock cognate 71 kDa protein[1,4,5]	1, **79**	P63018	70871	5.4	168, 407, 922	13, 31, 47	8, 20, 33	Cp
*Protein disulfide-isomerase[4,5]	**74**, 75	P04785	56951	4.8	613, 599, 2787	51, 55, 77	32, 32, 45	ER lumen, CM
*Protein disulfide-isomerase A3[1,2,4,5]	83	P11598	56623	5.9	393, 468, 1222	35, 41, 71	21, 26, 46	ER lumen
Proteolysis								
*α_1-antiproteinase[4]	86	P17475	46136	5.7	333, 311, 1087	33, 36, 52	16, 19, 23	sec
[+]*Protein AMBP: Bikunin and Trypstatin	23	Q64240	38851	5.8	48, 80, 736	10, 21, 69	4, 6, 24	sec
*Serine protease inhibitor A3K	80	P05545	46562	5.3	297, 549, 982	25, 37, 51	12, 14, 25	sec
*Ubiquitin fusion degradation protein 1 homolog	94	Q9ES53	34485	6.3	97, 62, 336	18, 12, 50	6, 3, 17	Nu, Cp
Structural proteins								
[+]β-Actin[1]/ γ-Actin	**2a**, 2b, 5, 78	P60711/ P63259	41737	5.3	75, 121, 117	28, 26, 17	10, 9, 6	Cp, Ck
[+]*Ezrin-radixin-moesin-binding phosphoprotein 50	21a	Q9JJ19	38830	5.7	884, 40, 87	83, 20, 29	31, 6, 10	Cp, CM
[+]Fibrinogen γ chain	21c	P02680	50633	5.9	42, 131, 55	23, 37, 13	9, 14, 7	sec
*Keratin, type II cytoskeletal 8	21b, **24**, 25, 78	Q10758	54019	5.8	3254, 122, 1339	90, 19, 78	65, 9, 52	Ck, Cp, Nu
*Na(+)/H(+) exchanger regulatory factor 3	75, **79**	Q9JJ40	56800	5.3	133, 254, 859	20, 30, 59	9, 17, 29	CM
*Protein SEC13 homolog	4	Q5XFW8	35548	5.2	195, 486, 447	24, 35, 64	5, 9, 17	ER, Nu
*Voltage-dependent anion-selective channel protein 1[1]	53	Q9Z2L0	30756	8.4	89, 83, 155	12, 10, 17	3, 3, 5	Mito, CM
Transport proteins								
*α2μ-Globulin[4]	19, 20a, **87**	P02761	20737	5.9	69, 101, 1045	20, 55, 71	4, 10, 17	Cp, sec
*Fatty acid binding protein 1[4,5]	63, **91**	P02692	14273	7.8	52, 99, 243	14, 36, 79	2, 5, 8	Cp
[+]*Protein AMBP: α_1-Microglobulin	23	Q64240	38851	5.8	48, 80, 736	10, 21, 69	4, 6, 24	sec
*Transthyretin[4,5]	92	P02767	15720	5.8	121, 300, 368	37, 52, 73	7, 13, 12	sec
*Vitamin D binding protein	80	P04276	53544	5.8	134, 276, 702	22, 42, 62	10, 18, 29	sec
Nucleotide metabolism								
*Multifunctional protein ADE2	51	P51583	47096	7.9	81, 50, 137	17, 16, 18	7, 8, 9	
*Putative L-aspartate dehydrogenase	61	Q5I0J9	31260	5.5	301, 87, 207	41, 16, 34	11, 5, 10	
*Heterogeneous nuclear ribonucleoprotein H1[2]	93	Q8VHV7	49188	5.9	100, 94, 515	14, 18, 44	6, 7, 16	Nu, Cp

Table 10 *(continued)*

Protein Name	Spot	UniProt ID	M_r [Da]	pI	Protein scores	Sequence coverage [%]	Peptides assigned to protein	Location
Miscellaneous								
*Acetyl-CoA acetyltransferase	50	P17764	44695	8.9	293, 517, 308	36, 44, 36	14, 22, 15	Mito
*Aflatoxin B1 aldehyde reductase member 2	96	Q8CG45	40675	6.3	115, 236, 490	19, 30, 50	5, 10, 16	Cp, Golgi
*Aldehyde dehydrogenase[1,3,5,6]	29, **86**	P11884	56488	6.7	269, 209, 660	26, 20, 49	14, 13, 25	Mito
+3α-Hydroxysteroid dehydrogenase[4,5]	**37**, 60	P23457	37028	6.7	106, 151, 140	22, 39, 29	8, 14, 10	Cp
*ATP synthase β subunit[1,3]	**4**, 74	P10719	56354	5.2	252, 253, 657	24, 23, 35	10, 9, 14	Mito
+δ-Aminolevulinic acid dehydratase	35	P06214	36032	6.3	177, 210, 176	28, 34, 19	10, 12, 7	Cp, ES
*Glycerol-3-phosphate dehydrogenase [NAD+][5]	33b, **60**	O35077	37453	6.2	329, 126, 143	41, 25, 25	16, 10, 10	Cp
+3-Mercaptopyruvate sulfurtransferase	30	P97532	32940	5.9	64, 131, 125	21, 34, 31	7, 11, 9	Cp, Mito
*Ppa1 protein[6]	4	Q499R7	37677	6.4	130, 119, 453	29, 11, 48	9, 4, 19	Cp
*Protein NDRG2	78	Q8VBU2	40779	5.2	158, 162, 344	12, 18, 56	4, 5, 13	Cp
*Regucalcin[5]	4	Q03336	33390	5.4	1109, 1263, 2623	90, 86, 88	42, 30, 37	Cp, Nu
+*Ribonuclease UK114[1,4,5]	**14**, 63	P52759	14303	7.8	2226, 169, 144	96, 34, 26	15, 4, 3	Mito, Cp, Nu. Px, ER
*Sulfite oxidase	83	Q07116	60806	6.3	140, 153, 466	16, 21, 52	8, 11, 22	Mito

Note:

- *β-Actin and γ-actin show 99 % sequence homology and thus in most cases it was not possible to determine which of both was present in the spots.*
- *Protein AMBP is a precursor protein which is synthesized in the liver and is then cleaved into α_1-microglobulin and bikunin/trypstatin, which are secreted separately. These two cleavage products have different functions and thus protein AMBP occurs twice in the protein list (in the groups "proteolysis" and "transport proteins"). Although there are two separate proteins after the cleavage, there is only one common accession number for protein AMBP.*

Comparison of theoretical and experimentally determined molecular masses and isoelectric points of the identified proteins

Most proteins identified showed experimentally determined (estimated from positions on the gel in relation to the protein marker) molecular masses and isoelectric points which were ≤ 10 kDa and ≤ 1.0 different from the theoretical values, respectively (see Annex, Tab. 21). However, in some cases the differences between theoretical and experimentally determined molecular mass values were higher than 10 kDa. In the case of long-chain fatty acid CoA ligase 1, the theoretical molecular mass of 79 kDa strongly differs from the experimentally determined molecular mass of 47 kDa. The reasons for this are not known, but a possible explanation may be that the protein was cleaved during sample preparation or that there are different forms of the protein in the cell. Literature data report the existence of a long-chain fatty acid CoA ligase 1 in Escherichia coli showing molecular masses of 45-50 kDa, but it is unknown whether this protein may also be present in mammalian cells (Kameda et al., 1985). Interestingly, all peptides detected for this protein are located within the first 370 amino acids of the protein sequence, suggesting that a truncated form of this protein was present in the spot.

Several proteins occurred in multiple spots

Analyses of 83 spots yielded only 61 identified proteins. This may in part be due to insufficient sample material in some gel plugs. Especially in the case of the less sensitive QTOF, a small amount of material may lead to failure of protein identification. Furthermore, several proteins were present in more than one spot. This is in line with literature data and is thought to be the result of posttranslational modifications resulting in mobility shifts (Ikehata et al., 2008; Koen et al., 2007; Koen and Hanzlik, 2002; Qiu et al., 1998). The groups of spots containing the same protein were either present on the same gel or on gels derived from different pH ranges or sample preparation methods. For example, S-adenosylmethionine synthetase isoform type-1 was found in spots 85 and 86 (53 kDa, pI 5.8 and 53 kDa, pI 5.7), which were both detected on the gel obtained after protein separation over the pH range 4-7 (membrane fraction). In contrast, heat shock cognate 71 kDa protein was identified in spots 1 and 79 (70 kDa, pI 5.3 and 70 kDa, pI 5.2), which were detected after protein separation over the pH range 4-7 (whole tissue homogenate and membrane fraction). In these cases, the same proteins were present in

spots with the same molecular mass, but slightly different pI values. On the other hand, it is also possible that the same protein occurs in spots with different molecular masses and same pI values, e.g. 78 kDa glucose-regulated protein, which was observed in spots 75 and 76 (70 kDa, pI 5.0 and 42 kDa, pI 5.0).

Several spots contain multiple proteins

It is important to point out that identification of furan target proteins by this approach is considered as tentative and that unambiguous identification requires additional confirmatory experiments, e.g. demonstration of furan-adducted peptides of individual proteins using mass spectrometry. This is particularly evident as a single spot was sometimes found to contain more than one protein, making it impossible to discern which of the proteins present in the spot carries the radiolabel. For example, spot 83 (58 kDa, pI 5.7) was found to contain the three proteins formimidoyltransferase-cyclodeaminase, sulfite oxidase, and protein disulfide-isomerase A3. The phenomenon of comigration of different proteins with similar molecular masses and isoelectric points into one spot is common if the sample is a complex mixture of many proteins and was also described in reports from groups using a similar approach (Koen et al., 2007; Qiu et al., 1998).

Proteins identified using less stringent criteria

In addition to the 61 proteins identified as putative furan target proteins, 37 further proteins were found which did not match the criteria set for protein identification (detected in all high dose animals (n=3), each with a sequence coverage of at least 10 % and at least 2 peptides). These proteins were either positively identified only in two of three high dose animals (both showing sequence coverages > 10 %) or they were detected in all three animals, but showed a sequence coverage < 10 % in one of the animals (see Annex, Tab. 23). These additional proteins were excluded from the detailed analysis, but were used to obtain clues as to which additional pathways may also be affected by covalent protein binding of furan metabolites.

Classes of furan target proteins

Regarding information on the protein properties taken from the Mascot search engine and UniProtKB database, we found that target proteins represent - among others - enzymes, transport proteins, structural proteins, and chaperones which predominantly localize to cytosol and mitochondria and participate in various cellular processes (Tab. 10).

Cysteine and lysine contents of identified furan target proteins

In order to establish whether there are protein properties that favor a protein to become a target for furan metabolites, the cysteine and lysine content of the proteins were determined (see Annex, Tab. 22). The cysteine content ranged from 0.3 to 5.9 % (mean 1.9 %), with two proteins not containing any cysteine residue (cytokeratin 8, ATP synthase β subunit), and the lysine content from 0.7 to 13.4 % (mean 6.9 %), calculated as number of cysteine or lysine residues/total number of amino acids in the protein. Considering that both cysteine and lysine are encoded by two different codons each, the theoretically calculated mean contents of cysteine and lysine in proteins are both 3.3 % (Miseta and Csutora, 2000). However, experimental approaches revealed a mean cysteine content in mammalian proteins of 2.3 % (Miseta and Csutora, 2000), while the mean lysine content of rat proteome was reported to be 5.5 % (Labenski et al., 2009). Thus, it seems that cysteine is underrepresented in the identified furan target proteins, whereas the mean lysine content of the target proteins is higher than average. This is in line with result from bioinformatic analyses which identified protein lysine - but not cysteine - content as a protein feature important to determine if a protein is likely to become adducted by reactive metabolites (Fang et al., 2009). In this respect, it is also interesting to note that some of the metabolites identified in bile and urine of rats treated with furan seem to represent degradation products of protein adducts formed through the reactions of BDA with cysteine and lysine residues in proteins (Hamberger et al., 2010a; Kellert et al., 2008b; Lu et al., 2009).

Commonalities and differences in target proteins of various compounds

Interestingly, 33/61 proteins identified also represent target proteins of other drugs/compounds thought to cause toxicity via reactive metabolite formation. This is of particular interest since establishing commonalities and differences in target proteins of different chemical compounds (and their reactive metabolites) may help to elucidate how covalent binding to proteins may be connected to cytotoxicity. To summarize the current knowledge on target proteins of various compounds and to gain a comprehensive overview of target proteins whose adduction may be involved in cytotoxicity, Hanzlik et al. established a target protein database (Hanzlik et al., 2007). A function of this database is the commonality matrix, which shows the number of target proteins which any two chemicals have in common. To date, the database includes information on the target proteins of 45 chemicals and a total of 352 target proteins (http://tpdb.medchem.ku.edu:8080/protein_database/). The target proteins in the database which are most often reported to be adducted by a compound are 56 kDa selenium-binding protein, 78 kDa glucose-regulated protein, glutathione S-transferase Mu 1, protein disulfide-isomerase, and serum albumin. Interestingly, two of these proteins (78 kDa glucose-regulated protein, protein disulfide-isomerase) were also identified as furan target proteins.

6.3.3 Protein adducts in rat liver following administration of furan at lower dose

In order to assess protein adduction at a lower dose closer to human exposure, liver proteins isolated form rats treated with the low dose of [3,4-^{14}C]-furan (0.1 mg/kg bw) were separated by 2D-GE and fluorography was performed.

Despite longer exposure times used for the detection of radioactively labeled spots on gels derived from low dose animals (30 weeks) as compared to high dose animals (10 weeks), spots on fluorographic films derived from low dose-treated animals were fewer and weaker compared to the spots detected on films obtained from high dose animals. This is consistent with the results obtained using liquid scintillation counting of the protein extracts, where it was shown that the amount of ^{14}C-furan bound to proteins in rat liver after administration of low dose furan was only about 10 % of the amount after treatment with the high dose. However, a similar spot pattern as found in high dose animals was observed on films from low dose animals (Fig. 22). Thus, the target proteins appear to be identical to those identified after high dose furan treatment.

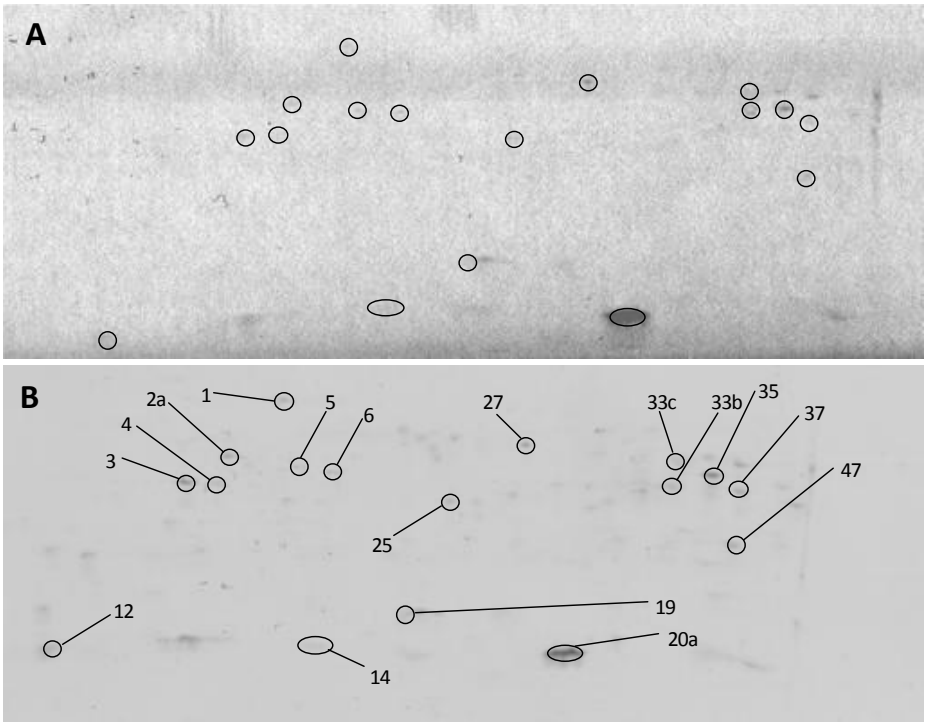

Figure 22 *Spot patterns of furan-adducted proteins obtained by separation of proteins extracts obtained from rats treated with a low dose of ^{14}C-furan (A) as compared to high dose ^{14}C-furan treatment (B). In both cases, similar spot patterns were observed. Proteins identified in the spots:* ***1*** *= Heat shock cognate 71 kDa protein;* ***2a*** *= Long-chain fatty acid CoA ligase 1 and β-Actin / γ-Actin;* ***3*** *= Thioredoxin-like protein 1;* ***4*** *= Regucalcin, ATP synthase β subunit, Protein SEC13 homolog, and Ppa1 protein;* ***5*** *= β-Actin / γ-Actin;* ***6*** *= Fructose-1,6-bisphosphatase 1;* ***12*** *= Thioredoxin-1;* ***14*** *= Ribonuclease UK114;* ***19*** *and* ***20a*** *= α2μ-Globulin;* ***25*** *= Keratin, type II cytoskeletal 8;* ***27*** *= α-Enolase;* ***33b*** *= Glycerol-3-phosphate dehydrogenase;* ***33c*** *= Isovaleryl-CoA dehydrogenase;* ***35*** *= δ-Amiolevulinic acid dehydratase;* ***37*** *= 3α-Hydroxysteroid dehydrogenase;* ***47*** *= Triosephosphate isomerase*

6.3.4 Protein binding in the non-target organ kidney

Since liquid scintillation counting revealed that covalent binding of furan to proteins is not restricted to the target organ of furan carcinogenicity (liver) but also occurs in the non-target organ kidney, we were interested if similar patterns of adducted proteins may be detected in both organs.

Comparison of the Coomassie Blue-stained 2D-gels suggested differential protein expression in liver and kidney tissue. In agreement with results from liquid scintillation counting, also films obtained from kidney tissue showed radioactive spots containing adducted proteins. Similar to the films derived from liver tissue of low dose treated animals, most spots on the fluorographic films obtained from kidney tissue were less intense than spots on films from liver tissue, although the exposure time for the kidney sample was about three times the exposure time for the liver sample. This is in line with the finding that the amount of radiolabeled furan covalently bound to proteins is around

3-4 fold higher in liver than in kidney tissue. Some but not all spots which were detected on films derived from liver tissue were also observed on films from kidney tissue (Fig. 23). Thus, it seems that liver and kidney share several target proteins.

Even though it appears that in both tissues similar proteins may be adducted, effects of furan administration on liver and kidneys were found to be quite different. While toxic lesions in rat liver tissue were already observed after 0.12 mg/kg bw furan p.o. for 90 days, microscopic examination of kidney tissue showed no signs of nephrotoxicity under these conditions (Gill et al., 2010). Statistically significant toxic kidney lesions were found only after furan high dose exposure (60 mg/kg bw) over 13 weeks (NTP, 1993). A possible explanation for this finding may be that the level of protein adduction in liver tissue was found to be about three times higher than in kidney tissue (6.3.1), suggesting that a higher amount of protein binding may result in increased toxicity.

Moreover, furan treatment at 2 mg/kg bw for 2 years was reported to induce hepatocellular adenomas and carcinomas as well as cholangiocarcinomas, whereas no tumors were observed in kidneys (NTP, 1993). This may also be due to different levels of protein adduction in both tissues.

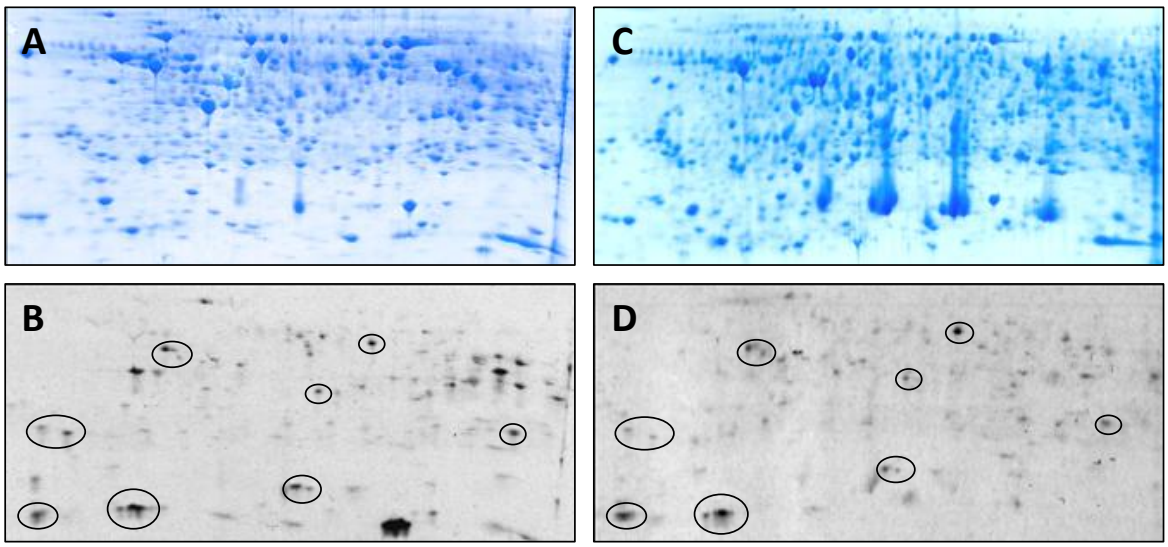

Figure 23 *Representative images of Coomassie Blue-stained gels obtained after protein separation by two-dimensional gel electrophoresis (pH range 4-7) (top) and their corresponding fluorographic film images (bottom) obtained from target organ liver (A, B) and non-target organ kidney (C, D). For analyses, protein extracts (900µg protein) from high dose animals (2 mg/kg bw) were used and the films were exposed to the gels for 10 weeks (liver) and 28 weeks (kidney). Apparently common spots between the films from both organs are marked with circles.*

6.3.5 Furan distribution in rat liver after oral administration of [3,4-^{14}C]-furan

In contrast to the hypothesis that different responses to furan treatment in liver lobes may be caused by diffusion from the stomach leading to high concentrations along the subcapsular surface of furan target lobes, no regions with higher concentrations of ^{14}C-labeled furan were observed in our study (Fig. 24). This suggests that under the conditions used in this study (single oral dose of 0.8 mg/kg bw and sacrifice 2 hours after administration) furan is evenly distributed across all liver lobes.

Alternatively, it was hypothesized that inter- and intralobular differences in liver perfusion or vascular lesions constricting blood supply may play a role in locally different susceptibilities of liver lobes to toxic furan effects (Mally et al., 2010). Interestingly, fibrinogen γ chain (FGG) was also identified as furan target. It was reported that mutations of FGG and subsequent exchange of an amino acid can result in malfunction of important FGG binding sites, leading to dysfibrinogenemia and an increased risk of thrombosis (Robert-Ebadi et al., 2008) (see paragraph on FGG in 8.3.3.6). Hence, binding of furan metabolites to FGG which may result in blocking of important binding sites of fibrinogen, may also increase the risk of thrombus formation. The occurrence of blood clots in small vessels and their resulting obstruction may lead to locally different blood flows. Thus, loss of function of FGG through furan adduct formation may represent a link between protein binding and the phenomenon of locally different susceptibility of liver lobes to furan toxicity.

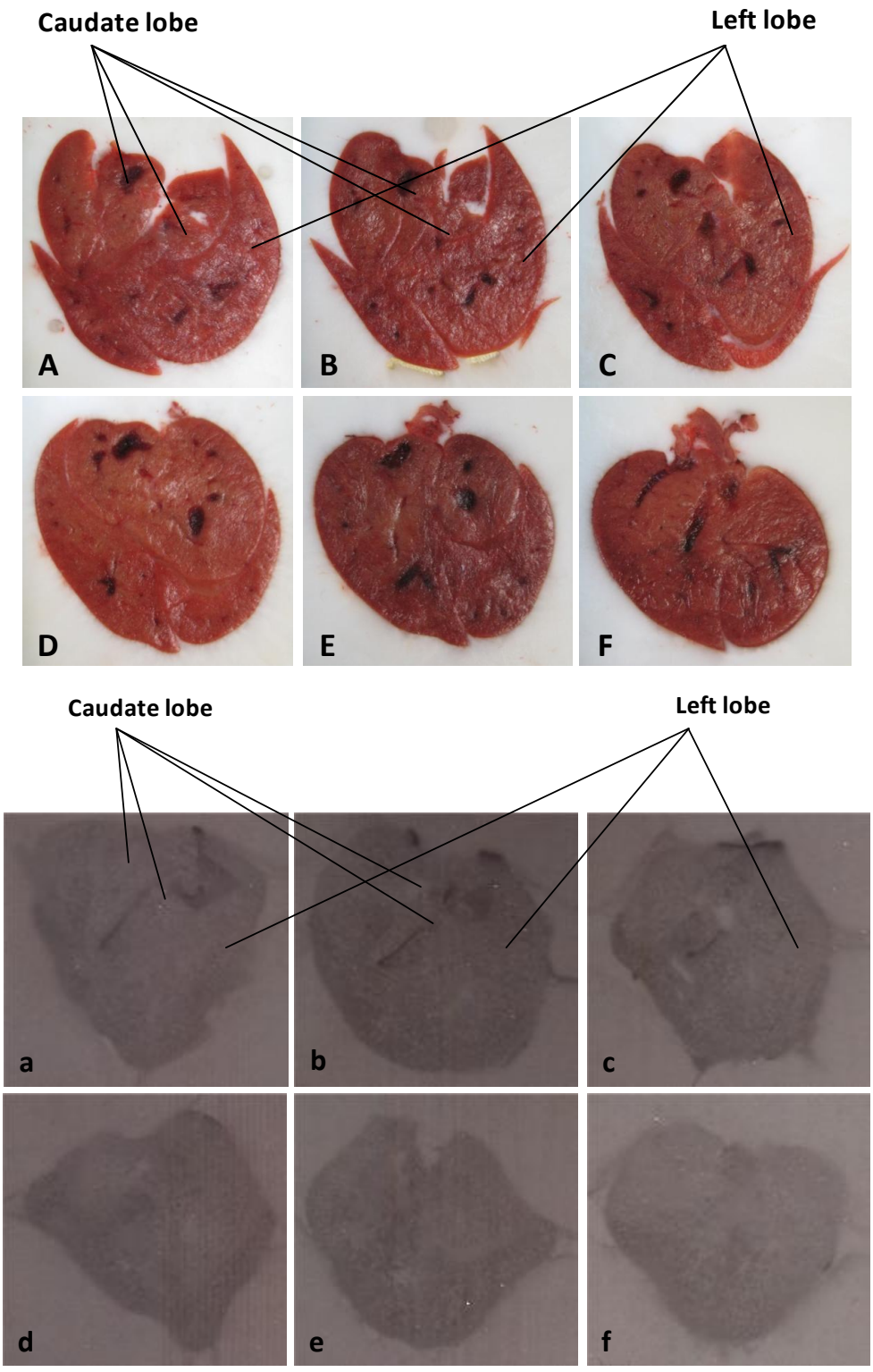

Figure 24 *Images of liver slices (A-F) and their corresponding autoradiographic images (a-f). The slices are shown in the order from dorsal to ventral (A-F and a-f), i. e. slice A is closest to the bottom and slice F is closest to the top of the casted tissue block. Furan appears to be evenly distributed over the whole liver.*

6.4 Conclusions

Liquid scintillation counting of protein extracts from rats treated with [3,4-^{14}C]-furan revealed a dose-dependent increase in the amount of radiolabeled compound covalently bound to proteins in both target (liver) and non-target (kidney) tissue of furan carcinogenicity. However, furan covalent protein binding occurred to a lesser extent in kidney than in liver tissue. Consistent with these results, fluorographic analysis of two-dimensional gels showed the presence of adducted proteins in both liver and kidney tissue. Furthermore, similar spot patterns but lower levels of overall protein adduction were observed in kidney tissue (as compared to liver tissue) and after administration of furan at the lower dose of 0.1 mg/kg bw (as compared to 2 mg/kg bw).

Separation of whole liver extracts and liver membrane fractions by two-dimensional gel electrophoresis and subsequent detection of radioactive protein adducts by fluorography led to the identification of 61 putative furan target proteins of furan reactive metabolites by mass spectrometry and Mascot database search. The identified proteins are derived from various cellular compartments, mainly mitochondria and cytosol, and serve various cellular functions.

From the 61 putative furan target proteins, 33 proteins also represent targets of other compounds known to form reactive metabolites. Gathering information on commonalities and differences in target proteins of various compounds, which are assumed to cause toxicity via reactive metabolite formation and subsequent protein binding, may help to elucidate mechanisms of toxicity.

In contrast to the hypothesis that the reasons for the different toxic responses to furan in rat liver lobes were due to locally different furan concentrations after oral administration (Hamadeh et al., 2004; Metzger and Schywalsky, 1992), furan appeared to be evenly distributed over all areas of the different liver lobes in our study.

7 CELLULAR AND FUNCTIONAL CONSEQUENCES OF FURAN PROTEIN BINDING IN RAT LIVER

7.1 Introduction

Furan administration at 2 mg/kg bw for 2 years was found to induce hepatotoxicity and liver tumors in rats (NTP, 1993), but the mechanisms involved are still poorly understood. Our study using radiolabeled furan revealed covalent furan binding to proteins at a level of approximately 1 adduct per 100 molecules of protein (calculated for a 25 kDa protein) in rat liver after administration of the known carcinogenic furan dose of 2 mg/kg bw (6.3.1). For a comprehensive understanding of molecular events which may link furan protein binding to the toxicity and carcinogenicity of furan, characterization of the cellular and functional consequences of furan administration is needed. For this purpose, a subacute toxicity study was conducted with rats receiving furan at a known carcinogenic dose (2 mg/kg bw) and at doses closer to estimated human exposure (0.1 and 0.5 mg/kg bw). In addition, also samples from a study using furan high dose (30 mg/kg bw) treatment were examined. Since furan administration at this dose was reported to cause extensive hepatotoxicity (Hickling et al., 2010a), it would be expected that the induced effects may be more pronounced than after the relatively low doses used in the subacute toxicity study.

A possible link between furan protein binding and the toxicity and carcinogenicity of furan may be reflected by activation of the unfolded protein response (UPR). Protein function requires proper folding of proteins, which is established and maintained by the endoplasmic reticulum (ER). It is well known that protein adduction by reactive metabolites, e.g. the furan metabolite BDA, may compromise the three-dimensional protein structure and may thus lead to accumulation of misfolded and nonfunctional proteins. To cope with accumulated proteins and to prevent toxicity associated with impaired protein function, cells may respond by activating the UPR. Activation of the UPR leads to increased transcription of genes encoding chaperones and components of the ER-associated degradation (ERAD) machinery, thereby increasing the cells capacity to recognize misfolded proteins and repair or target them for degradation by the proteasome. However, if the ER folding capacity is overwhelmed and homeostasis cannot be maintained, cell death may occur.

At present, three different sensors of ER stress have been identified, namely inositol-requiring protein-1 (IRE1), protein kinase RNA (PRK)-like ER kinase (PERK) and activating transcription factor-6 (ATF-6) (Ron and Walter, 2007). Upon activation, these sensors transmit their signal from the ER to the nucleus (via the Golgi and/or cytoplasm), resulting in transcription of unfolded protein response (UPR) target genes (Fig. 25). Activation of these signaling pathways is regulated in part by the chaperone glucose-regulated protein 78 (GRP78; BiP). Direct binding of misfolded proteins to BiP or the lumenal domain of IRE1 is thought to release BiP from IRE1, leading to oligomerization and autophosphorylation of IRE1, and subsequent cleavage of X-box binding protein-1 (XBP1) mRNA via IRE1 endoribonuclease activity. Spliced XBP1 protein translocates to the nucleus where it functions as a potent transcription factor and key regulator of the UPR (Ron and Walter, 2007). Thus, splicing of XBP1 mRNA and expression of UPR target genes function as indicators of ER stress and UPR (Samali et al., 2010) and were used in this study to determine if protein binding by furan triggers the UPR in rat liver.

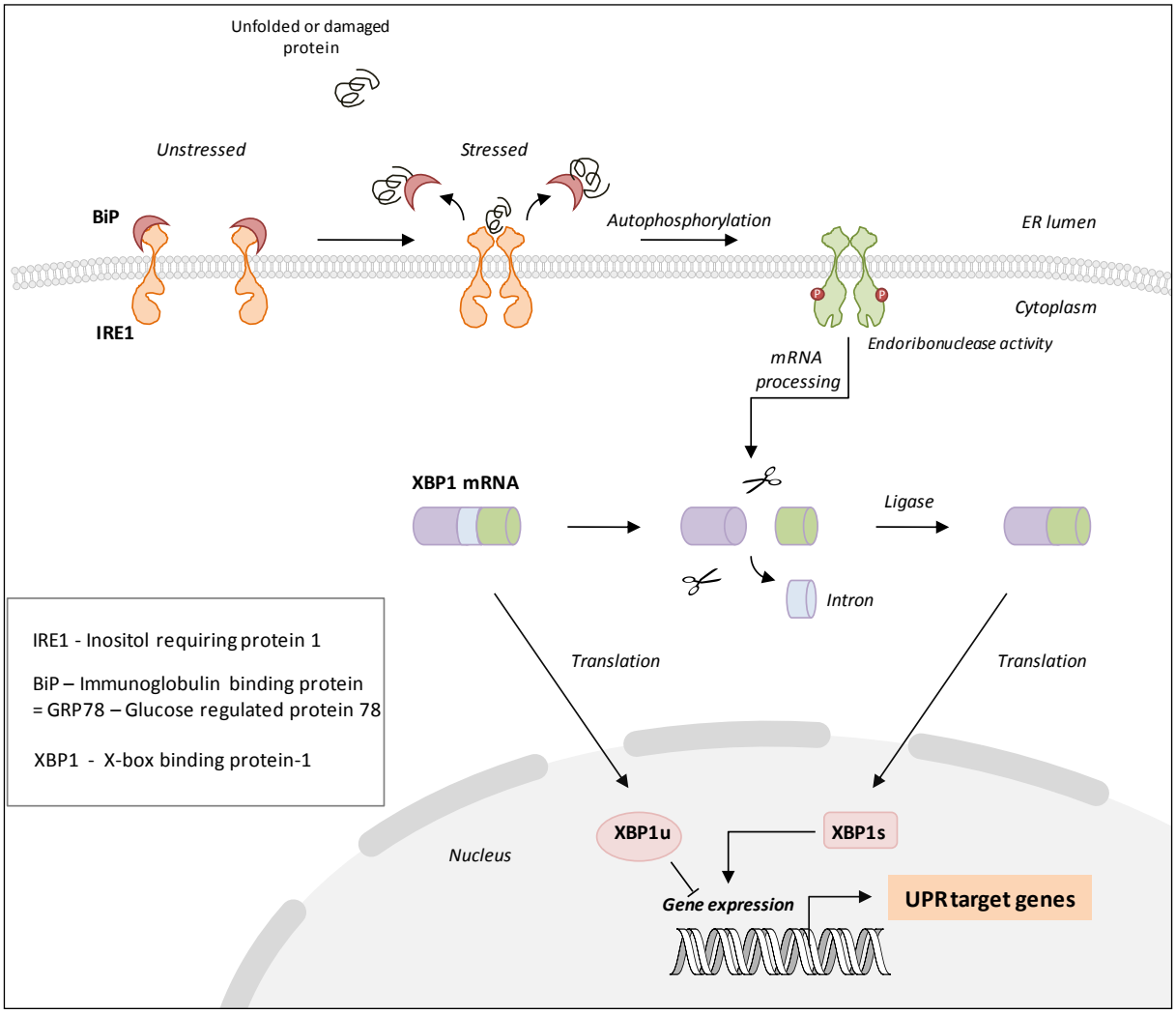

Figure 25 *UPR signaling via the ER stress sensor IRE1 (modified from Ron and Walter, 2007).*

7.2 Methods

7.2.1 Housing and treatment of animals

Male Fischer F344/N rats (aged 5-7 weeks on arrival, Harlan-Winkelmann GmbH, Borchen, Germany) were housed at standard laboratory conditions (climate cabinets, temperature 22 ± 2 °C, relative humidity 30-70 %, 12-15 air changes per hour, 12 hours light/dark cycle) in groups of 5 in Makrolon® type-4 cages with wire meshtops and standard softwood bedding. Rats received pelleted standard rat maintenance diet and tap-water ad libitum. After 2 weeks of acclimatization, animals received furan in corn oil (4 ml/kg bw) by gavage five days a week (Fig. 26). To assess furan toxicity at a known carcinogenic dose (2 mg/kg bw) and at lower doses closer to estimated human exposure, 4 dose groups of 0.0 mg/kg bw, 0.1 mg/kg bw, 0.5 mg/kg bw, and 2.0 mg/kg bw were used. Rats were transferred into metabolic cages for 24 hours prior to sacrifice to collect urine.

Viability, mortality, and clinical signs were recorded daily, body weights twice a week, and food and drinking water consumption weekly. After 5 days, 4 weeks or 6 weeks (4 weeks treatment + 2 weeks recovery), rats were anesthetized with CO_2 and sacrificed by cardiac puncture. The livers were removed, aliquoted, flash frozen in liquid nitrogen and stored at -80 °C or fixed in formalin and embedded in paraffin.

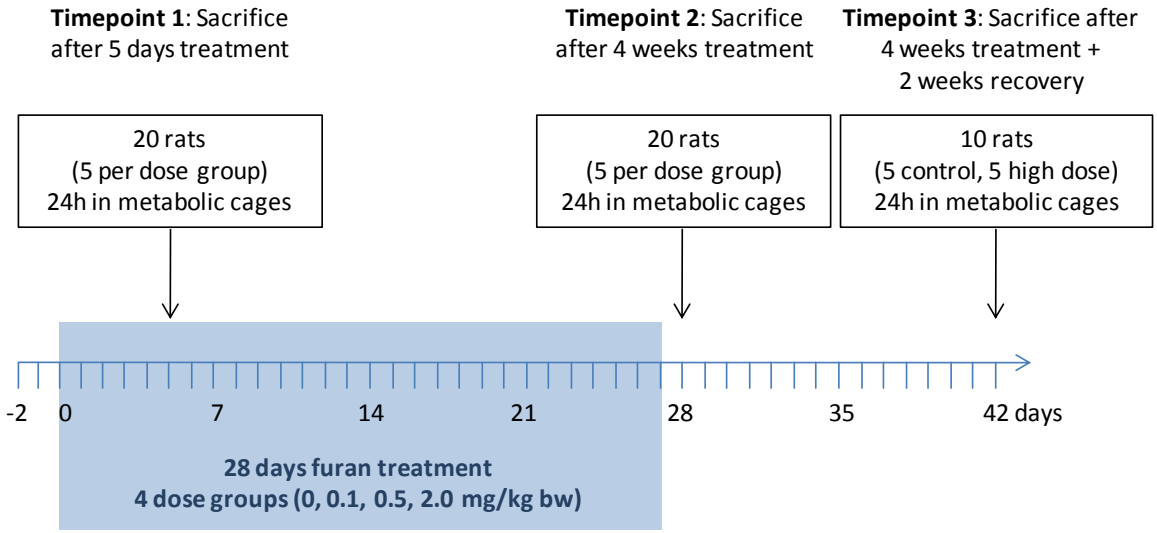

Figure 26 *Study design for the 28 days oral toxicity study.*

7.2.2 Analysis of clinical chemistry parameters for the assessment of furan hepatotoxicity

Blood and urine were analyzed at the Laboratory for Clinical Chemistry, University of Würzburg, using standard protocols. In urine, nitrite, protein, creatinine, glucose, ketones, urobilinogen, bilirubin, erythrocytes, and leukocytes were measured, while glucose, urea, creatinine, total bilirubin, total cholesterol, triglycerides, aspartate aminotransferase, alanine aminotransferase, lactate dehydrogenase, glutamate dehydrogenase, creatine kinase, alkaline phosphatase, γ-glutamyltransferase, total protein, albumin, globulin, and albumin/globulin ratio were determined in plasma.

7.2.3 Analysis of protein expression

To establish whether administration of furan at low doses causes changes in the expression of protein in liver tissue of furan-treated rats, proteins from the livers of 3 control and 3 high dose animals (2 mg/kg bw, 4 weeks) were divided into 4 subcellular fractions and separated by two-dimensional gel electrophoresis. The obtained gels were stained with silver, and analyzed using Ludesi Redfin3 software.

7.2.3.1 Subcellular fractionation and protein quantification

As described in 6.2.5, the FractionPREP^{TM} Cell Fractionation Kit (Biocat) was used to obtain four subcellular protein fractions (cytosolic, nuclear, membrane/particulate, and cytoskeletal fraction) from each sample. Subcellular fractionation was conducted using the right anterior liver lobes of 3 control and 3 high dose rats (2 mg/kg bw, 4 weeks). After fractionation, 300 µl acetone (-20 °C) was added to 100 µl of each fraction and the samples were left at 4 °C over night for the proteins to precipitate. The next day, the samples were centrifuged at 4 °C for 30 min (10,000 x g, Eppendorf Centrifuge 5403) and the pellets were dissolved in 100 µl sample solution. The protein concentrations of all fractions were determined by 2D Quant Kit as described in 6.2.3. The fractions were stored at –80 °C for further use.

7.2.3.2 Two-dimensional gel electrophoresis

Two-dimensional gel electrophoresis was conducted as described in 6.2.6 with the following changes: Liver protein extracts (subcellular fractions) containing 10 µg protein were diluted with rehydration solution (7M urea, 2M thiourea, 2 % CHAPS, 0.5 % IPG

Buffer pH 3-11 NL, 20 mM DTT, 0.002 % bromophenol blue) to a final volume of 210 µl. Isoelectric focusing was performed using Immobiline DryStrips pH 3-11 NL (11 cm) on a Multiphor II electrophoresis unit equipped with an additional frame (Immobiline Dry Strip Tray), a cooling unit (MultiTemp) and a power supply (Electrophoresis Power Supply EPS 3500) running 3500 V, 1 mA, 5 W, 2.9 kVh in the first step and 3500 V, 1 mA, 5 W, 9.1 kVh in the second step. After equilibration, for the second dimension two equilibrated IPG strips from the same subcellular fraction, one of a control and one of a high dose animal, were used on one ExcelGel SDS 2-D Homogeneous 12.5 (Fig. 27).

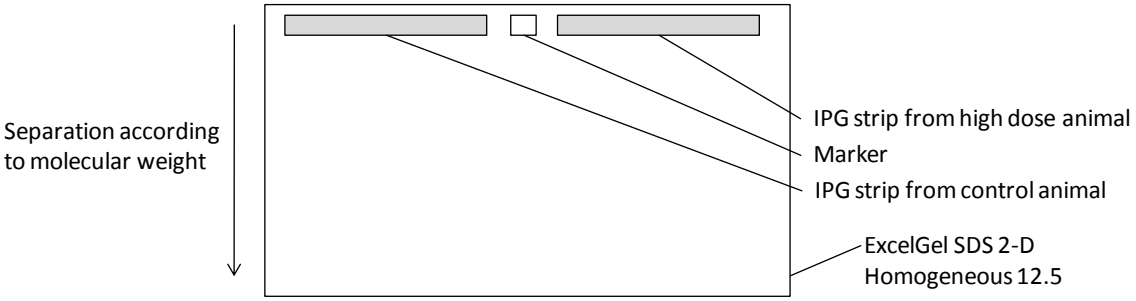

Figure 27 *Schematic view of positioning strips and marker on ExcelGel SDS 2-D Homogeneous 12.5 when two immobiline pH gradient (IPG) strips were used for the second dimension.*

7.2.3.3 Silver staining of protein gels

- **Fixing solution:** 125 ml deionized water, 100 ml ethanol, 25 ml acetic acid glacial
- **Sensitizing solution:** ethanol 75 ml, sodium thiosulfate (5 % w/v) 10 ml, sodium acetate 17 g, deionized water to 250 ml, before use 1.25 ml glutardialdehyde (25 % w/v) was added
- **Silver solution:** silver nitrate solution (2.5 % w/v) 25 ml, deionized water to 250 ml
- **Developing solution:** sodium carbonate 6.25 g, deionized water to 250 ml, before use 0.2 ml formaldehyde (37 % w/v) was added
- **Stop solution:** 3.65 g EDTA-Na_2•$2H_2O$, deionized water to 250 ml
- **Washing solution:** deionized water
- **Preserving solution:** glycerol (87 % w/w) 25 ml, deionized water to 250 ml

The gel was soaked in fixing solution for 30 min and washed three times in deionized water for 5 min. The sensitizing solution was added, the gel was left shaking for at least 30 min and was washed three times in deionized water for 10 min. The silver solution was added, the gel was left shaking for 20 min, and was rinsed twice in deionized water for one minute. After addition of the developing solution, the gel was left shaking for 3 min

and was transferred to the stop solution once the spots had reached the desired intensity. The gel was left shaking in the stop solution for 10 min. Deionized water was added and the gel was washed three times for 5 min. To prevent the gel from drying and cracking, the preserving solution was added and the gel was left shaking for 20 min. The gel was then shortly dried and scanned on a HP ScanJet 5550C flatbed scanner to obtain digital images. After the procedure, the gel was wrapped in plastic foil and kept at 4 °C.

7.2.3.4 Protein expression analysis

To establish whether the expression of proteins was altered through treatment with furan for 4 weeks, the silver stained images were analyzed using Ludesi Redfin3 software. For this purpose, the scanned gel images were converted into grey scale and uploaded into the online analyzing program. The software measured and compared the densities of the single spots between treated and control samples. The following settings were used for analysis: fold change ≥ 1.5, p-value ≤ 0.05, presence 100 %, and volume ≥ 1000.

7.2.4 Effect of furan treatment on the unfolded protein response

7.2.4.1 Samples used for analysis of the unfolded protein response

Frozen tissue from the caudate liver lobes of control and high dose animals (0 or 2 mg/kg bw, 4 weeks) derived from the 28 days oral toxicity study (7.2.1) were used for analysis.

Additional liver samples (caudate liver lobes) from an acute oral toxicity study on furan were kindly provided by H. Hoffmann (Hoffmann, 2010). In this study, male Fischer F344/N rats (200-250 g on arrival, Harlan-Winkelmann GmbH, Borchen, Germany) were housed in groups of 4 in Makrolon® type-4 cages with wire meshtops and standard softwood bedding at standard laboratory conditions (climate cabinets, temperature 22 ± 2 °C, relative humidity 30-70 %, 12-15 air changes per hour, 12 hours light/dark cycle). Rats received both pelleted standard rat maintenance diet and autoclaved tap-water ad libitum. After acclimatization, animals received a p.o. single dose of furan (30 mg/kg bw) in corn oil (4 ml/kg bw) or vehicle only. At sacrifice (24 hours post-dose), blood samples were taken by cardiac puncture and the livers were removed, separated into the different lobes and stored until further use. Plasma was analyzed at the Laboratory for Clinical Chemistry, University of Würzburg, using standard protocols. Moreover, light microscopic evaluation of liver slices stained with hematoxylin and eosin was performed.

7.2.4.2 Isolation of RNA from liver tissue using the RNeasy® Mini Kit

Isolation of the RNA was conducted using the RNeasy® Mini Kit, which is based on binding of RNA to the silica membranes of the RNeasy® Mini Spin Columns.

- **RNeasy® Mini Kit** (Qiagen): before use 300 µl β-mercaptoethanol is added to 30 ml RLT buffer (lysis buffer)
- **RNase-Free DNase Set** (Qiagen)**:** for preparation of the DNase I solution, 121 µl DNase I stock solution (1500 units in 550 µl DEPC-H_2O) is mixed with 847 µl digestion buffer (RDD buffer)

From each sample, 100 mg frozen tissue was homogenized in 2 ml lysis buffer (RLT buffer; contains guanidine thiocyanate) including β-mercaptoethanol in a manual tissue homogenizer. The chaotropic agent guanidine thiocyanate supports the cell lysis and, together with β-mercaptoethanol, protects the mRNAs by inactivation of mRNA-degrading enzymes (RNases) through reduction of their protein thiol groups. The homogenates were transferred into autoclaved Eppendorf caps and kept on ice until centrifugation for 10 min at 8000 rpm and 4 °C. The supernatant (350 µl) was transferred into autoclaved Eppendorf caps and 350 µl ethanol 70 % (RNase free) was added to increase the affinity of the mRNA to the column material and mixed by pipetting several times. The whole volume was transferred to a RNeasy® Mini column, the columns were centrifuged for 15 seconds at 11000 rpm and the collected liquid was discarded. As a washing step, 350 µl RW1 buffer (contains ethanol and guanidine thiocyanate) was added, the columns were centrifuged for 15 seconds at 11000 rpm and the liquid was discarded. DNase I solution (80 µl) was pipetted to the column to degrade remaining DNA, which would disturb the analyses of mRNA. The columns were then incubated for 15 min at room temperature. RW1 buffer (350 µl) was added to wash away the degraded DNA and the DNase I, the columns were centrifuged for 15 seconds at 11000 rpm and the liquid was discarded. The columns were placed into fresh tubes and a further washing step was conducted with 500 µl RPE buffer. After centrifugation of the columns for 15 seconds at 11000 rpm, the liquid was discarded. In the next step, 500 µl RPE buffer was added, the columns were centrifuged for 2 min at 11000 rpm, and the liquid was discarded. The columns were placed into fresh tubes and centrifuged for 1 minute at 14000 rpm to remove the remaining washing buffers from the columns. To elute the mRNAs, the columns were placed into fresh tubes and 30 µl RNase free water was added.

After incubating the columns for 1 minute at room temperature, they were centrifuged for 1 minute at 11000 rpm. The RNA content of the obtained liquid containing the isolated mRNAs was measured using a Nanodrop 2000C (Thermo Fisher Scientific) and a sample volume of 2 µl. The samples were stored at -80 °C until further use.

7.2.4.3 cDNA synthesis using the Verso™ cDNA Kit

The obtained RNA was transcribed into cDNA using the Verso™ cDNA Kit (Thermo Fisher Scientific). This kit contains Verso™ Enzyme Mix, which consists of Verso™ Reverse Transcriptase (RT) to synthesize cDNA strands and RNase inhibitors for protection of the template mRNA against degradation. Furthermore, cDNA synthesis buffer (5 x) for optimal reaction conditions, RT enhancer for removal of contaminating DNA, random hexamer (400 ng/µl), and dNTP mix are included in the kit.

Each sample was diluted with DEPC-H_2O to a concentration of 1 µg RNA in 11 µl. In order to obtain no-enzyme control (= RT control) samples, several samples were pooled: From each sample of control and treated rats (24 hours oral toxicity study) 0.9 µl was taken and 5.6 µl DEPC-H_2O was added (= RT_A), while from each sample of control and high dose rats (28 days oral toxicity study) 0.9 µl was taken and mixed with 5.6 µl DEPC-H_2O (= RT_B). Furthermore, a water control (= no-template control) was included consisting of 11 µl DEPC-H_2O without any RNA. To the 11 µl of sample or control, 1 µl random hexamer was added and the solutions were mixed by inverting. The samples were placed in the thermocycler (PTC-200™ Programmable Thermal Controller MJ) for 5 min at 70 °C for annealing of the hexamers and were then kept on ice. 8 µl Mastermix (containing 4 µl cDNA synthesis buffer (5 x), 2 µl dNTP mix, 1 µl RT enhancer, and 1 µl Verso™ Enzyme Mix) was added to the samples and the water control and mixed well by pipetting. To the RT controls, the components of the Mastermix were added in the same way, except that DEPC-H_2O was added instead of Verso™ Enzyme Mix so that no reverse transcriptase was present. Thus, no cDNA is produced and hence no PCR products should appear in later analyses unless the sample is contaminated. Also in the water control no PCR product should be visible since no RNA had been present as template. The samples and controls were placed in the thermocycler (PTC-200™ Programmable Thermal Controller MJ) and cDNA synthesis was conducted applying 47 °C for 50 min, 95 °C for 2 min, and then

cooling down to 4 °C. The thermocycler kept the samples at 4 °C until they were taken out of the machine. The cDNA was stored at -80 °C until further use.

7.2.4.4 Detection of XBP1 (X-box binding protein 1) mRNA splicing

Role of XBP1 in the unfolded protein response

An important step in the activation of the unfolded protein response is the cleavage of XBP1 mRNA to the spliced XBP1 mRNA by the cytoplasmic domain (endoribonuclease activity) of inositol-requiring protein-1 (IRE1). The spliced XBP1 mRNA migrates into the nucleus, where it functions as a transcription factor. Thus, the relation between unspliced and spliced XBP1 mRNA can indicate whether the unfolded protein response is activated in the cell. For this purpose, a PCR reaction for amplification of the cDNAs of XBP1 and GAPDH (housekeeping gene) was conducted, followed by separation of the obtained products on an agarose gel.

Principle of the polymerase chain reaction (PCR)

PCR is a fast and sensitive method to exponentially amplify a specific DNA sequence defined by the added primers through several cycles of an enzymatic reaction. One reaction cycle consists of three steps. During the first step (95 °C), the DNA is denatured to completely separate the two strands. Next, there is the hybridization step during which the primers anneal at specific DNA regions, followed by the synthesis step during which the enzyme polymerase specifically synthesizes the part of the DNA strand between the primers from deoxyribonucleotide triphosphates. Thus, the amount of DNA in the reaction mix should double after the completion of each cycle and amplify exponentially. However, the PCR reaction is usually linear during the starting cycles, continues in an exponential way and reaches a plateau at the end of the cycles. This is due to the fact that the activity of the enzyme decreases and the oligonucleotides start to hybridize amongst each other instead of reacting with the primers. Thus, in practice the exponential amplification occurs only at a level of 70-80 % and this reaction kinetic must be taken into account if quantification is conducted.

cDNA amplification by PCR

To detect whether the ratio between unspliced XBP1 mRNA (289 bp) and spliced XBP1 mRNA (263 bp) is altered by furan treatment, the cDNAs have to be amplified by PCR. The cDNAs used for analysis had a concentration of 50 ng/µl and GAPDH was used as a housekeeping gene. A total of 15 samples were examined including 12 cDNA samples obtained from control and furan-treated rats (1-12) and 3 control samples (13-16) (Tab. 11).

- **XBP1 forward (fw) primer** 5'-ccttgtggttgagaaccagg-3' (3 µM)
- **XBP1 reverse (rv) primer** 5'-ctagaggcttggtgtatac-3' (3 µM)
- **GAPDH forward primer** 5'-tgccactcagaagactgtgg-3' (3 µM)
- **GAPDH reverse primer** 5'-ggatgcagggatgatgttct-3' (3 µM)
- **cDNA** (50 ng/µl) of samples 1-12 (Tab. 11)
- **Thermo-Start PCR Mastermix** (2x) (Thermo Fisher Scientific)

Table 11 *Samples used for the detection of XBP1 mRNA splicing in livers of furan-treated rats. RT_A is the no-enzyme control of the pooled samples 1-6; RT_B is the no-enzyme control of the pooled samples 7-12.*

Sample number	Time point	Furan dose
1	24 hours	0 mg/kg bw
2	24 hours	0 mg/kg bw
3	24 hours	0 mg/kg bw
4	24 hours	30 mg/kg bw
5	24 hours	30 mg/kg bw
6	24 hours	30 mg/kg bw
7	4 weeks	0 mg/kg bw
8	4 weeks	0 mg/kg bw
9	4 weeks	0 mg/kg bw
10	4 weeks	2 mg/kg bw
11	4 weeks	2 mg/kg bw
12	4 weeks	2 mg/kg bw
13	No-enzyme control (RT_A)	
14	No-enzyme control (RT_B)	
15	No-template control (DEPC-H_2O)	

Table 12 *Composition of the PCR reaction mixture for the detection of XBP1 mRNA splicing in livers of furan-treated rats.*

Reagent	Volume/tube [µl]
Thermo-Start PCR Mastermix (2x)	12.5
Fw primer (3 µM)	2.5
Rv primer (3 µM)	2.5
DEPC-H_2O	5
Final Volume	22.5

To 22.5 µl PCR reaction mixture (Tab. 12), 2.5 µl cDNA or control was added and mixed by pipetting several times. The samples were then placed in the thermocycler (PTC-200™ Programmable Thermal Controller MJ) and incubated at 95 °C for 4 min. Then 40 reaction cycles followed, each consisting of 95 °C for 30 seconds (denaturating of the DNA strands), 55 °C for 30 seconds (annealing of the primers), and 72 °C for 45 seconds (elongation). After the last cycle, another 7 min at 72 °C were applied for the polymerase to complete the DNA synthesis. The thermocycler kept the samples at 4 °C until they were taken out of the machine. The PCR products were stored at -80 °C until further use.

Separation of the PCR products by agarose gel electrophoresis

- **10x TAE (Tris-Acetate-EDTA) buffer:** 48.4 g Tris-HCl, 11.42 ml acetic acid glacial, 20 ml EDTA (0.5 M) pH 8.0, 900 ml deionized water, the pH was adjusted with HCl (25 %) to pH 8.0, the solution was filled up to 1 liter with deionized water
- **1x TAE buffer:** 100 ml 10x TAE buffer, 900 ml deionized water
- **Gel loading dye**

Gel electrophoresis was conducted at room temperature using an Owl Separation Systems Model B1 connected to a DC Power Supply PS 3000. To prepare a 3.5 % agarose gel, 3.5 g agarose was heated in 100 ml 1x TAE buffer in the microwave until the agarose had dissolved. After a short time of cooling, the liquid gel was cast in a gel form with a 14-well gel comb and was left to cool down and to solidify. Then the cast gel was transferred into a gel chamber. The electrophoresis chamber was filled up with 1x TAE as running buffer until the gel was completely covered by a layer of liquid and the gel comb was removed. For each sample, 10 µl PCR product and 2 µl gel loading dye were mixed and loaded onto the agarose gel. One lane of the gel was used for the marker DNA ladder

(peqGOLD Orange 50 bp). The gel chamber was connected to the power supply and the gel was run at 80 V, 100 mA, and 9 W for 2 hours. After the run, the gel was placed in an ethidiumbromide (EtBr) bath containing 100 µl EtBr solution (1 % in water) in 100ml 1x TAE buffer for 30 min and was scanned with a FluorChemQ imaging system (Cell Biosciences) to obtain digital images.

7.2.4.5 Quantitative gene expression analysis of unfolded protein response target genes using TaqMan® probes

The DNA amplification can be quantified by the use of TaqMan® probes (5' nuclease assay). A TaqMan® probe represents an oligonucleotide that is designed to anneal within the DNA region of interest, i.e. the DNA region specifically amplified by the added primers, and contains a fluorophore covalently bound to its 5'-end and a quencher at the 3'-end. In this experiment, the fluorophore 6-carboxyfluorescein (acronym: FAM) and the quencher dihydrocyclopyrroloindole tripeptide minor groove binder (acronym: MGB) were used. When the probe is bound to the DNA in its original state, the fluorophore and the quencher are close to each other and any fluorescence signal, which is emitted by the fluorophore FAM after excitation, is suppressed by the quencher. During the amplification process, the enzyme DNA polymerase synthesizes the nascent strand and, through its 5' to 3' exonuclease activity, degrades the probe annealed to the DNA template (Fig. 28). After cleavage of the probe, the fragments are displaced from the template, the fluorophore and the quencher become separated, and the quenching effect is lost, thus allowing fluorescence of the fluorophore. The accumulation of the PCR products over time is directly proportional to the increasing fluorescence signals.

To calculate the amount of DNA in a sample, the threshold cycle value (C_t value) is used. The C_t value is defined as the number of cycles required for the accumulated fluorescence signals to exceed the background fluorescence level. The higher the amount of template was in the original sample, the faster, i.e. after less cycles, the C_t value is reached, which means there is an inversely proportional correlation between the C_t value and the amount of template in the sample.

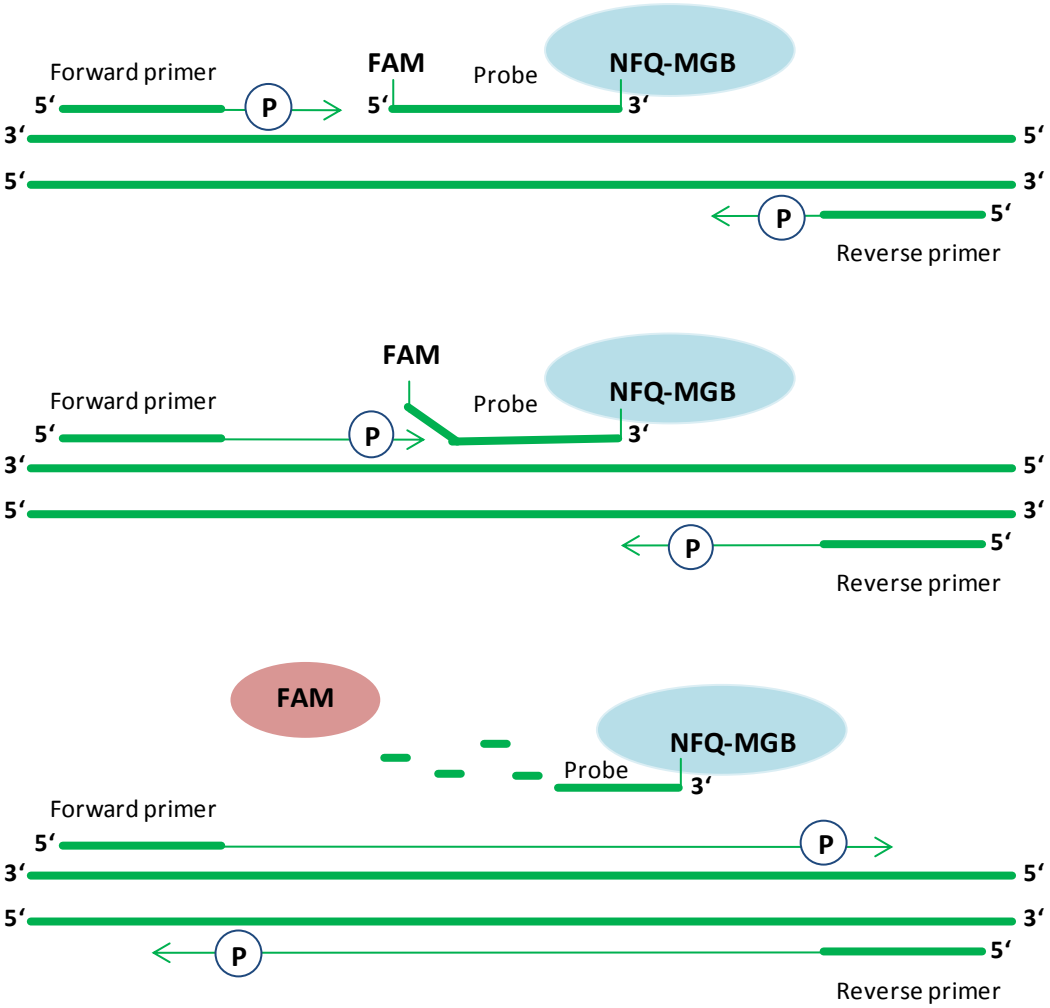

Figure 28 *Principle of quantitative real-time PCR using TaqMan® probes. Figure modified from http://www.hgbiochip.com/images/TaqMan.gif. FAM = fluorophore, NFQ = nonfluorescent quencher, MGB = minor groove binder, P = polymerase*

- **TaqMan® Gene Expression Assay**: Glucose-regulated protein 78 (GRP78); (Rn00565250_m1)
- **TaqMan® Gene Expression Assay**: Homocysteine-responsive endoplasmic reticulum-resident ubiquitin-like domain member 1 protein (Herpud1); (Rn00585371_m1)
- **TaqMan® Gene Expression Assay**: housekeeping gene Glyceraldehyde-3-phosphate dehydrogenase (GAPDH); (Rn99999916_s1)
- **TaqMan® Gene Expression Mastermix**
- **cDNA** (10 ng/µl) of samples 1-12 (Tab. 11)

Real-time PCR analysis was performed as described by Samali et al. 2010 using TaqMan® Gene Expression Assays, which contain two unlabeled primers (20 x stock concentration is 18 µM for each primer) and one specific 6-FAM dye-labeled TaqMan® MGB probe (20 x stock concentration is 5 µM), and TaqMan® Gene Expression Mastermix, which consists of the main components AmpliTaq Gold® DNA Polymerase UP (Ultra Pure) and deoxyribonucleotide triphosphates (dTNPs) (Samali et al., 2010).

The samples used for analysis were the same 15 samples described in 7.2.4.4 (Tab. 11), but were further diluted to a cDNA concentration of 10 ng/µl. In addition, a dilution series of one sample was pipetted diluting 1:1 with DEPC-H_2O every step (from S_1:2 until S_1:32) and included into each PCR run to obtain an internal control for the efficiency of the PCR reaction. According to the scheme (Tab. 14), 2 µl cDNA or control was pipetted into each well of a 96 well plate. 18 µl of the PCR reaction mixture (Tab. 13) was added and was mixed by pipetting several times. The plate was sealed with adhesive foil and transferred into the Roche LightCycler® 480.

Table 13 *Composition of PCR reaction mixtures for the determination of gene expression of GRP78 and Herpud1 in livers of furan-treated rats.*

TaqMan® PCR	Volume/well [µl]
TaqMan® Gene Expression Mastermix (2x)	10
TaqMan® Gene Expression Assay (20x)	1
DEPC-H_2O	7
Final Volume	18

Table 14 *Pipetting scheme used for the TaqMan® PCR analyses with housekeeping gene (rows A-D) and target gene (GRP78 or Herpud1) (rows E-H).*

	1	2	3	4	5	6	7	8	9	10	11	12
A	1	2	3	4	5	6	7	8	9	10	11	12
B	1	2	3	4	5	6	7	8	9	10	11	12
C	1	2	3	4	5	6	7	8	9	10	11	12
D	S_1:2	S_1:4	S_1:8	S_1:16	S_1:32	13	13	13	14	14	14	15
E	1	2	3	4	5	6	7	8	9	10	11	12
F	1	2	3	4	5	6	7	8	9	10	11	12
G	1	2	3	4	5	6	7	8	9	10	11	12
H	S_1:2	S_1:4	S_1:8	S_1:16	S_1:32	13	13	13	14	14	14	15

For analysis, the Roche LightCycler® 480 was run at 95 °C for 10 min to activate the enzyme. Then, 45 amplification cycles, each consisting of 15 seconds at 95 °C (denaturation) and 60 seconds at 60 °C (primer annealing and strand synthesis), were run. For data analysis, the software LightCycler® 480 SW 1.5 (Roche) was used. Gene expression was calculated as fold expression using the $\Delta\Delta$ C_t method. For this relative quantification, a normalization using a housekeeping gene was used. In this respect, it is important that the efficiency of the PCR reactions is the same or at least similar for both the housekeeping and the target gene in the same run. Under ideal conditions (efficiency of 100 %), the amount of template is doubled with every cycle which means the reaction shows an efficiency value of 2. However, in practice values between 1.8 and 2 occur and are regarded as adequate. To ensure that the amplification efficiency of the PCR runs is sufficient and comparable, a standard dilution series of one sample (S_1:2 to S_1:32) was included in every run for both the housekeeping and the target gene. The PCR efficiency was calculated using the standard dilution series and was found to be comparable for housekeeping and target gene in both runs: Values of 1.8 and 1.9 were determined for the runs of GRP78/GAPDH and Herpud1/GAPDH, respectively. Thus, a comparison with the aim to detect changes in gene expression could be conducted.

7.3 Results

7.3.1 Effect of furan on body and organ weights

Oral administration of furan at doses of 0, 0.1, 0.5 and 2 mg/kg bw for 4 weeks had no effect on the consumption of food and drinking water. Furthermore, no clinical signs of toxicity were observed. Determination of body and relative organ weights showed no treatment-related changes (Tab. 15).

Table 15 *Body weight and relative liver weight after furan administration for 4 weeks. Data are expressed as mean ± SD (n = 5/ dose group). Statistical analysis was performed by ANOVA and Dunnett's post-hoc test (*p<0.05, **p<0.01).*

	Furan dose (mg/kg bw)			
	0	0.1	0.5	2
Body weight initial (g)	125.2 ± 6.3	124.8 ± 4.4	126.6 ± 9.8	136.9 ± 5.6
Body weight final (g)	208.5 ± 8.7	207.5 ± 9.7	199.4 ± 13.7	212.6 ± 14.3
Relative liver weight (%)	3.4 ± 0.1	3.2 ± 0.1	3.1 ± 0.04**	3.3 ± 0.1

7.3.2 Effect of furan on clinical chemistry parameters

Furan treatment with 0, 0.1, 0.5 and 2 mg/kg bw had no significant effects on clinical chemistry parameters in plasma or urine except for a small, but dose-dependent increase in plasma cholesterol following 4 weeks treatment with furan, which returned to control levels after a 2 week recovery period (Mally et al., 2010). Furthermore, a slight decrease in glucose and alkaline phosphatase was observed, but these changes were not considered to be toxicologically relevant. No changes in liver enzymes indicative of hepatic injury were observed throughout the study (Tab. 16).

Table 16 *Clinical chemistry after furan administration for 4 weeks. Data are expressed as mean ± SD (n = 5/ dose group). Statistical analysis was performed by ANOVA and Dunnett's post-hoc test (*p<0.05, **p<0.01).*

	Furan dose (mg/kg bw)			
	0	0.1	0.5	2
Glucose (mg/dl)	164 ± 12	153 ± 6	150 ± 12	138 ± 20*
Creatinine (mg/dl)	0.3 ± 0.1	0.2 ± 0.1	0.3 ± 0.1	0.3 ± 0.1
Urea (mg/dl)	30.9 ± 3.0	29.4 ± 1.7	30.3 ± 1.6	34.2 ± 2.4
Total bilirubin (mg/dl)	0.0 ± 0.0	0.02 ± 0.05	0.02 ± 0.05	0.02 ± 0.05
Aspartate aminotransferase (U/l)	134 ± 19	132 ± 36	142 ± 56	168 ± 105
Alanine aminotransferase (U/l)	53.5 ± 5.2	58.8 ± 10.0	67.0 ± 29.2	81.1 ± 57.9
Glutamate dehydrogenase (U/l)	6.4 ± 0.7	7.4 ± 2.0	8 ± 3.2	11.2 ± 7.2
γ-Glutamyltransferase (U/l)	1.6 ± 0.7	2.2 ± 1.6	1.6 ± 0.9	1.9 ± 1.0
Alkaline phosphatase (U/l)	320 ± 35	278 ± 20*	259 ± 6**	264 ± 7.8**
Lactate dehydrogenase (U/l)	303 ± 78	255 ± 155	330 ± 216	457 ± 521
Creatinine kinase total (U/l)	1177 ± 300	982 ± 760	1004 ± 580	1344 ± 1350
Cholesterol (mg/dl)	48.6 ± 3.8	49.4 ± 3.2	53.6 ± 2.7	56.0 ± 3.5**
Triglycerides (mg/dl)	39.4 ± 9.3	59.6 ± 9.6*	53.6 ± 10.6	49.6 ± 7.6
Total protein (g/dl)	6.9 ± 0.2	6.6 ± 0.2	6.7 ± 0.3	6.9 ± 0.2

In contrast to animals which had received furan at doses of 0.1 to 2 mg/kg bw for 4 weeks, rats treated with a single furan dose of 30 mg/kg bw showed a strong increase in the plasma levels of aspartate aminotransferase, alanine aminotransferase, and glutamate dehydrogenase after 24 hours, indicative of substantial liver damage (Tab. 17) (Hoffmann, 2010). Furthermore, γ-glutamyltransferase was found to be elevated in plasma, while alkaline phosphatase and total bilirubin levels remained unchanged.

Table 17 *Clinical chemistry 24 hours after a single dose of furan (30 mg/kg bw). Data are expressed as mean ± SD (n = 4/ dose group). Statistical analysis was performed by unpaired t-test (*p<0.05, **p<0.01).*

	Control	**Furan (30 mg/kg bw, 24h)**
Total bilirubin [mg/dl]	0.0 ± 0.1	0.0 ± 0.1
Aspartate aminotransferase [U/l]	101 ± 16	853 ± 235**
Alanine aminotransferase [U/l]	65 ± 5	874 ± 232**
Glutamate dehydrogenase [U/l]	6 ± 1	800 ± 247**
γ-Glutamyltransferase [U/l]	0.6 ± 0.5	0.9 ± 0.4
Alkaline phosphatase [U/l]	361 ± 26	379 ± 43

7.3.3 Histopathological alterations after furan treatment

Consistent with the lack of effects of furan exposure on plasma transaminases, light microscopic evaluation of H&E (hematoxylin and eosin) stained liver sections did not reveal marked histopathological changes in response to furan treatment (2 mg/kg bw) for 28 days (Fig. 29A) (Mally et al., 2010). However, slight inflammation was observed in subcapsular regions of left liver lobes (Fig. 29C). Few apoptotic cells were seen in the various exposed livers, but at similar frequency as in the control livers.

In contrast, furan administration of 30 mg/kg bw induced extensive degeneration and inflammation within liver parenchyma and subcapsular areas after 24 hours (Fig. 29B, D). Consistent with these results, a similar study in rats using furan doses of 30 mg/kg bw also showed subcapsular and centrilobular necrosis and inflammation already at 24 hours after the first dose (Hickling et al., 2010a).

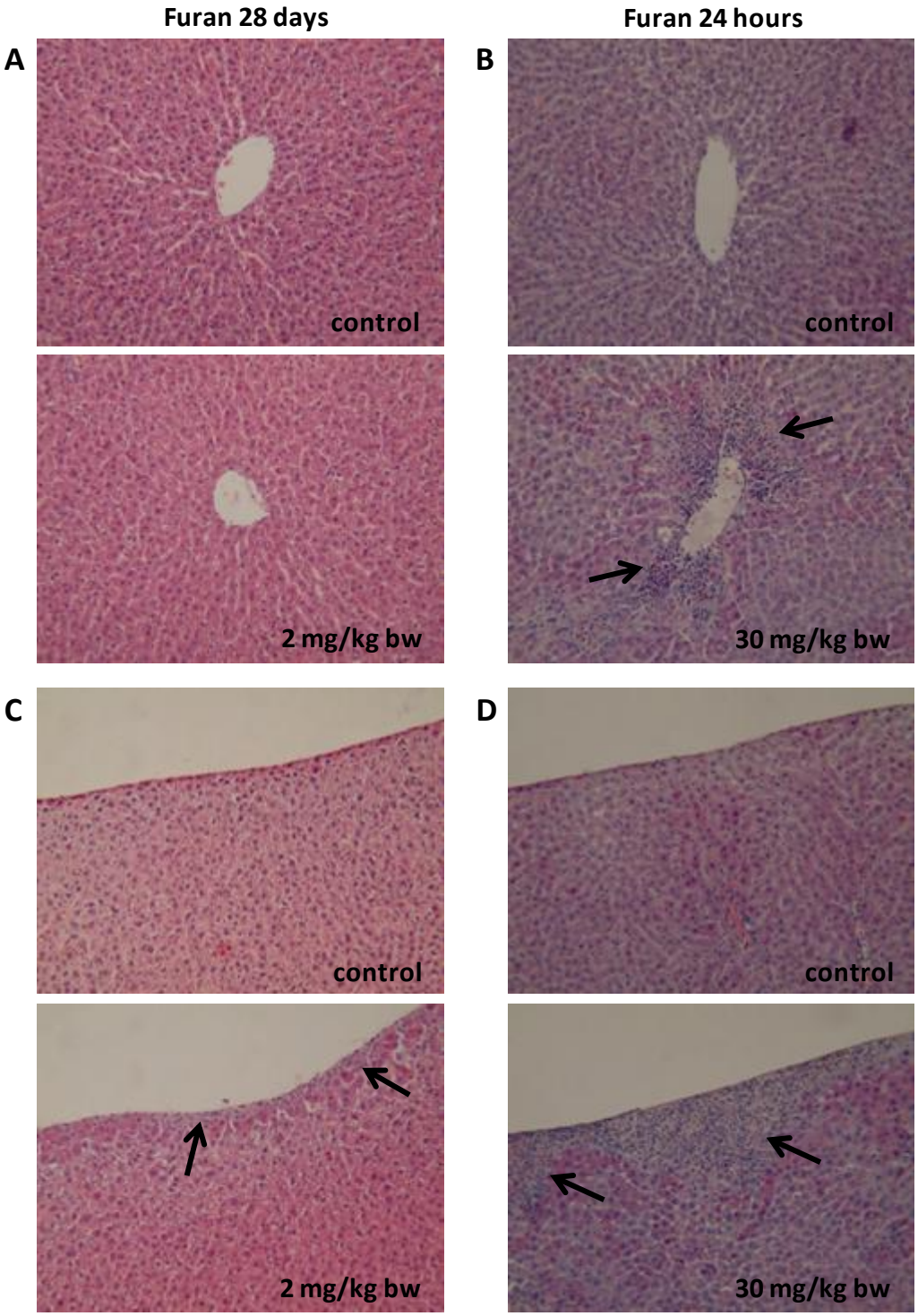

Figure 29 *Rat liver after furan administration (left liver lobes; hematoxylin and eosin stain). Treatment with 2 mg/kg bw furan for 28 days showed no marked treatment-related effects around the central vein (A). In contrast, furan administration of 30 mg/kg bw induced extensive degeneration and inflammation (arrows) in the parenchyma around the central vein after 24 hours (B). While slight subcapsular inflammation (arrows) was observed in livers of rats treated with 2 mg/kg bw furan for 28 days (C), extensive degeneration and inflammation (arrows) was observed in this area after administration of furan (30 mg/kg bw) after 24 hours (D).*

7.3.4 Alterations in protein expression after furan treatment

In good agreement with the overall absence of significant hepatotoxicity, proteomics analysis by 2D-GE did not reveal significant alterations in protein expression in livers of rats treated with furan at doses up to 2 mg/kg bw for 28 days (Fig. 30). For the cytosolic, membrane, nuclear and cytoskeletal fraction 911, 1221, 1061, and 728 protein spots were detected, respectively, none of which showed a significant treatment-related change.

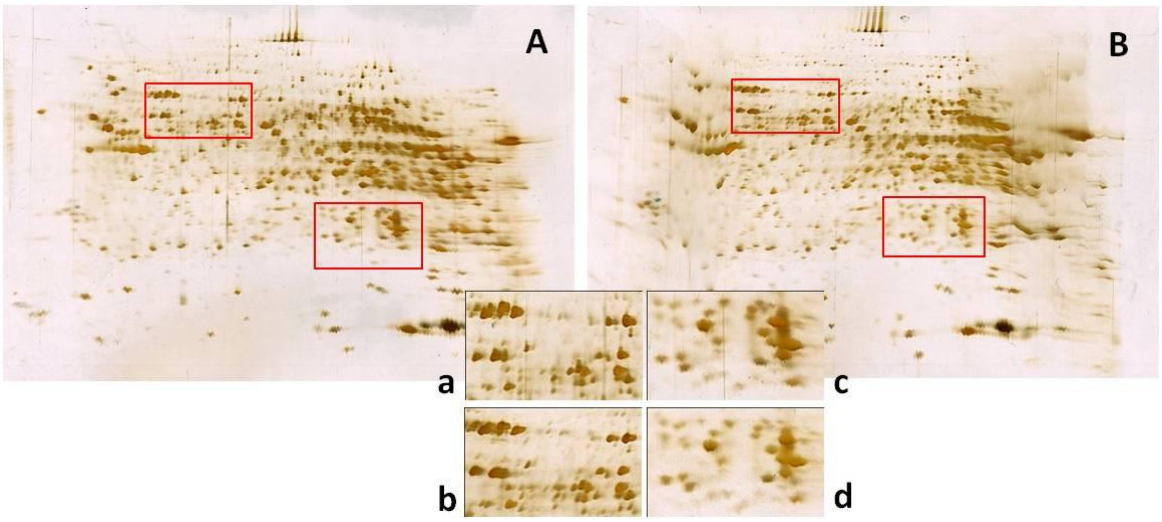

Figure 30 *Gel images of the cytosolic fraction of a control rat (A) and a rat treated with 2 mg/kg bw for 4 weeks (B) and two representative enlarged sections of A (a, c) and B (b, d) as indicated by the red rectangles. No changes in protein expression were evident after furan treatment.*

7.3.5 Impact of furan treatment on activation of the unfolded protein response

Splicing of XBP1 mRNA was analyzed in livers of furan treated rats by semiquantitative RT-PCR using primers designed to detect both unspliced and spliced XBP1 mRNA (Samali et al., 2010). Expression of key UPR target genes encoding GRP78, which we also identified as a protein target of furan, and Herpud1, one of the most highly inducible UPR targets, were analyzed using predesigned TaqMan® assays (Samali et al., 2010). Low levels of spliced XBP1 mRNA were detected in both control and furan treated samples (Fig. 31A). However, no treatment related effects on XBP1 mRNA splicing were evident. Consistent with these findings, gene expression analysis did not reveal upregulation of GRP78 and Herpud1 (Fig. 31B). Thus, under the conditions of our studies, protein binding of furan reactive metabolites does not appear to trigger an unfolded protein response. It is important to note that the unfolded protein response was not found to be activated at the high furan dose of 30 mg/kg bw, which was clearly shown to induce toxic effects in rat

liver, such as increases in liver enzymes indicative of hepatic injury and extensive hepatic degeneration and inflammation.

A

X box-binding protein 1 (XBP1) mRNA splicing

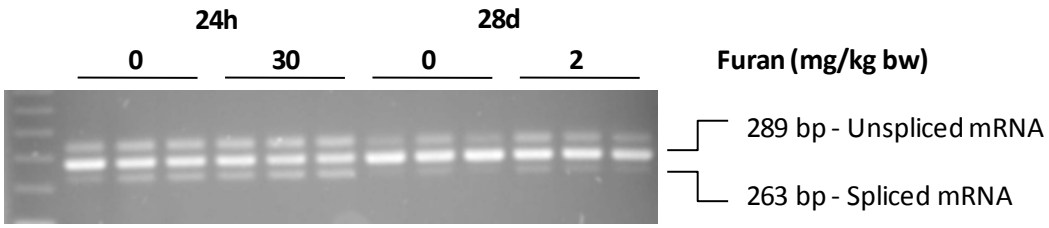

B

UPR target gene expression (TaqMan®)

Furan (mg/kg bw)	Treatment time	UPR target gene expression (fold change relative to controls) GRP78	HERP
0	24h	1.0 ± 0.43	1.0 ± 0.51
30	24h	0.96 ± 0.06	1.02 ± 0.08
0	28d	1.0 ± 0.05	1.0 ± 10
2	28d	0.82 ± 0.15	0.94 ± 0.33

Figure 31 *X-box binding protein 1 (XPB-1) mRNA splicing (A) and expression of unfolded protein response (UPR) target genes (B) in rat liver in response to treatment with furan. No treatment-related changes in either XBP-1 m RNA splicing or UPR target gene expression were evident. GRP78 = 78 kDa glucose-regulated protein, HERP = Herpud1 = homocysteine-inducible, endoplasmic reticulum stress-inducible, ubiquitin-like domain member 1*

7.4 Discussion

A subacute oral toxicity study was conducted to determine the cellular and functional consequences potentially associated with covalent protein binding after administration of a known carcinogenic dose (2 mg/kg bw) and at lower doses closer to estimated human exposure (0.5 and 0.1 mg/kg bw). After 28 days of furan administration, body and organ weight, clinical chemistry parameters, histopathological examination of liver tissue, and analysis of protein expression showed no evidence of hepatotoxic effects except for a slight and reversible increase in plasma cholesterol.

However, further analyses conducted within our group and by our collaborators revealed that furan treatment caused cellular and functional changes indicative of mild hepatotoxicity.

In line with findings that furan administration caused enhanced plasma levels of bile acids in female B6C3F1 mice (Fransson-Steen et al., 1997), furan treatment (2 mg/kg bw) for 4 weeks was found to induce a statistically significant increase of unconjugated bile acids in rat plasma (Mally et al., 2010). Considering the fact that plasma cholesterol was also observed to be slightly increased in this study, this indicates that furan may impair hepatobiliary transport. Since unconjugated bile acids are known to induce necrosis and apoptosis (Palmeira and Rolo, 2004), accumulation of unconjugated bile acids caused by impaired hepatobiliary transport may contribute to cellular injury.

Furthermore, assessment of cell proliferation in subcapsular areas of the left and caudate lobes revealed a statistically significant increase in the number of proliferating hepatocytes in high dose rats (2 mg/kg bw), suggesting that furan treatment may lead to proliferative changes even at doses which do not induce no significant hepatotoxicity. In support of this, an increase in cell proliferation without the occurrence of elevated liver enzymes indicative of hepatic injury was observed in rats after furan treatment with 8 mg/kg bw for 6 weeks (Wilson et al., 1992). In addition, the localization of lesions is consistent with previous studies at higher doses showing necrosis, inflammatory cell infiltration, proliferation and fibrotic changes developing from the subcapsular visceral surface and extending into the parenchyma (Hickling et al., 2010a).

Consistent with the proliferative changes observed after 4 weeks of furan administration, gene expression analysis of rat liver tissue revealed significant alterations in the expression of genes involved in cell-cycle control (Chen et al., 2010). In addition to cell-cycle control genes, also apoptosis-related genes were found to be altered, but in this group the greatest response was at 2 mg/kg bw. In contrast to these two groups of genes, no significant alterations in genes related to DNA damage response were seen at the dose levels used in the 28 days oral toxicity study, indicating that the levels of protein binding observed after treatment with 0.1 or 2 mg/kg bw furan (6.3.1) may not result in oxidative stress. This is in line with the finding that no significant changes on 8-oxo-7,8-dihydro-2´-deoxyguanosine (8-oxo-dG) levels were evident after furan treatment at doses of 2 mg/kg bw and below for 4 weeks (Mally et al., 2010).

Conversely, in a recent study performed with a high dose of furan (30 mg/kg bw) both expression changes of genes associated with DNA damage and increased levels of 8-oxo-dG indicative of oxidative DNA damage were observed (Hickling et al., 2010b).

In addition to the analyses on furan hepatotoxicity, we addressed the question whether protein binding by furan induces activation of the unfolded protein response (UPR) in rat liver. No signs for activation of the UPR were observed after furan administration of 2 mg/kg bw. Since furan treatment at this dose only resulted in slight evidence for toxic effects after 4 weeks, these findings suggest that furan does not lead to significant accumulation of misfolded proteins under these conditions. However, even at a high furan dose (30 mg/kg bw for 24 hours), which clearly showed hepatotoxic effects such as necrosis and inflammation (Hickling et al., 2010a) and which would be expected to induce cellular defense mechanisms, no activation of the UPR was evident in our experiments. Thus, protein adduct formation caused by furan treatment associated with marked hepatotoxicity did not appear to trigger the unfolded protein response. However, this finding may also indicate that cells lack the ability to adequately respond to protein damage and thus cannot activate the unfolded protein response despite the accumulation of damaged proteins. Support for this comes from the fact that loss of function of GRP 78, which was identified as a furan target protein, was reported to increase ER stress-induced cell death, presumably through inhibition of homeostatic responses to ER stress (e.g. UPR) (Martin et al., 2010). Hence, adduction of GRP78 by furan reactive metabolites may disrupt the cellular ability to activate the unfolded protein response, which may result in cell death. These events may play a role in furan-induced carcinogenicity.

7.5 Conclusions

The cellular and functional consequences of subacute furan administration which may be associated with covalent protein binding were determined to establish a link between protein adduct formation and the toxicity and carcinogenicity of furan. Furan treatment with the known carcinogenic dose of 2 mg/kg bw and below for 4 weeks was found not to induce marked hepatotoxicity, although a statistically significant increase of unconjugated bile acids and cholesterol in plasma was observed (Mally et al., 2010). This indicates that furan may impair hepatobiliary transport, which may contribute to cellular injury through hepatic accumulation of surface-active and hence toxic bile acids. Furthermore, increased cell proliferation and alterations in the expression of genes involved in cell-cycle control and apoptosis were observed, suggesting that chronic furan exposure may lead to

proliferative changes even at doses below the already known carcinogenic dose. Considering the collective findings of the subacute toxicity study, it seems that the levels of protein binding observed after furan administration of 2 and 0.1 mg/kg bw (6.3.1) may not be sufficient to induce pronounced hepatotoxicity. However, results from this study also suggest that protein binding may contribute to furan toxicity and carcinogenicity through mechanisms such as impairment of the hepatobiliary transport by adduct formation with involved transport proteins.

A further possible explanation how protein adduct formation may be linked to the toxicity and carcinogenicity of furan may be that covalent protein binding may compromise the three-dimensional protein structure and may thus lead to accumulation of misfolded and nonfunctional proteins in the endoplasmic reticulum (ER). This ER stress may then trigger the activation of the unfolded protein response (UPR), a cellular defense mechanism against accumulation of unfolded proteins. Upon activation of the UPR, splicing of XBP1 mRNA and expression of UPR target genes are specifically altered. However, neither altered XBP1 mRNA splicing nor expression changes of UPR target genes were evident in our experiments. This may either be due to the fact that not enough damaged and nonfunctional proteins accumulate in rat livers after administration of furan to trigger the UPR or may result from loss of function of a protein involved in activation of the UPR (GRP 78). In support of the latter, even a clearly hepatotoxic dose of furan did not appear to activate the UPR.

8 PATHWAY ANALYSIS AND BIOLOGICAL INTERPRETATION OF FURAN TARGET PROTEINS

8.1 Introduction

Covalent binding of furan reactive metabolites to cellular proteins, subsequent cell death and regenerative cell proliferation may represent important steps in the mechanism of furan toxicity and carcinogenicity in rat liver. To date, it is still unknown which proteins are critical for the development of cytotoxicity caused by protein adduct formation.

According to their functions, cellular proteins can be assigned to specific pathways. Since it is well known that adduct formation at proteins may lead to loss of their function, covalent binding to different proteins involved in the same pathway may result in disruption of this pathway. Using pathway mapping tools, we wanted to determine which pathways are enriched among the identified furan target proteins. Thus, identification of possibly impaired pathways may provide information regarding the cellular events that link cytotoxicity and adduct formation at the 61 identified furan target proteins.

Moreover, it was suggested that there may be individual proteins with key functions whose loss of function may lead to cytotoxicity. Hence, a literature research was conducted to better understand individual protein functions and to establish a mechanistic connection between loss of protein function and cytotoxicity.

8.2 Methods

8.2.1 Pathway mapping to identify significantly enriched pathways

To establish whether there are metabolic pathways which are specifically enriched among the 61 identified furan target proteins, a list of the UniProt IDs of the target proteins was copied and pasted into an online pathway analysis tool called Database for Annotation, Visualization and Integrated Discovery (DAVID, version 6.7) (http://david.abcc.ncifcrf.gov/) (Dennis, Sherman et al. 2003; Huang da, Sherman et al. 2009). The identifier "UNIPROT_ACCESSION" and the list type "Gene List" were selected for the protein list and the list was submitted for analysis. Then the functional annotation tool was used to view the results. The annotation summary results for the three gene ontology (GO) terms biological process, cellular compartment, and molecular functions and for the Kyoto Encyclopedia of Genes and Genomes (KEGG) pathways were selected. The enriched pathways showing p-values of less than 0.05 were inspected and

summarized. The DAVID software uses the EASE Score, a modified Fisher Exact p-Value, to measure whether an enrichment in annotation terms is significant. For the calculation of the EASE Score p-value for each annotation category, the total number of entries of the background list (i.e. the default background list of Rattus norvegicus), the total number of entries belonging to the annotation category, the total number of entries on the list which was uploaded into DAVID (61 target proteins), and the number of entries from the uploaded list which was assigned to the annotation category were considered.

To illustrate the considerations which are the basic of these calculations, a hypothetical example taken from the DAVID website is described: In an uploaded list containing 300 entries, 3 entries were found to be involved in a certain pathway (p53 signaling). The background list in this case includes 30000 entries, 40 of which participate in total in p53 signaling. The question is now whether 3/300 is more than random chance compared to the background of 40/30000. In this example, an EASE Score of 0.06 was calculated, which means, regarding a significance threshold of 0.05, that this specific enrichment is not statistically significant.

The pathway analysis was first conducted using the 61 furan target proteins. Moreover, a second analysis was performed with an extended protein list including the 61 already analyzed proteins and 37 additional proteins which had closely failed to meet the stringently set criteria for protein identification (6.3.2). The second analysis was done to find out whether these additional proteins may also participate in the pathways found to be enriched in the first analysis.

8.2.2 Literature search

Various sources such as PubMed (http://www.ncbi.nlm.nih.gov/pubmed) and the Protein Knowledgebase UniProtKB (http://www.uniprot.org/) were used to obtain information on individual target protein functions and loss of their functions.

8.2.3 Semiquantitative analysis to estimate the degree of protein adduction

To gather information as to which proteins appear to be most heavily adducted relative to their abundance in rat liver, a densitometric analysis was conducted. Therefore, Coomassie Blue-stained gels and their corresponding films obtained by fluorography were scanned on a HP ScanJet 5550C flatbed scanner to obtain digital images and densitometric analysis was performed using Ludesi Redfin3 (Ludesi) software. The relative ratios of the amount of radioactivity present in spots on the film (arbitrary units) and the total amount of protein as detected by Coomassie Blue staining (arbitrary units) were calculated for each spot. In the next step, the mean ratios and standard deviations were determined. This allowed ranking of target proteins according to the degree of protein adduction relative to the abundance of the protein. Ranking was performed separately for proteins isolated from gels derived from pH 4-7 (whole tissue extract), pH 6-9 (whole tissue extract), and pH 4-7 (membrane fraction) due to different exposure times and different amounts of protein loaded onto the gels.

8.3 Results and discussion

8.3.1 Significantly enriched pathways identified by pathway mapping

Pathway mapping of the 61 furan target proteins using DAVID revealed fatty acid, amino acid, and glucose metabolism as significantly enriched KEGG pathways with 7/61 (11.5 %), 7/61 (11.5 %), and 8/61 (13.1 %) proteins assigned to the annotation terms, respectively (Tab. 18). Similarly, the gene ontology category biological process glucose metabolic process (9/61, 14.8 %), nitrogen compound biosynthetic process (9/61, 14.8 %), and fatty acid metabolic process (6/61, 9.8 %) were found to be significantly enriched. The differences in the exact numbers of proteins assigned to the terms is due to the fact that the terms in KEGG pathways and gene ontology are not fully identical. Additionally, the gene ontology category biological process showed significant enrichment in the annotation terms oxidation/reduction (17/61, 27.9 %), generation of precursor metabolites and energy (11/61, 18 %), and cell redox homeostasis (5/61, 8.2 %). Furthermore, we found that a large number of proteins were derived from mitochondria (24/61, 39.3 %) and cytosol (21/61, 34.4 %).

It is important to note that the terms are not mutually exclusive and that some proteins may be assigned to more than one annotation term. For example, the protein aldehyde

dehydrogenase (P11884) was observed in all three, while the protein acetyl-CoA acetyltransferase (P17764) was found in two of the three enriched KEGG pathways.

Table 18 Enriched categories and terms as determined with the DAVID Gene-Enrichment and Functional Annotation Analysis *(Dennis et al., 2003; Huang da et al., 2009); *indicates number of proteins in the dataset that belong to this category, **indicates percentage of proteins in the dataset that belong to this category, *** p-Values were calculated with a modified Fisher exact test.*

Annotation category	Annotation term	Proteins assigned to annotation term	Count*	%**	p-Value***
KEGG pathway	Fatty acid metabolism	P13437, P14604, P15650, P15651, P17764, P18163, P11884	7	11.5	2.9×10^{-7}
	Valine, leucine and isoleucine degradation	P11884, P11960, P12007, P13437, P14604, P15651, P17764	7	11.5	5.0×10^{-7}
	Glycolysis / Gluconeogenesis	P00884, P04642, P04764, P04797, P11884, P16617, P19112, P48500	8	13.1	1.2×10^{-6}
Gene ontology Cellular component	Mitochondrion	O35077, O88989, P00481, P04642, P09034, P10719, P11232, P11884, P11960, P12007, P13437, P13803, P14604, P15650, P15651, P17764, P18163, P52759, P97532, Q07116, Q63716, Q8CG45, Q9JJ40, Q9Z2L0	24	39.3	4.9×10^{-9}
	Cytosol	O35077, O88989, P00884, P02692, P02761, P04642, P04764, P04797, P06214, P06761, P11232, P16617, P18163, P19112, P48500, P60711, P63018, Q07116, Q499R7, Q63716, Q9ES53	21	34.4	1.3×10^{-7}
Gene ontology Biological process	Oxidation/Reduction	O35077, O88989, P04642, P04797, P11232, P11884, P11960, P12007, P13803, P15650, P15651, P23457, Q07116, Q5I0J9, Q63716, Q8CG45, Q920J4	17	27.9	7.2×10^{-9}
	Generation of precursor metabolites and energy	O88989, P00884, P04642, P04764, P04797, P10719, P11232, P13803, P16617, P48500, Q920J4	11	18	9.7×10^{-8}
	Glucose metabolic process	O35077, O88989, P00884, P04642, P04764, P04797, P16617, P19112, P48500	9	14.8	1.2×10^{-6}
	Nitrogen compound biosynthetic process	O09171, P00481, P06214, P07824, P09034, P10719, P13444, P51583, Q5I0J9	9	14.8	1.1×10^{-4}
	Cell redox homeostasis	P04785, P11232, P11598, Q63716, Q920J4	5	8.2	1.9×10^{-4}
	Fatty acid metabolic process	P13437, P14604, P15650, P15651, P18163, P48500	6	9.8	1.6×10^{-3}
Gene ontology Molecular function	Electron carrier activity	P12007, P13803, P15650, P15651, Q07116	5	8.2	2.1×10^{-2}

In addition to the 61 proteins identified as putative furan target proteins, 37 further proteins were found which did not match our stringent criteria set for protein identification. These additional proteins have not been included in the detailed interpretation. However, since the additional proteins may also represent furan target proteins which may just have closely failed to meet the stringently set criteria, we were interested to see whether they provide further support to our findings regarding possible mechanisms involved in furan-mediated cytotoxicity and carcinogenicity. Thus, a further

analysis using DAVID was conducted in which the 37 additional proteins were included (Tab. 19).

Table 19 Enriched categories and terms as determined with the DAVID Gene-Enrichment and Functional Annotation Analysis *(Dennis et al., 2003; Huang da et al., 2009); *indicates number of proteins in the dataset that belong to this category, **indicates percentage of proteins in the dataset that belong to this category, *** p-Values were calculated with a modified Fisher exact test. Additional proteins assigned to the terms and newly observed terms are marked in red.*

Category	Term	Enriched proteins	Count*	%**	p-Value***
KEGG pathway	Fatty acid metabolism	P13437, P14604, P15650, P15651, P17764, P18163, P11884, Q9JLJ3	8	8.2	2.9×10^{-7}
	Valine, leucine and isoleucine degradation	P11884, P11960, P12007, P13437, P14604, P15651, P17425, P17764, P22791, P29266, Q99PU6, Q9JLJ3	12	12.4	1.2×10^{-12}
	Glycolysis / Gluconeogenesis	P00884, P04642, P04764, P04797, P11884, P16617, P19112, P48500, Q9JLJ3	9	9.3	3.2×10^{-6}
Gene ontology Cellular component	Mitochondrion	O35077, O88989, P00173, P00481, P04642, P09034, P10719, P11232, P11884, P11960, P12007, P13437, P13803, P14604, P15650, P15651, P15999, P17764, P18163, P22734, P22791, P24329, P29266, P41562, P51650, P52759, P60901, P70473, P97532, Q05982, Q07116, Q63060, Q63716, Q68FT4, Q6AYQ8, Q8CG45, Q99PU6, Q9JJ40, Q9JLJ3, Q9QZU7, Q9Z2L0	41	42.3	5.9×10^{-17}
	Cytosol	O35077, O88989, P00884, P02692, P02761, P04642, P04764, P04797, P06214, P06761, P11232, P16617, P17425, P18163, P19112, P22734, P25093, P25409, P41562, P48500, P50237, P60711, P63018, Q05982, Q07116, Q499R7, Q5RK09, Q63060, Q63716, Q6P9T8, Q9EQS0, Q9ES53, Q9JLJ3	33	34.0	7.4×10^{-12}
Gene ontology Biological process	Oxidation/Reduction	O35077, O88989, P00173, P04176, P04642, P04797, P11232, P11884, P11960, P12007, P13803, P15650, P15651, P23457, P29266, P32755, P41562, P51650, Q07116, Q5I0J9, Q5I0M4, Q63716, Q8CG45, Q920J4, Q9JLJ3, Q9QZU7,	26	26.8	5.6×10^{-13}
	Generation of precursor metabolites and energy	O88989, P00173, P00884, P04642, P04764, P04797, P10719, P11232, P13803, P15999, P16617, P41562, P48500, P51650, Q68FT4, Q920J4	16	16.5	1.2×10^{-10}
	Glucose metabolic process	O35077, O88989, P00884, P04642, P04764, P04797, P16617, P19112, P29266, P48500, P51650, Q9EQS0	12	12.4	4.9×10^{-8}
	Nitrogen compound biosynthetic process	O09171, P00481, P04176, P06214, P07824, P09034, P10719, P13444, P15999, P51583, Q05982, Q5I0J9, Q9JLJ3, Q9QZU7	14	14.4	5.9×10^{-7}
	Cell redox homeostasis	P04785, P11232, P11598, Q63716, Q920J4	5	5.2	1.1×10^{-3}
	Steroid metabolic process	P04276, P17425, P22734, P22791, P23457, P70473, Q6PAH0	7	7.2	1.3×10^{-3}
	Fatty acid metabolic process	P13437, P14604, P15650, P15651, P18163, P48500, P51650	7	7.2	2.3×10^{-3}
Gene ontology Molecular function	Electron carrier activity	P00173, P12007, P13803, P15650, P15651, Q07116, Q9QZU7	7	7.2	7.2×10^{-3}

In comparison to the first DAVID analysis, additional proteins were assigned to all terms except the gene ontology term cell redox homeostasis. The gene ontology term steroid metabolic process, which had not been observed in the first DAVID analysis, was found to be significantly enriched in the second analysis. In the category KEGG pathway, the terms fatty acid metabolism and glycolysis/gluconeogenesis both showed one additional protein, while 5 additional proteins were assigned to the term valine, leucine and isoleucine degradation. Thus, it appears that the degradation of the branched chain amino acids became more important. Moreover, 42.3 % (before: 39.3 %) of the proteins were now assigned to the gene ontology term mitochondrion, while the percentage of proteins in the dataset assigned to the cytosol did not change after analysis including the additional proteins (34.4 % vs. 34.0 %). Hence, it seems that a larger fraction of proteins is associated with the mitochondrion.

8.3.2 Adduction of proteins involved in glucose and fatty acid metabolism suggests impaired energy production as a mechanism of furan toxicity

Pathway mapping of the 61 furan target proteins using DAVID revealed that furan binds to a range of proteins involved in glycolysis/gluconeogenesis (α-enolase, fructose-bisphosphate aldolase B, fructose-1,6-bisphosphatase, glyceraldehyde-3-phosphate dehydrogenase, L-lactate dehydrogenase A chain, phosphoglycerate kinase 1, triosephosphate isomerase), mitochondrial fatty acid metabolism (long-chain fatty acid CoA ligase 1, short/long-chain specific acyl-CoA dehydrogenase, enoyl-CoA hydratase, 3-ketoacyl-CoA thiolase) and ATP synthesis (ATP synthase β subunit) (Fig. 32 and 33).

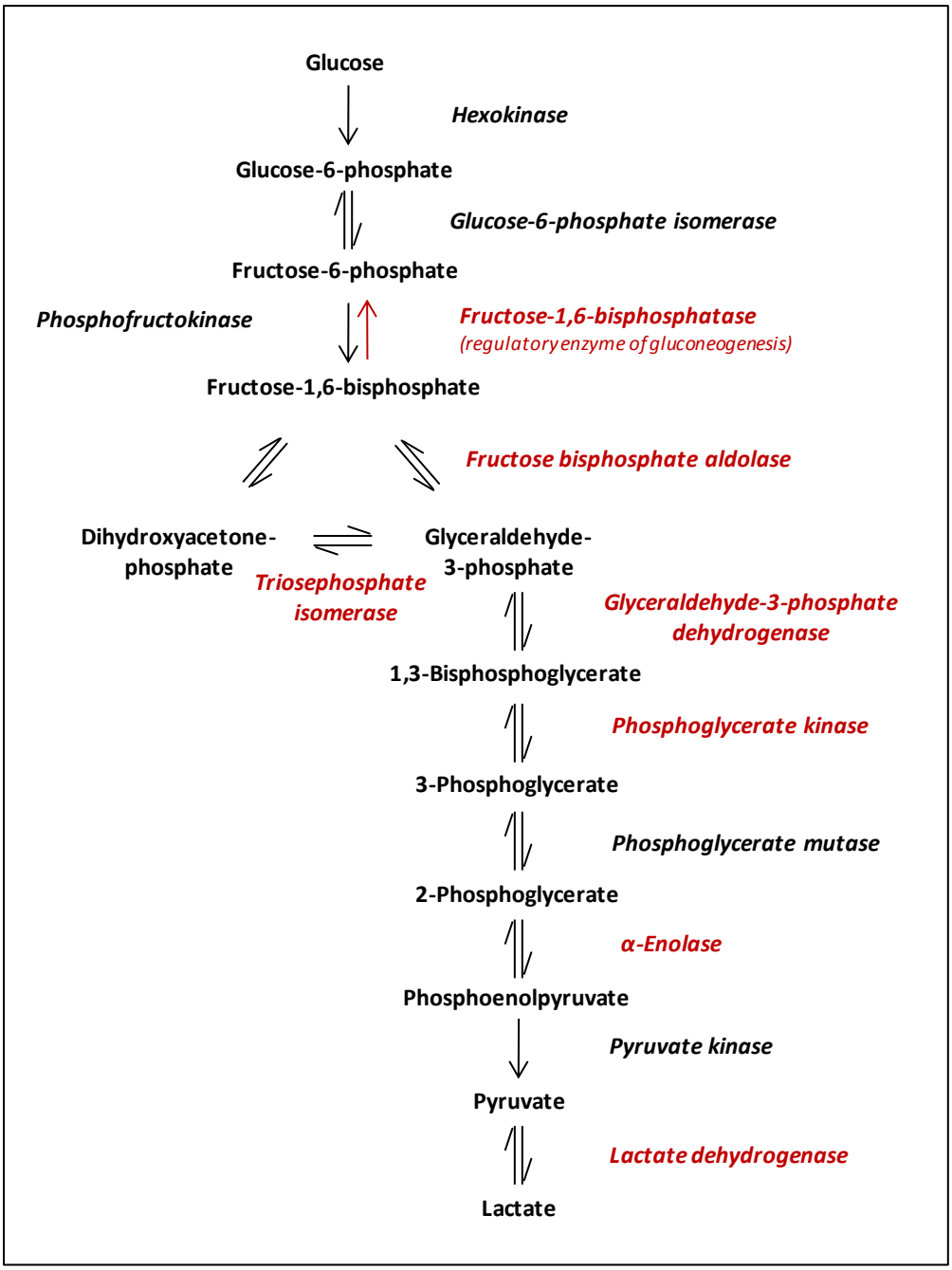

Figure 32 *Furan target proteins (red) involved in glycolysis and gluconeogenesis (modified from KEGG Pathway Database, http://www.genome.jp/kegg/pathway.html).*

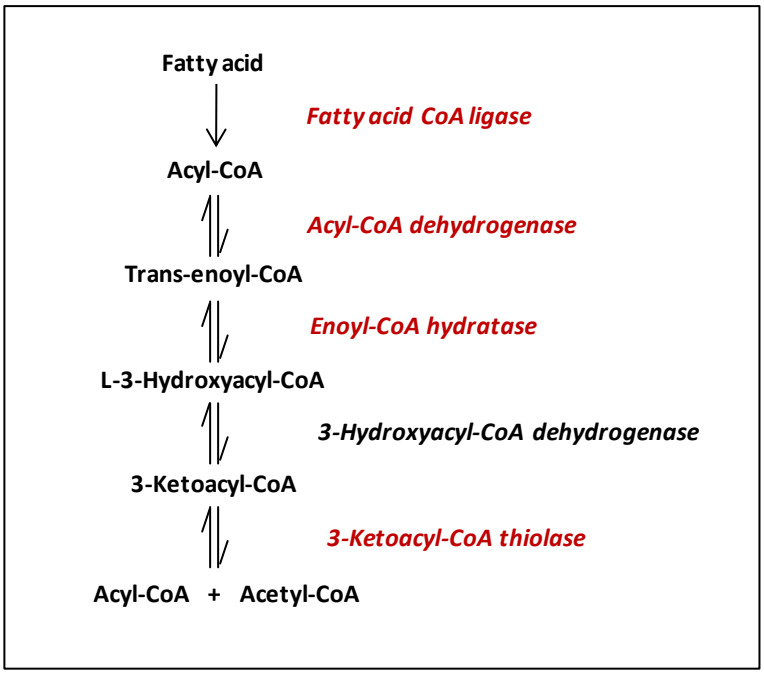

Figure 33 *Furan target proteins (red) involved in mitochondrial β-oxidation of fatty acids (modified from KEGG Pathway Database, http://www.genome.jp/kegg/pathway.html).*

Provided that covalent binding of furan actually results in an impaired or loss of protein function, it is possible that glycolysis/gluconeogenesis and mitochondrial β-oxidation may be disrupted. This may lead to a decreased supply of precursor metabolites crucial for the production of energy in the mitochondria, i.e. pyruvate and acetyl-CoA as final products of glycolysis and mitochondrial β-oxidation of fatty acids, respectively. Under physiological conditions, these precursors enter the citric acid cycle in the mitochondrial matrix, resulting in the formation of CO_2 and reduction equivalents $NADH/H^+$ and $FADH_2$. The obtained reduction equivalents are then oxidized by the respiratory chain, leading to the production of ATP. However, if there is a strong decrease in the concentration of the precursor compounds, the production of ATP may be decreased.

In addition, we found that furan also binds to several enzymes involved in degradation of amino acids (2-oxoisovalerate dehydrogenase subunit α, isovaleryl-CoA dehydrogenase, short-chain specific acyl-CoA dehydrogenase, enoyl-CoA hydratase, 3-ketoacyl-CoA thiolase, acetyl-CoA acetyltransferase, ornithine carbamoyltransferase, argininosuccinate synthase, arginase 1). Under physiological conditions, these amino acid degradation pathways also supply acetyl-CoA, pyruvate or other intermediates which enter the citric acid cycle and contribute to energy production (Fig. 34). Taken together, overall impairment of energy production may occur due to disruption of several different pathways which normally lead to formation of energy precursors (Fig. 35).

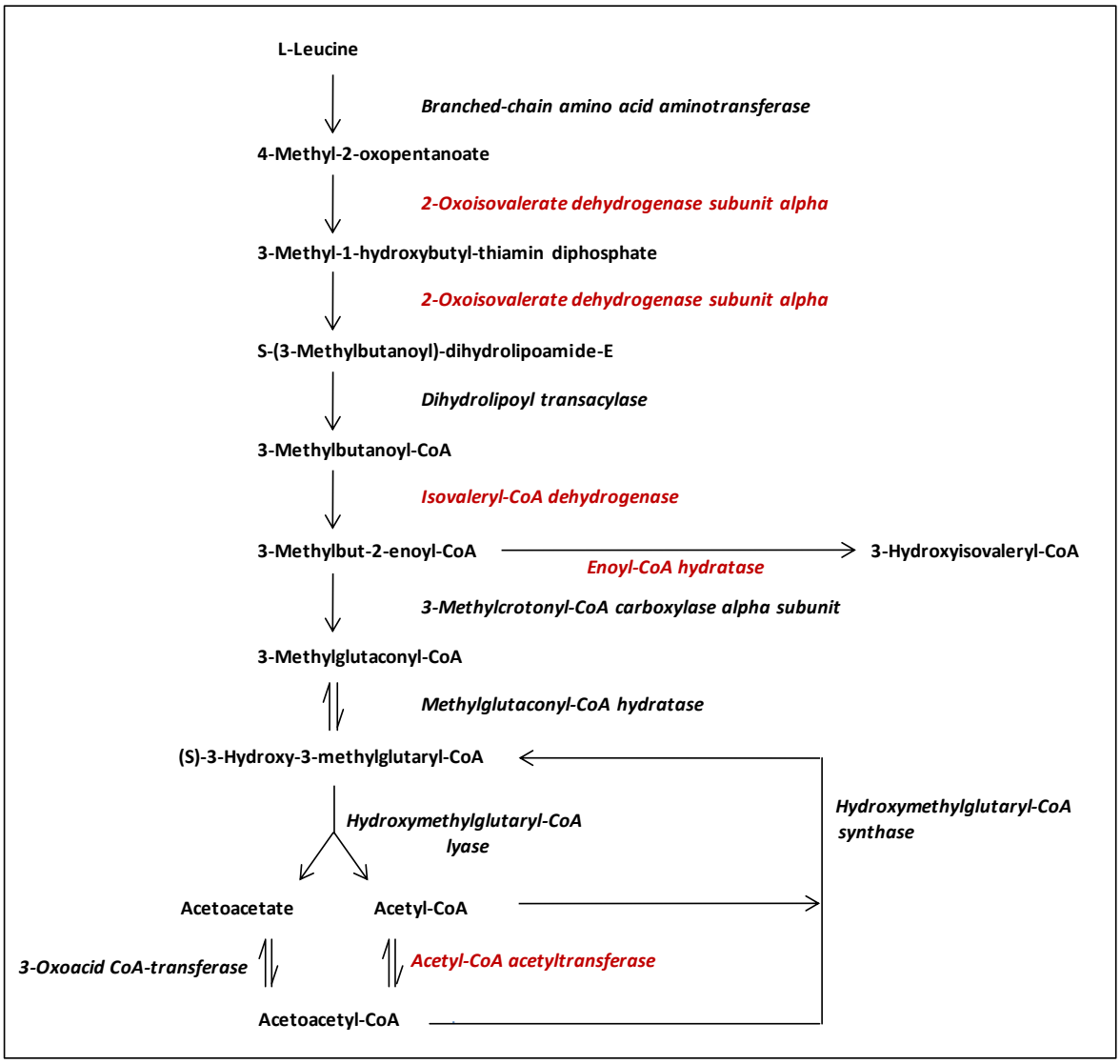

Figure 34 *Adducted proteins (red) involved in the degradation of branched chain amino acids exemplified by leucine (modified from KEGG Pathway Database, http://www.genome.jp/kegg/pathway.html).*

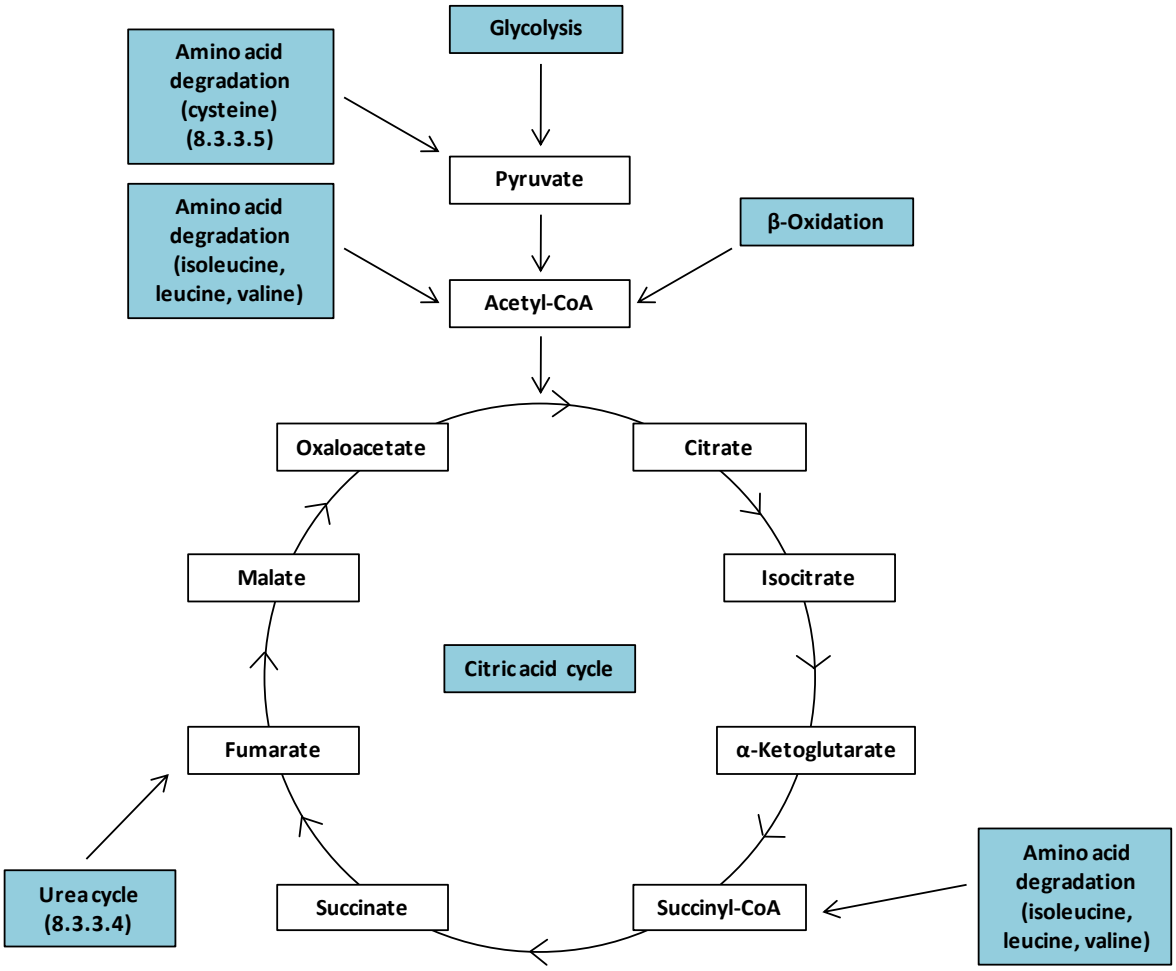

Figure 35 *Connection of cellular pathways potentially affected by furan protein binding (modified from KEGG Pathway Database, http://www.genome.jp/kegg/pathway.html).*

In addition to potential insufficient supply of precursor metabolites and reduction equivalents, the respiratory chain and the oxidative phosphorylation may also be disrupted since subunits of the electron transfer flavoprotein and the ATP synthase were identified as target proteins of furan reactive metabolites.

Inhibition of the mitochondrial β-oxidation and impairment of the respiratory chain (causing the formation of reactive oxygen species) were reported to result in severe cellular consequences leading to necrosis, inflammation, and fibrosis (Pessayre et al., 1999). Taken together, this suggests that furan cytotoxicity may result from ATP depletion and oxidative stress through decreased generation of acetyl-CoA and accumulation of free fatty acids, which act as mitochondrial uncouplers (Skulachev, 1991; Vickers, 2009) (Fig. 36). This is consistent with a study by Mugford et al. which demonstrates that uncoupling of hepatic oxidative phosphorylation is an early event in furan-mediated cell death (Mugford et al., 1997).

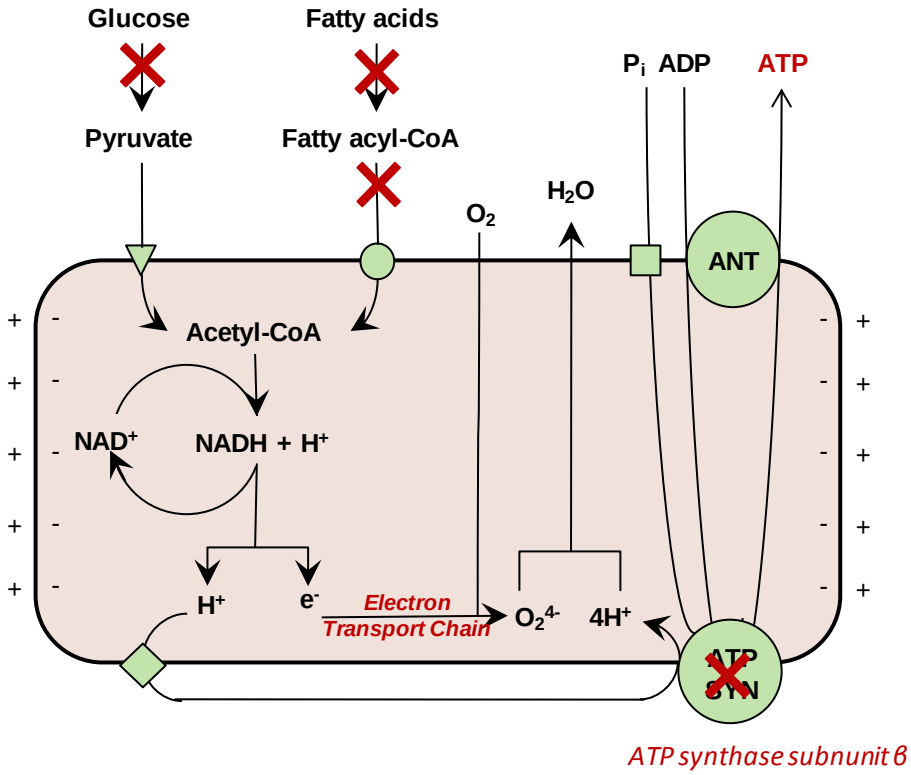

Figure 36 *Potential mechanistic link between furan toxicity and adducted proteins: impaired mitochondrial energy production and altered redox state due to binding to ATP synthase and enzymes involved in glycolysis and mitochondrial β-oxidation.*

While α-enolase, fructose-bisphosphate aldolase B, glyceraldehyde-3-phosphate dehydrogenase, phosphoglycerate kinase 1, and triosephosphate isomerase were shown to form adducts with hepatotoxic metabolites of thiobenzamide and bromobenzene (Ikehata et al., 2008; Koen et al., 2007), it is interesting to note that several of the enzymes involved in energy production, i.e. 3-ketoacyl-CoA thiolase, long-chain fatty acid CoA ligase 1, long-chain specific acyl-CoA dehydrogenase, fructose-bisphosphate aldolase B, glyceraldehyde-3-phosphate dehydrogenase, and ATP synthase β subunit were previously shown to represent targets of teucrin A, a hepatotoxic furan-containing compound found in the herb germander, which is bioactivated to an 1,4-enedial derivative structurally similar to *cis*-2-butene-1,4-dial (Druckova et al., 2007). Since teucrin A was shown to form adducts with several mitochondrial proteins, it was suggested that mitochondrial dysfunction may play a role in teucrin A-induced cytotoxicity (Druckova et al., 2007).

8.3.3 Potential link between furan toxicity and impaired function of individual target proteins

8.3.3.1 Proteins involved in transport processes across the mitochondrial membranes

Further support for mitochondrial toxicity as a key event in furan mediated cell death comes from the finding that **voltage-dependent anion-selective channel protein 1** (VDAC1, also known as porin) appears to be targeted by furan. VDAC1 is a pore-forming protein in the outer mitochondrial membrane, which facilitates exchange of metabolites such as ADP/ATP, succinate and citrate between the cytosol and mitochondria, thereby contributing to the regulation of mitochondrial energy metabolism (Lawen et al., 2005). Silencing of VDAC1 has been shown to impair mitochondrial ATP production (Abu-Hamad et al., 2006). In addition, there is increasing evidence to suggest that VDAC1 is a key player in apoptosis by forming complexes with Bcl-2 family proteins such as Bax, Bak, Bcl-2 and Bcl-XL and regulating cytochrome c release (Lawen et al., 2005; Shoshan-Barmatz et al.). Although the precise mechanism as to how binding of pro- and anti-apoptotic proteins to VDAC1 modulates mitochondrial permeability is still unknown, dissociation from VDAC1 may promote mitochondria-dependent apoptosis (Shoshan-Barmatz et al., 2010). Interestingly, VDAC1 has also been identified as a protein target of acrolein, a cytotoxic α,β-unsaturated aldehyde, which – similar to *cis*-2-butene-1,4-dial – preferentially reacts with thiol groups of cysteine residues (Mello et al., 2007). VDAC1 has been shown to contain two highly conserved cysteine residues, with Cys^{232} facing the VDAC pore, whereas the second cysteine residue (Cys^{127}) is oriented towards the lipid bilayer or may be exposed to the cytosol (Aram et al., 2010). Although recent work suggests that VDAC cysteine residues are not essential for VDAC channel activity and induction of apoptosis (Aram et al., 2010), the functional consequences of covalent binding of furan remain to be established.

The enzyme **cytosolic malate dehydrogenase** (MDH1), which was also reported to form adducts with thiobenzamide intermediates in vivo, participates in the malate-aspartate shuttle (Ikehata et al., 2008; Lo et al., 2005). The function of this shuttle system is the transport of reducing equivalents into the mitochondrium (Lo et al., 2005; Minarik et al., 2002). MDH1 mRNA expression was observed to correlate with the tissue's dependency on glucose (Lo et al., 2005), suggesting an important role of MDH1 in cellular energy supply. Independent of its catalytic activity, results from recent knockdown experiments indicate that MHD1 mediates glucose depletion-induced activation of p53, which was found to act as a central regulator of energy metabolism and to induce cell cycle arrest and cell death if energy is depleted (Lee et al., 2009). Considering these findings in combination with the above discussed furan-induced energy depletion through disturbed glucose and fatty acid metabolism and altered transport mechanisms, impaired MDH1 function may contribute to furan-mediated disruption of energy production resulting in cytotoxicity and cell death.

The **cytosolic glycerol-3-phosphate dehydrogenase** (GPDH-C), which was also identified as a target protein of bromobenzene (Koen et al., 2007), works in concert with the mitochondrial form (GPDH-M) of the enzyme to function as a glycerol-3-phosphate shuttle system, transporting electrons from cytosolic $NADH/H^+$ produced during glycolysis to the mitochondrial electron transport chain (Brisson et al., 2001). Through oxidation of $NADH/H^+$ to NAD^+, GPDH-C reduces dihydroxyacetone phosphate to glycerol-3-phosphate, which enters the mitochondrion and is oxidized back to dihydroxyacetone phosphate by GPDH-M, thereby reducing FAD to $FADH_2$ that can be used in the oxidative phosphorylation (Brisson et al., 2001). Although the glycerol-3-phosphate shuttle plays a role in brain and skeletal muscle, the malate-aspartate shuttle appears to be the predominant system in the liver (Brisson et al., 2001). However, since the malate-aspartate shuttle may also be impaired by furan binding to cytosolic malate dehydrogenase, combined loss of function of both shuttle systems may have pronounced negative effects on energy production in the liver and may thus result in cytotoxicity and cell death.

8.3.3.2 Proteins involved in redox regulation

Functional loss of **electron transfer flavoprotein subunit α** and **peroxiredoxin-1**, which participate in mitochondrial electron transfer and maintenance of redox homeostasis, respectively, may further contribute to altered redox state and subsequent induction of cell death. Owing to redox-sensitive cysteine residues, which may be targeted by furan, peroxiredoxins play an important role in antioxidative defense by reducing H_2O_2, peroxynitrite and lipid peroxides (Kalinina et al., 2008).

Furthermore, impaired **thioredoxin-1** (Trx-1) function could play a role in furan-induced toxicity. Trx-1, which was also identified as a target protein of thiobenzamide and bromobenzene in vivo (Ikehata et al., 2008; Koen et al., 2007), is ubiquitously expressed and is localized to cytosol and nucleus (Powis and Montfort, 2001). The thioredoxin family shows a highly conserved catalytic site containing one lysine and two cysteine residues (Powis and Montfort, 2001). Thioredoxins function by reducing disulfide residues of oxidized proteins through cysteine thiol-disulfide exchange, thereby regulating protein function. In turn, thioredoxin reductase reduces oxidized Trx back to its thiol form (Powis and Montfort, 2001). Mice overexpressing Trx show an enhanced life-span and ability to cope with oxidative stress (Mitsui et al., 2002), whereas mice homozygous with defects in the Trx gene die shortly after implantation (Matsui et al., 1996). In addition to regulation of the redox state of a cell, Trx is thought to participate in a variety of processes, including cell signaling via extra- and intracellular pathways and regulation of gene expression via interaction with transcription factors (Lillig and Holmgren, 2007). For instance, Trx has been reported to suppress cell death through inhibition of a mitogen-activated protein (MAP) kinase–kinase–kinase (i.e. apoptosis signal-regulating kinase 1) and the downstream c-Jun N-terminal kinase and p38 MAP kinase pathways (Ichijo et al., 1997; Niso-Santano et al., 2010; Saitoh et al., 1998). Collectively, these studies demonstrate that Trx protects against oxidative damage and cell death, suggesting that impaired Trx function mediated by covalent binding of furan reactive metabolites may contribute to furan toxicity and carcinogenicity.

Thioredoxin-like protein 1 (Txl-1) is expressed in various tissues and contains one N-terminal thioredoxin domain (Jimenez et al., 2006; Miranda-Vizuete et al., 1998). Similar to thioredoxin-1 (Trx-1), Txl-1 also acts as a reducing protein, but showed only 25 % of Trx-1 activity (Jimenez et al., 2006). In vitro, overexpression of Txl-1 was found to protect cells against cytotoxicity induced by glucose deprivation, but not against hydrogen peroxide-induced toxic effects (Jimenez et al., 2006). Knockdown of Txl-1 was shown to result in slightly elevated amounts of ubiquitin-protein conjugates in vitro, suggesting that Txl-1 may be involved in protein degradation by the ubiquitin-proteasome system (Andersen et al., 2009). Taken together, loss of Txl-1 function through adduct formation may lead to both impaired redox regulation and protein degradation and may thus promote furan-induced cytotoxicity.

Regucalcin (senescence marker protein 30), which was also reported to represent a target protein of bromobenzene (Koen et al., 2007), is a Ca^{2+} binding protein expressed in liver and kidney (Nakagawa and Yamaguchi, 2008). Regucalcin is involved in the maintenance of intracellular Ca^{2+} homeostasis by regulating the activity of Ca^{2+} pumps in the plasma membrane, endoplasmic reticulum and mitochondria (Yamaguchi, 2000), thereby protecting cells against intracellular calcium elevation and oxidative stress (Son et al., 2008). Importantly, regucalcin deficiency has been reported to cause generation of reactive oxygen species (Son et al., 2006). Thus, loss of regucalcin function through furan covalent binding may lead to increased cellular oxidative stress, which may result in cytotoxicity.

3-Mercaptopyruvate sulfurtransferase (MST) is present in the cytosol and mitochondria of a variety of organs (Nagahara and Nishino, 1996). It contains five cysteine residues, one of which is located in the active site and is important for protein function (Nagahara et al., 2007). MST catalyzes the transfer of sulfur from 3-mercaptopyruvate to various acceptor molecules. One possibility is the detoxification of cyanide through the reaction with 3-mercaptopyruvate, yielding pyruvate and thiocyanate (Nagahara and Nishino, 1996). Furthermore, MST participates in the anaerobic degradation of cysteine leading to the formation of sulfane sulfur-containing compounds (e.g. persulfides, thiosulfate, elemental sulfur, disulfides) (Iciek and Wlodek, 2001). These substances are presumably involved in

regulation of enzymes and receptors through modification of their thiol groups (Iciek and Wlodek, 2001). Sulfane sulfur-containing compounds were also found to have antioxidative effects in the cell through removal of free radicals and enhancement of antioxidative enzymes (e.g. glutathione peroxidase, glutathione reductase) (Iciek and Wlodek, 2001). Additionally, MST was reported to be involved in the cellular redox homeostasis together with thioredoxin (Nagahara et al., 2007). Thus, binding of furan metabolites may result in impaired cellular defense against oxidative stress and thus lead to cytotoxicity.

Considering the role of several putative furan target proteins in regulating redox state, it appears that adduction by furan may result in impaired antioxidant defense. In this respect, it is interesting to note that evidence of oxidative stress in form of increased 8-oxo-7,8-dihydro-2´-deoxyguanosine was seen after high dose furan exposure associated with substantial hepatotoxicity (Hickling et al., 2010b). In contrast, no increased levels of 8-oxo-7,8-dihydro-2´-deoxyguanosine were observed in response to furan treatment at 2 mg/kg bw for 28 days (Mally et al., 2010), suggesting that under the conditions of this study no oxidative stress is induced. This may indicate that the levels of protein binding observed after furan treatment at 2 mg/kg bw may not be high enough to affect the overall cellular antioxidative defense mechanisms. However, administration of furan at 2 mg/kg bw was reported to induce toxic and hyperplastic effects in rat liver after 90 days and to result in tumor formation after 2 years (Gill et al., 2010; NTP, 1993). Moreover, a recent study conducted with a high dose of furan (30 mg/kg bw) showed expression changes of genes associated with DNA damage and increased levels of 8-oxo-dG indicative of oxidative DNA damage (Hickling et al., 2010b). Thus, it is conceivable that the amount of protein binding observed after furan treatment at 2 mg/kg bw may not induce oxidative stress after 4 weeks of administration but may lead to oxidative stress after longer exposure times, thereby possibly contributing to toxicity and cancer.

8.3.3.3 Proteins involved in protein folding and proteolysis

Heat shock cognate 71 kDa protein (also called Hsc70, Hsp73, Hsp70-8, Hspa8) and **78 kDa glucose-regulated protein** (also known as heat shock 70 kDa protein 5, Hsp70-5, Hspa5, BiP), which were also identified as targets of teucrin A, thiobenzamide, and bromobenzene (Druckova et al., 2007; Ikehata et al., 2008; Koen et al., 2007), both belong to the heat shock protein 70 family**.** Proteins from this family show very similar sequences (Daugaard et al., 2007) and are highly conserved across different species (Kelley and Schlesinger, 1982). Heat shock cognate 71 kDa protein is constitutively expressed in various tissues including liver (Dworniczak and Mirault, 1987; O'Malley et al., 1985). It is thought to function predominantly as an ATP-dependent chaperone, directing processes critical for cell survival such as protein folding, assembly of protein complexes, intracellular protein transport, and protein degradation (Lindquist and Craig, 1988; Pelham, 1986; Rohde et al., 2005). Thus, loss of heat shock cognate 71 kDa protein function may lead to decreased chaperone activity, which may then cause toxicity through accumulation of unfolded and misfolded proteins.

Similarly, 78 kDa glucose-regulated protein (GRP78), which localizes to the lumen of the endoplasmic reticulum, regulates protein folding and proteasomal degradation by binding ATP-dependently to unfolded and misfolded proteins. Moreover, GRP78 was suggested to be the primary sensor of ER stress and thus important regulator of the unfolded protein response (as further described in chapter 7). Interestingly, recent data suggest that abrogation of GRP78 function can increase ER stress-induced cell death, presumably through inhibition of homeostatic responses to ER stress (Martin et al., 2010). This suggests that adduction of GRP78 by furan reactive metabolites may limit the cells ability to cope with damaged proteins due to reduced chaperone activity and failure to activate the UPR. It is worth noting that GRP78 was also shown to be targeted by teucrin A, a hepatotoxic furan derivative (Druckova et al., 2007).

Protein disulfide isomerase (PDI) and **protein disulfide isomerase A3** (PDIA3, Erp60, Erp57, 58 kDa glucose-regulated protein, p58), which were both reported to form adducts with thiobenzamide and bromobenzene (Druckova et al., 2007; Ikehata et al., 2008; Koen et al., 2007), are members of the thioredoxin superfamily and contain two catalytically active thioredoxin domains (Wilkinson and Gilbert, 2004). PDI was reported to be among the high abundance proteins in the ER where it functions as a chaperone, oxidoreductase

and isomerase, thereby preventing aggregation of misfolded proteins and oxidizing and/or reducing thiols and disulfides in order to restore proper protein folding (Wilkinson and Gilbert, 2004). Similarly, PDIA3 is a thiol oxidoreductase involved in the regulation of protein folding (Ni and Lee, 2007). Thus, impaired PDI and PDIA43 function through adduct formation with furan may contribute to accumulation of protein aggregates, thus enhancing cellular stress and toxicity. However, considering that PDI represents a high abundance protein in the ER, it is unclear if the level of adduction is sufficient to exert a significant effect on overall PDI function.

Ubiquitin fusion degradation protein 1 homolog (UB fusion protein 1, Ufd1l) belongs to the UFD1 family and represents the homolog to the yeast protein Ufd1, which is involved in the degradation of ubiquitin fusion proteins in yeast. Proper function of Udf1 appears to be required for cell survival (Johnson et al., 1995). Ufd1 is involved in regulation of the ATPase p97, a mediator of various cellular processes such as endoplasmic reticulum associated protein degradation (ERAD), membrane fusion, transcription factor activation, and cell cycle regulation (Meyer et al., 2000; Woodman, 2003). Binding of a complex including p97 and Ufd1 to ubiquitinated proteins mediates their transport from the ER to the cytosol for degradation by the proteasome (Ye et al., 2001). Thus, disturbance of Udf1 function through covalent binding of furan reactive metabolites may lead to impaired proteasomal protein degradation and thus accumulation of misfolded proteins.

α_1-Antiproteinase (α_1-antitrypsin, AAT, serpin A1), a glycoprotein predominantly expressed in liver is secreted into the plasma where it acts as a major serum serine protease inhibitor (Carlson et al., 1988; Rogers et al., 1983). AAT, which was also identified as a target of thiobenzamide (Ikehata et al., 2008), is an acute phase protein (Schreiber et al., 1989), which is induced during inflammatory processes (Perlmutter et al., 1989). Mutations within the α_1-antiproteinase gene were found to be associated with the formation of protein polymers in the endoplasmic reticulum (Fairbanks and Tavill, 2008). Inherited deficiency of α_1-antiproteinase predisposes affected individuals to liver diseases, including hepatocellular carcinoma, presumably as a result of the accumulated polymerization products within the cells (Fairbanks and Tavill, 2008). Thus, loss of AAT function may contribute to furan toxicity and carcinogenicity in rodent liver.

Serine protease inhibitor A3K (serpin A3K, kallikrein-binding protein, growth hormone-regulated proteinase inhibitor, SPI-2), which is highly expressed in liver, was first identified in human serum (Chao et al., 1986). It belongs to the serpin family and specifically inhibits the proteolytic activity of tissue kallikrein, a protease that releases kinins from kininogens (Bhoola et al., 1992; Chao et al., 1990). Knockdown of SerpinA3K by siRNA was shown to activate the canonical Wnt pathway, leading to an increase in cytosolic β-catenin and expression of Wnt target genes including c-myc and cyclin D1 (Zhang et al., 2010). These findings suggest that SerpinA3K has antiproliferative effects by blocking the canonical Wnt pathway. Thus, furan binding to Serpin A3K may contribute to carcinogenesis by abrogating the inhibitory effects of Serpin A3K on the Wnt pathway.

8.3.3.4 Proteins involved in the urea cycle

Three out of five enzymes involved in the urea cycle, i.e. **ornithine carbamoyltransferase, argininosuccinate synthase, and arginase 1,** were identified as putative furan target proteins (Fig. 37). Arginase 1 was also reported to represent a target protein of the reactive metabolites of thiobenzamide and bromobenzene in rat liver in vivo (Ikehata et al., 2008; Koen et al., 2007), while argininosuccinate synthase was found to be adducted by teucrin A intermediates (Druckova et al., 2007). The function of the urea cycle is the elimination of excess nitrogen by transformation of toxic ammonia derived from dietary sources and amino acid catabolism into easily excretable urea (Deignan et al., 2008). Although we cannot rule out that increased intracellular ammonia resulting from disruption of the hepatic urea cycle may induce local effects, hyperammonemia resulting from inherited deficiencies of urea cycle enzymes was reported to cause damage to the brain without inducing toxicity in other tissues (Walker, 2009). Thus, it is not evident if and how disruption of the urea cycle as such may contribute to furan toxicity in rat liver. However, **arginase 1**, a cytosolic enzyme which catalyzes the reaction of arginine to ornithine and urea, participates in the regulation of nitric oxide production by competing with nitric oxide synthase for their common substrate arginine (Maarsingh et al., 2009). Thus, decreased activity of the arginine-degrading enzyme arginase 1 may result in increased nitric oxide synthesis and subsequent toxicity caused by peroxynitrite (produced from reaction between NO and the superoxide anion) (Pacher et al., 2007).

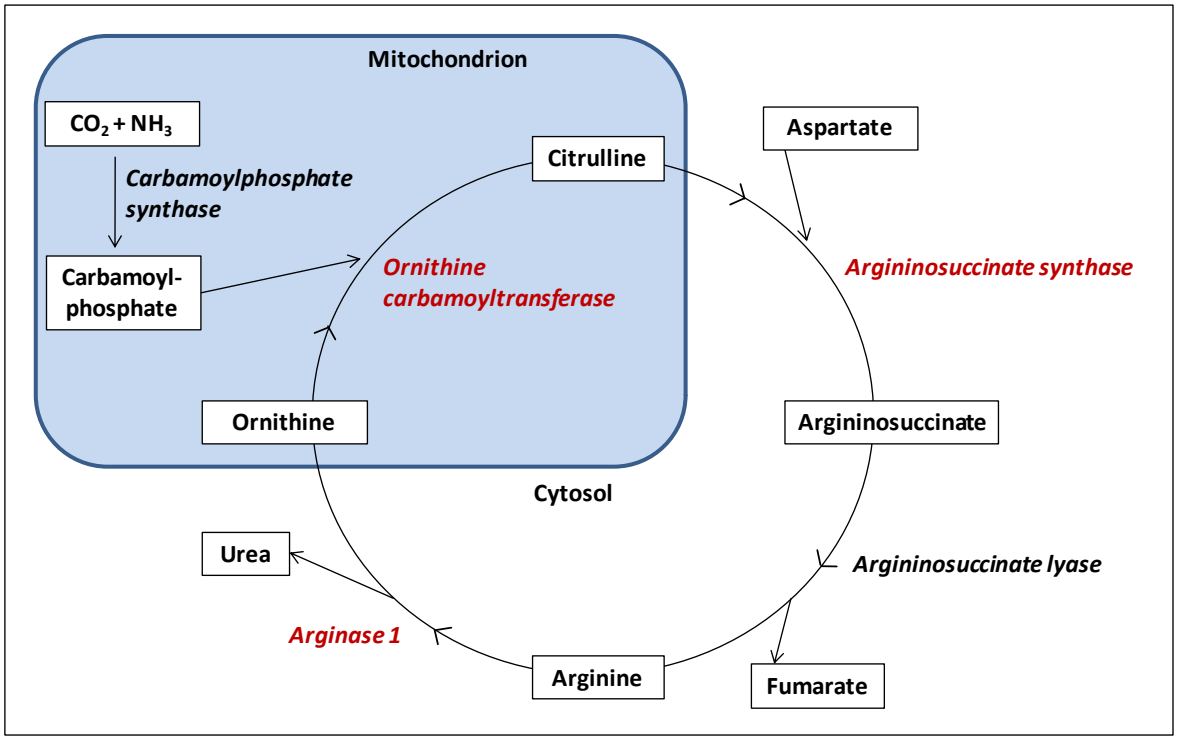

Figure 37 *Furan target proteins (red) involved in the urea cycle (modified from KEGG Pathway Database, http://www.genome.jp/kegg/pathway.html).*

8.3.3.5 Proteins involved in the metabolism of sulfur-containing amino acids

The conversion of methionine to homocysteine via S-adenosylmethionine and S-adenosylhomocysteine represents an important pathway for transmethylation reactions. It can be followed either by transsulfuration to form cysteine or by remethylation to regenerate methionine (Baric, 2009). Several enzymes are involved in these pathways and two of these enzymes also represent putative target proteins of furan adduct formation, i.e. S-adenosylmethionine synthetase isoform type-1 and betaine-homocysteine S-methyltransferase 1 (Fig. 38).

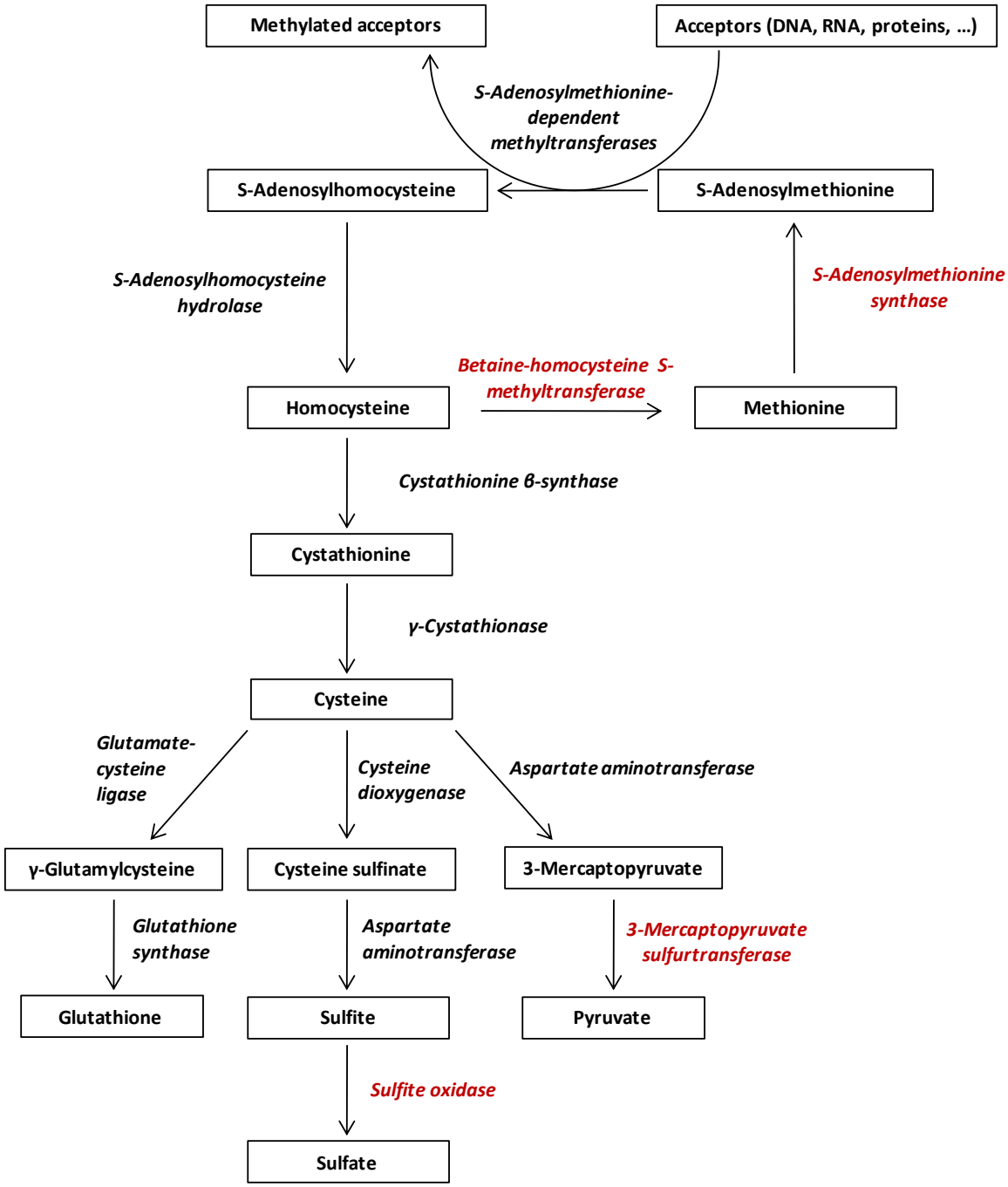

Figure 38 *Metabolism of the sulfur-containing amino acids methionine, homocysteine, and cysteine (modified from KEGG Pathway Database, http://www.genome.jp/kegg/pathway.html, Baric 2009, and Tan 2005). Furan target proteins are marked in red.*

S-Adenosylmethionine synthetase isoform type-1 (methionine adenosyltransferase 1, MAT 1) is expressed in the liver and transfers the adenosyl group of ATP to the amino acid methionine, thereby producing S-adenosylmethionine (SAM), which represents the main biological methyl donor (Baric, 2009; Ulrey et al., 2005). Substrates of SAM-dependent transmethylation reactions are DNA, RNA, proteins, neurotransmitters, and phospholipids (Ulrey et al., 2005). Knockout of the MAT 1 gene in mice led to increased

plasma levels of methionine and a decreased hepatic content of S-adenosylmethionine and glutathione, while S-adenosylhomocysteine levels and global DNA methylation were not altered (Lu et al., 2001). In MAT 1 knockout mice, liver hyperplasia, inflammation and macrovesicular steatosis were observed. Furthermore, a study using MAT 1 knockout mice revealed changes in the expression of genes involved in lipid and glucose metabolism accompanied by hyperglycemia, induction of CYP2E1 and mitochondrial uncoupling protein 2, enhanced triglyceride and decreased hepatic glutathione content, and increased lipid peroxidation (Martinez-Chantar et al., 2002). Importantly, MAT 1 knockout mice also showed increased incidences of hepatocellular carcinoma. Although no changes in the global DNA methylation were observed in MAT 1 knockout mice, it may well be possible that the methylation state of promoter regions of individual genes may be altered. The methylation state of a gene promoter region is known to affect gene expression. Increased or decreased methylation can lead to silencing or overexpression of the gene, respectively (Ulrey et al., 2005). Thus, hypermethylation of tumor suppressor genes or hypomethylation of oncogenes can promote tumor initiation. In this respect, the increased incidences of hepatocellular carcinoma reported in MAT 1 knockout mice may represent the final step in a chain of events leading from lack of functional MAT 1 protein via decreased SAM levels and altered methylation of cancer-related genes to cancer development. No changes in global DNA methylation were evident after furan treatment for 28 days in both male mice (2, 4, 8 and 15 mg/kg bw) and male rats (0.1, 0.5, 2 mg/kg bw) (Chen et al., 2010; Cordelli et al., 2010). Moreover, in male rats furan treatment did not appear to alter DNA methylation status of five different genes relevant to carcinogenesis (Chen et al., 2010). Thus, it is unclear whether loss of MAT 1 function caused by covalent binding of furan reactive metabolites may contribute to furan-induced liver carcinogenicity.

Betaine-homocysteine S-methyltransferase 1 (BHMT1) is a high abundance protein in the liver of most mammals (0.6-1.6 % of total protein), which catalyzes the formation of methionine from homocysteine through transmethylation, thereby converting betaine to dimethylglycine (Pajares and Perez-Sala, 2006). Druckova et al. showed that BHMT1 represents a target protein of the hepatotoxic compound teucrin A which forms a reactive metabolite structurally similar to *cis*-2-butene-1,4-dial (Druckova et al., 2007).

Inhibition of BHMT1 expression in vitro was associated with impaired homocysteine metabolism and induction of ER stress (Ou et al., 2007). However, BHMT1 represents a high abundance protein and the remethylation of homocysteine to methionine is also possible through other enzymes like methionine synthase. Thus, it is unclear whether adduct formation at BHMT1 by furan and teucrin A may result in reduction of overall BHMT1 function and disturbed methionine and homocysteine metabolism.

Sulfite oxidase (SO), an enzyme present in the mitochondrial intermembrane space of many mammalian tissues including liver, catalyzes the oxidation and detoxification of sulfite to sulfate as a final reaction in the metabolism of sulfur amino acids, thereby transferring electrons to its physiological electron acceptor cytochrome c (Feng et al., 2007; Woo et al., 2003). Cytochrome c is a small heme-containing protein located in the inner mitochondrial membrane, which participates in the respiratory chain through shuttling electrons between the complexes III (cytochrome reductase) and IV (cytochrome c oxidase). Thus, SO contributes to energy production by passing on electrons obtained from the reduction of sulfite to the respiratory chain. Patients suffering from SO deficiency show severe neurological, but no hepatic symptoms (Tan et al., 2005). The loss of SO function through binding of furan metabolites may lead to an accumulation of sulfites, but there is no evidence whether this may also affect liver function or have hepatotoxic effects.

8.3.3.6 Structural proteins

Actin, one of the most abundant proteins present in eukaryotic cells (Schleicher and Jockusch, 2008), is a key component of the cytoskeleton, which provides mechanical support, allows cell motility, and participates in the regulation of intracellular signaling. Although impaired function of actin may have detrimental effects on cells, we consider that covalent binding of furan reactive metabolites to a small fraction of this high abundance protein is unlikely to affect overall protein function.

The protein **Ezrin-radixin-moesin-binding phosphoprotein 50** (EBP50), also known as Na^+/H^+ exchanger regulatory factor 1, was reported to participate in protein complexes, which anchor and stabilize transmembrane receptors and transporters at the plasma

membrane and regulate their activity (Georgescu et al., 2008). In hepatocytes and cholangiocytes, EBP50 was found to be localized to the apical membrane where it was suggested to play a role in organization and regulation of bile secretory proteins (Fouassier et al., 2001). In line with this, it was reported that in EBP50 knockout mice the transport protein mrp2 (multidrug resistance-associated protein 2) was decreased to 70 % and that bile flow was reduced to approximately 70 % together with a 50 % reduction in glutathione excretion, while bile acid and bilirubin excretion were not altered (Li et al., 2010). These findings indicate that EBP50 is involved in the canalicular expression of mrp2, which regulates glutathione-dependent, bile acid-independent bile flow (Li et al., 2010). Thus, covalent binding of furan metabolites to EBP50 and possible loss of its function may result in decreased bile flow. In addition to transporters and receptors, EPB50 can also bind further ligands such as β-catenin (mitogenic and possibly oncogenic) and localize them to the cell membrane, thereby preventing the ligands from translocating to cytoplasm and nucleus where they may induce cellular effects (e.g. cell growth) (Georgescu et al., 2008). Although the role of EBP50 in cancer is still not fully established, the aforementioned findings suggest that EBP50 may act as a tumor suppressor when located at the membrane (Georgescu et al., 2008). Consequently, loss of EBP50 function, e.g. due to furan adduct formation, may disrupt interactions between EBP50 and its ligands and cause their redistribution to the cytoplasm and/or nucleus. There, EBP50 may act in an oncogenic manner and promote cell growth, possibly via formation of complexes with mediators like β-catenin (Georgescu et al., 2008). In support of this, siRNA-mediated knockdown of EBP50 in proliferating cholangiocytes was shown to result in strong reduction of bromodeoxyuridine incorporation, indicating that EBP50 may participate in the regulation of cell proliferation (Fouassier et al., 2009).

Fibrinogen γ chain (FGG) is one of the three fibrinogen chains which are synthesized in hepatocytes and are combined to yield fibrinogen (Vu and Neerman-Arbez, 2007). During the coagulation process, fibrinogen is cleaved by thrombin to fibrin that forms a clot by polymerization (Vu and Neerman-Arbez, 2007). Several mutations of the genes encoding the fibrinogen chains in humans have been reported, with patients developing quantitative (hypo-, afibrinogenemia) or qualitative (dysfibrinogenemia) fibrinogen alterations (Undas et al., 2009). Nearly half of these cases were associated with either

bleeding (hypo- or afibrinogenemia) or thrombosis (dysfibrinogenemia) (Undas et al., 2009). It was reported that mutations resulting in the exchange of amino acids in FGG can lead to dysfibrinogenemia and an increased risk of thrombosis (Robert-Ebadi et al., 2008). This may be due to the fact that thrombin binding to altered fibrinogen is impaired and excessive thrombin in the blood circulation may result in thrombosis. A further explanation may be that changes in FGG may lead to reduced binding of tissue plasminogen activator and thus decreased fibrinolysis. This is supported by the finding that the structure of clots containing altered fibrinogen varies from normal clots (Robert-Ebadi et al., 2008). A third factor possibly contributing to an increased risk of thrombosis in patients with dysfibrinogenemia may be the loss of functionality of a certain site at FGG that is responsible for correct polymerization of fibrinogen. The binding of furan metabolites to FGG may result in blocking of important binding sites of fibrinogen and an increased risk of thrombus formation. The occurrence of blood clots in small vessels and their resulting obstruction may lead to locally different blood flows. It was hypothesized that inter- and intralobular differences in liver perfusion or vascular lesions constricting blood supply may play a role in locally different susceptibilities of liver lobes to toxic furan effects (Mally et al., 2010). Thus, loss of function of FGG through furan adduct formation may represent a link between protein binding and the phenomenon of the regional susceptibility of liver lobes to furan toxicity.

Keratin, type II cytoskeletal 8 (cytokeratin-8, CK-8) is a member of the family of intermediate filaments (IF). IFs are important for mechanical stability of the cell, intracellular organization, and transport (Gonias et al., 2001). In the liver, CK-8 is highly expressed in hepatocytes, oval cells and cholangiocytes (Strnad et al., 2008). Although CK-8/CK-18 knockout mice have been shown to be more susceptible to liver injury (Strnad et al., 2008), it is questionable if furan binding to this high abundance protein results in significant loss of overall protein function.

Na(+)/H(+) exchanger regulatory factor 3 (NHERF3, diphor-1, clamp, PDZK1) is a scaffold protein that is expressed in epithelia and endothelia of several organs including liver (Kocher and Krieger, 2009). NHERF3 contains four binding domains, which interact with different partner proteins such as receptors (e.g. high density lipoprotein (HDL) receptor

SR-BI (scavenger receptor class B type I)), ion channels and ion transporters (Hu et al., 2009; Kocher and Krieger, 2009). In studies using NHERF3 knockout mice, nearly total loss of hepatic SR-BI protein expression, hypercholesterolemia and enlarged HDL particles were observed (Kocher et al., 2003). Thus, it was suggested that NHERF3 represents an adaptor protein for the regulation of hepatic HDL receptor levels and may hence be involved in reverse cholesterol transport (Kocher and Krieger, 2009). SR-BI null mice were reported to show increased plasma levels of cholesterol, probably as a result of decreased selective cholesterol uptake (Rigotti et al., 1997). Moreover, it was observed that in NHERF3 knockout mice an organic anion transporting polypeptide (Oatp1a1) was not correctly localized to the liver cell surface as in wildtype mice, but was present at intracellular structures, indicating that NHERF3 is responsible for targeting Oatp1a1 to the basolateral cell membrane where it can exert its transport functions (Wang et al., 2005b). Oatp1a1 was reported to be involved in the basolateral uptake of a variety of molecules such as enalapril and different bile acids derivatives into hepatocytes (Chang et al., 2005; Zsembery et al., 2000). Knockout of Oatp1a/1b in mice was reported to result in increased plasma levels of unconjugated bile acids (van de Steeg et al., 2010). Furan administration (2 mg/kg bw, 4 weeks) induced a statistically significant increase in unconjugated bile acids and a slight increase in cholesterol in rat plasma (Mally et al., 2010). These findings may represent a possible hint that loss of NHERF3 function through binding of furan metabolites may result in disrupted regulation of NHERF3 partner proteins, which may, for example, lead to impaired transport function of Oatp1a1 or inhibition of SR-BI-mediated cholesterol uptake.

Protein SEC13 homolog (SEC13l1) is the mammalian form of the yeast SEC13 protein (Tang et al., 1997). SEC13l is a part of and plays a structural role in the coat protein complex II (COPII) and in the nuclear pore complex (NPC) (Brohawn and Schwartz, 2009; Stagg et al., 2006). COPII is involved in the vesicular transport of proteins from the rough endoplasmic reticulum to the Golgi apparatus (anterograde transport), whereas the NPCs provide the possibility to exchange various molecules between the cytosol and the nucleus (Siniossoglou et al., 2000; Stagg et al., 2006). Depletion of SEC13l was found to inhibit ER-Golgi transport in normal rat kidney (NRK) cells (Tang et al., 1997). Yeast SEC13 mutants were shown to display disrupted nuclear envelopes and NPCs (Siniossoglou et al.,

2000). Considering the various and essential roles of SEC13l1, binding of furan metabolites and subsequent loss of protein function may lead to impaired vesicular transport and nonfunctional NPCs, which may result in cell death.

8.3.3.7 Transport proteins

α2μ-Globulin belongs to the lipocalin family whose members bind and transport small lipophilic molecules such as pheromones (Cuervo et al., 1999; Pervaiz and Brew, 1987). α2μ-globulin is extensively synthesized in male rat liver, secreted into plasma and degraded in lysosomes in kidney epithelial cells (Hard et al., 1993). It is well established that non-covalent binding of certain chemicals can prevent lysosomal degradation of α2μ-globulin, leading to accumulation within proximal tubules cells and subsequent tubule damage. Furthermore, covalent binding of thiobenzamide metabolites, which are associated with hepatotoxicity, to α2μ-globulin was reported (Ikehata et al., 2008). Based on our current understanding of the role and function of α2μ-globulin and the fact that α2μ-globulin is expressed in male rats only whereas no sex differences exist with regard to furan toxicity and carcinogenicity, it appears that covalent binding of furan to α2μ-globulin is unlikely to contribute to furan hepatotoxicity.

Transthyretin (thyroxine binding prealbumin), which is synthesized predominantly in the liver and the choroid plexus (brain), was first known as a binding and transport protein of thyroxine and retinol in serum and cerebrospinal fluid (Buxbaum and Reixach, 2009; Fleming et al., 2009). Transthyretin was also reported to represent a target protein of thiobenzamide (Ikehata et al., 2008). Transthyretin or its mutant forms were found to be involved in the pathogenesis of some forms of amyloidoses, diseases associated with the extracellular aggregation and deposition of misfolded proteins leading to impaired organ function (Buxbaum and Reixach, 2009). While the nervous system and heart represent the main targets of these diseases, deposition of aggregates in the liver and impaired hepatic function have not been reported (Buxbaum and Reixach, 2009). Transthyretin was suggested to participate – together with albumin – in detoxification of a variety of small endogenous and exogenous molecules by transporting them to the liver for metabolism or to the kidneys for excretion (Buxbaum and Reixach, 2009). Interestingly, binding of these small molecules seems to stabilize the tetrameric form of transthyretin and thus

decrease the formation of aggregates (Buxbaum and Reixach, 2009). Considering the role of transthyretin in the detoxification of small molecules, this protein may have cytoprotective effects by binding the reactive furan metabolite *cis*-2-butene-1,4-dial.

Vitamin D binding protein (DBP, Gc globulin) is formed in the liver and is excreted into the plasma where it represents the main carrier of vitamin D and its metabolites (Speeckaert et al., 2006). DBP also binds free G-actin monomers released from injured or dying cells in order to prevent their polymerization in the extracellular space, thereby protecting from organ dysfunction and vascular obstruction (Speeckaert et al., 2006). DBP shows a rapid turnover rate and is highly polymorphic (Speeckaert et al., 2006). It was reported that DBP null mice expressing no DBP showed normal viability, fertility, size and appearance (Safadi et al., 1999). Impaired DBP function through furan adduct formation may lead to increased polymerization of actin in the extracellular space. However, there is no evidence so far to suggest that this effect may be involved in furan-induced liver toxicity and carcinogenicity.

8.3.3.8 Proteins involved in the metabolism of nucleotides and nucleic acids

Heterogeneous nuclear ribonucleoprotein H1 (hnrnp H1) represents an isoform of hnrnp H, which belongs to a family of RNA binding proteins, heterogeneous nuclear ribonucleoproteins (hnrnps), that are ubiquitously expressed and participate in the processing of pre-mRNAs and mRNAs, i.e. regulation of splicing and alternative splicing, polyadenylation, capping, transcriptional regulation, export from the nucleus into the cytoplasm, localization, stability, and translation (Chaudhury et al., 2010). For this purpose, hnrnps together with further proteins are associated with mRNAs in mixed complexes, which are formed specifically with each mRNA species and do not only act as a simple packaging unit, but also play an important role in mRNA development by carrying the information about mRNA processing (Dreyfuss et al., 2002). Since also pro- and antiapoptotic effects of hnrnp H1 were reported (Garneau et al., 2005; Rauch et al., 2010), loss of hnrnp H1 function through binding of furan metabolites may cause impaired mRNA processing and influence apoptosis. These effects may contribute to furan cytotoxicity and carcinogenicity.

Little information is available about the mammalian or eukaryotic **L-aspartate dehydrogenase**. However, the enzyme was characterized in the bacterium Thermotoga maritima and in the archaeon Archaeoglobus fulgidus (Yang et al., 2003; Yoneda et al., 2006). In Thermotoga maritima, L-aspartate dehydrogenase is thought to be involved in the de novo biosynthesis of NAD^+ from L-aspartate where it catalyzes the first step, i.e. the conversion of L-aspartate to iminoaspartate, which is unstable and can decompose to oxalacetate and ammonia (Yang et al., 2003). Since it remains unknown whether L-aspartate dehydrogenase exerts the same function in mammals, it is difficult to suggest a connection to furan-induced toxicity.

Multifunctional protein ADE2 is an octameric and bifunctional enzyme that contains the domains for phosphoribosylaminoimidazole-succinocarboxamide synthase and phosphoribosylaminoimidazole carboxylase, both of which participate in purine metabolism where they catalyze two consecutive steps in the chain of reactions from 5-phosphoribosyl-1-pyrophosphate to inosine-5'-monophosphate formation (Li et al., 2007; Zhang et al., 2008). Loss of function of this bifunctional enzyme through binding of furan metabolites may impair de novo purine biosynthesis. However, since normal cells, in contrast to tumor cells, mainly use the salvage pathway to cover their purine demands (Li et al., 2007), functional inactivation through adduct formation does not appear to have a strong influence on the cellular purine pool and thus may not play a major role in the pathogenesis of furan-induced toxicity.

8.3.3.9 Intracellular transport of bile acids

It is well known that deficiency of bile acid transport proteins (e.g. bile salt export pump, multidrug-resistant protein 3) in the cell membrane of hepatocytes may play a role in the pathophysiology of cholestatic liver disease (Pellicoro and Faber, 2007), which includes accumulation of toxic bile acids resulting in mitochondrial dysfunction and cell death via damage to biological membranes (Palmeira and Rolo, 2004; Perez and Briz, 2009).

Furan administration was reported to result in elevated plasma levels of endogenous metabolites normally excreted in bile such as cholesterol and bilirubin (Hamadeh et al., 2004; Mally et al., 2010). Moreover, treatment with furan was shown to cause elevated levels of bile acids in mice and rats (Fransson-Steen et al., 1997; Mally et al., 2010).

Therefore, it has been suggested that furan may interfere with hepatobiliary transport mechanisms through covalent binding of furan reactive metabolites to transport proteins located in the cell membranes of hepatocytes. However, adduct formation directly at these membrane transporters was not confirmed in our study as no membrane transporters were identified as furan target proteins. Nevertheless, furan may interfere with bile acid transport since two intracellular bile acid transport proteins were identified as furan targets, i.e. **3α-hydroxysteroid dehydrogenase** (3α-HSD, Akr1C9) and **liver fatty acid binding protein** (L-FABP, FABP1) (Alrefai and Gill, 2007).

3α-HSD, which was previously shown to be adducted by reactive metabolites of both thiobenzamide and bromobenzene (Ikehata et al., 2008; Koen et al., 2007), is highly expressed in the liver (MacLeod et al., 2010) and is involved in the metabolism of various compounds such as steroid hormones and glucocorticoids (Usui et al., 1994). In vitro, inhibition of bile acid binding to 3α-HSD by indomethacin was shown to cause redistribution of bile acids from the cytosol out of the cell into the media, suggesting that loss of function of 3α-HSD may induce decreased uptake, increased sinusoidal reflux, and decreased excretion of bile acids into bile (Alrefai and Gill, 2007). Thus, loss of function of 3α-HSD by covalent binding of furan may impair hepatobiliary transport, hence contributing to furan-induced cytotoxicity.

Liver fatty acid binding protein (L-FABP, FABP1), which was identified as a target protein of thiobenzamide and bromobenzene (Ikehata et al., 2008; Koen et al., 2007), is a high abundance protein, accounting for 2-6 % of the cytosolic protein in rat liver cells (Sorof, 1994). L-FABP has various functions in the uptake and metabolism of long chain fatty acids (LCFA) and protects the cells from deleterious effects of free fatty acids through binding of LCFAs and LCFA-CoAs (Atshaves et al., 2010). Several studies using L-FABP null mice yielded inconsistent results regarding the influence of L-FABP gene ablation on different parameters such as bile acid pool size and biliary lipid secretion (Martin et al., 2005; Xie et al., 2009). Considering these findings, together with the fact that L-FABP is a high abundance protein, it is unclear whether or to what extent loss of L-FABP function through furan adduct formation may have cellular consequences. Additionally, stable transfection of L-FABP into non-L-FABP-expressing liver cells improved their ability to

cope with oxidative stress, suggesting antioxidant and cytoprotective roles of L-FABP (Wang et al., 2005a). Interestingly, chemically reactive intermediates, including prostaglandins containing α,β-unsaturated carbonyls and electrophilic metabolites of the genotoxic hepatocarcinogen 2-acetylaminofluorene, were found to covalently bind to L-FABP, thereby apparently inhibiting cell proliferation (Sorof, 1994). It has been speculated that this covalent modification blocked or decreased the L-FABP binding capacity for endogenous mitogenic ligands (e.g. unsaturated fatty acids, peroxisome proliferators), thereby interfering with the proliferative effects of these ligands (Sorof, 1994).

8.3.3.10 Miscellaneous

Aflatoxin B1 aldehyde reductase member 2 (rAFAR2-2, AKR7A2, succinic semialdehyde reductase) belongs to the aldo-keto reductase family 7 and was found to be located to the Golgi apparatus, where it catalyzes the synthesis of γ-hydroxybutyrate (GHB) from succinic semialdehyde and presumably facilitates its secretion (Kelly et al., 2002). Regarding the function of rAFAR2-2, there seems to be no evidence for a potential connection between loss of protein function and furan toxicity.

Mitochondrial **aldehyde dehydrogenase** (ALDH-2), which represents a common target of furan, teucrin A, bromobenzene, and acetaminophen (Druckova et al., 2007; Koen et al., 2007; Qiu et al., 1998), is expressed predominantly in the liver and kidneys. Its role is to metabolize aliphatic and aromatic aldehydes, including detoxification of reactive aldehydes formed during oxidative stress, such as malondialdehyde and 4-hydroxynonenal (Crabb et al., 2004; Wenzel et al., 2008). The catalytic site of ALDH-2 contains three cysteine residues (Wenzel et al., 2008), which may be targeted by cis-2-butene-1,4-dial, potentially during an attempt to metabolize this reactive furan metabolite. Loss of function through covalent binding of furan reactive metabolites may then lead to decreased ability to detoxify endogenous aldehydes, leading to increased oxidative stress and cytotoxicity.

δ-Aminolevulinic acid dehydratase (ALAD, porphobilinogen synthase) is involved in the formation of porphobilinogen through asymmetric condensation of two molecules of δ-aminolevulinic acid (Jaffe, 2004). Porphobilinogen and δ-aminolevulinic acid represent

important intermediates in the biosynthesis of tetrapyrrole pigments, such as porphyrin, which is further used to produce heme (Jaffe, 2004). Hereditary deficiency of ALAD, which occurs as acute hepatic porphyria, was reported, but occurs very rarely (Jaffe and Stith, 2007). The clinical manifestations in patients showing a decrease in ALAD activity down to less than 10 % include colicky abdominal pain, vomiting, and polyneuropathy (Doss et al., 2004; Thunell et al., 1987). Thus, it is not evident whether and how inactivation of δ-aminolevulinic acid dehydratase may be involved in furan-induced toxicity in rat liver.

Formimidoyltransferase-cyclodeaminase (FTCD) is a bifunctional and homooctameric enzyme consisting of the domains glutamate formimidoyltransferase (FT) and formimidoyltetrahydrofolate cyclodeaminase (CD) (Murley and MacKenzie, 1997). FTCD catalyzes two successive reactions, thereby connecting histidine degradation with folate metabolism (Mao et al., 2004). Additionally, FTCD was reported to be associated with the Golgi apparatus and to be involved in the assembly of vimentin intermediate filaments, suggesting that FTCD functions as a mediator between the Golgi apparatus and the cytoskeleton, a function that appears to be independent of its catalytic activity (Bashour and Bloom, 1998; Gao and Sztul, 2001; Mao et al., 2004). FTCD was also found to be located at the centrosome where it presumably provides the centriole tubulins with glutamate required for stabilization through polyglutamylation (Hagiwara et al., 2006). Moreover, glutamate formimidoyltransferase deficiency with modest neurological symptoms was observed in humans (Hilton et al., 2003). Impaired protein function of FTCD through binding of furan metabolites may result in disturbed catalytic activity and/or disrupted cell structure. However, it is unclear how these effects may contribute to furan cytotoxicity.

NDRG2 (N-myc downstream-regulated gene 2) was found to be expressed in the cytoplasm of a variety of tissues including brain, heart, and liver (Yao et al., 2008). NDRG2 overexpression was shown to cause cell cycle arrest, enhanced apoptosis, and inhibition of tumor invasion via suppression of NFκB activity (Kim et al., 2009; Yao et al., 2008), suggesting antiproliferative, proapoptotic and antimetastatic functions of NDRG2. Overall, it appears that loss of NDRG2 function through covalent binding of furan may play a role

in promoting cell proliferation and tumorigenesis rather than participating in furan-mediated cytotoxicity.

The finding that **ppa1 protein (inorganic pyrophosphatase 1, PPase)** was identified as a putative target of furan, might further support the hypothesis that furan toxicity may be mediated through impaired energy production. Ppa1 protein, a highly conserved cytoplasmic enzyme present in many cells and tissues, mainly the liver, catalyzes the hydrolysis of diphosphate (pyrophosphate) yielding two molecules of phosphate (Shatton et al., 1983). This cleavage represents an exergonic reaction and provides energy that is needed for unfavorable cellular processes, such as the activation of fatty acids for degradation (Lundin et al., 1991; Shatton et al., 1983). This important role of ppa1 protein which consists of enabling and driving forward many unfavorable metabolic processes indicates the importance of ppa1 protein for cell survival (Lundin et al., 1991). In line with this assumption, disruption of the ppa1 gene was reported to result in cell death in yeast (Lundin et al., 1991). Thus, impaired protein function through binding of furan metabolites to ppa1 protein may contribute to disruption of metabolic pathways, such as fat metabolism, amino acid activation, glycogen synthesis, and urea synthesis (Guynn et al., 1974; Panda et al., 2007). In line with this, ppa1 protein was also observed to be adducted during the occurrence of acetaminophen-induced hepatotoxicity, which was shown to be associated with impaired mitochondrial energy metabolism in the liver (Katyare and Satav, 1989; Qiu et al., 1998).

Ribonuclease UK114 (Perchloric acid soluble protein, 14.5 kDa translational inhibitor protein), which is mainly expressed in liver and kidneys, was reported to effectively inhibit protein synthesis in a rabbit reticulocyte lysate system through its endoribonucleolytic activity (Antonenkov et al., 2007; Chong et al., 2008; Morishita et al., 1999). Furthermore, ribonuclease UK114 was observed to be induced after activation of ER stress, suggesting that it participates in cellular stress response (Kanouchi et al., 2005). While it was reported that overexpression of ribonuclease UK114 caused decreased cell proliferation in a rat kidney, hepatocyte, and hepatoma cell line, contradictory findings were observed in HepG2 cells (Chong et al., 2008; Kanouchi et al., 2001). Thus, it remains unclear whether ribonuclease UK114 actually represents a tumor suppressor. It is hence

not evident which effect adduct formation through furan reactive metabolites and possible loss of protein function may have on cell proliferation. However, considering the possible role of ribonuclease UK144 in ER stress response, impaired protein function due to furan binding may result in disturbed cellular defense mechanisms. Interestingly, ribonuclease UK114 was also identified as a target protein of thiobenzamide and bromobenzene (Ikehata et al., 2008; Koen et al., 2007).

After its synthesis in the liver, the precursor **protein AMBP** is transported to the Golgi system where it is cleaved into two separately secreted proteins, i.e. **α_1-microglobulin** and **bikunin** (inter-α-trypsin inhibitor light chain) (Akerstrom et al., 2000; Lindqvist et al., 1992). Moreover, the proteinase inhibitor **trypstatin** identified in rat peritoneal mast cell granules was shown to consist of an amino acid sequence identical with the C-terminal part of bikunin, thus indicating that it is also derived from the protein AMBP (Itoh et al., 1994). The reason for the phenomenon of cosynthesis of α_1-microglobulin and bikunin is still unknown since the obtained proteins can also be expressed independently (Akerstrom et al., 2000).

The glycoprotein **α_1-microglobulin** is a member of the lipocalin family and is mainly localized in liver, plasma, and kidneys (Akerstrom et al., 2000). α_1-microglobulin was found to form complexes in plasma with various binding partners, such as IgA, albumin, and mutated versions of coagulation factors, probably via the free cysteine residue Cys^{34} (Akerstrom et al., 2000). It is unclear whether and how loss of α_1-microglobulin may contribute to furan toxicity and carcinogenicity.

Bikunin is a monomeric glycoprotein mainly expressed in the liver and contains two domains which show proteinase inhibitor activity and include three characteristically arranged disulfide bonds (Fries and Blom, 2000). Female mice deficient in the bikunin gene showed infertility, which occurred presumably due to disturbed formation of extracellular oocyte matrix, indicating that bikunin function may be essential for the extracellular matrix (Zhuo et al., 2001). The results of several studies suggested that bikunin exerts an antiinflammatory function through suppression of proteolysis, which is usually activated during inflammation, through stabilization of the extracellular matrix, through inhibition of expression and translation of inflammatory cytokines, and through disruption of the inflammatory cascade (Kobayashi, 2006). In various studies, it was

reported that furan administration resulted in inflammation, which is assumed to contribute to tissue damage and tumor formation (Gill et al., 2010; Hamadeh et al., 2004; NTP, 1993; Wilson et al., 1992). Thus, loss of function of bikunin through adduct formation may enhance the inflammatory effects of furan and may hence be involved in furan-mediated cytotoxicity and carcinogenesis.

8.3.4 Estimation of the degree of protein adduction

To estimate the relative degree of covalent protein adduction, the ratios of the amount of radioactivity and the total amount of protein were calculated for each spot. The mean ratios and standard deviations were determined (see Annex, Fig. 39). Ranking of target proteins was conducted according to the degree of protein adduction relative to the abundance of the protein (Tab. 20). Based on these semiquantitative analyses, some of the most adducted proteins were found to be structural proteins (keratin type II cytoskeletal 8, actin β/γ) and transport proteins (α2μ-globulin, fatty acid binding protein 1). Furthermore, proteins involved in detoxification (aldehyde dehydrogenase) and redox homeostasis (thioredoxin-1, peroxiredoxin-1), glucose (glyceraldehyde-3-phosphate dehydrogenase, triosephosphate isomerase) and lipid metabolism (short-chain specific acyl-CoA dehydrogenase, isovaleryl-CoA dehydrogenase), as well as the ER stress sensor 78 kDa glucose-regulated protein, showed a relatively high level of adduction. These findings further support a potential role of impaired energy production, altered redox balance and reduced ability to cope with misfolded proteins in furan toxicity.

Table 20 *Ranking of furan target proteins based on densitometry of protein spots on Coomassie Blue stained gels and spots obtained by fluorography (Ratio film/gel). ++++ = ratio > 100, +++ = ratio 50-100, ++ = 25-50, + = < 25*

Level of adduction	pH range 4-7, whole tissue extract	pH range 6-9, whole tissue extract	pH range 4-7, membrane fraction
++++	α2μ-Globulin Thioredoxin-1	Short-chain specific acyl-CoA dehydrogenase Arginase 1 Glyceraldehyde-3-phosphate dehydrogenase	78 kDa Glucose-regulated protein
+++	Aldehyde dehydrogenase	Peroxiredoxin-1 Isovaleryl-CoA dehydrogenase	Fatty acid binding protein 1 Keratin type II cytoskeletal 8 Actin β/γ Protein NDRG2 Triosephosphate isomerase
++	Keratin, type II cytoskeletal 8 δ-Amiolevulinic acid dehydratase Long-chain fatty acid CoA ligase 1 Actin β/γ Ribonuclease UK114 Heat shock cognate 71 kDa protein Triosephosphate isomerase	Ornithine carbamoyltransferase Argininosuccinate synthase 3-Ketoacyl-CoA thiolase Enoyl-CoA hydratase	Heat shock cognate 71 kDa protein, Na(+)/H(+)exchanger regulatory factor 3
+	Thioredoxin-like protein 1 Protein AMBP Glycerol-3-phosphate dehydrogenase Fructose-1,6-bisphosphatase 1 3α-Hydroxysteroid dehydrogenase Fibrinogen γ chain Malate dehydrogenase Actin β/γ Keratin, type II cytoskeletal 8 α-Enolase Ezrin-radixin-moesin-binding phosphoprotein 50 Isovaleryl-CoA dehydrogenase α2μ-Globulin 3-Mercaptopyruvate sulfurtransferase Regucalcin ATP synthase β subunit Protein SEC13 homolog Ppa1 protein	Putative L-aspartate dehydrogenase Electron transfer flavoprotein subunit α Acetyl-CoA acetyltransferase Fructose-bisphosphate aldolase B L-lactate dehydrogenase A chain Voltage-dependent anion-selective channel protein 1 Argininosuccinate synthase Betaine-homocysteine S-methyltransferase 1 3-Ketoacyl-CoA thiolase Phosphoglycerate kinase 1 Multifunctional protein ADE2 Glycerol-3-phosphate dehydrogenase 3α-Hydroxysteroid dehydrogenase Ornithine carbamoyltransferase Ribonuclease UK114 Fatty acid binding protein 1	Ubiquitin fusion degradation protein 1 homolog S-Adenosylmethionine synthetase isoform type-1 2-Oxoisovalerate dehydrogenase subunit α α_1-Antiproteinase Aldehyde dehydrogenase Heterogeneous nuclear ribonucleoprotein H1 Long-chain specific acyl-CoA dehydrogenase Aflatoxin B1 aldehyde reductase member 2 Transthyretin α2μ-Globulin Protein disulfide-isomerase A3 Formimidoyltransferase-cyclodeaminase Sulfite oxidase Serine protease inhibitor A3K, Vitamin D-binding protein, Protein disulfide-isomerase ATP synthase β subunit 78 kDa Glucose-regulated protein Na(+)/H(+) exchanger regulatory factor 3

8.4 Conclusions

Pathway mapping analysis showed that the 61 identified furan target proteins are mainly derived from cytosol and mitochondria and participate in various cellular pathways, predominantly fatty acid, amino acid, and glucose metabolism. Furthermore, several target proteins were found to be involved in cell redox homeostasis. While it is not known if adduct formation at proteins through furan actually leads to loss of protein function, we tried to establish which cellular consequences may result from inhibited functions of the 61 furan target proteins and how these cellular effects may be linked to cytotoxicity.

First, disrupted function of proteins involved in glycolysis/gluconeogenesis, mitochondrial fatty acid metabolism, degradation of amino acids and ATP synthesis may lead to a decreased supply of precursor metabolites for the production of energy in the mitochondria, reduced mitochondrial energy production, ATP depletion and oxidative stress. These findings suggest that furan cytotoxicity may be mediated through mitochondrial dysfunction and energy depletion. This is consistent with a study by Mugford et al. which demonstrated that uncoupling of hepatic oxidative phosphorylation is involved in furan-mediated cell death (Mugford et al., 1997).

Second, furan was also found to bind to proteins participating in cellular redox regulation (electron transfer flavoprotein subunit α, peroxiredoxin-1, thioredoxin-1, thioredoxin-like protein 1, regucalcin, 3-mercaptopyruvate sulfurtransferase). A loss of function of these proteins may lead to oxidative stress in the cell and thus promote mitochondrial dysfunction, thereby contributing to furan-induced cytotoxicity.

Third, loss of function of proteins participating in protein folding and proteolysis (heat shock cognate 71 kDa protein, 78 kDa glucose-regulated protein, protein disulfide isomerase, protein disulfide isomerase A3, ubiquitin fusion degradation protein 1 homolog, α_1-antiproteinase, serine protease inhibitor A3K, protein AMBP) may lead to impaired detection of damaged proteins and disruption of protein repair and degradation in the cell, resulting in an increased load of damaged and nonfunctional proteins.

Besides the potential malfunction of whole pathways due to loss of functions of several participating proteins, adduction of individual proteins with key functions may also be involved in furan toxicity and carcinogenicity. For instance, loss of function of proteins involved in transport processes across the mitochondrial membranes (voltage-dependent anion-selective channel protein 1, cytosolic malate dehydrogenase, cytosolic glycerol-3-

phosphate dehydrogenase) may contribute to mitochondrial dysfunction and thus to cytotoxicity. Furthermore, proteins involved in processes such as cell signaling (canonical Wnt pathway: serine protease inhibitor A3K), DNA methylation (S-adenosylmethionine synthetase isoform type-1), blood coagulation (fibrinogen γ chain), and bile acid transport (3α-hydroxysteroid dehydrogenase) may participate in furan-induced cytotoxicity and carcinogenicity.

A semiquantitative analysis to estimate the amount of radioactivity covalently bound to proteins in various spots showed that structural proteins (keratin type II cytoskeletal 8, actin β/γ) and transport proteins (α2μ-globulin, fatty acid binding protein 1) were among the most adducted furan targets. These proteins are mostly high abundance proteins and hence adduction of a small fraction of these proteins through furan metabolites may not per se contribute to cytotoxicity. Thus, their role in furan toxicity is unclear. However, it has been proposed that these proteins may detoxify and/or inactivate reactive furan metabolites, thus protecting proteins which may be less abundant but perhaps more important for cell survival (Hoivik et al., 1996).

9 FINAL CONCLUSIONS AND FUTURE PERSPECTIVES

Furan administration was shown to induce hepatotoxicity and liver tumors in rodents (NTP, 1993), but the mechanisms involved in furan toxicity and carcinogenicity remain to be elucidated. Irrespective of its genotoxic potential, results from previous studies suggest that furan toxic and carcinogenic effects may at least partly be mediated through a non-genotoxic mechanism including covalent binding to proteins, leading to cytotoxicity and subsequent regenerative cell proliferation (Burka et al., 1991; Lu et al., 2009; Wilson et al., 1992). In support of this, our data confirm that furan forms covalent protein adducts in rat liver, both at a known carcinogenic dose (2 mg/kg bw) and at a dose closer to estimated human exposure (0.1 mg/kg bw). While it is well established that protein binding may result in cytotoxicity (Evans et al., 2004), the cellular events involved are still poorly understood. In this context, two mechanistic links between protein adduct formation and furan toxicity are conceivable.

The first possible link is that covalent binding of reactive metabolites to cellular proteins may disrupt their proper folding and lead to accumulation of unfolded or damaged proteins in the endoplasmic reticulum (ER). In response to this ER stress, activation of the unfolded protein response (UPR) may be triggered to cope with the accumulated proteins. The UPR is a cellular pathway which enhances the cells capacity to recognize misfolded proteins and repair or target them for degradation by the proteasome. However, if the ER stress through accumulated proteins is too extensive and homeostasis cannot be maintained, cytotoxicity may occur.

Activation of the UPR leads to enhanced splicing of X-box binding protein-1 (XBP1) mRNA and specific alterations of expression of UPR target genes. In our experiments, neither altered XBP1 mRNA splicing nor expression changes of UPR target genes were evident. Thus, it appears that the amount of damaged and nonfunctional proteins accumulated in rat livers after treatment with either a known carcinogenic or an acutely hepatotoxic furan dose is not high enough to trigger activation of the UPR. Another possible explanation, however, may be that activation of the UPR cannot work properly due to loss of function of a protein involved in this process. Indeed, it may well be possible that adduction and inhibition of GRP78, the primary sensor of ER stress, may prevent activation of the UPR (Martin et al., 2010).

The second possibility for a mechanistic link between protein adduct formation and furan toxicity is that protein binding by a compound may lead to impaired function of individual proteins or whole pathways, which may result in disruption of cell/tissue homeostasis and may cause toxicity. Moreover, it has also been recognized that adduction of some proteins may be critical to injury, whereas covalent binding to others is not (Zhou et al., 2005). To establish how furan protein binding may be involved in furan-induced liver toxicity and carcinogenicity, we identified putative target proteins of furan reactive metabolites.

Our data demonstrate that furan binds to a large number of proteins localized predominantly in the cytosol and mitochondria. Among the most adducted furan targets were structural proteins and transport proteins. However, their contribution to the mechanism of furan toxicity is not apparent. It is conceivable that binding to these high abundance proteins may lead to detoxification/inactivation of reactive furan metabolites, thus preventing damage and loss of function of proteins which may be less abundant but perhaps more important for cell survival.

In contrast, the finding that furan binds to a range of enzymes involved in glucose metabolism, mitochondrial β-oxidation and ATP synthesis suggests that furan toxicity may involve impaired mitochondrial energy production and oxidative stress through mitochondrial uncoupling. This is in line with data showing that uncoupling of hepatic oxidative phosphorylation is an early event in furan-mediated cell death (Mugford et al., 1997). In addition, adduct formation with proteins participating in the maintenance of redox homeostasis and protein folding/degradation mechanisms may result in reduced ability to cope with cellular/oxidative stress, including accumulation of misfolded proteins.

Besides the potential malfunction of whole pathways due to loss of functions of several participating proteins, loss of function of individual proteins which are involved in cellular processes such as transport processes across the mitochondrial membranes, cell signaling, DNA methylation, blood coagulation, and bile acid transport may also play a role in furan-induced cytotoxicity and carcinogenicity, e.g. through altered gene expression due to changes in gene methylation state or impaired hepatobiliary transport.

Commonalities and differences in target proteins of various chemical compounds (and their reactive metabolites) may help to elucidate how covalent binding to proteins may

be connected to toxicity and/or carcinogenicity. In the context of possible commonalities in target proteins, it is interesting to note that 33 of the 61 identified furan target proteins also represent target proteins of other drugs/compounds thought to cause toxicity via reactive metabolite formation. These 33 proteins predominantly relate to carbohydrate metabolism, redox regulation, and protein folding, suggesting that targeting and inhibiting these cellular functions may represent common events contributing to toxicity. However, not all drugs that target proteins are necessarily also carcinogenic. Thus, it may be hypothesized that inactivation of some proteins through adduct formation may relate to cytotoxicity, while inactivation of other proteins may promote carcinogenicity.

In summary, our data suggest that functional loss of several individual proteins and pathways, most notably mitochondrial energy production, redox regulation and protein folding, may combine to disrupt cell homeostasis and cause hepatocyte cell death. However, further work is needed to establish if adduction by furan reactive metabolites results in loss of individual protein function. In this respect, key questions that remain to be addressed are (i) to what extent peptides/proteins are adducted, (ii) which residues and sites of the proteins are adducted, i.e. catalytic and/or non-active sites, and (iii) what the turn-over rate of the protein is, i.e. how fast the damaged protein will be repaired. Recent approaches to address these questions are described below.

Determination of protein covalent modification sites

In order to experimentally establish whether and to what extent the identified putative target proteins of furan reactive metabolites actually lose their function and thus may be involved in furan toxicity, it is necessary to both determine the sites of covalent modification and assess the functionality of the protein after adduct formation.

Several studies addressing these questions have already been conducted for various substances and impaired or even loss of protein function through adduct formation by reactive compounds has been described. For instance, the α,β-unsaturated aldehyde acrolein showing a structure similar to BDA was found to covalently bind to a functionally important cysteine residue (Cys^{215}) in the active site of protein tyrosine phosphatase 1B, thus causing irreversible inactivation of the protein (Seiner et al., 2007). The experimental approach used by Seiner et al. consisted of the incubation of protein tyrosine

phosphatase 1B with acrolein and subsequent analysis of the purified tryptic digest using MALDI-TOF and ESI-QTOF mass spectrometry. MALDI-TOF analysis of the peptides revealed the presence of five adducted peptides. Among these adducted peptides, there was also the one containing the active site of the protein. To identify the sites of acrolein modification in the active site, this peptide was further analyzed using ESI-QTOF mass spectrometry. This analysis showed increased masses corresponding to acrolein adducts for certain b- and y-ions which identified cysteine Cys^{215} as the site of modification. Furthermore, Seiner et al. conducted inactivation assays, which demonstrated time-dependent inactivation of the protein tyrosine phosphatase 1B by acrolein. In addition to the modification of cysteine residues, acrolein was also reported to covalently form adducts at protein histidine and lysine residues and to inhibit protein disulfide isomerase, one of the proteins identified in our studies (Carbone et al., 2005; Seiner et al., 2007).

Furthermore, two other α,β-unsaturated aldehydes, the lipid peroxidation products 4-hydroxynonenal (4-HNE) and 4-oxononenal (4-ONE), were shown to react with the cytoskeletal protein tubulin and form protein cross-links, thus inhibiting proper protein function, i.e. the ability to form polymeric microtubules (Stewart et al., 2007). It has already been shown that impaired microtubule formation may be a result of adduct formation at both cysteine and lysine residues of tubulin. Additionally, both 4-HNE and 4-ONE were known to have the ability to modify cysteine, histidine, and lysine residues. Thus, the exact adduction sites of 4-HNE and 4-ONE at tubulin were determined. 4-HNE was observed to covalently bind to different cysteine residues in tubulin, $Cys^{347\alpha}$, $Cys^{376\alpha}$, and $Cys^{303\beta}$, while for 4-ONE, which represents a rapid and very potent inductor of cross-links, it could not be determined at which residues adduct formation occurred (Stewart et al., 2007). Based on their results, the authors concluded that most tubulin adducts and cross-links of 4-HNE and 4-ONE were formed through covalent binding to lysine residues and had only mild inhibiting effects on protein function, whereas formation of adducts and cross-links at cysteine residues dramatically reduced the ability of tubulin to polymerize (Stewart et al., 2007). 4-HNE was not only found to inhibit the function of tubulin, but was also reported to covalently modify the enzyme creatine kinase at its active site residues His^{66}, His^{191}, Cys^{283}, and His^{296}, thus leading to reduced enzyme activity, which may finally result in cell death (Eliuk et al., 2007).

Many different study designs and experimental procedures have been reported for the determination of the sites of covalent protein modification and to address this question, a method similar to the one described by Eliuk et al. could be applied for furan target proteins (Eliuk et al., 2007).

In brief, the protein of interest was incubated with the reactive compound in vitro at different concentrations ranging from a very high concentration to achieve a maximum of adduct formation for the development of a suitable analytical method down to a physiological or pathophysiological concentration to mimic in vivo conditions. After the reaction, the protein was isolated and digested into peptides, which were separated by liquid chromatography and analyzed by mass spectrometry. With knowledge about the amino acid sequence and the amino acid residues most likely to be adducted on one hand and information on the nature of the different modifications on the other hand, the obtained peak lists were searched for the masses of modified peptides as calculated from the masses of unmodified peptide plus its assumed modification(s). Furthermore, using the MS/MS fragment data of the modified peptides it can be determined which y- and b-ions show a mass shift corresponding to specific modifications, thus establishing which amino acid residues are adducted.

This experimental setup is suitable to detect the binding sites at a certain protein in vitro and predict possible binding sites in vivo. However, in vivo several additional factors which make the detection of covalently modified peptides very difficult have to be taken into account. These factors include very low levels of protein adduction, insufficient sequence coverage for proteins in the mass spectrometry analyses, and the occurrence of modifications at multiple sites within a protein. Koen et al. were only able to determine a binding site (Cys^{111}) of bromobenzene reactive metabolites at glutathione-S-transferase (GST) subunits in rat liver after the use of high accuracy and high sensitivity mass spectrometry and previous enrichment of GST with a glutathione-agarose affinity column (Koen et al., 2006).

Data from several in vivo studies indicate that furan has the ability to modify cysteine and lysine residues and that the bifunctionality of BDA can lead to the formation of cross-links between these residues (Chen et al., 1997; Peterson et al., 2005). Thus, a wide variety of different protein modifications can occur, making it difficult to predict the nature of the adducts. However, unambiguous detection of the modification sites in putative furan

target proteins, as conducted for protein targets of thiobenzamide in rat liver (Ikehata et al., 2008), is needed for assessing whether the function of the adducted proteins may be impaired. For this purpose, an approach similar to the one applied by Ikehata et al. may also be used in the case of furan (Ikehata et al., 2008). A possible problem, however, may be the level of protein adduct formation after furan treatment (286 pmol equiv/mg protein), which is around 100 times lower than the amount of adduction seen after thiobenzamide administration (25.6 and 36.8 nmol equiv/mg protein for cytosolic and microsomal proteins, respectively) (Ikehata et al., 2008). Therefore, it may be more difficult to detect the amino acid residues adducted after furan administration and for this purpose higher furan doses would be needed.

To identify the protein sites of adduct formation, Ikehata et al. administered a 1:1 mixture of thiobenzamide and thiobenzamide-d_5 to rats and, after protein isolation, two-dimensional gel electrophoresis, spot excision, tryptic digest and FT-ICR mass spectrometry, searched for pairs of m/z peaks showing similar intensities and a mass difference of 5 units (Ikehata et al., 2008). In the next step, it was ensured that the masses of these peptide ion peak pairs did not correspond to the masses of theoretically predicted peptides. After subtraction of the modification mass from the mass of the adducted peptide, the mass of the unmodified peptide was obtained and again compared to theoretical peptide masses to identify the peptide. Since adduct formation by thiobenzamide metabolites can occur at the lysine residue and the enzyme trypsin cleaves after lysine, also a missed cleavage site should be visible in the peptide spectra. Furthermore, exact adduct location in the peptide was conducted using MS/MS analyses (Ikehata et al., 2008).

Determination of protein function after adduct formation

A further important question regarding the role of covalent protein modification in cytotoxicity is whether adduct formation will result in impaired or even loss of protein function. This can be addressed using specific assays determining the activity of an enzyme in biological fluids or tissues. However, problems can occur if specific activity assays are not available for a certain enzyme or if a protein does not represent an enzyme, but e.g. a structural protein, making it hard to find parameters to measure their functionality.

In the context of assessing protein functionality, it is also interesting to determine the subcellular location and the turnover rate of the proteins. Changes in the subcellular location of a protein, which can be established by immunohistochemistry, might indicate that it is more or less active than in controls or even that its functions are altered, such as in the case of ezrin-radixin-moesin-binding phosphoprotein 50 (Georgescu et al., 2008). The protein turnover rate is a parameter of high significance regarding the manifestation of protein adduct-mediated toxic effects in the cell, because it expresses how fast a damaged protein can be replaced by a new and functional one. Proteins with a high turnover rate are replaced faster than proteins showing a low turnover rate, thus having less possibility to introduce cytotoxicity. For determination of protein turnover, Doherty et al. applied a method referred to as dynamic SILAC (stable isotope labeling by amino acids in cell culture), which monitors the incorporation of stable isotope amino acid precursors in proteins using one-dimensional gel electrophoresis, in-gel digestion, and LC-MS/MS analysis (Doherty et al., 2009).

Mitochondrial toxicity

As described above, the fact that several target proteins are involved in mitochondrial energy production, suggests that furan toxicity may be mediated by mitochondrial toxicity and impaired energy production. Consistently, Mugford et al. reported that mitochondrial uncoupling might represent an early event in furan-induced cytotoxicity (Mugford et al., 1997). In these studies relatively high furan doses were used and thus it might be interesting to find out to what extent ATP depletion and mitochondrial toxicity might occur at lower doses, e.g. doses as used in the 28 day oral toxicity study. However, this was beyond the scope of this work.

Common protein properties

It has been suggested that finding commonalities in target proteins and their protein properties might elucidate a general mechanism of protein adduct-induced toxicity. By building up a target protein database and applying bioinformatic tools, Hanzlik et al. provided first insights into this field (Fang et al., 2009; Hanzlik et al., 2009; Hanzlik et al., 2007). However, the currently available information on target proteins of toxic metabolites in vivo appears to be insufficient to reveal a general mechanism of toxicity.

In addition to the abundance and turnover of a protein, also further protein properties such as cysteine or lysine content may determine which proteins are adducted by reactive metabolites. For instance, it was reported that acylating electrophilic metabolites prefer modification of lysine residues of proteins, whereas alkylating agents mainly form adducts with cysteine, lysine, and histidine side chains (Fang et al., 2009).

10 SUMMARY

Furan was recently found to be present in a variety of food items that undergo heat treatment. It is known to act as a potent hepatotoxin and liver carcinogen in rodents. In a 2-year bioassay, chronic furan administration to rats was shown to cause hepatocellular adenomas and carcinomas and very high incidences of cholangiocarcinomas even at the lowest furan dose tested (2.0 mg/kg bw) (NTP, 1993). However, the mechanisms of furan-induced tumor formation are poorly understood.

Furan is metabolized by cytochrome P450 (CYP) enzymes, predominantly CYP2E1, to its major metabolite *cis*-2-butene-1,4-dial (BDA) (Chen et al., 1995; Kedderis et al., 1993). BDA is thought to be the key mediator of furan toxicity and carcinogenicity (Carfagna et al., 1993; Fransson-Steen et al., 1997; Mugford et al., 1997) and was shown to react with cellular nucleophiles such as nucleosides (Byrns et al., 2002; Byrns et al., 2004) and amino acid residues (Chen et al., 1997) in vitro.

It is well known that covalent protein binding may lead to cytotoxicity, but the cellular mechanisms involved remain to be elucidated. Since covalent binding of reactive intermediates to a target protein may result in loss of protein function and subsequent damage to the cell, the aim of this study was to identify furan target proteins to establish their role in the pathogenesis of furan-associated liver toxicity and carcinogenicity.

In order to identify target proteins of furan reactive metabolites, male F344/N rats were administered [3,4-^{14}C]-furan. Liquid scintillation counting of protein extracts revealed a dose-dependent increase of radioactivity covalently bound to liver proteins. After separation of the liver protein extracts by two-dimensional gel electrophoresis and subsequent detection of radioactive spots by fluorography, target proteins of reactive furan intermediates were identified by mass spectrometry and database search via Mascot. A total of 61 putative target proteins were consistently found to be adducted in 3 furan-treated rats. The identified proteins represent - among others - enzymes, transport proteins, structural proteins and chaperones. Pathway mapping tools revealed that target proteins are predominantly located in the cytosol and mitochondria and participate in glucose metabolism, mitochondrial β-oxidation of fatty acids, and amino acid degradation. These findings together with the fact that ATP synthase β subunit was also identified as a putative target protein strongly suggest that binding of furan reactive metabolites to proteins may result in mitochondrial injury, impaired cellular energy

production, and altered redox state, which may contribute to cell death. Moreover, several proteins involved in the regulation of redox homeostasis represent putative furan target proteins. Loss of function of these proteins by covalent binding of furan reactive metabolites may impair cellular defense mechanisms against oxidative stress, which may also result in cell death. Besides the potential malfunction of whole pathways due to loss of functions of several participating proteins, loss of function of individual proteins which are involved in various cellular processes such as transport processes across the mitochondrial membranes, cell signaling, DNA methylation, blood coagulation, and bile acid transport may also contribute to furan-induced cytotoxicity and carcinogenicity.

Covalent binding of reactive metabolites to cellular proteins may result in accumulation of high amounts of unfolded or damaged proteins in the endoplasmic reticulum (ER). In response to this ER stress, the cell can activate the unfolded protein response (UPR) to repair or degrade damaged proteins. To address whether binding of furan reactive metabolites to cellular proteins triggers activation of the UPR, semiquantitative PCR and TaqMan® real-time PCR were performed. In the case of UPR activation, semiquantitative PCR should show enhanced splicing of X-box binding protein-1 (XBP1) mRNA (transcription factor and key regulator of the UPR) and TaqMan® real-time PCR should determine an increased expression of UPR target genes. However, our data showed no evidence for activation of the UPR in the livers of rats treated either with a single hepatotoxic dose or with a known carcinogenic dose for 4 weeks. This suggests either that furan administration does not induce ER stress through accumulation of damaged proteins or that activation of the UPR is disrupted. Consistent with the latter, glucose-regulated protein 78 (GRP78), identified as a target protein in our study, represents an important mediator involved in activation of the UPR whose inhibition was shown to impair induction of the UPR (Martin et al., 2010). Thus, adduct formation and inactivation of GRP78 by furan metabolites may disturb activation of the UPR. In addition to impaired activation of UPR, protein repair and degradation functions may be altered, because several proteins involved in these processes also represent target proteins of furan and thus may show impaired functionality.

Taken together, our data suggest that covalent binding of furan reactive metabolites to several proteins may result in impaired protein function and thus disruption of cellular functions, most notably mitochondrial energy production, redox regulation, and protein

folding and degradation, which may combine to disrupt cell homeostasis and cause hepatocyte cell death. However, further work is needed to establish whether protein adduction by furan reactive metabolites results in loss of individual protein function.

11 ZUSAMMENFASSUNG

Im Rahmen von Untersuchungen der U.S. Food and Drug Administration (FDA) wurde im Jahr 2004 bekannt, dass Furan in verschiedensten hitzebehandelten Lebensmitteln vorkommt. Durch Tierstudien des National Toxicology Programs (NTP) aus den 90er Jahren wusste man bereits, dass Furan hepatotoxische und leberkanzerogene Wirkungen in Nagern verursacht. In diesen Studien wurden nach chronischer Verabreichung von Furan an Ratten über einen Zeitraum von 2 Jahren bereits bei der niedrigsten getesteten Dosis von 2 mg/kg Körpergewicht hepatozelluläre Adenome und Karzinome sowie sehr hohe Inzidenzen von Cholangiokarzinomen beobachtet (NTP, 1993). Die Mechanismen, die der Tumorentstehung durch Furan zugrunde liegen, sind jedoch bis heute nicht ausreichend untersucht.

Furan wird durch Enzyme der Cytochrom P450 (CYP) Familie, vor allem durch CYP2E1, zu seinem Hauptmetaboliten cis-2-Buten-1,4-dial (BDA) verstoffwechselt (Chen et al., 1995; Kedderis et al., 1993). Der reaktive Furan-Metabolit BDA kann in vitro mit zellulären Nukleophilen wie Nukleosiden und Aminosäureresten reagieren (Byrns et al., 2002; Byrns et al., 2004; Chen et al., 1997). Verschiedene Untersuchungen weisen darauf hin, dass die toxischen und kanzerogenen Effekte von Furan hauptsächlich durch BDA vermittelt werden (Carfagna et al., 1993; Fransson-Steen et al., 1997; Mugford et al., 1997).

Es ist seit langem bekannt, dass kovalente Bindung an Proteine zu Zytotoxizität führen kann. Der zugrunde liegende Mechanismus ist bislang noch ungeklärt. Es wird jedoch vermutet, dass die kovalente Bindung von reaktiven Metaboliten an Proteine zu deren Funktionsverlust führt, was wiederum fatale Konsequenzen für die Zellen haben kann. Eine Identifizierung der Zielproteine von Furan, d.h. jener Proteine an denen eine Adduktbildung durch reaktive Metabolite von Furan erfolgt, könnte daher Aufschluss über deren mögliche Rolle in der Pathogenese der durch Furan induzierten Lebertoxizität und -kanzerogenität geben.

Um die Zielproteine reaktiver Furan-Metabolite zu identifizieren, wurde [3,4-^{14}C]-Furan an männliche F344/N Ratten verabreicht. Durch Flüssigkeitsszintillationszählung der Proteinextrakte wurde ein dosisabhängiger Anstieg der kovalent an Leberproteine gebundenen Radioaktivität ermittelt. Nach der Auftrennung der Leberproteinextrakte durch zweidimensionale Gelelektrophorese und der Detektion der radioaktiven Spots

durch Fluorographie wurden die Zielproteine reaktiver Furan-Metabolite durch Massenspektrometrie und Datenbanksuche (Mascot-Datenbank) identifiziert. In 3 Ratten, die mit Furan behandelt worden waren, wurden übereinstimmend 61 mögliche Zielproteine von Furan identifiziert. Unter diesen Zielproteinen waren unter anderem Enzyme, Transportproteine, Strukturproteine und Chaperones vertreten. Die Zuordnung der identifizierten Proteine zu zellulären Signal- und Stoffwechselwegen mittels spezieller Software zeigte, dass die Zielproteine hauptsächlich aus dem Zytosol und den Mitochondrien stammen und an Glucosemetabolismus, mitochondrieller β-Oxidation von Fettsäuren und dem Abbau von Aminosäuren beteiligt sind. Außerdem wurde auch die β-Untereinheit der ATP-Synthase als mögliches Zielprotein identifiziert. Diese Ergebnisse weisen stark darauf hin, dass die Bindung reaktiver Furan-Metabolite an Proteine zur Schädigung der Mitochondrien, Beeinträchtigung der zellulären Energieproduktion und verändertem Redox-Status führen und damit zum Zelltod beitragen könnte. Weiterhin befanden sich unter den möglichen Zielproteinen auch Proteine, die für die Regulation der Redox-Homöostase in der Zelle verantwortlich sind. Ein Funktionsverlust dieser Proteine durch die kovalente Bindung reaktiver Furan-Metabolite könnte eine verminderte Fähigkeit der Zelle oxidativen Stress abzuwehren zur Folge haben, was wiederum zum Zelltod führen könnte. Zusätzlich dazu, dass die kovalente Modifikation mehrerer Proteine aus dem gleichen Stoffwechselweg dessen Gesamtfunktion beeinträchtigen kann, ist es außerdem möglich, dass Adduktbildung an einzelnen Proteinen mit Schlüsselfunktionen in der Aufrechterhaltung der Zellhomöostase toxische Effekte auslösen kann. Ein Funktionsverlust dieser Proteine, die z.B. in Transportprozesse durch Mitochondrienmembranen, zelluläre Signalwege, DNA-Methylierung, Blutgerinnung und Gallensäuren-Transport involviert sind, könnte ebenfalls an den zytotoxischen und kanzerogenen Wirkungen von Furan beteiligt sein.

Die kovalente Bindung reaktiver Furan-Metabolite an zelluläre Proteine kann zu einer Akkumulation großer Mengen an ungefalteten oder beschädigten Proteinen im endoplasmatischen Retikulum (ER) führen. Als Antwort auf diesen sogenannten ER-Stress kann die Zelle den Unfolded Protein Response (UPR) aktivieren, einen zellulären Signalweg um vermehrt beschädigte Proteine zu reparieren oder abzubauen. Um festzustellen, ob die Bindung reaktiver Furan-Metabolite an zelluläre Proteine eine Aktivierung des UPR auslöst, wurden semiquantitative PCR und Real-Time-PCR Analysen

durchgeführt. Nach einer Aktivierung des UPR sollte die semiquantitative PCR das vermehrte Auftreten gespleißter X-box binding protein-1 (XBP1) mRNA zeigen, die als Transkriptionsfaktor die Expression der UPR-Zielgene auslöst. Weiterhin sollte im Falle einer UPR-Aktivierung eine erhöhte Expression der Zielgene des UPR durch Real-Time-PCR sichtbar werden. Unsere Daten zeigen jedoch keine Hinweise auf eine Aktivierung des UPR in der Rattenleber, weder nach Verabreichung einer einzigen hepatotoxischen Dosis noch nach Behandlung über 4 Wochen mit einer bekanntlich kanzerogenen Dosis. Diese Ergebnisse lassen vermuten, dass nach der Verabreichung von Furan entweder kein ER-Stress durch Akkumulation beschädigter Proteine entsteht oder die Aktivierung des UPR beeinträchtigt ist. Für Letzteres spricht, dass das Glucose-regulierte Protein 78 (GRP78), das eine wichtige Mediatorfunktion bei der Aktivierung des UPR aufweist und durch dessen Inhibition die Aktivierung des UPR behindert werden kann (Martin et al., 2010), in unseren Untersuchungen als ein Zielprotein von Furan identifiziert wurde. Es erscheint daher möglich, dass kovalente Modifikation von GRP78 durch reaktive Furan-Metabolite die Aktivierung des UPR beeinträchtigt. Zusätzlich dazu ist es außerdem möglich, dass Reparatur- und Degradierungsfunktionen der Zelle nicht vollständig funktionsfähig sind, weil einige Proteine, die an diesen Prozessen teilnehmen, auch als Zielproteine von Furan identifiziert wurden und daher in ihrer Funktionalität beeinträchtigt sein können.

Zusammenfassend weisen unsere Daten darauf hin, dass die kovalente Bindung reaktiver Furan-Metabolite an verschiedenste Proteine zu deren beeinträchtigter Funktion führen könnte, was wiederum eine Störung der zellulären Funktionen zur Folge haben könnte. Im Fall von Furan scheint es vor allem zur Beeinträchtigung der mitochondriellen Energieproduktion, der Redox-Regulation sowie der Proteinfaltung und des -abbaus zu kommen, was im Zusammenspiel den Zelltod von Hepatozyten herbeiführen könnte. Um jedoch eindeutig zu klären, ob die Furan-bedingte Adduktbildung an Proteinen tatsächlich zu einem Funktionsverlust der betroffenen Proteine führt, sind weitere Untersuchungen nötig.

12 REFERENCES

Abu-Hamad, S., Sivan, S., and Shoshan-Barmatz, V. (2006). The expression level of the voltage-dependent anion channel controls life and death of the cell. Proc Natl Acad Sci U S A *103*, 5787-5792.

Akerstrom, B., Logdberg, L., Berggard, T., Osmark, P., and Lindqvist, A. (2000). alpha(1)-Microglobulin: a yellow-brown lipocalin. Biochim Biophys Acta *1482*, 172-184.

Alrefai, W.A., and Gill, R.K. (2007). Bile acid transporters: structure, function, regulation and pathophysiological implications. Pharm Res *24*, 1803-1823.

Andersen, K.M., Madsen, L., Prag, S., Johnsen, A.H., Semple, C.A., Hendil, K.B., and Hartmann-Petersen, R. (2009). Thioredoxin Txnl1/TRP32 is a redox-active cofactor of the 26 S proteasome. J Biol Chem *284*, 15246-15254.

Antonenkov, V.D., Ohlmeier, S., Sormunen, R.T., and Hiltunen, J.K. (2007). UK114, a YjgF/Yer057p/UK114 family protein highly conserved from bacteria to mammals, is localized in rat liver peroxisomes. Biochem Biophys Res Commun *357*, 252-257.

Aram, L., Geula, S., Arbel, N., and Shoshan-Barmatz, V. (2010). VDAC1 cysteine residues: topology and function in channel activity and apoptosis. Biochem J *427*, 445-454.

Asif, A.R., Armstrong, V.W., Voland, A., Wieland, E., Oellerich, M., and Shipkova, M. (2007). Proteins identified as targets of the acyl glucuronide metabolite of mycophenolic acid in kidney tissue from mycophenolate mofetil treated rats. Biochimie *89*, 393-402.

Atshaves, B.P., Martin, G.G., Hostetler, H.A., McIntosh, A.L., Kier, A.B., and Schroeder, F. (2010). Liver fatty acid-binding protein and obesity. J Nutr Biochem.

Baric, I. (2009). Inherited disorders in the conversion of methionine to homocysteine. J Inherit Metab Dis *32*, 459-471.

Bashour, A.M., and Bloom, G.S. (1998). 58K, a microtubule-binding Golgi protein, is a formiminotransferase cyclodeaminase. J Biol Chem *273*, 19612-19617.

Bhoola, K.D., Figueroa, C.D., and Worthy, K. (1992). Bioregulation of kinins: kallikreins, kininogens, and kininases. Pharmacol Rev *44*, 1-80.

Brisson, D., Vohl, M.C., St-Pierre, J., Hudson, T.J., and Gaudet, D. (2001). Glycerol: a neglected variable in metabolic processes? Bioessays *23*, 534-542.

Brohawn, S.G., and Schwartz, T.U. (2009). Molecular architecture of the Nup84-Nup145C-Sec13 edge element in the nuclear pore complex lattice. Nat Struct Mol Biol *16*, 1173-1177.

Burka, L.T., Washburn, K.D., and Irwin, R.D. (1991). Disposition of [14C]furan in the male F344 rat. J Toxicol Environ Health *34*, 245-257.

Buxbaum, J.N., and Reixach, N. (2009). Transthyretin: the servant of many masters. Cell Mol Life Sci *66*, 3095-3101.

Byrns, M.C., Predecki, D.P., and Peterson, L.A. (2002). Characterization of nucleoside adducts of cis-2-butene-1,4-dial, a reactive metabolite of furan. Chem Res Toxicol *15*, 373-379.

Byrns, M.C., Vu, C.C., and Peterson, L.A. (2004). The formation of substituted 1,N6-etheno-2'-deoxyadenosine and 1,N2-etheno-2'-deoxyguanosine adducts by cis-2-butene-1,4-dial, a reactive metabolite of furan. Chem Res Toxicol *17*, 1607-1613.

Carbone, D.L., Doorn, J.A., Kiebler, Z., and Petersen, D.R. (2005). Cysteine modification by lipid peroxidation products inhibits protein disulfide isomerase. Chem Res Toxicol *18*, 1324-1331.

Carfagna, M.A., Held, S.D., and Kedderis, G.L. (1993). Furan-induced cytolethality in isolated rat hepatocytes: correspondence with in vivo dosimetry. Toxicol Appl Pharmacol *123*, 265-273.

Carlson, J.A., Rogers, B.B., Sifers, R.N., Hawkins, H.K., Finegold, M.J., and Woo, S.L. (1988). Multiple tissues express alpha 1-antitrypsin in transgenic mice and man. J Clin Invest *82*, 26-36.

Chang, C., Pang, K.S., Swaan, P.W., and Ekins, S. (2005). Comparative pharmacophore modeling of organic anion transporting polypeptides: a meta-analysis of rat Oatp1a1 and human OATP1B1. J Pharmacol Exp Ther *314*, 533-541.

Chao, J., Chai, K.X., Chen, L.M., Xiong, W., Chao, S., Woodley-Miller, C., Wang, L.X., Lu, H.S., and Chao, L. (1990). Tissue kallikrein-binding protein is a serpin. I. Purification, characterization, and distribution in normotensive and spontaneously hypertensive rats. J Biol Chem *265*, 16394-16401.

Chao, J., Tillman, D.M., Wang, M.Y., Margolius, H.S., and Chao, L. (1986). Identification of a new tissue-kallikrein-binding protein. Biochem J *239*, 325-331.

Chaudhury, A., Chander, P., and Howe, P.H. (2010). Heterogeneous nuclear ribonucleoproteins (hnRNPs) in cellular processes: Focus on hnRNP E1's multifunctional regulatory roles. RNA *16*, 1449-1462.

Chen, L.J., Hecht, S.S., and Peterson, L.A. (1995). Identification of cis-2-butene-1,4-dial as a microsomal metabolite of furan. Chem Res Toxicol *8*, 903-906.

Chen, L.J., Hecht, S.S., and Peterson, L.A. (1997). Characterization of amino acid and glutathione adducts of cis-2-butene-1,4-dial, a reactive metabolite of furan. Chem Res Toxicol *10*, 866-874.

Chen, T., Mally, A., Ozden, S., and Chipman, J.K. (2010). Low Doses of the Carcinogen Furan Alter Cell Cycle and Apoptosis Gene Expression in Rat Liver Independent of DNA Methylation. Environ Health Perspect.

Chong, C.L., Huang, S.F., Hu, C.P., Chen, Y.L., Chou, H.Y., Chau, G.Y., Shew, J.Y., Tsai, Y.L., Chen, C.T., Chang, C.*, et al.* (2008). Decreased expression of UK114 is related to the differentiation status of human hepatocellular carcinoma. Cancer Epidemiol Biomarkers Prev *17*, 535-542.

Cordelli, E., Leopardi, P., Villani, P., Marcon, F., Macri, C., Caiola, S., Siniscalchi, E., Conti, L., Eleuteri, P., Malchiodi-Albedi, F.*, et al.* (2010). Toxic and genotoxic effects of oral administration of furan in mouse liver. Mutagenesis *25*, 305-314.

Crabb, D.W., Matsumoto, M., Chang, D., and You, M. (2004). Overview of the role of alcohol dehydrogenase and aldehyde dehydrogenase and their variants in the genesis of alcohol-related pathology. Proc Nutr Soc *63*, 49-63.

Crews, C., and Castle, L. (2007). A review of the occurence, formation and analysis of furan in heat-processed foods. Trends in Food Science & Technology *18*, 365-372.

Cuervo, A.M., Hildebrand, H., Bomhard, E.M., and Dice, J.F. (1999). Direct lysosomal uptake of alpha 2-microglobulin contributes to chemically induced nephropathy. Kidney Int *55*, 529-545.

Daugaard, M., Rohde, M., and Jaattela, M. (2007). The heat shock protein 70 family: Highly homologous proteins with overlapping and distinct functions. FEBS Lett *581*, 3702-3710.

Deignan, J.L., Cederbaum, S.D., and Grody, W.W. (2008). Contrasting features of urea cycle disorders in human patients and knockout mouse models. Mol Genet Metab *93*, 7-14.

Dennis, G., Jr., Sherman, B.T., Hosack, D.A., Yang, J., Gao, W., Lane, H.C., and Lempicki, R.A. (2003). DAVID: Database for Annotation, Visualization, and Integrated Discovery. Genome Biol *4*, P3.

Doherty, M.K., Hammond, D.E., Clague, M.J., Gaskell, S.J., and Beynon, R.J. (2009). Turnover of the human proteome: determination of protein intracellular stability by dynamic SILAC. J Proteome Res *8*, 104-112.

Dooley, G.P., Reardon, K.F., Prenni, J.E., Tjalkens, R.B., Legare, M.E., Foradori, C.D., Tessari, J.E., and Hanneman, W.H. (2008). Proteomic analysis of diaminochlorotriazine adducts in wistar rat pituitary glands and LbetaT2 rat pituitary cells. Chem Res Toxicol *21*, 844-851.

Doss, M.O., Stauch, T., Gross, U., Renz, M., Akagi, R., Doss-Frank, M., Seelig, H.P., and Sassa, S. (2004). The third case of Doss porphyria (delta-amino-levulinic acid dehydratase deficiency) in Germany. J Inherit Metab Dis *27*, 529-536.

Dreyfuss, G., Kim, V.N., and Kataoka, N. (2002). Messenger-RNA-binding proteins and the messages they carry. Nat Rev Mol Cell Biol *3*, 195-205.

Druckova, A., and Marnett, L.J. (2006). Characterization of the amino acid adducts of the enedial derivative of teucrin A. Chem Res Toxicol *19*, 1330-1340.

Druckova, A., Mernaugh, R.L., Ham, A.J., and Marnett, L.J. (2007). Identification of the protein targets of the reactive metabolite of teucrin A in vivo in the rat. Chem Res Toxicol *20*, 1393-1408.

Durling, L.J., Svensson, K., and Abramsson-Zetterberg, L. (2007). Furan is not genotoxic in the micronucleus assay in vivo or in vitro. Toxicol Lett *169*, 43-50.

Dworniczak, B., and Mirault, M.E. (1987). Structure and expression of a human gene coding for a 71 kd heat shock 'cognate' protein. Nucleic Acids Res *15*, 5181-5197.

EFSA (2004). Report of the Scientific Panel on Contaminants in the Food Chain on provisional findings on furan in food. The EFSA Journal *137*, 1-20.

EFSA (2009a). Furan in heat processed food products including home cooked food products and ready-to-eat products. SCIENTIFIC REPORT submitted to EFSA.

EFSA (2009b). Results on the monitoring of furan levels in food. EFSA Scientific Report *304*, 1-23.

Egle, J.L., Jr., and Gochberg, B.J. (1979). Respiratory retention and acute toxicity of furan. Am Ind Hyg Assoc J *40*, 310-314.

Eliuk, S.M., Renfrow, M.B., Shonsey, E.M., Barnes, S., and Kim, H. (2007). active site modifications of the brain isoform of creatine kinase by 4-hydroxy-2-nonenal correlate with reduced enzyme activity: mapping of modified sites by Fourier transform-ion cyclotron resonance mass spectrometry. Chem Res Toxicol *20*, 1260-1268.

Evans, D.C., Watt, A.P., Nicoll-Griffith, D.A., and Baillie, T.A. (2004). Drug-protein adducts: an industry perspective on minimizing the potential for drug bioactivation in drug discovery and development. Chem Res Toxicol *17*, 3-16.

Fairbanks, K.D., and Tavill, A.S. (2008). Liver disease in alpha 1-antitrypsin deficiency: a review. Am J Gastroenterol *103*, 2136-2141; quiz 2142.

Fan, X., Huang, L., and Sokorai, K.J. (2008). Factors Affecting Thermally Induced Furan Formation. J Agric Food Chem.

Fang, J., Koen, Y.M., and Hanzlik, R.P. (2009). Bioinformatic analysis of xenobiotic reactive metabolite target proteins and their interacting partners. BMC Chem Biol *9*, 5.

Feng, C., Tollin, G., and Enemark, J.H. (2007). Sulfite oxidizing enzymes. Biochim Biophys Acta *1774*, 527-539.

Fleming, C.E., Nunes, A.F., and Sousa, M.M. (2009). Transthyretin: more than meets the eye. Prog Neurobiol *89*, 266-276.

Fouassier, L., Duan, C.Y., Feranchak, A.P., Yun, C.H., Sutherland, E., Simon, F., Fitz, J.G., and Doctor, R.B. (2001). Ezrin-radixin-moesin-binding phosphoprotein 50 is expressed at the apical membrane of rat liver epithelia. Hepatology *33*, 166-176.

Fouassier, L., Rosenberg, P., Mergey, M., Saubamea, B., Claperon, A., Kinnman, N., Chignard, N., Jacobsson-Ekman, G., Strandvik, B., Rey, C*., et al.* (2009). Ezrin-radixin-moesin-binding phosphoprotein (EBP50), an estrogen-inducible scaffold protein, contributes to biliary epithelial cell proliferation. Am J Pathol *174*, 869-880.

Fransson-Steen, R., Goldsworthy, T.L., Kedderis, G.L., and Maronpot, R.R. (1997). Furan-induced liver cell proliferation and apoptosis in female B6C3F1 mice. Toxicology *118*, 195-204.

Fries, E., and Blom, A.M. (2000). Bikunin--not just a plasma proteinase inhibitor. Int J Biochem Cell Biol *32*, 125-137.

Gao, Y., and Sztul, E. (2001). A novel interaction of the Golgi complex with the vimentin intermediate filament cytoskeleton. J Cell Biol *152*, 877-894.

Garneau, D., Revil, T., Fisette, J.F., and Chabot, B. (2005). Heterogeneous nuclear ribonucleoprotein F/H proteins modulate the alternative splicing of the apoptotic mediator Bcl-x. J Biol Chem *280*, 22641-22650.

Georgescu, M.M., Morales, F.C., Molina, J.R., and Hayashi, Y. (2008). Roles of NHERF1/EBP50 in cancer. Curr Mol Med *8*, 459-468.

Gill, S., Bondy, G., Lefebvre, D.E., Becalski, A., Kavanagh, M., Hou, Y., Turcotte, A.M., Barker, M., Weld, M., Vavasour, E*., et al.* (2010). Subchronic oral toxicity study of furan in Fischer-344 rats. Toxicol Pathol *38*, 619-630.

Gonias, S.L., Hembrough, T.A., and Sankovic, M. (2001). Cytokeratin 8 functions as a major plasminogen receptor in select epithelial and carcinoma cells. Front Biosci *6*, D1403-1411.

Guynn, R.W., Veloso, D., Lawson, J.W., and Veech, R.L. (1974). The concentration and control of cytoplasmic free inorganic pyrophosphate in rat liver in vivo. Biochem J *140*, 369-375.

Hagiwara, H., Tajika, Y., Matsuzaki, T., Suzuki, T., Aoki, T., and Takata, K. (2006). Localization of Golgi 58K protein (formiminotransferase cyclodeaminase) to the centrosome. Histochem Cell Biol *126*, 251-259.

Hamadeh, H.K., Jayadev, S., Gaillard, E.T., Huang, Q., Stoll, R., Blanchard, K., Chou, J., Tucker, C.J., Collins, J., Maronpot, R*., et al.* (2004). Integration of clinical and gene expression endpoints to explore furan-mediated hepatotoxicity. Mutat Res *549*, 169-183.

Hamberger, C., Kellert, M., Schauer, U.M., Dekant, W., and Mally, A. (2010a). Hepatobiliary toxicity of furan: Identification of furan metabolites in bile of male F344/N rats. Drug Metab Dispos.

Hamberger, C., Moro, S., Malfatti, M., Turteltaub, K., Dekant, W., and Mally, A. (2010b). Analysis of DNA binding of [3,4-14C]-furan in rat liver by accelerator mass spectrometry. (Poster). Society of Toxicology 49th Annual Meeting, Salt Lake City, 2010 The Toxicologist, Supplement to Toxicological Sciences.

Hanzlik, R.P., Fang, J., and Koen, Y.M. (2009). Filling and mining the reactive metabolite target protein database. Chem Biol Interact *179*, 38-44.

Hanzlik, R.P., Koen, Y.M., Theertham, B., Dong, Y., and Fang, J. (2007). The reactive metabolite target protein database (TPDB)--a web-accessible resource. BMC Bioinformatics *8*, 95.

Hard, G.C., Rodgers, I.S., Baetcke, K.P., Richards, W.L., McGaughy, R.E., and Valcovic, L.R. (1993). Hazard evaluation of chemicals that cause accumulation of alpha 2u-globulin, hyaline droplet nephropathy, and tubule neoplasia in the kidneys of male rats. Environ Health Perspect *99*, 313-349.

Hickling, K., Hitchcock, J.M., Chipman, J.K., Hammond, T.G., and Evans, J.G. (2010a). Induction and progression of cholangiofibrosis in rat liver injured by oral administration of furan. Toxicologic Pathology *38*, 213-229.

Hickling, K.C., Hitchcock, J.M., Oreffo, V., Mally, A., Coleman, R., Hammond, T.G., Evans, J.G., and Chipman, J.K. (2010b). Evidence of oxidative stress and associated DNA damage, increased proliferative drive and altered gene expression in rat liver produced by the cholangiocarcinogenic agent furan. Toxicologic Pathology *38*, 230-243.

Hilton, J.F., Christensen, K.E., Watkins, D., Raby, B.A., Renaud, Y., de la Luna, S., Estivill, X., MacKenzie, R.E., Hudson, T.J., and Rosenblatt, D.S. (2003). The molecular basis of glutamate formiminotransferase deficiency. Hum Mutat *22*, 67-73.

Hoffmann, H. (2010). Untersuchungen zur Beteiligung von bakterieller Translokation an der Hepatotoxizität von Furan. Diplomarbeit Universität Würzburg.

Hoivik, D.J., Manautou, J.E., Tveit, A., Mankowski, D.C., Khairallah, E.A., and Cohen, S.D. (1996). Evidence suggesting the 58-kDa acetaminophen binding protein is a preferential target for acetaminophen electrophile. Fundam Appl Toxicol *32*, 79-86.

Hu, S., Song, E., Tian, R., Ma, S., Yang, T., Mu, Y., Li, Y., Shao, C., Gao, S., and Gao, Y. (2009). Systematic analysis of a simple adaptor protein PDZK1: ligand identification, interaction and functional prediction of complex. Cell Physiol Biochem *24*, 231-242.

Huang da, W., Sherman, B.T., and Lempicki, R.A. (2009). Systematic and integrative analysis of large gene lists using DAVID bioinformatics resources. Nat Protoc *4*, 44-57.

IARC (1995). Furan. Dry Cleaning, Some Chlorinated Solvents and Other Industrial Chemicals. International Agency for Research on Cancer (IARC) Monograph *63*, 393.

Ichijo, H., Nishida, E., Irie, K., ten Dijke, P., Saitoh, M., Moriguchi, T., Takagi, M., Matsumoto, K., Miyazono, K., and Gotoh, Y. (1997). Induction of apoptosis by ASK1, a mammalian MAPKKK that activates SAPK/JNK and p38 signaling pathways. Science *275*, 90-94.

Iciek, M., and Wlodek, L. (2001). Biosynthesis and biological properties of compounds containing highly reactive, reduced sulfane sulfur. Pol J Pharmacol *53*, 215-225.

Ikehata, K., Duzhak, T.G., Galeva, N.A., Ji, T., Koen, Y.M., and Hanzlik, R.P. (2008). Protein targets of reactive metabolites of thiobenzamide in rat liver in vivo. Chem Res Toxicol *21*, 1432-1442.

Itoh, H., Ide, H., Ishikawa, N., and Nawa, Y. (1994). Mast cell protease inhibitor, trypstatin, is a fragment of inter-alpha-trypsin inhibitor light chain. J Biol Chem *269*, 3818-3822.

Jaffe, E.K. (2004). The porphobilinogen synthase catalyzed reaction mechanism. Bioorg Chem *32*, 316-325.

Jaffe, E.K., and Stith, L. (2007). ALAD porphyria is a conformational disease. Am J Hum Genet *80*, 329-337.

Jimenez, A., Pelto-Huikko, M., Gustafsson, J.A., and Miranda-Vizuete, A. (2006). Characterization of human thioredoxin-like-1: potential involvement in the cellular response against glucose deprivation. FEBS Lett *580*, 960-967.

Johnson, E.S., Ma, P.C., Ota, I.M., and Varshavsky, A. (1995). A proteolytic pathway that recognizes ubiquitin as a degradation signal. J Biol Chem *270*, 17442-17456.

Kalinina, E.V., Chernov, N.N., and Saprin, A.N. (2008). Involvement of thio-, peroxi-, and glutaredoxins in cellular redox-dependent processes. Biochemistry (Mosc) *73*, 1493-1510.

Kameda, K., Suzuki, L.K., and Imai, Y. (1985). Further purification, characterization and salt activation of acyl-CoA synthetase from Escherichia coli. Biochim Biophys Acta *840*, 29-36.

Kanouchi, H., Matsumoto, M., Taga, M., Yamada, K., Oka, T., Tone, S., and Minatogawa, Y. (2005). Nuclear transfer of perchloric acid-soluble protein by endoplasmic reticulum stressors. Protein Sci *14*, 2344-2349.

Kanouchi, H., Tachibana, H., Oka, T., and Yamada, K. (2001). Recombinant expression of perchloric acid-soluble protein reduces cell proliferation. Cell Mol Life Sci *58*, 1340-1343.

Katyare, S.S., and Satav, J.G. (1989). Impaired mitochondrial oxidative energy metabolism following paracetamol-induced hepatotoxicity in the rat. Br J Pharmacol *96*, 51-58.

Kedderis, G.L., Carfagna, M.A., Held, S.D., Batra, R., Murphy, J.E., and Gargas, M.L. (1993). Kinetic analysis of furan biotransformation by F-344 rats in vivo and in vitro. Toxicol Appl Pharmacol *123*, 274-282.

Kellert, M., Brink, A., Richter, I., Schlatter, J., and Lutz, W.K. (2008a). Tests for genotoxicity and mutagenicity of furan and its metabolite cis-2-butene-1,4-dial in L5178Y tk(+/-) mouse lymphoma cells. Mutat Res.

Kellert, M., Wagner, S., Lutz, U., and Lutz, W.K. (2008b). Biomarkers of furan exposure by metabolic profiling of rat urine with liquid chromatography-tandem mass spectrometry and principal component analysis. Chem Res Toxicol *21*, 761-768.

Kelley, P.M., and Schlesinger, M.J. (1982). Antibodies to two major chicken heat shock proteins cross-react with similar proteins in widely divergent species. Mol Cell Biol *2*, 267-274.

Kelly, V.P., Sherratt, P.J., Crouch, D.H., and Hayes, J.D. (2002). Novel homodimeric and heterodimeric rat gamma-hydroxybutyrate synthases that associate with the Golgi apparatus define a distinct subclass of aldo-keto reductase 7 family proteins. Biochem J *366*, 847-861.

Kim, A., Kim, M.J., Yang, Y., Kim, J.W., Yeom, Y.I., and Lim, J.S. (2009). Suppression of NF-kappaB activity by NDRG2 expression attenuates the invasive potential of highly malignant tumor cells. Carcinogenesis *30*, 927-936.

Klaunig, J.E., Kamendulis, L.M., and Xu, Y. (2000). Epigenetic mechanisms of chemical carcinogenesis. Hum Exp Toxicol *19*, 543-555.

Kobayashi, H. (2006). Endogenous anti-inflammatory substances, inter-alpha-inhibitor and bikunin. Biol Chem *387*, 1545-1549.

Kocher, O., and Krieger, M. (2009). Role of the adaptor protein PDZK1 in controlling the HDL receptor SR-BI. Curr Opin Lipidol *20*, 236-241.

Kocher, O., Yesilaltay, A., Cirovic, C., Pal, R., Rigotti, A., and Krieger, M. (2003). Targeted disruption of the PDZK1 gene in mice causes tissue-specific depletion of the high density lipoprotein receptor scavenger receptor class B type I and altered lipoprotein metabolism. J Biol Chem *278*, 52820-52825.

Koen, Y.M., Gogichaeva, N.V., Alterman, M.A., and Hanzlik, R.P. (2007). A proteomic analysis of bromobenzene reactive metabolite targets in rat liver cytosol in vivo. Chem Res Toxicol *20*, 511-519.

Koen, Y.M., and Hanzlik, R.P. (2002). Identification of seven proteins in the endoplasmic reticulum as targets for reactive metabolites of bromobenzene. Chem Res Toxicol *15*, 699-706.

Koen, Y.M., Yue, W., Galeva, N.A., Williams, T.D., and Hanzlik, R.P. (2006). Site-specific arylation of rat glutathione s-transferase A1 and A2 by bromobenzene metabolites in vivo. Chem Res Toxicol *19*, 1426-1434.

Labenski, M.T., Fisher, A.A., Lo, H.H., Monks, T.J., and Lau, S.S. (2009). Protein electrophile-binding motifs: lysine-rich proteins are preferential targets of quinones. Drug Metab Dispos *37*, 1211-1218.

Lawen, A., Ly, J.D., Lane, D.J., Zarschler, K., Messina, A., and De Pinto, V. (2005). Voltage-dependent anion-selective channel 1 (VDAC1)--a mitochondrial protein, rediscovered as a novel enzyme in the plasma membrane. Int J Biochem Cell Biol *37*, 277-282.

Lee, S.M., Kim, J.H., Cho, E.J., and Youn, H.D. (2009). A nucleocytoplasmic malate dehydrogenase regulates p53 transcriptional activity in response to metabolic stress. Cell Death Differ *16*, 738-748.

Li, M., Wang, W., Soroka, C.J., Mennone, A., Harry, K., Weinman, E.J., and Boyer, J.L. (2010). NHERF-1 binds to Mrp2 and regulates hepatic Mrp2 expression and function. J Biol Chem *285*, 19299-19307.

Li, S.X., Tong, Y.P., Xie, X.C., Wang, Q.H., Zhou, H.N., Han, Y., Zhang, Z.Y., Gao, W., Li, S.G., Zhang, X.C.*, et al.* (2007). Octameric structure of the human bifunctional enzyme PAICS in purine biosynthesis. J Mol Biol *366*, 1603-1614.

Lillig, C.H., and Holmgren, A. (2007). Thioredoxin and related molecules--from biology to health and disease. Antioxid Redox Signal *9*, 25-47.

Limacher, A., Kerler, J., Conde-Petit, B., and Blank, I. (2007). Formation of furan and methylfuran from ascorbic acid in model systems and food. Food Addit Contam *24 Suppl 1*, 122-135.

Lindquist, S., and Craig, E.A. (1988). The heat-shock proteins. Annu Rev Genet *22*, 631-677.

Lindqvist, A., Bratt, T., Altieri, M., Kastern, W., and Akerstrom, B. (1992). Rat alpha 1-microglobulin: co-expression in liver with the light chain of inter-alpha-trypsin inhibitor. Biochim Biophys Acta *1130*, 63-67.

Lo, A.S., Liew, C.T., Ngai, S.M., Tsui, S.K., Fung, K.P., Lee, C.Y., and Waye, M.M. (2005). Developmental regulation and cellular distribution of human cytosolic malate dehydrogenase (MDH1). J Cell Biochem *94*, 763-773.

Lu, D., Sullivan, M.M., Phillips, M.B., and Peterson, L.A. (2009). Degraded protein adducts of cis-2-butene-1,4-dial are urinary and hepatocyte metabolites of furan. Chem Res Toxicol *22*, 997-1007.

Lu, S.C., Alvarez, L., Huang, Z.Z., Chen, L., An, W., Corrales, F.J., Avila, M.A., Kanel, G., and Mato, J.M. (2001). Methionine adenosyltransferase 1A knockout mice are predisposed to liver injury and exhibit increased expression of genes involved in proliferation. Proc Natl Acad Sci U S A *98*, 5560-5565.

Lundin, M., Baltscheffsky, H., and Ronne, H. (1991). Yeast PPA2 gene encodes a mitochondrial inorganic pyrophosphatase that is essential for mitochondrial function. J Biol Chem *266*, 12168-12172.

Maarsingh, H., Zaagsma, J., and Meurs, H. (2009). Arginase: a key enzyme in the pathophysiology of allergic asthma opening novel therapeutic perspectives. Br J Pharmacol *158*, 652-664.

MacLeod, A.K., Kelly, V.P., Higgins, L.G., Kelleher, M.O., Price, S.A., Bigley, A.L., Betton, G.R., and Hayes, J.D. (2010). Expression and localization of rat aldo-keto reductases and induction of the 1B13 and 1D2 isoforms by phenolic antioxidants. Drug Metab Dispos *38*, 341-346.

Mally, A., Graff, C., Schmal, O., Moro, S., Hamberger, C., Schauer, U.M., Bruck, J., Ozden, S., Sieber, M., Steger, U.*, et al.* (2010). Functional and proliferative effects of repeated low-dose oral administration of furan in rat liver. Mol Nutr Food Res.

Mao, Y., Vyas, N.K., Vyas, M.N., Chen, D.H., Ludtke, S.J., Chiu, W., and Quiocho, F.A. (2004). Structure of the bifunctional and Golgi-associated formiminotransferase cyclodeaminase octamer. EMBO J *23*, 2963-2971.

Marinari, U.M., Ferro, M., Sciaba, L., Finollo, R., Bassi, A.M., and Brambilla, G. (1984). DNA-damaging activity of biotic and xenobiotic aldehydes in Chinese hamster ovary cells. Cell Biochem Funct *2*, 243-248.

Maronpot, R.R., Giles, H.D., Dykes, D.J., and Irwin, R.D. (1991). Furan-induced hepatic cholangiocarcinomas in Fischer 344 rats. Toxicol Pathol *19*, 561-570.

Martin, G.G., Atshaves, B.P., McIntosh, A.L., Mackie, J.T., Kier, A.B., and Schroeder, F. (2005). Liver fatty-acid-binding protein (L-FABP) gene ablation alters liver bile acid metabolism in male mice. Biochem J *391*, 549-560.

Martin, S., Hill, D.S., Paton, J.C., Paton, A.W., Birch-Machin, M.A., Lovat, P.E., and Redfern, C.P. (2010). Targeting GRP78 to enhance melanoma cell death. Pigment Cell Melanoma Res *23*, 675-682.

Martinez-Chantar, M.L., Corrales, F.J., Martinez-Cruz, L.A., Garcia-Trevijano, E.R., Huang, Z.Z., Chen, L., Kanel, G., Avila, M.A., Mato, J.M., and Lu, S.C. (2002). Spontaneous oxidative stress and liver tumors in mice lacking methionine adenosyltransferase 1A. FASEB J *16*, 1292-1294.

Matsui, M., Oshima, M., Oshima, H., Takaku, K., Maruyama, T., Yodoi, J., and Taketo, M.M. (1996). Early embryonic lethality caused by targeted disruption of the mouse thioredoxin gene. Dev Biol *178*, 179-185.

Mello, C.F., Sultana, R., Piroddi, M., Cai, J., Pierce, W.M., Klein, J.B., and Butterfield, D.A. (2007). Acrolein induces selective protein carbonylation in synaptosomes. Neuroscience *147*, 674-679.

Metzger, H.P., and Schywalsky, M. (1992). Intraorgan differences of blood flow, oxygen supply and glycogen content in the multilobular liver of normal and hemorrhagic rats. Int J Microcirc Clin Exp *11*, 67-83.

Meyer, B., Papasotiriou, D.G., and Karas, M. (2010). 100% protein sequence coverage: a modern form of surrealism in proteomics. Amino Acids.

Meyer, H.H., Shorter, J.G., Seemann, J., Pappin, D., and Warren, G. (2000). A complex of mammalian ufd1 and npl4 links the AAA-ATPase, p97, to ubiquitin and nuclear transport pathways. EMBO J *19*, 2181-2192.

Miller, J.A., and Miller, E.C. (1948). The carcinogenicity of certain derivatives of p-dimethylaminozobenz in the rat. J Exp Med *87*, 139-156.

Minarik, P., Tomaskova, N., Kollarova, M., and Antalik, M. (2002). Malate dehydrogenases--structure and function. Gen Physiol Biophys *21*, 257-265.

Miranda-Vizuete, A., Gustafsson, J.A., and Spyrou, G. (1998). Molecular cloning and expression of a cDNA encoding a human thioredoxin-like protein. Biochem Biophys Res Commun *243*, 284-288.

Miseta, A., and Csutora, P. (2000). Relationship between the occurrence of cysteine in proteins and the complexity of organisms. Mol Biol Evol *17*, 1232-1239.

Mitsui, A., Hamuro, J., Nakamura, H., Kondo, N., Hirabayashi, Y., Ishizaki-Koizumi, S., Hirakawa, T., Inoue, T., and Yodoi, J. (2002). Overexpression of human thioredoxin in transgenic mice controls oxidative stress and life span. Antioxid Redox Signal *4*, 693-696.

Morishita, R., Kawagoshi, A., Sawasaki, T., Madin, K., Ogasawara, T., Oka, T., and Endo, Y. (1999). Ribonuclease activity of rat liver perchloric acid-soluble protein, a potent inhibitor of protein synthesis. J Biol Chem *274*, 20688-20692.

Mugford, C.A., Carfagna, M.A., and Kedderis, G.L. (1997). Furan-mediated uncoupling of hepatic oxidative phosphorylation in Fischer-344 rats: an early event in cell death. Toxicol Appl Pharmacol *144*, 1-11.

Murley, L.L., and MacKenzie, R.E. (1997). Monofunctional domains of formiminotransferase-cyclodeaminase retain similar conformational stabilities outside the bifunctional octamer. Biochim Biophys Acta *1338*, 223-232.

Nagahara, N., and Nishino, T. (1996). Role of amino acid residues in the active site of rat liver mercaptopyruvate sulfurtransferase. CDNA cloning, overexpression, and site-directed mutagenesis. J Biol Chem *271*, 27395-27401.

Nagahara, N., Yoshii, T., Abe, Y., and Matsumura, T. (2007). Thioredoxin-dependent enzymatic activation of mercaptopyruvate sulfurtransferase. An intersubunit disulfide bond serves as a redox switch for activation. J Biol Chem *282*, 1561-1569.

Nakagawa, T., and Yamaguchi, M. (2008). Nuclear localization of regucalcin is enhanced in culture with protein kinase C activation in cloned normal rat kidney proximal tubular epithelial NRK52E cells. Int J Mol Med *21*, 605-610.

Nesvizhskii, A.I., and Aebersold, R. (2004). Analysis, statistical validation and dissemination of large-scale proteomics datasets generated by tandem MS. Drug Discov Today *9*, 173-181.

Ni, M., and Lee, A.S. (2007). ER chaperones in mammalian development and human diseases. FEBS Lett *581*, 3641-3651.

Niso-Santano, M., Gonzalez-Polo, R.A., Bravo-San Pedro, J.M., Gomez-Sanchez, R., Lastres-Becker, I., Ortiz-Ortiz, M.A., Soler, G., Moran, J.M., Cuadrado, A., and Fuentes, J.M. (2010). Activation of apoptosis signal-regulating kinase 1 is a key factor in paraquat-induced cell death: modulation by the Nrf2/Trx axis. Free Radic Biol Med *48*, 1370-1381.

NTP, U.S.D.o.H.a.H.S., Public Health Service, Research Triangle Park, NC. (1993). Toxicology and Carcinogenesis Studies of Furan (CAS No. 110-00-9) in F344/N Rats and B6C3F1 Mice (Gavage Studies). National Toxicology Program Technical Report Series *402*, 1-286.

O'Malley, K., Mauron, A., Barchas, J.D., and Kedes, L. (1985). Constitutively expressed rat mRNA encoding a 70-kilodalton heat-shock-like protein. Mol Cell Biol *5*, 3476-3483.

Ou, X., Yang, H., Ramani, K., Ara, A.I., Chen, H., Mato, J.M., and Lu, S.C. (2007). Inhibition of human betaine-homocysteine methyltransferase expression by S-adenosylmethionine and methylthioadenosine. Biochem J *401*, 87-96.

Pacher, P., Beckman, J.S., and Liaudet, L. (2007). Nitric oxide and peroxynitrite in health and disease. Physiol Rev *87*, 315-424.

Pajares, M.A., and Perez-Sala, D. (2006). Betaine homocysteine S-methyltransferase: just a regulator of homocysteine metabolism? Cell Mol Life Sci *63*, 2792-2803.

Palmeira, C.M., and Rolo, A.P. (2004). Mitochondrially-mediated toxicity of bile acids. Toxicology *203*, 1-15.

Panda, H., Pandey, R.S., Debata, P.R., and Supakar, P.C. (2007). Age-dependent differential expression and activity of rat liver cytosolic inorganic pyrophosphatase gene. Biogerontology *8*, 517-525.

Pelham, H.R. (1986). Speculations on the functions of the major heat shock and glucose-regulated proteins. Cell *46*, 959-961.

Pellicoro, A., and Faber, K.N. (2007). Review article: The function and regulation of proteins involved in bile salt biosynthesis and transport. Aliment Pharmacol Ther *26 Suppl 2*, 149-160.

Perez Locas, C., and Yaylayan, V.A. (2004). Origin and mechanistic pathways of formation of the parent furan--a food toxicant. J Agric Food Chem *52*, 6830-6836.

Perez, M.J., and Briz, O. (2009). Bile-acid-induced cell injury and protection. World J Gastroenterol *15*, 1677-1689.

Perlmutter, D.H., May, L.T., and Sehgal, P.B. (1989). Interferon beta 2/interleukin 6 modulates synthesis of alpha 1-antitrypsin in human mononuclear phagocytes and in human hepatoma cells. J Clin Invest *84*, 138-144.

Pervaiz, S., and Brew, K. (1987). Homology and structure-function correlations between alpha 1-acid glycoprotein and serum retinol-binding protein and its relatives. FASEB J *1*, 209-214.

Pessayre, D., Mansouri, A., Haouzi, D., and Fromenty, B. (1999). Hepatotoxicity due to mitochondrial dysfunction. Cell Biol Toxicol *15*, 367-373.

Peterson, L.A., Cummings, M.E., Chan, J.Y., Vu, C.C., and Matter, B.A. (2006). Identification of a cis-2-butene-1,4-dial-derived glutathione conjugate in the urine of furan-treated rats. Chem Res Toxicol *19*, 1138-1141.

Peterson, L.A., Cummings, M.E., Vu, C.C., and Matter, B.A. (2005). Glutathione trapping to measure microsomal oxidation of furan to cis-2-butene-1,4-dial. Drug Metab Dispos *33*, 1453-1458.

Peterson, L.A., Naruko, K.C., and Predecki, D.P. (2000). A reactive metabolite of furan, cis-2-butene-1,4-dial, is mutagenic in the Ames assay. Chem Res Toxicol *13*, 531-534.

Powis, G., and Montfort, W.R. (2001). Properties and biological activities of thioredoxins. Annu Rev Pharmacol Toxicol *41*, 261-295.

Qiu, Y., Benet, L.Z., and Burlingame, A.L. (1998). Identification of the hepatic protein targets of reactive metabolites of acetaminophen in vivo in mice using two-dimensional gel electrophoresis and mass spectrometry. J Biol Chem *273*, 17940-17953.

Ramsby, M.L., Makowski, G.S., and Khairallah, E.A. (1994). Differential detergent fractionation of isolated hepatocytes: biochemical, immunochemical and two-dimensional gel electrophoresis characterization of cytoskeletal and noncytoskeletal compartments. Electrophoresis *15*, 265-277.

Rauch, J., O'Neill, E., Mack, B., Matthias, C., Munz, M., Kolch, W., and Gires, O. (2010). Heterogeneous nuclear ribonucleoprotein H blocks MST2-mediated apoptosis in cancer cells by regulating A-Raf transcription. Cancer Res *70*, 1679-1688.

Rehm, H. (2006). Der Experimentator Proteinbiochemie/Proteomics. 5. Auflage, Elsevier GmbH, München.

Richter, C., Schweizer, M., Cossarizza, A., and Franceschi, C. (1996). Control of apoptosis by the cellular ATP level. FEBS Lett *378*, 107-110.

Rigotti, A., Trigatti, B.L., Penman, M., Rayburn, H., Herz, J., and Krieger, M. (1997). A targeted mutation in the murine gene encoding the high density lipoprotein (HDL) receptor scavenger receptor class B type I reveals its key role in HDL metabolism. Proc Natl Acad Sci U S A *94*, 12610-12615.

Robert-Ebadi, H., Le Querrec, A., de Moerloose, P., Gandon-Laloum, S., Borel Derlon, A., and Neerman-Arbez, M. (2008). A novel Asp344Val substitution in the fibrinogen gamma chain (fibrinogen Caen) causes dysfibrinogenemia associated with thrombosis. Blood Coagul Fibrinolysis *19*, 697-699.

Rogers, J., Kalsheker, N., Wallis, S., Speer, A., Coutelle, C.H., Woods, D., and Humphries, S.E. (1983). The isolation of a clone for human alpha 1-antitrypsin and the detection of alpha 1-antitrypsin in mRNA from liver and leukocytes. Biochem Biophys Res Commun *116*, 375-382.

Rohde, M., Daugaard, M., Jensen, M.H., Helin, K., Nylandsted, J., and Jaattela, M. (2005). Members of the heat-shock protein 70 family promote cancer cell growth by distinct mechanisms. Genes Dev *19*, 570-582.

Ron, D., and Walter, P. (2007). Signal integration in the endoplasmic reticulum unfolded protein response. Nat Rev Mol Cell Biol *8*, 519-529.

Safadi, F.F., Thornton, P., Magiera, H., Hollis, B.W., Gentile, M., Haddad, J.G., Liebhaber, S.A., and Cooke, N.E. (1999). Osteopathy and resistance to vitamin D toxicity in mice null for vitamin D binding protein. J Clin Invest *103*, 239-251.

Saitoh, M., Nishitoh, H., Fujii, M., Takeda, K., Tobiume, K., Sawada, Y., Kawabata, M., Miyazono, K., and Ichijo, H. (1998). Mammalian thioredoxin is a direct inhibitor of apoptosis signal-regulating kinase (ASK) 1. EMBO J *17*, 2596-2606.

Samali, A., Fitzgerald, U., Deegan, S., and Gupta, S. (2010). Methods for monitoring endoplasmic reticulum stress and the unfolded protein response. Int J Cell Biol *2010*, 830307.

Schleicher, M., and Jockusch, B.M. (2008). Actin: its cumbersome pilgrimage through cellular compartments. Histochem Cell Biol *129*, 695-704.

Schreiber, G., Tsykin, A., Aldred, A.R., Thomas, T., Fung, W.P., Dickson, P.W., Cole, T., Birch, H., De Jong, F.A., and Milland, J. (1989). The acute phase response in the rodent. Ann N Y Acad Sci *557*, 61-85; discussion 85-66.

Seiner, D.R., LaButti, J.N., and Gates, K.S. (2007). Kinetics and mechanism of protein tyrosine phosphatase 1B inactivation by acrolein. Chem Res Toxicol *20*, 1315-1320.

Shatton, J.B., Williams, A., and Weinhouse, S. (1983). Subcellular distribution of inorganic pyrophosphatase activity in various normal and neoplastic cell types. Cancer Res *43*, 3742-3747.

Shoshan-Barmatz, V., De Pinto, V., Zweckstetter, M., Raviv, Z., Keinan, N., and Arbel, N. (2010). VDAC, a multi-functional mitochondrial protein regulating cell life and death. Mol Aspects Med.

Siniossoglou, S., Lutzmann, M., Santos-Rosa, H., Leonard, K., Mueller, S., Aebi, U., and Hurt, E. (2000). Structure and assembly of the Nup84p complex. J Cell Biol *149*, 41-54.

Skulachev, V.P. (1991). Fatty acid circuit as a physiological mechanism of uncoupling of oxidative phosphorylation. FEBS Lett *294*, 158-162.

Son, T.G., Kim, S.J., Kim, K., Kim, M.S., Chung, H.Y., and Lee, J. (2008). Cytoprotective roles of senescence marker protein 30 against intracellular calcium elevation and oxidative stress. Arch Pharm Res *31*, 872-877.

Son, T.G., Zou, Y., Jung, K.J., Yu, B.P., Ishigami, A., Maruyama, N., and Lee, J. (2006). SMP30 deficiency causes increased oxidative stress in brain. Mech Ageing Dev *127*, 451-457.

Sorof, S. (1994). Modulation of mitogenesis by liver fatty acid binding protein. Cancer Metastasis Rev *13*, 317-336.

Speeckaert, M., Huang, G., Delanghe, J.R., and Taes, Y.E. (2006). Biological and clinical aspects of the vitamin D binding protein (Gc-globulin) and its polymorphism. Clin Chim Acta *372*, 33-42.

Stagg, S.M., Gurkan, C., Fowler, D.M., LaPointe, P., Foss, T.R., Potter, C.S., Carragher, B., and Balch, W.E. (2006). Structure of the Sec13/31 COPII coat cage. Nature *439*, 234-238.

Stewart, B.J., Doorn, J.A., and Petersen, D.R. (2007). Residue-specific adduction of tubulin by 4-hydroxynonenal and 4-oxononenal causes cross-linking and inhibits polymerization. Chem Res Toxicol *20*, 1111-1119.

Strnad, P., Stumptner, C., Zatloukal, K., and Denk, H. (2008). Intermediate filament cytoskeleton of the liver in health and disease. Histochem Cell Biol *129*, 735-749.

Tan, W.H., Eichler, F.S., Hoda, S., Lee, M.S., Baris, H., Hanley, C.A., Grant, P.E., Krishnamoorthy, K.S., and Shih, V.E. (2005). Isolated sulfite oxidase deficiency: a case report with a novel mutation and review of the literature. Pediatrics *116*, 757-766.

Tang, B.L., Peter, F., Krijnse-Locker, J., Low, S.H., Griffiths, G., and Hong, W. (1997). The mammalian homolog of yeast Sec13p is enriched in the intermediate compartment and is essential for protein transport from the endoplasmic reticulum to the Golgi apparatus. Mol Cell Biol *17*, 256-266.

Thunell, S., Holmberg, L., and Lundgren, J. (1987). Aminolaevulinate dehydratase porphyria in infancy. A clinical and biochemical study. J Clin Chem Clin Biochem *25*, 5-14.

Tirmenstein, M.A., and Nelson, S.D. (1989). Subcellular binding and effects on calcium homeostasis produced by acetaminophen and a nonhepatotoxic regioisomer, 3'-hydroxyacetanilide, in mouse liver. J Biol Chem *264*, 9814-9819.

Ulrey, C.L., Liu, L., Andrews, L.G., and Tollefsbol, T.O. (2005). The impact of metabolism on DNA methylation. Hum Mol Genet *14 Spec No 1*, R139-147.

Undas, A., Zdziarska, J., Iwaniec, T., Stepien, E., Skotnicki, A.B., de Moerloose, P., and Neerman-Arbez, M. (2009). Fibrinogen Krakow: a novel hypo/dysfibrinogenemia mutation in fibrinogen gamma chain (Asn325Ile) affecting fibrin clot structure and function. Thromb Haemost *101*, 975-976.

Usui, E., Okuda, K., Kato, Y., and Noshiro, M. (1994). Rat hepatic 3 alpha-hydroxysteroid dehydrogenase: expression of cDNA and physiological function in bile acid biosynthetic pathway. J Biochem *115*, 230-237.

van de Steeg, E., Wagenaar, E., van der Kruijssen, C.M., Burggraaff, J.E., de Waart, D.R., Elferink, R.P., Kenworthy, K.E., and Schinkel, A.H. (2010). Organic anion transporting polypeptide 1a/1b-knockout mice provide insights into hepatic handling of bilirubin, bile acids, and drugs. J Clin Invest *120*, 2942-2952.

Vickers, A.E. (2009). Characterization of hepatic mitochondrial injury induced by fatty acid oxidation inhibitors. Toxicol Pathol *37*, 78-88.

Vu, D., and Neerman-Arbez, M. (2007). Molecular mechanisms accounting for fibrinogen deficiency: from large deletions to intracellular retention of misfolded proteins. J Thromb Haemost *5 Suppl 1*, 125-131.

Walker, V. (2009). Ammonia toxicity and its prevention in inherited defects of the urea cycle. Diabetes Obes Metab *11*, 823-835.

Wang, G., Gong, Y., Anderson, J., Sun, D., Minuk, G., Roberts, M.S., and Burczynski, F.J. (2005a). Antioxidative function of L-FABP in L-FABP stably transfected Chang liver cells. Hepatology *42*, 871-879.

Wang, P., Wang, J.J., Xiao, Y., Murray, J.W., Novikoff, P.M., Angeletti, R.H., Orr, G.A., Lan, D., Silver, D.L., and Wolkoff, A.W. (2005b). Interaction with PDZK1 is required for expression of organic anion transporting protein 1A1 on the hepatocyte surface. J Biol Chem *280*, 30143-30149.

Wenzel, P., Muller, J., Zurmeyer, S., Schuhmacher, S., Schulz, E., Oelze, M., Pautz, A., Kawamoto, T., Wojnowski, L., Kleinert, H*., et al.* (2008). ALDH-2 deficiency increases cardiovascular oxidative stress--evidence for indirect antioxidative properties. Biochem Biophys Res Commun *367*, 137-143.

Wilkinson, B., and Gilbert, H.F. (2004). Protein disulfide isomerase. Biochim Biophys Acta *1699*, 35-44.

Wilson, D.M., Goldsworthy, T.L., Popp, J.A., and Butterworth, B.E. (1992). Evaluation of genotoxicity, pathological lesions, and cell proliferation in livers of rats and mice treated with furan. Environ Mol Mutagen *19*, 209-222.

Woo, W.H., Yang, H., Wong, K.P., and Halliwell, B. (2003). Sulphite oxidase gene expression in human brain and in other human and rat tissues. Biochem Biophys Res Commun *305*, 619-623.

Woodman, P.G. (2003). p97, a protein coping with multiple identities. J Cell Sci *116*, 4283-4290.

Xie, Y., Newberry, E.P., Kennedy, S.M., Luo, J., and Davidson, N.O. (2009). Increased susceptibility to diet-induced gallstones in liver fatty acid binding protein knockout mice. J Lipid Res *50*, 977-987.

Yamaguchi, M. (2000). Role of regucalcin in calcium signaling. Life Sci *66*, 1769-1780.

Yang, Z., Savchenko, A., Yakunin, A., Zhang, R., Edwards, A., Arrowsmith, C., and Tong, L. (2003). Aspartate dehydrogenase, a novel enzyme identified from structural and functional studies of TM1643. J Biol Chem *278*, 8804-8808.

Yao, L., Zhang, J., and Liu, X. (2008). NDRG2: a Myc-repressed gene involved in cancer and cell stress. Acta Biochim Biophys Sin (Shanghai) *40*, 625-635.

Ye, Y., Meyer, H.H., and Rapoport, T.A. (2001). The AAA ATPase Cdc48/p97 and its partners transport proteins from the ER into the cytosol. Nature *414*, 652-656.

Yoneda, K., Kawakami, R., Tagashira, Y., Sakuraba, H., Goda, S., and Ohshima, T. (2006). The first archaeal L-aspartate dehydrogenase from the hyperthermophile Archaeoglobus fulgidus: gene cloning and enzymological characterization. Biochim Biophys Acta *1764*, 1087-1093.

Zhang, B., Abreu, J.G., Zhou, K., Chen, Y., Hu, Y., Zhou, T., He, X., and Ma, J.X. (2010). Blocking the Wnt pathway, a unifying mechanism for an angiogenic inhibitor in the serine proteinase inhibitor family. Proc Natl Acad Sci U S A *107*, 6900-6905.

Zhang, Y., Morar, M., and Ealick, S.E. (2008). Structural biology of the purine biosynthetic pathway. Cell Mol Life Sci *65*, 3699-3724.

Zhou, S., Chan, E., Duan, W., Huang, M., and Chen, Y.Z. (2005). Drug bioactivation, covalent binding to target proteins and toxicity relevance. Drug Metab Rev *37*, 41-213.

Zhuo, L., Yoneda, M., Zhao, M., Yingsung, W., Yoshida, N., Kitagawa, Y., Kawamura, K., Suzuki, T., and Kimata, K. (2001). Defect in SHAP-hyaluronan complex causes severe female infertility. A study by inactivation of the bikunin gene in mice. J Biol Chem *276*, 7693-7696.

Zsembery, A., Thalhammer, T., and Graf, J. (2000). Bile Formation: a Concerted Action of Membrane Transporters in Hepatocytes and Cholangiocytes. News Physiol Sci *15*, 6-11.

13 ANNEX

13.1 Comparison between theoretical and experimentally determined molecular masses (M_r) and isoelectric points (pI) of target proteins

Table 21 *Comparison between theoretical and experimentally determined protein data (continued on next pages); theoretical protein mass and pI were taken from the UniProtKB database and the Mascot search engine, respectively. Experimentally determined protein molecular mass (M_r exp) and pI (pI exp) were obtained from the spot positions on the 2D-gels in comparison to the protein marker used and the pH range of the IPG strip. Discrepancies between theoretical and experimentally determined protein mass may be due to the facts that the protein was cleaved during sample preparation or that there are different forms of the protein in the cell. Discrepancies between theoretical and experimentally determined pI are in line with literature data and are thought to be the result of posttranslational modifications resulting in mobility shifts (Koen et al., 2007, Koen and Hanzlik, 2002, Qiu et al., 1998, Ikehata et al., 2008).*

Protein Name	Spot	UniProt ID	M_r theoretical [kDa]	M_r exp [kDa]	pI theoretical	pI exp
Carbohydrate metabolism						
[+]α-enolase	27	P04764	47	55	6.2	5.9
*Fructose-bisphosphate aldolase B	50	P00884	40	49	8.7	8.0
[+]Fructose-1,6-bisphosphatase 1	6	P19112	40	45	5.5	5.4
*Glyceraldehyde-3-phosphate dehydrogenase	52	P04797	36	45	8.4	7.2
*L-Lactate dehydrogenase A chain	53	P04642	36	40	8.5	7.2
[+]Malate dehydrogenase	2b	O88989	36	53	6.2	5.2
	31			37		6.2
*Phosphoglycerate kinase 1	51	P16617	45	52	8.0	7.5
*Triosephosphate isomerase	47	P48500	27	26	6.5	6.5
	97			25		6.4
Lipid metabolism						
*Enoyl-CoA hydratase	64	P14604	32	31	6.4	6.3
*3-Ketoacyl-CoA thiolase	**51**	P13437	42	52	8.1	7.5
	55			54		6.9
[+]Long-chain fatty acid CoA ligase 1	2a	P18163	78	49	6.6	5.2
*Long-chain specific acyl-CoA dehydrogenase	93	P15650	48	46	7.6	6.4
*Short-chain specific acyl-CoA dehydrogenase	59	P15651	45	46	8.5	6.2
Amino acid metabolism, urea cycle						
*Arginase 1	59	P07824	35	46	6.8	6.2
*Argininosuccinate synthase	**51**	P09034	46	52	7.6	7.5
	55			54		6.9
*Betaine-homocysteine S-methyltransferase 1	51	O09171	45	52	8.0	7.5
*Formimidoyltransferase-cyclodeaminase	83	O88618	59	58	5.8	5.7
*Isovaleryl-CoA dehydrogenase	33c	P12007	46	48	8.0	6.3
	58			53		6.3
*Ornithine carbamoyltransferase	**55**	P00481	40	54	9.1	6.9
	60			44		6.3
*2-Oxoisovalerate dehydrogenase subunit α	85	P11960	50	53	7.7	5.8

Table 21 *(continued)*

Protein Name	Spot	UniProt ID	M_r theoretical [kDa]	M_r exp [kDa]	pI theoretical	pI exp
*S-Adenosylmethionine synthetase isoform type-1	**85**	P13444	44	53	5.6	5.8
	86			53		5.7
Redox regulation						
*Electron transfer flavoprotein subunit α	61	P13803	35	40	8.6	6.4
*Peroxiredoxin-1	62	Q63716	22	25	8.3	6.7
+*Thioredoxin-1	12	P11232	12	13	4.8	4.6
+*Thioredoxin-like protein 1	3	Q920J4	32	40	4.8	5.0
Protein folding						
*78 kDa Glucose-regulated protein	**75**	P06761	72	70	5.1	5.0
	76			42		5.0
*Heat shock cognate 71 kDa protein	1	P63018	71	70	5.4	5.3
	79			70		5.2
*Protein disulfide-isomerase	**74**	P04785	57	62	4.8	4.8
	75			70		5.0
*Protein disulfide-isomerase A3	83	P11598	57	58	5.9	5.7
Proteolysis						
*α_1-antiproteinase	86	P17475	46	53	5.7	5.7
+*Protein AMBP: Bikunin and Trypstatin	23	Q64240	39	50	5.8	5.7
*Serine protease inhibitor A3K	80	P05545	47	58	5.3	5.4
*Ubiquitin fusion degradation protein 1 homolog	94	Q9ES53	34	43	6.3	6.4
Structural proteins						
+β-Actin	**2a**	P60711	42	49	5.3	5.2
	2b			53		5.2
	5			50		5.4
	78			48		5.1
+*Ezrin-radixin-moesin-binding phosphoprotein 50	21a	Q9JJ19	39	55	5.7	5.6
+Fibrinogen γ chain	21c	P02680	51	55	5.9	5.6
+γ-Actin	**2a**	P63259	42	49	5.3	5.2
	2b			53		5.2
	5			50		5.4
	78			48		5.1
*Keratin, type II cytoskeletal 8	21b	Q10758	54	58	5.8	5.6
	24			60		5.7
	25			39		5.7
	78			48		5.1

Table 21 *(continued)*

Protein Name	Spot	UniProt ID	M_r theoretical [kDa]	M_r exp [kDa]	pI theoretical	pI exp
*Na(+)/H(+) exchanger regulatory factor 3	75	Q9JJ40	57	70	5.3	5.0
	79			70		5.2
*Protein SEC13 homolog	4	Q5XFW8	36	41	5.2	5.2
*Voltage-dependent anion-selective channel protein 1	53	Q9Z2L0	31	40	8.4	7.2
Transport proteins						
*α2μ-Globulin	19	P02761	21	16	5.9	5.6
	20a			13		6.0
	87			17		5.5
*Fatty acid binding protein 1	63	P02692	14	14	7.8	6.4
	91			14		5.9
+*Protein AMBP: α_1-microglobulin	23	Q64240	39	50	5.8	5.7
*Transthyretin	92	P02767	16	14	5.8	6.0
*Vitamin D binding protein	80	P04276	54	58	5.8	5.4
Nucleotide metabolism						
*Multifunctional protein ADE2	51	P51583	47	52	7.9	7.5
*Putative L-aspartate dehydrogenase	61	Q5I0J9	31	40	5.5	6.4
*Heterogeneous nuclear ribonucleoprotein H1	93	Q8VHV7	49	46	5.9	6.4

Table 21 *(continued)*

Protein Name	Spot	UniProt ID	M_r theoretical [kDa]	M_r exp [kDa]	pI theoretical	pI exp
Miscellaneous						
*Acetyl-CoA acetyltransferase	50	P17764	45	49	8.9	8.0
*Aflatoxin B1 aldehyde reductase member 2	96	Q8CG45	41	38	6.3	6.4
*Aldehyde dehydrogenase	29	P11884	56	40	6.7	6.1
	86			53		5.7
+3α-Hydroxysteroid dehydrogenase	**37**	P23457	37	40	6.7	6.5
	60			44		6.3
*ATP synthase β subunit	**4**	P10719	56	41	5.2	5.2
	74			62		4.8
+δ-aminolevulinic acid dehydratase	35	P06214	36	40	6.3	6.4
*Glycerol-3-phosphate dehydrogenase [NAD+]	33b	O35077	37	41	6.2	6.3
	60			44		6.3
+3-Mercaptopyruvate sulfurtransferase	30	P97532	33	36	5.9	6.1
*Ppa1 protein	4	Q499R7	38	41	6.4	5.2
*Protein NDRG2	78	Q8VBU2	41	48	5.2	5.1
*Regucalcin	4	Q03336	33	41	5.4	5.2
+*Ribonuclease UK114	**14**	P52759	14	13	7.8	5.4
	63			14		6.4
*Sulfite oxidase	83	Q07116	61	58	6.3	5.7

13.2 Amino acid sequences of the identified proteins

Data on amino acid sequences were taken from the online database Protein Knowledgebase (UniProtKB, http://www.uniprot.org/).

13.2.1 Carbohydrate metabolism

α-Enolase

```
        10         20         30         40         50         60
MSILKIHARE IFDSRGNPTV EVDLYTAKGL FRAAVPSGAS TGIYEALELR DNDKTRFMGK

        70         80         90        100        110        120
GVSKAVEHIN KTIAPALVSK KLNVVEQEKI DQLMIEMDGT ENKSKFGANA ILGVSLAVCK

       130        140        150        160        170        180
AGAVEKGVPL YRHIADLAGN PEVILPVPAF NVINGGSHAG NKLAMQEFMI LPVGASSFRE

       190        200        210        220        230        240
AMRIGAEVYH NLKNVIKEKY GKDATNVGDE GGFAPNILEN KEALELLKSA IAKAGYTDQV

       250        260        270        280        290        300
VIGMDVAASE FYRAGKYDLD FKSPDDASRY ITPDQLADLY KSFIKDYPVV SIEDPFDQDD

       310        320        330        340        350        360
WDAWQKFTAT AGIQVVGDDL TVTNPKRIAK AAGEKSCNCL LLKVNQIGSV TESLQACKLA

       370        380        390        400        410        420
QSNGWGVMVS HRSGETEDTF IADLVVGLCT GQIKTGAPCR SERLAKYNQI LRIEEELGSK

       430
AKFAGRSFRN PLAK
```

Fructose-bisphosphate aldolase B

```
         10         20         30         40         50         60
MAHRFPALTS EQKKELSEIA QRIVANGKGI LAADESVGTM GNRLQRIKVE NTEENRRQFR

         70         80         90        100        110        120
ELLFSVDNSI SQSIGGVILF HETLYQKDSQ GKLFRNILKE KGIVVGIKLD QGGAPLAGTN

        130        140        150        160        170        180
KETTIQGLDG LSERCAQYKK DGVDFGKWRA VLRISDQCPS SLAIQENANA LARYASICQQ

        190        200        210        220        230        240
NGLVPIVEPE VLPDGDHDLE HCQYVSEKVL AAVYKALNDH HVYLEGTLLK PNMLTAGHAC

        250        260        270        280        290        300
TKKYTPEQVA MATVTALHRT VPAAVPSICF LSGGMSEEDA TLNLNAIYRC PLPRPWKLSF

        310        320        330        340        350        360
SYGRALQASA LAAWGGKAAN KKATQEAFMK RAVANCQAAQ GQYVHTGSSG AASTQSLFTA


SYTY
```

Fructose-1,6-bisphosphatase 1

```
         10         20         30         40         50         60
MVDHAPFETD ISTLTRFVLE EGRKAGGTGE MTQLLNSLCT AIKAISSAVR QAGIAQLYGI

         70         80         90        100        110        120
AGSTNVTGDQ VKKLDILSND LVINMLKSSY ATCVLVSEED THAIIIEPEK RGKYVVCFDP

        130        140        150        160        170        180
LDGSSNIDCL ASIGTIFGIY RKTSANEPSE KDALQPGRNL VAAGYALYGS ATMLVLAMNC

        190        200        210        220        230        240
GVNCFMLDPS IGEFILVDRD VKIKKKGNIY SINEGYAKDF DPAINEYIQR KKFPPDNSAP

        250        260        270        280        290        300
YGARYVGSMV ADVHRTLVYG GIFLYPANKK NPSGKLRLLY ECNPIAYVME KAGGLATTGN

        310        320        330        340        350        360
EDILDIVPTE IHQKAPVIMG STEDVQEFLE IYNKDKAKSR PSLPLPQSRA RESPVHSICD


ELF
```

Glyceraldehyde-3-phosphate dehydrogenase

```
         10          20          30          40          50          60
MVKVGVNGFG RIGRLVTRAA FSCDKVDIVA INDPFIDLNY MVYMFQYDST HGKFNGTVKA

         70          80          90         100         110         120
ENGKLVINGK PITIFQERDP ANIKWGDAGA EYVVESTGVF TTMEKAGAHL KGGAKRVIIS

        130         140         150         160         170         180
APSADAPMFV MGVNHEKYDN SLKIVSNASC TTNCLAPLAK VIHDNFGIVE GLMTTVHAIT

        190         200         210         220         230         240
ATQKTVDGPS GKLWRDGRGA AQNIIPASTG AAKAVGKVIP ELNGKLTGMA FRVPTPNVSV

        250         260         270         280         290         300
VDLTCRLEKP AKYDDIKKVV KQAAEGPLKG ILGYTEDQVV SCDFNSNSHS STFDAGAGIA

        310         320         330
LNDNFVKLIS WYDNEYGYSN RVVDLMAYMA SKE
```

L-Lactate dehydrogenase A chain

```
         10          20          30          40          50          60
MAALKDQLIV NLLKEEQVPQ NKITVVGVGA VGMACAISIL MKDLADELAL VDVIEDKLKG

         70          80          90         100         110         120
EMMDLQHGSL FLKTPKIVSS KDYSVTANSK LVIITAGARQ QEGESRLNLV QRNVNIFKFI

        130         140         150         160         170         180
IPNVVKYSPQ CKLLIVSNPV DILTYVAWKI SGFPKNRVIG SGCNLDSARF RYLMGERLGV

        190         200         210         220         230         240
HPLSCHGWVL GEHGDSSVPV WSGVNVAGVS LKSLNPQLGT DADKEQWKDV HKQVVDSAYE

        250         260         270         280         290         300
VIKLKGYTSW AIGLSVADLA ESIMKNLRRV HPISTMIKGL YGIKEDVFLS VPCILGQNGI

        310         320         330
SDVVKVTLTP DEEARLKKSA DTLWGIQKEL QF
```

Malate dehydrogenase

```
         10          20          30          40          50          60
MSEPIRVLVT GAAGQIAYSL LYSIGNGSVF GKDQPIILVL LDITPMMGVL DGVLMELQDC

         70          80          90         100         110         120
ALPLLQDVIA TDKEEVAFKD LDVAVLVGSM PRREGMERKD LLKANVKIFK SQGAALEKYA

        130         140         150         160         170         180
KKSVKVIVVG NPANTNCLTA SKSAPSIPKE NFSCLTRLDH NRAKSQIALK LGVTADDVKN

        190         200         210         220         230         240
VIIWGNHSST QYPDVNHAKV KLQGKEVGVY EALKDDSWLK GEFITTVQQR GAAVIKARKL

        250         260         270         280         290         300
SSAMSAAKAI SDHIRDIWFG TPEGEFVSMG VISDGNSYGV PDDLLYSFPV VIKNKTWKFV

        310         320         330
EGLPINDFSR EKMDLTAKEL TEEKETAFEF LSSA
```

Phosphoglycerate kinase 1

```
         10          20          30          40          50          60
MSLSNKLTLD KLDVKGKRVV MRVDFNVPMK NNQITNNQRI KAAVPSIKFC LDNGAKSVVL

         70          80          90         100         110         120
MSHLGRPDGV PMPDKYSLEP VAAELKSLLG KDVLFLKDCV GSEVENACAN PAAGTVILLE

        130         140         150         160         170         180
NLRFHVEEEG KGKDASGNKV KAEPAKIDAF RASLSKLGDV YVNDAFGTAH RAHSSMVGVN

        190         200         210         220         230         240
LPQKAGGFLM KKELNYFAKA LESPERPFLA ILGGAKVADK IQLINNMLDK VNEMIIGGGM

        250         260         270         280         290         300
AFTFLKVLNN MEIGTSLYDE EGAKIVKDLM AKAEKNGVKI TLPVDFVTAD KFDENAKTGQ

        310         320         330         340         350         360
ATVASGIPAG WMGLDCGTES SKKYAEAVAR AKQIVWNGPV GVFEWEAFAR GTKSLMDEVV

        370         380         390         400         410
KATSRGCITI IGGGDTATCC AKWNTEDKVS HVSTGGGASL ELLEGKVLPG VDALSNV
```

Triosephosphate isomerase

```
         10          20          30          40          50          60
MAPSRKFFVG GNWKMNGRKK CLGELICTLN AAKLPADTEV VCAPPTAYID FARQKLDPKI

         70          80          90         100         110         120
AVAAQNCYKV TNGAFTGEIS PGMIKDLGAT WVVLGHSERR HIFGESDELI GQKVNHALSE

        130         140         150         160         170         180
GLGVIACIGE KLDEREAGIT EKVVFEQTKA IADNVKDWCK VVLAYEPVWA IGTGKTATPQ

        190         200         210         220         230         240
QAQEVHEKLR GWLKCNVSEG VAQCTRIIYG GSVTGATCKE LASQPDVDGF LVGGASLKPE

FVDIINAKQ
```

13.2.2 Lipid metabolism

Enoyl-CoA hydratase

```
        10         20         30         40         50         60
MAALRALLPR ACNSLLSPVR CPEFRRFASG ANFQYIITEK KGKNSSVGLI QLNRPKALNA

        70         80         90        100        110        120
LCNGLIEELN QALETFEEDP AVGAIVLTGG EKAFAAGADI KEMQNRTFQD CYSGKFLSHW

       130        140        150        160        170        180
DHITRIKKPV IAAVNGYALG GGCELAMMCD IIYAGEKAQF GQPEILLGTI PGAGGTQRLT

       190        200        210        220        230        240
RAVGKSLAME MVLTGDRISA QDAKQAGLVS KIFPVETLVE EAIQCAEKIA NNSKIIVAMA

       250        260        270        280        290
KESVNAAFEM TLTEGNKLEK KLFYSTFATD DRREGMSAFV EKRKANFKDH
```

3-Ketoacyl-CoA thiolase

```
        10         20         30         40         50         60
MALLRGVFIV AAKRTPFGAY GGLLKDFTAT DLTEFAARAA LSAGKVPPET IDSVIVGNVM

        70         80         90        100        110        120
QSSSDAAYLA RHVGLRVGVP TETGALTLNR LCGSGFQSIV SGCQEICSKD AEVVLCGGTE

       130        140        150        160        170        180
SMSQSPYSVR NVRFGTKFGL DLKLEDTLWA GLTDQHVKLP MGMTAENLAA KYNISREDCD

       190        200        210        220        230        240
RYALQSQQRW KAANEAGYFN EEMAPIEVKT KKGKQTMQVD EHARPQTTLE QLQNLPPVFK

       250        260        270        280        290        300
KEGTVTAGNA SGMSDGAGVV IIASEDAVKK HNFTPLARVV GYFVSGCDPA IMGIGPVPAI

       310        320        330        340        350        360
TGALKKAGLS LKDMDLIDVN EAFAPQFLAV QKSLDLDPSK TNVSGGAIAL GHPLGGSGSR

       370        380        390
ITAHLVHELR RRGGKYAVGS ACIGGGQGIS LIIQNTA
```

Long-chain fatty acid CoA ligase 1

```
        10         20         30         40         50         60
MEVHELFRYF RMPELIDIRQ YVRTLPTNTL MGFGAFAALT TFWYATRPKA LKPPCDLSMQ

        70         80         90        100        110        120
SVEVTGTTEG VRRSAVLEDD KLLLYYYDDV RTMYDGFQRG IQVSNDGPCL GSRKPNQPYE

       130        140        150        160        170        180
WISYKQVAEM AECIGSALIQ KGFKPCSEQF IGIFSQNRPE WVTIEQGCFT YSMVVVPLYD

       190        200        210        220        230        240
TLGTDAITYI VNKAELSVIF ADKPEKAKLL LEGVENKLTP CLKIIVIMDS YDNDLVERGQ

       250        260        270        280        290        300
KCGVEIIGLK ALEDLGRVNR TKPKPPEPED LAIICFTSGT TGNPKGAMVT HQNIMNDCSG

       310        320        330        340        350        360
FIKATESAFI ASPEDVLISF LPLAHMFETV VECVMLCHGA KIGFFQGDIR LLMDDLKVLQ

       370        380        390        400        410        420
PTIFPVVPRL LNRMFDRIFG QANTSVKRWL LDFASKRKEA ELRSGIVRNN SLWDKLIFHK

       430        440        450        460        470        480
IQSSLGGKVR LMITGAAPVS ATVLTFLRAA LGCQFYEGYG QTECTAGCCL SLPGDWTAGH

       490        500        510        520        530        540
VGAPMPCNYI KLVDVEDMNY QAAKGEGEVC VKGANVFKGY LKDPARTAEA LDKDGWLHTG

       550        560        570        580        590        600
DIGKWLPNGT LKIIDRKKHI FKLAQGEYIA PEKIENIYLR SEAVAQVFVH GESLQAFLIA

       610        620        630        640        650        660
IVVPDVEILP SWAQKRGFQG SFEELCRNKD INKAILEDMV KLGKNAGLKP FEQVKGIAVH

       670        680        690
PELFSIDNGL LTPTLKAKRP ELRNYFRSQI DELYSTIKI
```

Long-chain specific acyl-CoA dehydrogenase

```
        10         20         30         40         50         60
MAARLLLRSL RVLSARSATL PPPSARCSHS GAEARLETPS AKKLTDIGIR RIFSSEHDIF

        70         80         90        100        110        120
RESVRKFFQE EVIPYHEEWE KAGEVSRELW EKAGKQGLLG INIAEKHGGI GGDLLSTAVT

       130        140        150        160        170        180
WEEQAYSNCT GPGFSLHSDI VMPYIANYGT KEQIEQFIPQ MTAGKCIGAI AMTEPGAGSD

       190        200        210        220        230        240
LQGVRTNAKR SGSDWILNGS KVFITNGWLS DLVIVVAVTN REARSPAHGI SLFLVENGMK

       250        260        270        280        290        300
GFIKGKKLHK MGMKAQDTAE LFFEDVRLPA SALLGEENKG FYYLMQELPQ ERLLIADLAI

       310        320        330        340        350        360
SACEFMFEET RNYVRQRKAF GKTVAHIQTV QHKLAELKTN ICVTRAFVDS CLQLHETKRL

       370        380        390        400        410        420
DSASASMAKY WASELQNTVA YQCVQLHGGW GYMWEYPIAK AYVDARVQPI YGGTNEIMKE

       430
LIARQIVSDS
```

Short-chain specific acyl-CoA dehydrogenase

```
        10         20         30         40         50         60
MAAALLARAG GSLGRALRAR DWRRLHTVYQ SVELPETHQM LRQTCRDFAE KELVPIAAQL

        70         80         90        100        110        120
DKEHLFPTSQ VKKMGELGLL AMDVPEELSG AGLDYLAYSI ALEEISRGCA STGVIMSVNN

       130        140        150        160        170        180
SLYLGPILKF GSSQQKQQWI TPFTNGDKIG CFALSEPGNG SDAGAASTTA REEGDSWVLN

       190        200        210        220        230        240
GTKAWITNSW EASATVVFAS TDRSRQNKGI SAFLVPMPTP GLTLGKKEDK LGIRASSTAN

       250        260        270        280        290        300
LIFEDCRIPK ENLLGEPGMG FKIAMQTLDM GRIGIASQAL GIAQASLDCA VKYAENRHAF

       310        320        330        340        350        360
GAPLTKLQNI QFKLADMALA LESARLLTWR AAMLKDNKKP FTKESAMAKL AASEAATAIS

       370        380        390        400        410
HQAIQILGGM GYVTEMPAER YYRDARITEI YEGTSEIQRL VIAGHLLRSY RS
```

13.2.3 Amino acid metabolism, urea cycle

Arginase 1

```
        10         20         30         40         50         60
MSSKPKPIEI IGAPFSKGQP RGGVEKGPAA LRKAGLVEKL KETEYNVRDH GDLAFVDVPN

        70         80         90        100        110        120
DSPFQIVKNP RSVGKANEQL AAVVAETQKN GTISVVLGGD HSMAIGSISG HARVHPDLCV

       130        140        150        160        170        180
IWVDAHTDIN TPLTTSSGNL HGQPVAFLLK ELKGKFPDVP GFSWVTPCIS AKDIVYIGLR

       190        200        210        220        230        240
DVDPGEHYII KTLGIKYFSM TEVDKLGIGK VMEETFSYLL GRKKRPIHLS FDVDGLDPVF

       250        260        270        280        290        300
TPATGTPVVG GLSYREGLYI TEEIYKTGLL SGLDIMEVNP TLGKTPEEVT RTVNTAVALT

       310        320
LSCFGTKREG NHKPETDYLK PPK
```

Argininosuccinate synthase

```
        10         20         30         40         50         60
MSSKGSVVLA YSGGLDTSCI LVWLKEQGYD VIAYLANIGQ KEDFEEARKK ALKLGAKKVF

        70         80         90        100        110        120
IEDVSKEFVE EFIWPAVQSS ALYEDRYLLG TSLARPCIAR KQVEIAQREG AKYVSHGATG

       130        140        150        160        170        180
KGNDQVRFEL TCYSLAPQIK VIAPWRMPEF YNRFKGRNDL MEYAKQHGIP IPVTPKSPWS

       190        200        210        220        230        240
MDENLMHISY EAGILENPKN QAPPGLYTKT QDPAKAPNTP DVLEIEFKKG VPVKVTNVKD

       250        260        270        280        290        300
GTTHSTSLDL FMYLNEVAGK HGVGRIDIVE NRFIGMKSRG IYETPAGTIL YHAHLDIEAF

       310        320        330        340        350        360
TMDREVRKIK QGLGLKFAEL VYTGFWHSPE CEFVRHCIDK SQERVEGKVQ VSVFKGQVYI

       370        380        390        400        410
LGRESPLSLY NEELVSMNVQ GDYEPIDATG FININSLRLK EYHRLQSKVT AK
```

Betaine-homocysteine S-methyltransferase 1

```
         10          20          30          40          50          60
MAPIAGKKAK RGILERLNAG EVVIGDGGFV FALEKRGYVK AGPWTPEAAV EHPEAVRQLH

         70          80          90         100         110         120
REFLRAGSNV MQTFTFYASE DKLENRGNYV AEKISGQKVN EAACDIARQV ADEGDALVAG

        130         140         150         160         170         180
GVSQTPSYLS CKSETEVKKI FHQQLEVFMK KNVDFLIAEY FEHVEEAVWA VEALKTSGKP

        190         200         210         220         230         240
IAATMCIGPE GDLHGVSPGE CAVRLVKAGA AIVGVNCHFD PSTSLQTIKL MKEGLEAARL

        250         260         270         280         290         300
KAYLMSHALA YHTPDCGKQG FIDLPEFPFG LEPRVATRWD IQKYAREAYN LGVRYIGGCC

        310         320         330         340         350         360
GFEPYHIRAI AEELAPERGF LPPASEKHGS WGSGLDMHTK PWIRARARKE YWQNLRIASG

        370         380         390         400
RPYNPSMSKP DAWGVTKGAA ELMQQKEATT EQQLRALFEK QKFKSAQ
```

Formimidoyltransferase-cyclodeaminase

```
         10          20          30          40          50          60
MSQLVECVPN FSEGNNQEVI DAISQAISQT PGCVLLDVDA GPSTNRTVYT FVGQPECVVE

         70          80          90         100         110         120
GALSAARTAS QLIDMRKHKG EHPRMGALDV CPFIPVRGVS MDECVLCAKA FGQRLAEELN

        130         140         150         160         170         180
VPVYLYGEAA QMPSRQTLPA IRAGEYEALP EKLKQAEWVP DFGPSSFVPS WGATVTGARK

        190         200         210         220         230         240
FLIAFNINLL STKEQAHRIA LNLREQGRGK DQPGRLKKVQ GIGWYLEEKN LAQVSTNLLD

        250         260         270         280         290         300
FEVTALHTVY EEARREAQEL NLPVVGSQLV GLVPLKALLD AAAFYCDKEK LFVLEEEHRI

        310         320         330         340         350         360
RLVVNRLGLD SLAPFDPKER IIEYLVPDSG PEQSLLDASL RAFVREVGAR SAAPGGGSVA

        370         380         390         400         410         420
AAVAALGAAL ASMVGQMTYG RRQFDHLDST MRRLIPPFHA ASAQLTSLVD ADARAFAACL

        430         440         450         460         470         480
GAIKLPKNTP EERDRRTCAL QEGLRQAVAV PLKLAETVSQ LWPALQELAQ CGNLSCLSDL

        490         500         510         520         530         540
QVAAKALETG VFGAYFNVLI NLKDMTDDVF KEKTRHRISS LLQEAKTQAA LVLGSLEARK
```

E

Isovaleryl-CoA dehydrogenase

```
        10         20         30         40         50         60
MATAVRLLGR RVSSWRLRPL PSPLAVPQRA HSMLPVDDDI NGLNEEQKQL RHTISKFVQE

        70         80         90        100        110        120
NLAPKAQEID QSNDFKNLRE FWKQLGSLGV LGITAPVQYG GSGLGYLEHV LVMEEISRAS

       130        140        150        160        170        180
AAVGLSYGAH SNLCINQIVR NGNEAQKEKY LPKLISGEFI GALAMSEPNA GSDVVSMRLK

       190        200        210        220        230        240
AEKKGDHYVL NGNKFWITNG PDADVLVVYA KTDLTAVPAS RGITAFIVEK DMPGFSTSKK

       250        260        270        280        290        300
LDKLGMRGSN TCELVFEDCK VPAANILSQE SKGVYVLMSG LDLERLVLAG GPLGIMQAVL

       310        320        330        340        350        360
DHTIPYLHVR EAFGQKIGQF QLMQGKMADM YTRLMACRQY VYNVARACDE GHITAKDCAG

       370        380        390        400        410        420
VILYTAECAT QVALDGIQCL GGNGYINDFP MGRFLRDAKL YEIGGGTSEV RRLVIGRAFN

ADFR
```

Ornithine carbamoyltransferase

```
        10         20         30         40         50         60
MLSNLRILLN KAALRKAHTS MVRNFRYGKP VQSQVQLKGR DLLTLKNFTG EEIQYMLWLS

        70         80         90        100        110        120
ADLKFRIKQK GEYLPLLQGK SLGMIFEKRS TRTRLSTETG FALLGGHPSF LTTQDIHLGV

       130        140        150        160        170        180
NESLTDTARV LSSMTDAVLA RVYKQSDLDI LAKEATIPIV NGLSDLYHPI QILADYLTLQ

       190        200        210        220        230        240
EHYGSLKGLT LSWIGDGNNI LHSIMMSAAK FGMHLQAATP KGYEPDPNIV KLAEQYAKEN

       250        260        270        280        290        300
GTRLSMTNDP LEAARGGNVL ITDTWISMGQ EDEKKKRLQA FQGYQVTMKT AKVAASDWTF

       310        320        330        340        350
LHCLPRKPEE VDDEVFYSPR SLVFPEAENR KWTIMAVMVS LLTDYSPVLQ KPKF
```

2-Oxoisovalerate dehydrogenase subunit α

```
        10         20         30         40         50         60
SAAKIWRPSR GLRQAALLLL GRPGARGLAR FHPSRQQQQQ FPSLDDKPQF PGASAEFVDK

        70         80         90        100        110        120
LEFIQPNVIS GIPIYRVMDR QGQIINPSED PHLPQEEVLK LYRSMTLLNT MDRILYESQR

       130        140        150        160        170        180
QGRISFYMTN YGEEGTHVGS AAALERTDLV FGQYREAGVL MYRDYPLELF MAQCYGNVSD

       190        200        210        220        230        240
PGKGRQMPVH YGCKERHFVT ISSPLATQIP QAVGAAYAAK RANANQIVIC YFGEGAASEG

       250        260        270        280        290        300
DAHAGFNFAA TLECPIIFFC RNNGYAISTP TSEQYRGDGI AARGPGYGIM SIRVDGNDVF

       310        320        330        340        350        360
AVYNATKEAR RRAVAENQPF LIEAMTYRIG HHSTSDDSSA YRSVDEVNYW DKQDHPISRL

       370        380        390        400        410        420
RQYLLNQGWW DEEQEKAWRK QSRKKVMEAF EQAERKLKPN PSLLFSDVYQ EMPAQLRRQQ

       430        440
ESLARHLQTY GEHYPLDHFD K
```

S-Adenosylmethionine synthetase isoform type-1

```
        10         20         30         40         50         60
MNGPVDGLCD HSLSEEGAFM FTSESVGEGH PDKICDQISD AVLDAHLKQD PNAKVACETV

        70         80         90        100        110        120
CKTGMVLLCG EITSMAMIDY QRVVRDTIKH IGYDDSAKGF DFKTCNVLVA LEQQSPDIAQ

       130        140        150        160        170        180
CVHLDRNEED VGAGDQGLMF GYATDETEEC MPLTIVLAHK LNTRMADLRR SGVLPWLRPD

       190        200        210        220        230        240
SKTQVTVQYV QDNGAVIPVR VHTIVISVQH NEDITLEAMR EALKEQVIKA VVPAKYLDED

       250        260        270        280        290        300
TIYHLQPSGR FVIGGPQGDA GVTGRKIIVD TYGGWGAHGG GAFSGKDYTK VDRSAAYAAR

       310        320        330        340        350        360
WVAKSLVKAG LCRRVLVQVS YAIGVAEPLS ISIFTYGTSK KTERDELLEV VNKNFDLRPG

       370        380        390
VIVRDLDLKK PIYQKTACYG HFGRSEFPWE VPKKLVF
```

13.2.4 Redox regulation

Electron transfer flavoprotein subunit α

```
        10         20         30         40         50         60
MFRAAAPGQL RRAASLLRFQ STLVIAEHAN DSLAPITLNT ITAAGRLGGE VSCLVAGTKC

        70         80         90        100        110        120
DKVVQDLCKV AGVAKVLVAQ HDAYKGLLPE ELTPLILETQ KQFSYTHICA GASAFGKNLL

       130        140        150        160        170        180
PRVAAKLNVA PVSDIIEIKS PDTFVRTIYA GNALCTVKCD EKVKVFSVRG TSFEAAAASG

       190        200        210        220        230        240
GSASSEKAPS SSSAGISEWL DQKLTKSDRP ELTGAKVVVS GGRGLKSGEN FKLLYDLADQ

       250        260        270        280        290        300
LHAAVGASRA AVDAGFVPND MQVGQTGKIV APELYIAVGI SGAIQHLAGM KDSKTIVAIN

       310        320        330
KDPEAPIFQV ADYGIVADLF KVVPEMTEIL KKK
```

Peroxiredoxin-1

```
        10         20         30         40         50         60
MSSGNAKIGH PAPSFKATAV MPDGQFKDIS LSDYKGKYVV FFFYPLDFTF VCPTEIIAFS

        70         80         90        100        110        120
DRAEEFKKLN CQVIGASVDS HFCHLAWINT PKKQGGLGPM NIPLVSDPKR TIAQDYGVLK

       130        140        150        160        170        180
ADEGISFRGL FIIDDKGILR QITINDLPVG RSVDEILRLV QAFQFTDKHG EVCPAGWKPG

       190
SDTIKPDVNK SKEYFSKQK
```

Thioredoxin-1

```
        10         20         30         40         50         60
MVKLIESKEA FQEALAAAGD KLVVVDFSAT WCGPCKMIKP FFHSLCDKYS NVVFLEVDVD

        70         80         90        100
DCQDVAADCE VKCMPTFQFY KKGQKVGEFS GANKEKLEAT ITEFA
```

Thioredoxin-like protein 1

```
         10          20          30          40          50          60
MVGVKPVGSD PDFQPELSGA GSRLAVVKFT MRGCGPCLRI APAFSSMSNK YPQAVFLEVD

         70          80          90         100         110         120
VHQCQGTAAT NNISATPTFL FFRNKVRIDQ YQGADAVGLE EKIKQHLEND PGSNEDTDIP

        130         140         150         160         170         180
KGYMDLMPFI NKAGCECLNE SDEHGFDNCL RKDLSFLESD CDEQLLITVA FNQPVKLYSM

        190         200         210         220         230         240
KFQGPDNGQG PKYVKIFINL PRSMDFEEAE RSEPTQALEL TEDDIKEDGI VPLRYVKFQN

        250         260         270         280
VNSVTLFVQS NQGEEETTRI SYFTFIGTPV QATNMNDFKR VVGKKGESH
```

13.2.5 Protein folding

78 kDa Glucose-regulated protein

```
        10         20         30         40         50         60
MKFTVVAAAL LLLCAVRAEE EDKKEDVGTV VGIDLGTTYS CVGVFKNGRV EIIANDQGNR

        70         80         90        100        110        120
ITPSYVAFTP EGERLIGDAA KNQLTSNPEN TVFDAKRLIG RTWNDPSVQQ DIKFLPFKVV

       130        140        150        160        170        180
EKKTKPYIQV DIGGGQTKTF APEEISAMVL TKMKETAEAY LGKKVTHAVV TVPAYFNDAQ

       190        200        210        220        230        240
RQATKDAGTI AGLNVMRIIN EPTAAAIAYG LDKREGEKNI LVFDLGGGTF DVSLLTIDNG

       250        260        270        280        290        300
VFEVVATNGD THLGGEDFDQ RVMEHFIKLY KKKTGKDVRK DNRAVQKLRR EVEKAKRALS

       310        320        330        340        350        360
SQHQARIEIE SFFEGEDFSE TLTRAKFEEL NMDLFRSTMK PVQKVLEDSD LKKSDIDEIV

       370        380        390        400        410        420
LVGGSTRIPK IQQLVKEFFN GKEPSRGINP DEAVAYGAAV QAGVLSGDQD TGDLVLLDVC

       430        440        450        460        470        480
PLTLGIETVG GVMTKLIPRN TVVPTKKSQI FSTASDNQPT VTIKVYEGER PLTKDNHLLG

       490        500        510        520        530        540
TFDLTGIPPA PRGVPQIEVT FEIDVNGILR VTAEDKGTGN KNKITITNDQ NRLTPEEIER

       550        560        570        580        590        600
MVNDAEKFAE EDKKLKERID TRNELESYAY SLKNQIGDKE KLGGKLSPED KETMEKAVEE

       610        620        630        640        650
KIEWLESHQD ADIEDFKAKK KELEEIVQPI ISKLYGSGGP PPTGEEDTSE KDEL
```

Heat shock cognate 71 kDa protein

```
         10          20          30          40          50          60
MSKGPAVGID LGTTYSCVGV FQHGKVEIIA NDQGNRTTPS YVAFTDTERL IGDAAKNQVA

         70          80          90         100         110         120
MNPTNTVFDA KRLIGRRFDD AVVQSDMKHW PFMVVNDAGR PKVQVEYKGE TKSFYPEEVS

        130         140         150         160         170         180
SMVLTKMKEI AEAYLGKTVT NAVVTVPAYF NDSQRQATKD AGTIAGLNVL RIINEPTAAA

        190         200         210         220         230         240
IAYGLDKKVG AERNVLIFDL GGGTFDVSIL TIEDGIFEVK STAGDTHLGG EDFDNRMVNH

        250         260         270         280         290         300
FIAEFKRKHK KDISENKRAV RRLRTACERA KRTLSSSTQA SIEIDSLYEG IDFYTSITRA

        310         320         330         340         350         360
RFEELNADLF RGTLDPVEKA LRDAKLDKSQ IHDIVLVGGS TRIPKIQKLL QDFFNGKELN

        370         380         390         400         410         420
KSINPDEAVA YGAAVQAAIL SGDKSENVQD LLLLDVTPLS LGIETAGGVM TVLIKRNTTI

        430         440         450         460         470         480
PTKQTQTFTT YSDNQPGVLI QVYEGERAMT KDNNLLGKFE LTGIPPAPRG VPQIEVTFDI

        490         500         510         520         530         540
DANGILNVSA VDKSTGKENK ITITNDKGRL SKEDIERMVQ EAEKYKAEDE KQRDKVSSKN

        550         560         570         580         590         600
SLESYAFNMK ATVEDEKLQG KINDEDKQKI LDKCNEIISW LDKNQTAEKE EFEHQQKELE

        610         620         630         640
KVCNPIITKL YQSAGGMPGG MPGGFPGGGA PPSGGASSGP TIEEVD
```

Protein disulfide-isomerase

```
         10         20         30         40         50         60
MLSRALLCLA LAWAARVGAD ALEEEDNVLV LKKSNFAEAL AAHNYLLVEF YAPWCGHCKA

         70         80         90        100        110        120
LAPEYAKAAA KLKAEGSEIR LAKVDATEES DLAQQYGVRG YPTIKFFKNG DTASPKEYTA

        130        140        150        160        170        180
GREADDIVNW LKKRTGPAAT TLSDTAAAES LVDSSEVTVI GFFKDAGSDS AKQFLLAAEA

        190        200        210        220        230        240
VDDIPFGITS NSDVFSKYQL DKDGVVLFKK FDEGRNNFEG EITKEKLLDF IKHNQLPLVI

        250        260        270        280        290        300
EFTEQTAPKI FGGEIKTHIL LFLPKSVSDY DGKLSNFKKA AEGFKGKILF IFIDSDHTDN

        310        320        330        340        350        360
QRILEFFGLK KEECPAVRLI TLEEEMTKYK PESDELTAEK ITQFCHHFLE GKIKPHLMSQ

        370        380        390        400        410        420
ELPEDWDKQP VKVLVGKNFE EVAFDEKKNV FVEFYAPWCG HCKQLAPIWD KLGETYKDHE

        430        440        450        460        470        480
NIVIAKMDST ANEVEAVKVH SFPTLKFFPA SADRTVIDYN GERTLDGFKK FLESGGQDGA

        490        500
GDNDDLDLEE ALEPDMEEDD DQKAVKDEL
```

Protein disulfide-isomerase A3

```
         10         20         30         40         50         60
MRFSCLALLP GVALLLASAL LASASDVLEL TDENFESRVS DTGSAGLMLV EFFAPWCGHC

         70         80         90        100        110        120
KRLAPEYEAA ATRLKGIVPL AKVDCTANTN TCNKYGVSGY PTLKIFRDGE EAGAYDGPRT

        130        140        150        160        170        180
ADGIVSHLKK QAGPASVPLR TEDEFKKFIS DKDASVVGFF RDLFSDGHSE FLKAASNLRD

        190        200        210        220        230        240
NYRFAHTNVE SLVKEYDDNG EGITIFRPLH LANKFEDKIV AYTEKKMTSG KIKKFIQESI

        250        260        270        280        290        300
FGLCPHMTED NKDLIQGKDL LTAYYDVDYE KNTKGSNYWR NRVMMVAKTF LDAGHKLNFA

        310        320        330        340        350        360
VASRKTFSHE LSDFGLESTT GEIPVVAIRT AKGEKFVMQE EFSRDGKALE RFLQEYFDGN

        370        380        390        400        410        420
LKRYLKSEPI PETNEGPVKV VVAESFDDIV NAEDKDVLIE FYAPWCGHCK NLEPKYKELG

        430        440        450        460        470        480
EKLSKDPNIV IAKMDATAND VPSPYEVKGF PTIYFSPANK KLTPKKYEGG RELNDFISYL

        490        500
QREATNPPII QEEKPKKKKK AQEDL
```

13.2.6 Proteolysis

α_1-Antiproteinase

```
         10         20         30         40         50         60
MAPSISRGLL LLAALCCLAP SFLAEDAQET DTSQQDQSPT YRKISSNLAD FAFSLYRELV

         70         80         90        100        110        120
HQSNTSNIFF SPMSITTAFA MLSLGSKGDT RKQILEGLEF NLTQIPEADI HKAFHHLLQT

        130        140        150        160        170        180
LNRPDSELQL NTGNGLFVNK NLKLVEKFLE EVKNNYHSEA FSVNFADSEE AKKVINDYVE

        190        200        210        220        230        240
KGTQGKIVDL MKQLDEDTVF ALVNYIFFKG KWKRPFNPEH TRDADFHVDK STTVKVPMMN

        250        260        270        280        290        300
RLGMFDMHYC STLSSWVLMM DYLGNATAIF LLPDDGKMQH LEQTLTKDLI SRFLLNRQTR

        310        320        330        340        350        360
SAILYFPKLS ISGTYNLKTL LSSLGITRVF NNDADLSGIT EDAPLKLSQA VHKAVLTLDE

        370        380        390        400        410
RGTEAAGATV VEAVPMSLPP QVKFDHPFIF MIVESETQSP LFVGKVIDPT R
```

Protein AMBP: Bikunin and Trypstatin

```
         10         20         30         40         50         60
MQGLGALFLL LTACLTLKAD NVPTLPDIQV QENFNEARIY GKWFNLAVGS TCPWLRRIKN

         70         80         90        100        110        120
KMSVSTLVLQ EGATEAEISV TSTQWRKGVC EEISGVYQKT DIDGKFLYHK SKWNATLESY

        130        140        150        160        170        180
VVHTNYDEYA IFLTKKFSHR HGPTITAKLY GREPQLRDSL LQEFREVALS VGIPENSIVF

        190        200        210        220        230        240
MADRGECVPG DREVESTSFA RARRAVLPQE NEGSGSEPLI TGTLKKEDSC QLNYSEGPCL

        250        260        270        280        290        300
GMQQKYYYNG ASMACETFQY GGCLGNGNNF ASEKECLQTC RTIAACNLPI VQGPCRAFAE

        310        320        330        340
LWAFDAAQGK CIQFIYGGCK GNGNKFYSEK ECKEYCGVPG DGYEELTRS
```

Serine protease inhibitor A3K

```
        10         20         30         40         50         60
MAFIAALGLL MAGICPAVLC DGILGRDTLP HEDQGKGRQL HSLTLASINT DFTLSLYKKL

        70         80         90        100        110        120
ALRNPDKNVV FSPLSISAAL AILSLGAKDS TMEEILEVLK FNLTEITEEE IHQGFGHLLQ

       130        140        150        160        170        180
RLSQPEDQAE INTGSALFID KEQPILSEFQ EKTRALYQAE AFVADFKQCN EAKKFINDYV

       190        200        210        220        230        240
SNQTQGKIAE LFSELDERTS MVLVNYLLFK GKWKVPFNPN DTFESEFYLD EKRSVKVPMM

       250        260        270        280        290        300
KIKDLTTPYI RDEELSCSVL ELKYTGNASA LFILPDQGKM QQVESSLQPE TLKKWKDSLR

       310        320        330        340        350        360
PRIISELRMP KFSISTDYNL EEVLPELGIR KIFSQQADLS RITGTKNLHV SQVVHKAVLD

       370        380        390        400        410
VDETGTEGAA ATAVTAALKS LPQTIPLLNF NRPFMLVITD NNGQSVFFMG KVTNPM
```

Ubiquitin fusion degradation protein 1 homolog

```
        10         20         30         40         50         60
MFSFNMFDHP IPRVFQNRFS TQYRCFSVSM LAGPNDRSDV EKGGKIIMPP SALDQLSRLN

        70         80         90        100        110        120
ITYPMLFKLT NKNSDRMTHC GVLEFVADEG ICYLPHWMMQ NLLLEEGGLV QVESVNLQVA

       130        140        150        160        170        180
TYSKFQPQSP DFLDITNPKA VLENALRNFA CLTTGDVIAI NYNEKIYELR VMETKPDKAV

       190        200        210        220        230        240
SIIECDMNVD FDAPLGYKEP ERPVQHEESI EGEADHSGYA GEVGFRAFSG SGNRLDGKKK

       250        260        270        280        290        300
GVEPSPSPIK PGDIKRGIPN YEFKLGKITF IRNSRPMVKK VEEDEAGGRF VAFSGEGQSL


RKKGRKP
```

13.2.7 Structural proteins

β-Actin

```
         10          20          30          40          50          60
MDDDIAALVV DNGSGMCKAG FAGDDAPRAV FPSIVGRPRH QGVMVGMGQK DSYVGDEAQS

         70          80          90         100         110         120
KRGILTLKYP IEHGIVTNWD DMEKIWHHTF YNELRVAPEE HPVLLTEAPL NPKANREKMT

        130         140         150         160         170         180
QIMFETFNTP AMYVAIQAVL SLYASGRTTG IVMDSGDGVT HTVPIYEGYA LPHAILRLDL

        190         200         210         220         230         240
AGRDLTDYLM KILTERGYSF TTTAEREIVR DIKEKLCYVA LDFEQEMATA ASSSSLEKSY

        250         260         270         280         290         300
ELPDGQVITI GNERFRCPEA LFQPSFLGME SCGIHETTFN SIMKCDVDIR KDLYANTVLS

        310         320         330         340         350         360
GGTTMYPGIA DRMQKEITAL APSTMKIKII APPERKYSVW IGGSILASLS TFQQMWISKQ

        370
EYDESGPSIV HRKCF
```

Ezrin-radixin-moesin-binding phosphoprotein 50

```
         10          20          30          40          50          60
MSADAAAGEP LPRLCCLEKG PNGYGFHLHG EKGKVGQFIR LVEPGSPAEK SGLLAGDRLV

         70          80          90         100         110         120
EVNGENVEKE THQQVVSRIR AALNAVRLLV VDPETDEQLK KLGVPIREEL LRAQEKSEHT

        130         140         150         160         170         180
EPPAAADTKK AGDQNEAEKS HLERCELRPR LCTMKKGPNG YGFNLHSDKS KPGQFIRAVD

        190         200         210         220         230         240
PDSPAEASGL RAQDRIVEVN GVCMEGKQHG DVVSAIKAGG DEAKLLVVDK ETDEFFKKCR

        250         260         270         280         290         300
VTPSQEHLDG PLPEPFSNGE IQKENSREAL VEPASESPRP ALARSASSDT SEELNAQDSP

        310         320         330         340         350
KRHDSTEPSS TSSSSDPILD FNISLAVAKE RAHQKRSSKR APQMDWSKKN ELFSNL
```

Fibrinogen γ chain

```
         10         20         30         40         50         60
MNWSLQLRSF ILCWALLLLS PTGLAQYTAT RDNCCILDER FGSYCPTTCG ISDFLNSYQT

         70         80         90        100        110        120
DVDTDLQTLE NILQRAENRT TEAKELIKAI QVYYNPDQPP KPGMIEGATQ KSKKMVEEIL

        130        140        150        160        170        180
KYEALLLTHE SSIRYLQDIY TSNKQKITNL KQKVAQLEAQ CQEPCKDSVR IHDTTGKDCQ

        190        200        210        220        230        240
DIANKGAKES GLYFIRPLKA TQQFLVYCEI DGSGNGWTVL QKRLDGSVDF KKNWIQYKEG

        250        260        270        280        290        300
FGHLSPTGTT EFWLGNEKIH LISMQSTIPY ALRIQLKDWS GRTSTADYAM FRVGPESDKY

        310        320        330        340        350        360
RLTYAYFIGG DAGDAFDGYD FGDDPSDKFF TSHNGMHFST WDNDNDKFEG NCAEQDGSGW

        370        380        390        400        410        420
WMNKCHAGHL NGVYYQGGTY SKSSTPNGYD NGIIWATWKT RWYSMKETTM KIIPFNRLSI

        430        440
GDGQQHHMGG SKQVSVEHEV DVEYP
```

γ-Actin

```
         10         20         30         40         50         60
MEEEIAALVI DNGSGMCKAG FAGDDAPRAV FPSIVGRPRH QGVMVGMGQK DSYVGDEAQS

         70         80         90        100        110        120
KRGILTLKYP IEHGIVTNWD DMEKIWHHTF YNELRVAPEE HPVLLTEAPL NPKANREKMT

        130        140        150        160        170        180
QIMFETFNTP AMYVAIQAVL SLYASGRTTG IVMDSGDGVT HTVPIYEGYA LPHAILRLDL

        190        200        210        220        230        240
AGRDLTDYLM KILTERGYSF TTTAEREIVR DIKEKLCYVA LDFEQEMATA ASSSSLEKSY

        250        260        270        280        290        300
ELPDGQVITI GNERFRCPEA LFQPSFLGME SCGIHETTFN SIMKCDVDIR KDLYANTVLS

        310        320        330        340        350        360
GGTTMYPGIA DRMQKEITAL APSTMKIKII APPERKYSVW IGGSILASLS TFQQMWISKQ

        370
EYDESGPSIV HRKCF
```

Keratin, type II cytoskeletal 8

```
         10          20          30          40          50          60
MSVRVTQKSY KMSTSGPRAF SSRSFTSGPG ARISSSSFSR VGSSSSSFRG SLGGFGGAGV

         70          80          90         100         110         120
GGITAVTVNQ SLLNPLKLEV DPNIQAVRTQ EKEQIKTLNN KFASFIDKVR FLEQQNKMLE

        130         140         150         160         170         180
TKWSLLQQQK TSRSNMDNMF ESYINNLRRQ LEALGQEKLK LEVELGNMQG LVEDFKNKYE

        190         200         210         220         230         240
DEINKRTEME NEFVLIKKDV DEAYMNKVEL ESRLEGLTDE INFLRQIHEE EIRELQSQIS

        250         260         270         280         290         300
DTSVVLSMDN SRSLDMDSII AEVRAQYEEI ANRSRAEAET MYQIKYEELQ TLAGKHGDDL

        310         320         330         340         350         360
RRSKTEISEM NRNISRLQAE IDALKGQRAT LEAAIADAEQ RGELAVKDAN AKLEDLKNAL

        370         380         390         400         410         420
QKAKQDMARQ LREYQELMNV KLALDIEIAT YRKLLEGEES RLESGMQNMS IHTKTTSGYA

        430         440         450         460         470         480
GGLSSSYGGL TSPGFSYGMS SFQPGFGSVG GSSTYSRTKA VVVKKIETRD GKLVSESSDI


MSK
```

Na(+)/H(+) exchanger regulatory factor 3

```
         10          20          30          40          50          60
MASTFNPRCC KLSKKEGQNY GFFLRIEKDT DGHLVRVIEE GSPAEKAGLL DGDRVLRING

         70          80          90         100         110         120
VFVDKEEHAQ VVDLVRKSGN SVTLLVLDGD SYEKAVKHQV DLKELDQSPR EPALNEKKPD

        130         140         150         160         170         180
LGMNGGVETC AQPRLCYLVK EGNSFGFSLK TIQGKKGVFL TDITPQGVAM KAGVLADDHL

        190         200         210         220         230         240
IEVNGENVEN ASHEEVVEKV TKSGSRIMFL LVDKETARCH SEQKTPFKRE TASLKLLPHQ

        250         260         270         280         290         300
PRVVVIKKGS NGYGFYLRAG PEQKGQIIKD IEPGSPAEAA GLKNNDLVVA VNGESVEALD

        310         320         330         340         350         360
HDGVVEMIRN GGDQTTLLVL DKEADRIYSL ARFSPLLYCQ SQELPNGSVK EAPAPISAPL

        370         380         390         400         410         420
EAPGSATTED VGDHKPKLCR LIKEDDSYGF HLNAIRGQPG SFVKEVQQGG PADKAGLENE

        430         440         450         460         470         480
DIIIEVNGEN VQDEPYDRVV ERIKSSGEHV TLLVCGKVAY SYFQAKKIPI LSSLADPLVA

        490         500         510         520
GPDAKGETEH DSAESTKDSS HPARDRTLSA ASHSSSNSED TVM
```

Protein SEC13 homolog

```
        10         20         30         40         50         60
MVSVINTVDT SHEDMIHDAQ MDYYGTRLAT CSSDRSVKIF DVRNGGQILI ADLRGHEGPV

        70         80         90        100        110        120
WQVAWAHPMY GNILASCSYD RKVIIWKEEN GTWEKTHEHS GHDSSVNSVC WAPHDYGLIL

       130        140        150        160        170        180
ACGSSDGAIS LLTYTGEGQW EVKKINNAHT IGCNAVSWAP AVVPGSLIDQ PSGQKPNYIK

       190        200        210        220        230        240
KFASGGCDNL IKLWREEEDG QWKEEQKLEA HSDWVRDVAW APSIGLPTST IASCSQDGRV

       250        260        270        280        290        300
FIWTCDDASG NMWSPKLLHK FNDVVWHVSW SITANILAVS GGDNKVTLWK ESVDGQWVCI

       310        320
SDVNKGQGSV SASITEGQQN EQ
```

Voltage-dependent anion-selective channel protein 1

```
        10         20         30         40         50         60
MAVPPTYADL GKSARDVFTK GYGFGLIKLD LKTKSENGLE FTSSGSANTE TTKVNGSLET

        70         80         90        100        110        120
KYRWTEYGLT FTEKWNTDNT LGTEITVEDQ LARGLKLTFD SSFSPNTGKK NAKIKTGYKR

       130        140        150        160        170        180
EHINLGCDVD FDIAGPSIRG ALVLGYEGWL AGYQMNFETS KSRVTQSNFA VGYKTDEFQL

       190        200        210        220        230        240
HTNVNDGTEF GGSIYQKVNK KLETAVNLAW TAGNSNTRFG IAAKYQVDPD ACFSAKVNNS

       250        260        270        280
SLIGLGYTQT LKPGIKLTLS ALLDGKNVNA GGHKLGLGLE FQA
```

13.2.8 Transport proteins

α2μ-Globulin

```
         10          20          30          40          50          60
MKLLLLLLCL GLTLVCGHAE EASSTRGNLD VAKLNGDWFS IVVASNKREK IEENGSMRVF

         70          80          90         100         110         120
MQHIDVLENS LGFKFRIKEN GECRELYLVA YKTPEDGEYF VEYDGGNTFT ILKTDYDRYV

        130         140         150         160         170         180
MFHLINFKNG ETFQLMVLYG RTKDLSSDIK EKFAKLCEAH GITRDNIIDL TKTDRCLQAR


G
```

Fatty acid binding protein 1

```
         10          20          30          40          50          60
MNFSGKYQVQ SQENFEPFMK AMGLPEDLIQ KGKDIKGVSE IVHEGKKVKL TITYGSKVIH

         70          80          90         100         110         120
NEFTLGEECE LETMTGEKVK AVVKMEGDNK MVTTFKGIKS VTEFNGDTIT NTMTLGDIVY


KRVSKRI
```

Protein AMBP: α_1-Microglobulin

```
         10          20          30          40          50          60
MQGLGALFLL LTACLTLKAD NVPTLPDIQV QENFNEARIY GKWFNLAVGS TCPWLRRIKN

         70          80          90         100         110         120
KMSVSTLVLQ EGATEAEISV TSTQWRKGVC EEISGVYQKT DIDGKFLYHK SKWNATLESY

        130         140         150         160         170         180
VVHTNYDEYA IFLTKKFSHR HGPTITAKLY GREPQLRDSL LQEFREVALS VGIPENSIVF

        190         200         210         220         230         240
MADRGECVPG DREVESTSFA RARRAVLPQE NEGSGSEPLI TGTLKKEDSC QLNYSEGPCL

        250         260         270         280         290         300
GMQQKYYYNG ASMACETFQY GGCLGNGNNF ASEKECLQTC RTIAACNLPI VQGPCRAFAE

        310         320         330         340
LWAFDAAQGK CIQFIYGGCK GNGNKFYSEK ECKEYCGVPG DGYEELTRS
```

Transthyretin

```
         10          20          30          40          50          60
MASLRLFLLC LAGLIFASEA GPGGAGESKC PLMVKVLDAV RGSPAVDVAV KVFKKTADGS

         70          80          90         100         110         120
WEPFASGKTA ESGELHGLTT DEKFTEGVYR VELDTKSYWK ALGISPFHEY AEVVFTANDS

        130         140
GHRHYTIAAL LSPYSYSTTA VVSNPQN
```

Vitamin D binding protein

```
        10         20         30         40         50         60
MKRVLVLLLA LAFGHALERG RDYEKDKVCQ ELSTLGKDDF RSLSLILYSR KFPSSTFEQV

        70         80         90        100        110        120
SQLVKEVVSL TEECCAEGAD PNCYDTRTSE LSIKSCESDA PFPVHPGTSE CCTKEGLERK

       130        140        150        160        170        180
LCMAALSHQP QEFPAYVEPT NDEICEAFRK DPKGFADQFL FEYSSNYGQA PLPLLVGYTK

       190        200        210        220        230        240
SYLSMVGSCC TSAKPTVCFL KERLQMKQLL LLTTMSNRVC SQYAAYGKEK SRMSHLIKLA

       250        260        270        280        290        300
QKVPTANLED VLPLAEDLTE ILSRCCKSTS EDCMARELPE HTLKICGNLS KKNSKFEECC

       310        320        330        340        350        360
YETTPMGIFM CSYFMPTAEP LQLPAIKLPT SKDLCGQSAT QAMDQYTFEL SRRTQVPEVF

       370        380        390        400        410        420
LSKVLDTTLK TLRECCDTQD SVSCFSTQSP LMKRQLTSFI EKGQEMCADY SENTFTEYKK

       430        440        450        460        470
KLAERLRTKM PNASPEELAD MVAKHSDFAS KCCSINSPPR YCSSQIDAEM RDILQS
```

13.2.9 Nucleotide metabolism

Multifunctional protein ADE2

```
        10         20         30         40         50         60
MATAEVLNIG RKLYEGKTKE VYELLDSPGR VLLQSKDQIT AGNAARKNHL EGKAAISNKI

        70         80         90        100        110        120
TSCIFQLLQE AGIKTAFTKK CGETAFIAPQ CEMIPIEWVC RRIATGSFLK RNPGVKEGYR

       130        140        150        160        170        180
FYPPKVEMFF KDDANNDPQW SEEQLIAAKF CFAGLVIGQT EVDIMSHATQ AIFEILEKSW

       190        200        210        220        230        240
LPQNCTLVDM KIEFGVDVTT KEIVLADVID NDSWRLWPSG DRSQQKDKQS YRDLKEVTPE

       250        260        270        280        290        300
GLQMVKKNFE WVADRVELLL KSNSQCRVVV LMGSTSDLGH CEKIKKACGN FGIPCELRVT

       310        320        330        340        350        360
SAHKGPDETL RIKAEYEGDG IPTVFVAVAG RSNGLGPVMS GNTAYPVISC PPITADWGAQ

       370        380        390        400        410        420
DVWSSLRLPS GIGCSTILSP EGSAQFAAQI FGLNNHLVWA KLRASKLNTW ISLKQADKKI


RECNL
```

Putative L-aspartate dehydrogenase

```
        10         20         30         40         50         60
MDASMVPRVP HKVGVVGYGR LGQSLVSRLL AQGSELGLEL VFVWNRDPGR MAGSVPPALQ

        70         80         90        100        110        120
LEDLTTLEER HPDLVVEVAH PKIIHESGVQ ILRHANLLVG SPSALADQTT ERQLLEASNH

       130        140        150        160        170        180
WGHTVFVARG ALWGCEDISR LDAAGGLQSL RVTMATHPDG FRLEGPLAAA HSSGPRTVLY

       190        200        210        220        230        240
EGPVRGLCPL APRNSNTMAA AALAAPSLGF DRVIGVLVAD LSLTDMHVVD VELTGPQGPQ

       250        260        270        280        290
AAALPCTPTE RTQPSLALSL APLLLQPSGT AYWAAVSFPP DLGSASAEFP PLPLLSP
```

Heterogeneous nuclear ribonucleoprotein H1

```
        10         20         30         40         50         60
MMLGAEGGEG FVVKVRGLPW SCSADEVQRF FSDCKIQNGA QGIRFIYTRE GRPSGEAFVE

        70         80         90        100        110        120
LESEDEVKLA LKKKDRETMGH RYVEVFKSNN VEMDWVLKHT GPNSPDTAND GFVRLRGLPF

       130        140        150        160        170        180
GCSEEEIVQF FSGLEIVPNG ITLPVDFQGR STGEAFVQFA SQEIAEKALK KHKERIGHRY

       190        200        210        220        230        240
IEIFKSSRAE VRTHYDPPRK LMAMQRPGPY DRPGAGRGYN SIGRGAGFER MRRGAYGGGY

       250        260        270        280        290        300
GGYDDYNGYN DGYGFGSDRF GRDLNYCFSG MSDHRYGDGG STFQSTTGHC VHMRGLPYRA

       310        320        330        340        350        360
TENDIYNFFS PLNPVRVHIE TGPDGRVTGE ADVEFATHED AVAAMSKDKA NMQHRYVELF

       370        380        390        400        410        420
LNSTAGASGG AYEHRYVELF LNSTAGASGG AYGSQMMGGM GLSNQSSYGG PASQQLSGGY

       430        440
GGGYGGQSSM SGYDQVLQEN SSDFQSNIA
```

13.2.10 Miscellaneous

Acetyl-CoA acetyltransferase

```
        10         20         30         40         50         60
MAALAVLHGV VRRPLLRGLL QEVRCLGRSY ASKPTLNDVV IVSATRTPIG SFLGSLASQP

        70         80         90        100        110        120
ATKLGTIAIQ GAIEKAGIPK EEVKEVYMGN VIQGGEGQAP TRQATLGAGL PIATPCTTVN

       130        140        150        160        170        180
KVCASGMKAI MMASQSLMCG HQDVMVAGGM ESMSNVPYVM SRGATPYGGV KLEDLIVKDG

       190        200        210        220        230        240
LTDVYNKIHM GNCAENTAKK LSISREEQDK YAIGSYTRSK EAWDAGKFAN EITPITISVK

       250        260        270        280        290        300
GKPDVVVKED EEYKRVDFSK VPKLKTVFQK ENGTVTAANA STLNDGAAAV VLMTAEAAQR

       310        320        330        340        350        360
LKVKPLARIA AFADAAVDPI DFPLAPAYAV PKVLKYAGLK KEDIAMWEVN EAFSVVVLAN

       370        380        390        400        410        420
IKMLEIDPQK VNVHGGAVSL GHPIGMSGAR IVVHLAHALK QGEFGLASIC NGGGGASAVL


IEKL
```

Aflatoxin B1 aldehyde reductase member 2

```
        10         20         30         40         50         60
MLRAVSRAVS RAAVRCAWRS GPSVARPLAM SRSPAPRAVS GAPLRPGTVL GTMEMGRRMD

        70         80         90        100        110        120
ASASAATVRA FLERGLNELD TAFMYCDGQS ESILGSLGLG LGSGDCTVKI ATKANPWDGK

       130        140        150        160        170        180
SLKPDSVRSQ LETSLKRLQC PRVDLFYLHA PDHGTPIVET LQACQQLHQE GKFVELGLSN

       190        200        210        220        230        240
YASWEVAEIY TLCKSNGWIL PTVYQGMYNA TTRQVETELL PCLRYFGLRF YAYNPLAGGL

       250        260        270        280        290        300
LTGKYRYEDK DGKQPEGRFF GNSWSETYRN RFWKEHHFEA IALVEKALKT TYGTSAPSMT

       310        320        330        340        350        360
SAALRWMYHH SQLQGTRGDA VILGMSSLEQ LEQNLAATEE GPLEPAVVEA FNQAWNVVAH


ECPNYFR
```

Aldehyde dehydrogenase

```
         10          20          30          40          50          60
MLRAALSTAR RGPRLSRLLS AAATSAVPAP NQQPEVFCNQ IFINNEWHDA VSKKTFPTVN

         70          80          90         100         110         120
PSTGEVICQV AEGNKEDVDK AVKAAQAAFQ LGSPWRRMDA SDRGRLLYRL ADLIERDRTY

        130         140         150         160         170         180
LAALETLDNG KPYVISYLVD LDMVLKCLRY YAGWADKYHG KTIPIDGDFF SYTRHEPVGV

        190         200         210         220         230         240
CGQIIPWNFP LLMQAWKLGP ALATGNVVVM KVAEQTPLTA LYVANLIKEA GFPPGVVNIV

        250         260         270         280         290         300
PGFGPTAGAA IASHEDVDKV AFTGSTEVGH LIQVAAGSSN LKRVTLELGG KSPNIIMSDA

        310         320         330         340         350         360
DMDWAVEQAH FALFFNQGQC CCAGSRTFVQ EDVYDEFVER SVARAKSRVV GNPFDSRTEQ

        370         380         390         400         410         420
GPQVDETQFK KILGYIKSGQ QEGAKLLCGG GAAADRGYFI QPTVFGDVKD GMTIAKEEIF

        430         440         450         460         470         480
GPVMQILKFK TIEEVVGRAN NSKYGLAAAV FTKDLDKANY LSQALQAGTV WINCYDVFGA

        490         500         510
QSPFGGYKMS GSGRELGEYG LQAYTEVKTV TVKVPQKNS
```

3α-Hydroxysteroid dehydrogenase

```
         10          20          30          40          50          60
MDSISLRVAL NDGNFIPVLG FGTTVPEKVA KDEVIKATKI AIDNGFRHFD SAYLYEVEEE

         70          80          90         100         110         120
VGQAIRSKIE DGTVKREDIF YTSKLWSTFH RPELVRTCLE KTLKSTQLDY VDLYIIHFPM

        130         140         150         160         170         180
ALQPGDIFFP RDEHGKLLFE TVDICDTWEA MEKCKDAGLA KSIGVSNFNC RQLERILNKP

        190         200         210         220         230         240
GLKYKPVCNQ VECHLYLNQS KMLDYCKSKD IILVSYCTLG SSRDKTWVDQ KSPVLLDDPV

        250         260         270         280         290         300
LCAIAKKYKQ TPALVALRYQ LQRGVVPLIR SFNAKRIKEL TQVFEFQLAS EDMKALDGLN

        310         320
RNFRYNNAKY FDDHPNHPFT DE
```

ATP synthase β subunit

```
        10         20         30         40         50         60
MLSLVGRVAS ASASGALRGL NPLAALPQAH LLLRTAPAGV HPARDYAAQS SAAPKAGTAT

        70         80         90        100        110        120
GQIVAVIGAV VDVQFDEGLP PILNALEVQG RESRLVLEVA QHLGESTVRT IAMDGTEGLV

       130        140        150        160        170        180
RGQKVLDSGA PIKIPVGPET LGRIMNVIGE PIDERGPIKT KQFAPIHAEA PEFIEMSVEQ

       190        200        210        220        230        240
EILVTGIKVV DLLAPYAKGG KIGLFGGAGV GKTVLIMELI NNVAKAHGGY SVFAGVGERT

       250        260        270        280        290        300
REGNDLYHEM IESGVINLKD ATSKVALVYG QMNEPPGARA RVALTGLTVA EYFRDQEGQD

       310        320        330        340        350        360
VLLFIDNIFR FTQAGSEVSA LLGRIPSAVG YQPTLATDMG TMQERITTTK KGSITSVQAI

       370        380        390        400        410        420
YVPADDLTDP APATTFAHLD ATTVLSRAIA ELGIYPAVDP LDSTSRIMDP NIVGSEHYDV

       430        440        450        460        470        480
ARGVQKILQD YKSLQDIIAI LGMDELSEED KLTVSRARKI QRFLSQPFQV AEVFTGHMGK

       490        500        510        520
LVPLKETIKG FQQILAGDYD HLPEQAFYMV GPIEEAVAKA DKLAEEHGS
```

δ-Aminolevulinic acid dehydratase

```
        10         20         30         40         50         60
MHHQSVLHSG YFHPLLRAWQ TTPSTVSATN LIYPIFVTDV PDDVQPIASL PGVARYGVNQ

        70         80         90        100        110        120
LEEMLRPLVE AGLRCVLIFG VPSRVPKDEQ GSAADSEDSP TIEAVRLLRK TFPTLLVACD

       130        140        150        160        170        180
VCLCPYTSHG HCGLLSENGA FLAEESRQRL AEVALAYAKA GCQVVAPSDM MDGRVEAIKA

       190        200        210        220        230        240
ALLKHGLGNR VSVMSYSAKF ASCFYGPFRD AAQSSPAFGD RRCYQLPPGA RGLALRAVAR

       250        260        270        280        290        300
DIQEGADILM VKPGLPYLDM VQEVKDKHPE LPLAVYQVSG EFAMLWHGAK AGAFDLRTAV

       310        320        330
LESMTAFRRA GADIIITYFA PQLLKWLKEE
```

Glycerol-3-phosphate dehydrogenase [NAD+]

```
         10          20          30          40          50          60
MAGKKVCIVG SGNWGSAIAK IVGSNASQLA HFDPRVTMWV FEEDIGGRKL TEIINTQHEN

         70          80          90         100         110         120
VKYLPGHKLP PNVVAVPDVV QAATGADILV FVVPHQFIGK ICDQLKGHLK ANTIGISLIK

        130         140         150         160         170         180
GIDEGPNGLK LISEVIGESL GIPMSVLMGA NIASEVAEEK FCETTIGCKD PAQGQLLKEL

        190         200         210         220         230         240
MQTPNFRITV VQEVDTVEIC GALKNIVAVG AGFCDGLGFG DNTKAAVIRL GLMEMIAFAK

        250         260         270         280         290         300
LFCSGSVSSA TFLESCGVAD LITTCYGGRN RKVAEAFART GKSIEQLEKE MLNGQKLQGP

        310         320         330         340
QTARELHSIL QHKGLVDKFP LFTAVYKVCY EGQPVGEFIC CLQNHPEHM
```

3-Mercaptopyruvate sulfurtransferase

```
         10          20          30          40          50          60
MAAPQLFRAL VSAQWVAEAL KSPRASQPLK LLDASWYLPK LGRDARREFE ERHIPGAAFF

         70          80          90         100         110         120
DIDRCSDHTS PYDHMLPSAT HFADYAGSLG VSAATHVVIY DGSDQGLYSA PRVWWMFRAF

        130         140         150         160         170         180
GHHSVSLLDG GFRYWLSQNL PISSGKSPSE PAEFCAQLDP SFIKTHEDIL ENLDARRFQV

        190         200         210         220         230         240
VDARAAGRFQ GTQPEPRDGI EPGHIPGSVN IPFTEFLTSE GLEKSPEEIQ RLFQEKKVDL

        250         260         270         280         290
SKPLVATCGS GVTACHVVLG AFLCGKPDVP VYDGSWVEWY MRAQPEHVIS QGRGKTL
```

Ppa1 protein

```
         10          20          30          40          50          60
PAGQLVVRRR ELPPRYNRSE AGLCGCVAVQ RRRRRHRHIS DTMSSFSSEE RAAPFTLEYR

         70          80          90         100         110         120
VFIKNEKGQY ISPFHDVPIY ADKDVFHMVV EVPRWSNAKM EIATKDPLNP IKQDVKKGKL

        130         140         150         160         170         180
RYVANLFPYK GYIWNYGAIP QTWEDPGHSD EHTGCCGDND PIDVCEIGSK VCARGEIIRV

        190         200         210         220         230         240
KVLGILAMID EGETDWKVIA INVDDPDAAN YHDISDVERL KPGYLEATVD WFRRYKVPDG

        250         260         270         280         290         300
KPENEFAFNA EFKNKEFAVD IIKNTHDYWK ALVTKKTDGK GISCMNTTVS ESPFKCDPDA

        310         320         330
AKAIVDALPP PCESACALPM DVDKWFHHQK N
```

Protein NDRG2

```
         10         20         30         40         50         60
MAELQEVQIT EEKPLLPGQT PEAAKEAELA ARILLDQGQT HSVETPYGSV TFTVYGTPKP

         70         80         90        100        110        120
KRPAIFTYHD VGLNYKSCFQ PLFQFGDMQE IIQNFVRVHV DAPGMEEGAP VFPLGYQYPS

        130        140        150        160        170        180
QDQLADMIPC ILQYLNFSTI IGVGVGAGAY ILSRYALNHP DTVEGLVLIN IDPNAKGWMD

        190        200        210        220        230        240
WAAHKLTGLT SSIPEMILGH LFSQEELSGN SELIQKYRSL ITHAPNLENI ELYWNSYNNR

        250        260        270        280        290        300
RDLNFERGGE MTLKCPVMLV VGDQAPHEDA VVECNSKLDP TQTSFLKMAD SGGQPQLTQP

        310        320        330        340        350        360
GKLTEAFKYF VQGMGYMASS CMTRLSRSRT ASLTSAASID GSRSRSRTLS QSSESGTLPS

        370
GPPGHTMEVS C
```

Regucalcin

```
         10         20         30         40         50         60
MSSIKIECVL RENYRCGESP VWEEASKCLL FVDIPSKTVC RWDSISNRVQ RVGVDAPVSS

         70         80         90        100        110        120
VALRQSGGYV ATIGTKFCAL NWEDQSVFIL AMVDEDKKNN RFNDGKVDPA GRYFAGTMAE

        130        140        150        160        170        180
ETAPAVLERH QGSLYSLFPD HSVKKYFDQV DISNGLDWSL DHKIFYYIDS LSYTVDAFDY

        190        200        210        220        230        240
DLPTGQISNR RTVYKMEKDE QIPDGMCIDV EGKLWVACYN GGRVIRLDPE TGKRLQTVKL

        250        260        270        280        290
PVDKTTSCCF GGKDYSEMYV TCARDGMSAE GLLRQPDAGN IFKITGLGVK GIAPYSYAG
```

Ribonuclease UK114

```
         10         20         30         40         50         60
MSSIIRKVIS TSKAPAAIGA YSQAVLVDRT IYVSGQIGMD PSSGQLVPGG VAEEAKQALK

         70         80         90        100        110        120
NLGEILKAAG CDFTNVVKTT VLLADINDFG TVNEIYKTYF QGNLPARAAY QVAALPKGSR

        130
IEIEAIAVQG PFTTAGL
```

Sulfite oxidase

```
        10         20         30         40         50         60
MLPRLYRSVA VGLPRAIRAK STPLRLCIQA CSSSDSLKPQ HPSLTFSDDN SRTRGWKVMG

        70         80         90        100        110        120
TLIGLGAVLA YHDHRCRASQ ESPRIYSKED VRSHNNLKTG VWVTLGSEVF DVTKFVDLHP

       130        140        150        160        170        180
GGQSKLMLAA GGPLEPFWAL YAVHNQPHVR ELLAEYKIGE LNPEDRMSPP LEASDPYSND

       190        200        210        220        230        240
PMRHPALRIN SQRPFNAEPP PELLTESYIT PNPIFFTRNH LPVPNLDPDT YRLHVVGAPG

       250        260        270        280        290        300
GQSLSLSLDD LHKFPKHEVT VTLQCAGNRR SEMNKVKEVK GLEWRTGAIS TARWAGARLC

       310        320        330        340        350        360
DVLAQAGHRL RETEAHVCFE GLDSDPTGTA YGASIPLARA MDPQAEVLLA YEMNGQPLPR

       370        380        390        400        410        420
DHGFPVRVVV PGVVGARHVK WLGRVSVESE ESYSHWQRRD YKGFSPSVDW DTVDFDLAPS

       430        440        450        460        470        480
IQELPIQSAI TQPQDGTTVE SGEVIIKGYA WSGGGRAVIR VDVSMDGGLT WQEAELEGEE

       490        500        510        520        530        540
QHPRKAWAWR IWQLKAHVPA EQKELNIICK AVDDSYNVQP DTVAPIWNLR GVLSNAWHRV


HVQVVP
```

13.3 Summary of protein cysteine and lysine contents

Table 22 ***Cysteine and lysine contents of furan target proteins*** *(continued on next pages). Protein sequence data obtained from UniProt database. The % values for cysteine and lysine are calculated as number of cysteine or lysine amino acid residues/total number of amino acids.*

Protein Name	Spot	ID	M_r	pI	Total number of amino acids	Cysteine		Lysine	
						Number	%	Number	%
Carbohydrate metabolism									
α-Enolase	27	P04764	47128	6.16	434	6	1.4	36	8.3
Fructose-bisphosphate aldolase B	50	P00884	39618	8.66	364	8	2.2	23	6.3
Fructose-1,6-bisphosphatase 1	6	P19112	39609	5.54	363	8	2.2	24	6.6
Glyceraldehyde-3-phosphate dehydrogenase	52	P04797	35828	8.43	333	5	1.5	26	7.8
L-Lactate dehydrogenase A chain	53	P04642	36451	8.45	332	5	1.5	28	8.4
Malate dehydrogenase	2b, 31	O88989	36483	6.16	334	3	0.9	30	9.0
Phosphoglycerate kinase 1	51	P16617	44538	8.02	417	7	1.7	41	9.8
Triosephosphate isomerase	47, 97	P48500	26849	6.51	249	9	3.6	21	8.4
Lipid metabolism									
Enoyl-CoA hydratase	64	P14604	31516	6.41	290	7	2.4	22	7.6
3-Ketoacyl-CoA thiolase	51, 55	P13437	41871	8.09	397	7	1.8	23	5.8
Long-chain fatty acid CoA ligase 1	2a	P18163	78179	6.60	699	18	2.6	49	7.0
Long-chain specific acyl-CoA dehydrogenase	93	P15650	47873	7.63	430	7	1.6	26	6.0
Short-chain specific acyl-CoA dehydrogenase	59	P15651	44765	8.47	412	5	1.2	22	5.3
Amino acid metabolism, urea cycle									
Arginase 1	59	P07824	34973	6.76	323	3	0.9	26	7.7
Argininosuccinate synthase	51, 55	P09034	46496	7.63	412	5	1.2	34	8.3
Betaine-homocysteine S-methyltransferase 1	51	O09171	44976	8.01	407	8	2.0	30	7.4
Formimidoyltransferase-cyclodeaminase	83	O88618	58914	5.80	541	11	2.0	24	4.4
Isovaleryl-CoA dehydrogenase	33c, 58	P12007	46435	8.03	424	8	1.9	23	5.4
Ornithine carbamoyltransferase	55, 60	P00481	39886	9.12	354	1	0.3	26	7.3
2-Oxoisovalerate dehydrogenase subunit α	85	P11960	50164	7.68	441	5	1.1	16	3.6
S-Adenosylmethionine synthetase isoform type-1	85, 86	P13444	43698	5.61	397	10	2.5	25	6.3
Redox regulation									
Electron transfer flavoprotein subunit α	61	P13803	34951	8.62	333	6	1.8	26	7.8
Peroxiredoxin-1	62	Q63716	22109	8.27	199	4	2.0	19	9.5
Thioredoxin-1	12	P11232	11673	4.80	105	6	5.7	12	11.4
Thioredoxin-like protein 1	3	Q920J4	32249	4.84	289	7	2.4	18	5.9

Table 22 *(continued)*

Protein Name	Spot	ID	M_r	pI	Total number of amino acids	Cysteine		Lysine	
						Number	%	Number	%
Protein folding									
78 kDa Glucose-regulated protein	75, 76	P06761	72347	5.07	654	3	0.5	61	9.3
Heat shock cognate 71 kDa protein	1, 79	P63018	70871	5.43	646	4	0.6	54	8.4
Protein disulfide-isomerase	74, 75	P04785	56951	4.82	509	7	1.4	51	10.0
Protein disulfide-isomerase A3	83	P11598	56623	5.88	505	8	1.6	50	9.9
Proteolysis									
α_1-Antiproteinase	86	P17475	46136	5.70	411	3	0.7	26	6.3
Protein AMBP: Bikunin and Trypstatin	23	Q64240	38851	5.77	349	16	4.6	21	6.0
Serine protease inhibitor A3K	80	P05545	46562	5.31	416	4	1.0	30	7.2
Ubiquitin fusion degradation protein 1 homolog	94	Q9ES53	34485	6.27	307	5	1.6	22	7.2
Structural proteins									
β-Actin	2a, 2b, 5	P60711	41737	5.29	375	6	1.6	19	5.1
Ezrin-radixin-moesin-binding phosphoprotein 50	21a	Q9JJ19	38830	5.70	356	6	1.7	28	7.9
Fibrinogen γ chain	21c	P02680	50633	5.85	445	11	2.5	31	7.0
γ-Actin	2a, 2b, 5, 78	P63259	41793	5.29	375	6	1.6	19	5.1
Keratin, type II cytoskeletal 8	21b, 24, 25, 78	Q10758	54019	5.82	483	/	/	35	7.2
Na(+)/H(+) exchanger regulatory factor 3	75, 79	Q9JJ40	56800	5.23	523	7	1.3	41	7.8
Protein SEC13 homolog	4	Q5XFW8	35548	5.15	322	9	2.8	17	5.3
Voltage-dependent anion-selective channel protein 1	53	Q9Z2L0	30756	8.35	283	2	0.7	25	8.9
Transport proteins									
α2μ-Globulin	19, 20a, 87	P02761	20737	5.85	181	5	2.8	14	7.7
Fatty acid binding protein 1	63, 91	P02692	14273	7.79	127	1	0.8	17	13.4
Protein AMBP: α_1-Microglobulin	23	Q64240	38851	5.77	349	16	4.6	21	6.0
Transthyretin	92	P02767	15720	5.76	147	2	1.4	9	6.1
Vitamin D binding protein	80	P04276	53544	5.76	476	28	5.9	36	7.6
Nucleotide metabolism									
Multifunctional protein ADE2	51	P51583	47096	7.87	425	13	3.1	43	10.1
Putative L-aspartate dehydrogenase	61	Q5I0J9	31260	5.52	297	3	1.0	2	0.7
Heterogeneous nuclear ribonucleoprotein H1	93	Q8VHV7	49188	5.93	449	5	1.1	15	3.3

Table 22 *(continued)*

Protein Name	Spot	ID	M_r	pI	Total number of amino acids	Cysteine		Lysine	
						Number	%	Number	%
Miscellaneous									
Acetyl-CoA acetyltransferase	50	P17764	44695	8.92	424	6	1.4	33	7.8
Aflatoxin B1 aldehyde reductase member 2	96	Q8CG45	40675	6.27	367	8	2.2	13	3.5
Aldehyde dehydrogenase	29, 86	P11884	56488	7.63	519	9	1.7	31	6.0
3α-Hydroxysteroid dehydrogenase	37, 60	P23457	37028	6.67	322	9	2.8	28	8.7
ATP synthase β subunit	4, 74	P10719	56354	4.92	529	/	/	23	4.3
δ-aminolevulinic acid dehydratase	35	P06214	36032	6.32	330	8	2.4	12	3.6
Glycerol-3-phosphate dehydrogenase [NAD+]	33b, 60	O35077	37453	6.16	349	12	3.4	24	6.9
3-Mercaptopyruvate sulfurtransferase	30	P97532	32940	5.88	297	5	1.7	11	3.7
Ppa1 protein	4	Q499R7	37677	6.65	331	10	3.0	27	8.2
Protein NDRG2	78	Q8VBU2	40779	5.16	371	6	1.6	13	3.5
Regucalcin	4	Q03336	33390	5.40	299	10	3.3	19	6.4
Ribonuclease UK114	14, 63	P52759	14303	7.77	137	1	0.7	8	5.8
Sulfite oxidase	83	Q07116	60806	5.86	546	7	1.3	20	3.7

13.4 Possible additional target proteins of furan

Table 23 ***Further putative target proteins of reactive furan metabolites*** *(continued on next page)*

Protein data obtained from Mascot search engine and UniProt database following peptide analysis by FT-ICR (LTQ FT Ultra™, Thermo Scientific) or ESI-QTOF-MS/MS⁺ (Q-TOF Ultima Global, Waters). Proteins in this category were either found in three different animals showing once a sequence coverage < 10 % or were only observed in two animals, but both with a sequence coverage of > 10 %. Cs = cytosol, CM = cell membrane, Cp = cytoplasm, Mito = mitochondrion, ER = endoplasmic reticulum, Ck = cytoskeletal, ES = extracellular space, sec = secreted, Nu = nucleus, Ms = microsome, Px = peroxisome*

Protein	Spot	ID	M_r	pI	Found in 3 animals, but sequence coverage was once less than 10 %	Found in 2 animals, but twice > 10 %	Location
Carbohydrate metabolism							
*Transaldolase	60	Q9EQS0	37624	6.57		x	Cp
Amino acid metabolism, urea cycle							
*Alanine aminotransferase 1	98	P25409	55872	6.08		x	Cp
*Branched-chain α-keto acid dihydrolipoyl acyltransferase	98	Q99PU6	20825	5.21		x	Mito
*Fumarylacetoacetase	57	P25093	46231	6.67	x		
*3-Hydroxyisobutyrate dehydrogenase	61	P29266	36741	8.58		x	Mito
*4-Hydroxyphenylpyruvate dioxygenase	58	P32755	45312	6.29	x		Cp, ER, Golgi, CM
	94	P32755	45312	6.29		x	Cp, ER, Golgi, CM
*Phenylalanine-4-hydroxylase	24	P04176	52303	5.76		x	
*Succinate semialdehyde dehydrogenase	98	P51650	52669	6.40		x	Mito
Redox regulation							
*Cytochrome b5	70	P00173	11400	5.26		x	ER, Ms
Proteolysis							
*Cytosolic non-specific dipeptidase	80	Q6Q0N1	53116	5.43		x	Cp
*Proteasome subunit α type-6	64	P60901	27838	6.34	x		Cp, Nu
Structural proteins							
*Tubulin β2C chain	74	Q6P9T8	50225	4.79		x	Ck
Nucleotide metabolism							
*Nucleoside diphosphate kinase A	87	Q05982	17296	5.96		x	Cp, Nu
*Poly(RC) binding protein 2	94	Q6AYU5	37987	6.66		x	Cp

Table 23 *(continued)*

Protein	Spot	ID	M_r	pI	Found in 3 animals, but sequence coverage was once less than 10 %	Found in 2 animals, but twice > 10 %	Location
Miscellaneous							
+*Aldo-keto reductase family 1, member C13	+37	Q5I0M4	37503	6.47		x	
	*60	Q5I0M4	37503	6.47		x	
*α2-HS-glycoprotein	98	P24090	38757	6.05		x	sec
+*Annexin A3	25	P14669	36569	5.96		x	
*Apolipoprotein E	82	Q6PAH0	35798	5.23		x	CM, Golgi
*ATP synthase subunit α	62	P15999	55347	8.28		x	Mito
+*Catechol-O-methyltransferase	9	P22734	29806	5.41	x		CM, Cp
+*Cysteine sulfinic acid decarboxylase	29	Q64611	55841	6.84	x		
*Fumarylacetoacetate hydrolase domain containing 1	97	Q6AYQ8	24750	7.62		x	
*γ-Butyrobetaine dioxygenase	94	Q9QZU7	45031	6.23		x	Cp
Glycerate kinase	*24	Q0VGK3	55495	5.84		x	Cp
	+*25	Q0VGK3	55495	5.84		x	Cp
*Glycerol kinase	80	Q63060	58238	5.49		x	Cp, CM, Mito
*Guanine nucleotide binding protein, β polypeptide 2-like 1	54	P63245	35529	7.60		x	CM
*Ig kappa chain C region, A allele	64	P01836	11896	4.99		x	
*Isocitrate dehydrogenase [NADP] cytoplasmic	57	P41562	47047	6.53		x	Cp
*Rhodanese	54	P24329	33384	7.84	x		Mito
+*Suclg2 protein	23	Q68FT4	41980	5.64		x	Mito
+*Sulfotransferase 1C1	29	P50237	35865	6.09		x	Cp
*4-Trimethylaminobutyraldehyde dehydrogenase	24	Q9JLJ3	54928	6.31		x	Cp
	98	Q9JLJ3	54928	6.31		x	Cp
Protein biosynthesis							
+*Eukaryotic translation initiation factor 3, subunit 4	23	Q5RK09	35914	5.69		x	Cp
+*Eukaryotic translation initiation factor 6	8	Q3KRD8	27067	4.63	x		
Steroid metabolism							
*α-Methylacyl-CoA racemase	94	P70473	40035	6.22	x		Mito, Px
*HMG-CoA synthase 1	83	P17425	58025	5.58		x	Cp
+*HMG-CoA synthase 2	25	P22791	57306	8.86		x	Mito

13.5 Densitometry data

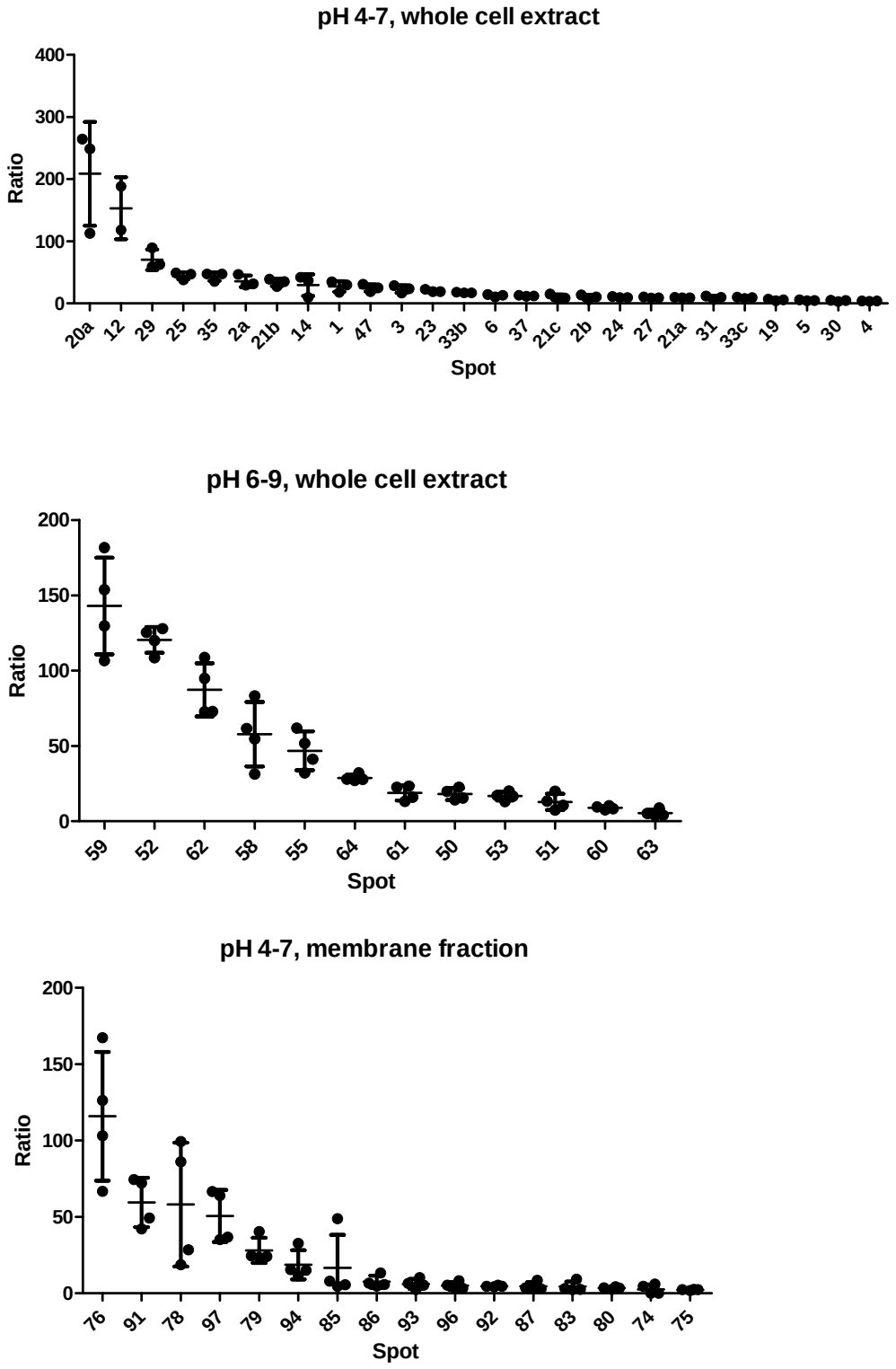

Figure 39 *Scatter blots showing the different ratio values for each spot plus their means and standard deviation. For identity of the proteins identified in the various spots see Tab. 24.*
Top: pH 4-7, whole tissue extract, 900 µg protein, 10 weeks exposure time, n=3
Middle: pH 6-9, whole tissue extract, 500 µg protein, 16 weeks exposure time, n=4
Bottom: pH 4-7, membrane fraction, 900 µg protein, 24 weeks exposure time, n=4

Table 24 *Summary of the proteins identified in the different protein spots.*

Spot	Protein	Spot	Protein
1	Heat shock cognate 71 kDa protein	**55**	Ornithine carbamoyltransferase Argininosuccinate synthase 3-Ketoacyl-CoA thiolase
2a	Long-chain fatty acid CoA ligase 1 β-Actin / γ-Actin		
2b	Malate dehydrogenase β-Actin / γ-Actin	**58**	Isovaleryl-CoA dehydrogenase
		59	Short-chain specific acyl-CoA dehydrogenase Arginase 1
3	Thioredoxin-like protein 1		
4	Regucalcin ATP synthase β subunit Protein SEC13 homolog Ppa1 protein	**60**	Glycerol-3-phosphate dehydrogenase [NAD+] 3α-Hydroxysteroid dehydrogenase Ornithine carbamoyltransferase
		61	Putative L-aspartate dehydrogenase Electron transfer flavoprotein subunit α
5	β-Actin / γ-Actin		
6	Fructose-1,6-bisphosphatase 1	**62**	Peroxiredoxin-1
12	Thioredoxin-1	**63**	Ribonuclease UK114 Fatty acid binding protein 1
14	Ribonuclease UK114		
19	α2μ-Globulin	**64**	Enoyl-CoA hydratase
20a	α2μ-Globulin	**74**	Protein disulfide-isomerase ATP synthase β subunit
21a	Ezrin-radixin-moesin-binding phosphoprotein 50		
21b	Keratin, type II cytoskeletal 8	**75**	78 kDa Glucose-regulated protein Protein disulfide-isomerase Na(+)/H(+) exchanger regulatory factor 3
21c	Fibrinogen γ chain		
23	Protein AMBP		
24	Keratin, type II cytoskeletal 8	**76**	78 kDa Glucose-regulated protein
25	Keratin, type II cytoskeletal 8	**78**	Keratin, type II cytoskeletal 8 β-Actin / γ-Actin Protein NDRG2
27	α-Enolase		
29	Aldehyde dehydrogenase		
30	3-Mercaptopyruvate sulfurtransferase	**79**	Heat shock cognate 71 kDa protein Na(+)/H(+) exchanger regulatory factor 3
31	Malate dehydrogenase		
33b	Glycerol-3-phosphate dehydrogenase	**80**	Serine protease inhibitor A3K Vitamin D-binding protein
33c	Isovaleryl-CoA dehydrogenase		
35	δ-Aminolevulinic acid dehydratase	**83**	Protein disulfide-isomerase A3 Formimidoyltransferase-cyclodeaminase Sulfite oxidase
37	3α-Hydroxysteroid dehydrogenase		
47	Triosephosphate isomerase		
50	Acetyl-CoA acetyltransferase Fructose-bisphosphate aldolase B	**85**	S-Adenosylmethionine synthetase isoform type-1 2-Oxoisovalerate dehydrogenase subunit α
51	Argininosuccinate synthase Betaine-homocysteine S-methyltransferase 1 3-Ketoacyl-CoA thiolase Phosphoglycerate kinase 1 Multifunctional protein ADE2	**86**	α_1-Antiproteinase Aldehyde dehydrogenase S-Adenosylmethionine synthetase isoform type-1
		87	α2μ-Globulin
		91	Fatty acid binding protein 1
52	Glyceraldehyde-3-phosphate dehydrogenase	**92**	Transthyretin
53	L-lactate dehydrogenase A chain Voltage-dependent anion-selective channel protein 1	**93**	Heterogeneous nuclear ribonucleoprotein H1 Long-chain specific acyl-CoA dehydrogenase
		94	Ubiquitin fusion degradation protein 1 homolog
		96	Aflatoxin B1 aldehyde reductase member 2
		97	Triosephosphate isomerase

14 PUBLICATIONS

14.1 Presentations at international meetings

Mally, A., Graff, C., **Moro, S.**, Hamberger, C., Schauer, U.M., Brück, J., Özden, S., Sieber, M., Steger, U., Hard, G.C., Chipman, J.K., Schrenk, D., and Dekant, W. Furan in Food: 28 Day Oral Toxicity and Cell proliferation in Male F344/N Rats. (Poster) Society of Toxicology 48th Annual Meeting, Baltimore, 2009. The Toxicologist, Supplement to Toxicological Sciences

Moro, S., Hamberger, C., Dekant, W., Chipman, K. and Mally, A. Identification of target proteins of furan in rat liver. (Oral presentation + Poster) 46th Congress of the European Society of Toxicology, Dresden, 2009. Toxicology Letters, Vol. 189S

Hamberger, C., **Moro, S.**, Malfatti, M., Turteltaub, K., Mally, A., Dekant, W. Analysis of DNA binding of furan in rat liver by accelerator mass spectrometry. (Oral presentation + Poster) 46th Congress of the European Society of Toxicology, Dresden, 2009. Toxicology Letters, Vol. 189S

Moro, S., Hamberger, C., Dekant, W., Chipman, K. and Mally, A. Identification of target proteins of furan in rat liver. (Poster) Society of Toxicology 49th Annual Meeting, Salt Lake City, 2010. The Toxicologist, Supplement to Toxicological Sciences

Hamberger, C., **Moro, S.**, Malfatti, M., Turteltaub, K., Dekant, W., Mally, A. Analysis of DNA binding of [3,4-^{14}C]-furan in rat liver by accelerator mass spectrometry. (Poster) Society of Toxicology 49th Annual Meeting, Salt Lake City, 2010. The Toxicologist, Supplement to Toxicological Sciences

14.2 Publication

Mally, A., Graff, C., Schmal, O., **Moro, S.**, Hamberger, C., Schauer, U.M., Brück, J., Özden, S., Sieber, M., Steger, U., Schrenk, D., Hard, G.C., Chipman, J.K. and Dekant, W. Functional and proliferative effects of repeated low-dose oral administration of furan in rat liver. Mol. Nutr. Food Res. 2010, *54*, 1-12

15 ACKNOWLEDGEMENTS

First of all, I would like to thank PD Dr. Angela Mally and Prof. Dr. Wolfgang Dekant for giving me the opportunity to work on this interesting PhD project. Thank you for your understanding and your support. I am deeply grateful that I had the chance to spend a few months working in England and to present the results of my work at meetings and international conferences.

I would like to thank Prof. Dr. Ulrike Holzgrabe for supervising my PhD thesis on behalf of the Faculty for Chemistry and Pharmacy.

I am very thankful to our cooperation partner Prof. J. Kevin Chipman for giving me the possibility to perform a part of my work at the School of Biosciences (The University of Birmingham).

I would like to thank Antony Jones, Lorraine Wallace, Dr. Jonathan James, and Dr. Cleidiane Zampronio for kindly supporting me in the mass spectrometry analyses. I am also grateful to my friends and colleagues at the University of Birmingham. I had a really great time with you - during the working hours as well as at tea times and curries.

Financial support by the DFG (Deutsche Forschungsgemeinschaft) is gratefully acknowledged. Furthermore, I would like to thank all participants of the FP6 European Union funded project “Role of genetic and non-genetic mechanisms in furan risk” for kind cooperation.

I am thankful to Christian Dees, Reinhold Krug, and Dr. Benjamin Mentzel for helping me with the radioactive work and measuring samples for me.

Thank you to Michaela Bekteshi, Ursula Tatsch, Heike Keim-Heusler, Caroline Kröcher, and Elisabeth Rüb-Spiegel for excellent technical assistance and animal care. Moreover, I am very grateful to all my colleagues from the working groups of PD Dr. Angela Mally and Prof. Dr. Wolfgang Dekant for the nice and friendly working atmosphere.

I am particularly thankful to Silvi, Dana, Melli, Caro, Tinka, and Marion for countless helpful discussions, for your optimism, for your friendship, and for your support (private and scientific).

Finally, I would like to express my special thanks to my dear parents. Thank you for your unlimited support during my years of study and my PhD work and for your patience and encouragement while I was writing up the thesis! I would also like to thank the rest of my familiy and my friends who always supported me.